AD-A062 289 DAVID TAYLOR MODEL BASIN WASHINGTON D C AERODYNAMICS LAB F/G 16/4.2
TRANSONIC WIND-TUNNEL TESTS OF A 1/15-SCALE MODEL OF THE TALOS --ETC(U)
MAR 61 M E MCDONALD

UNCLASSIFIED AERO-1002 NL

1 OF 3
ADA
062289

NAVY DEPARTMENT

THE DAVID W. TAYLOR MODEL BASIN

AERODYNAMICS LABORATORY

WASHINGTON 7, D.C.

TRANSONIC WIND-TUNNEL TESTS OF A 1/15-SCALE MODEL OF THE TALOS 6c1 MISSILE

(Title Unclassified)

by

Michael J. McDonald

Approved for unlimited distribution

Public Access

11

March 1961

(14)

Aero Report 1002

CANCELLED

AERODYNAMICS LABORATORY
DAVID TAYLOR MODEL BASIN
UNITED STATES NAVY
WASHINGTON, D. C.

(6)

TRANSONIC WIND-TUNNEL TESTS OF A 1/15-SCALE MODEL OF THE TALOS 6c1 MISSILE

by

(10) Michael E. McDonald

(11) Mar 61

(12) 196 p.

SUMMARY

Tests of a 1/15-scale model of the TALOS 6c1 missile were performed in the TMB 7- by 10-Foot Transonic Wind Tunnel for a Mach number range of 0.7 to 1.17, at angles of attack of -4° to 10°, and roll angles of 0° and -45°.

The investigation included evaluation of the effects of ram-air bleed at the base of the second stage and the longitudinal stability and control effectiveness of the missile.

The data are presented without analysis.

SYMBOLS

The aerodynamic force and moment coefficients are based on the maximum area and diameter of the missile body and are referred to the axes system given in Figure 1.

d	reference length (1.868 inches)
M	free-stream Mach number
q	free-stream dynamic pressure, pounds per square foot
R	Reynolds number per foot

CANCELLED

400 036

4/B

S_b area at the base of the model (0.0068 square foot)

S_d area at the model maximum diameter (0.0190 square foot)

C_A axial-force coefficient

C_N normal-force coefficient

C_m pitching-moment coefficient

C_l rolling-moment coefficient

C_n yawing-moment coefficient

C_Y side-force coefficient

i average incidence of wings b and d, in degrees (positive when the leading edges are deflected toward wing a) (See Figure 2)

i' average incidence of wings a and c, in degrees (positive when the leading edges are deflected toward control panel d) (See Figure 2)

δ differential deflection of wings b and d from the nominal incidence values, in degrees (a positive value indicates deflections that tend to produce a positive rolling moment)

δ' differential deflection of wings a and c from the nominal incidence values, in degrees (a positive value indicates deflections that tend to produce a positive rolling moment)

α angle of attack, in degrees (See Figure 1)

ϕ angle of roll, in degrees (See Figure 1)

Configuration Notation

B_{22} vented missile body with the following:

homing and fuse antenna	4 each
pressure probe on cowl	1
beacon and beam rider antenna	1 each
flash signals on base	2

R_5 booster body including:

launching lugs	4
vented head cap	

H_{10}	longitudinal housing plus large turbine exhaust louvers	4 each
W	missile wings	
T_{10}	missile tail (full-scale span, 23 inches)	4
F_{18}	booster fins	4
C	internal vent cover	1

INTRODUCTION

The TALOS is a surface-to-air, supersonic guided missile and utilizes a ram-jet second stage, which is propelled to operating velocity by a solid-propellant booster rocket.

An investigation was conducted at the request of the Bureau of Weapons (Reference 1) to determine the effect, upon stability and control, of a ram-inlet bleed at the base of the second stage of a 1/15-scale model TALOS 6c1 missile. The longitudinal stability characteristics and effects of various components of the missile were also investigated.

The Mach number range of the tests was from 0.7 to 1.17, the angle-of-attack range was from -4° to 10°, and the roll angles were 0° and -45°.

The tests were performed at the David Taylor Model Basin in September 1960, under the technical direction of the Johns Hopkins Applied Physics Laboratory and the Bendix Corporation.

APPARATUS AND METHODS

TUNNEL

This test was conducted in the 7- by 10-Foot Transonic Wind Tunnel at the David Taylor Model Basin, which is described in Reference 2. Sketches of the major tunnel components and test section are presented in Figures 3 and 4, respectively.

The distribution of the center-line free-stream Mach number in the testing region is shown in Figure 5. The deviations from the free-stream Mach number in the testing region are generally less than ±0.005 for Mach numbers below 1.0. The deviations increase with speed, but are never greater than ±0.01.

MODEL

A 1/15-scale model of the TALOS 6c1 was supplied for these tests. The missile body has a nearly constant circular cross section. It has four controllable wings and fixed tail surfaces on the second stage and four fixed booster fins on the first stage. Various protuberances, representing launching lugs, antennas, beacon lights, pressure probes, and external housings were attached to the model during the tests. Several of these configurations are shown in Figures 6 and 7. For the basic model configurations, the ram-inlet air was exhausted, by internal ducting of the second stage, through a series of bleed ports located around the circumference of the body (see Figure 8). An internal vent cover could be inserted to prevent the bleeding of ram air.

The small scale of the model dictated several internal modifications in adapting the model to an internal, six-component strain-gage balance. It was necessary for the balance to extend through the booster stage into the second stage. A flat-plate cross strut provided support for a balance locking screw. The upstream end of the screw and the exposed end of the balance were covered with conical fairings (see Figure 8). The depth to which the balance could be inserted into the model was restricted so that the effective cross-sectional area remained constant in the vicinity of the bleed passages. In this position, a small portion of the balance protruded from the rear of the model; however, all areas equipped with gages were inside the model.

TESTS AND MEASUREMENTS

As explained above, the model was attached to a six-component strain-gage balance. It was supported by a remotely controlled, cantilevered, sting support system. The angle of attack was measured by movement of the sting; it was adjusted for deflection due to aerodynamic loads. To obtain roll, the model was rotated manually on the strain-gage balance so that the forces and moments were always obtained in the axes system defined in Figure 1. Base pressure of the model was recorded by pressure transducers through static pressure orifices located inside the model base. A model fouling system was established by insulating the entire model from the support and balance system and providing a low-voltage circuit directly to the model. Schlieren photographs were taken at small angles of attack and several Mach numbers for representative configurations.

Various configurations of the model were investigated as shown in Table 1. Removable components consisted of internal vent cover, wings, tails, and booster fins.

The angle-of-attack range for the tests was from -4° to 10°. The angle of roll was either 0° (flight attitude) or -45° (launch attitude). The Mach numbers investigated were 0.70, 0.90, 1.06, and 1.17. The tests were conducted at a stagnation pressure of approximately one-half atmosphere and at a Reynolds number per foot of 1.6×10^6 to 2.2×10^6.

CORRECTIONS AND ACCURACY

No corrections have been made for the effects of tunnel blockage, since it is generally accepted that this effect is negligible for small blockage ratios. The angle of attack has been corrected for deflection due to aerodynamic load and is believed to be accurate within ±0.1°. However, no attempt has been made to correct for sting interference effects beyond

adjusting the axial force measurement to the condition of free-stream static pressure at the base of the model. No corrections have been made for internal losses due to bleed air flow through the missile.

The nominal Mach numbers given in the figures are accurate to within ±0.003. The repeatability and accuracy of the aerodynamic coefficients at three Mach numbers, taking into account calibrations of the strain-gage balance, are believed to be as follows:

Component	Mach number		
	0.7	0.9	1.17
C_A	±0.08	±0.07	±0.05
C_N	±0.25	±0.20	±0.14
C_m	±0.14	±0.12	±0.08
C_n	±0.14	±0.12	±0.08
C_Y	±0.08	±0.07	±0.05
C_l	±0.05	±0.04	±0.03

PRESENTATION OF RESULTS

The coefficients presented herein are referred to the missile axes system with the origin located at full-scale body station 241 (see Figures 1 and 2). The maximum body diameter and cross-sectional area were used as reference dimensions.

The variation of aerodynamic coefficients with angle of attack is presented for both roll angles in Figures 9 through 16. The pitching-moment coefficient is plotted versus the normal-force coefficient in Figures 17 through 24. In addition, the

lateral coefficients for some tests are given in Figures 9 to 11, to show the effect of control-surface deflections. An index of the configurations, the test conditions, figure numbers, and page numbers is given in Table 1.

Schlieren photographs of various configurations for several Mach numbers and angles of attack are presented in Figures 25 to 30.

It has been observed that:

1. The effect of Mach number on the slope of the curves of normal-force coefficient and pitching-moment coefficient versus angle of attack is small.

2. The effect of bleed air on the longitudinal characteristics of the missile appears to be slight.

3. For several configurations an unexplainable change in the pitching-moment and normal-force coefficients occurred between an angle of attack of -3° and -1° at a Mach number of 0.90.

The results are presented without further analysis.

Aerodynamics Laboratory
David Taylor Model Basin
Washington, D. C.
March 1961

REFERENCES

1. BUWEPS CONF ltr RAAD-341:JM Ser 037212 of 19 Aug 1960
2. Thomas, Walter S. The David Taylor Model Basin 7- by 10-Foot Transonic Wind Tunnel Facility. Wash., Jul 1960. 35 l. illus. (David Taylor Model Basin. Aero Rpt. 985)

Table 1

Index to Test Conditions

Configuration	Roll Angle ϕ in degrees	Incidence Angle in degrees		Deflection Angle in degrees		Mach Number	Figure	Page
		i	i'	δ	δ'			
$B_{22}R_5H_{10}W$	-45	0	0	0	0	(a)	9a,17a	14-23, 129
		-10	-10	0	0	(a)	9b,17b	24-26, 130
		-15	-15	0	0	(b)	9c,17c	27-29, 131
		0	0	5	5	(a)	9d,17d	30-35, 132
	0	0	0	0	0	(a)	9e,17e	36-38, 133
		-10	0	0	0	(a)	9f,17f	39-41, 134
$B_{22}R_5H_{10}W T_{10}$	-45	0	0	0	0	(a)	10a,18a	42-47, 135
		-10	-10	0	0	(a)	10b,18b	48-50, 136
		-15	-15	0	0	(b)	10c,18c	51-53, 137
		0	0	5	5	(a)	10d,18d	54-59, 138
	0	0	0	0	0	(a)	10e,18e	60-62, 139
		-10	0	0	0	(a)	10f,18f	63-65, 140
$B_{22}R_5H_{10}W T_{10}F_{18}$	-45	0	0	0	0	(a)	11a,19a	66-71, 141
		-5	-5	0	0	(a)	11b,19b	72-74, 142
		-10	-10	0	0	(a)	10c,19c	75-77, 143
		-15	-15	0	0	(b)	11d,19d	78-80, 144
		0	0	5	5	(a)	11e,19e	81-86, 145
	0	0	0	0	0	(a)	11f,19f	87-89, 146
		-5	0	0	0	(a)	11g,19g	90-92, 147
		-10	0	0	0	(a)	11h,19h	93-95, 148
$B_{22}R_5H_{10}$	-45	-	-	-	-	(c)	12, 20	96-101, 149-150
$B_{22}R_5H_{10}F_{18}$	-45	-	-	-	-	(d)	13, 21	102-110, 151-153
$B_{22}R_5H_{10}T_{10}$	-45	-	-	-	-	(a)	14, 22	111-113, 154
$B_{22}R_5H_{10}WC$	0	0	0	0	0	(e)	15a,23a	114-116, 155
		-5	0	0	0	(f)	15b,23b	117-119, 156
		-10	0	0	0	(e)	15c,23c	120-122, 157
$B_{22}R_5H_{10}W T_{10}F_{18}C$	0	0	0	0	0	(f)	16a,24a	123-125, 158
		-10	0	0	0	(f)	16b,24b	126-128, 159

a 0.70, 0.90, 1.06, 1.17

b 0.70

c 0.70, 0.90, 0.95, 0.975, 1.06, 1.10, 1.17

d 0.70, 0.90, 0.95, 0.975, 1.00, 1.02, 1.04, 1.06, 1.17

e 0.90, 1.17

f 1.17

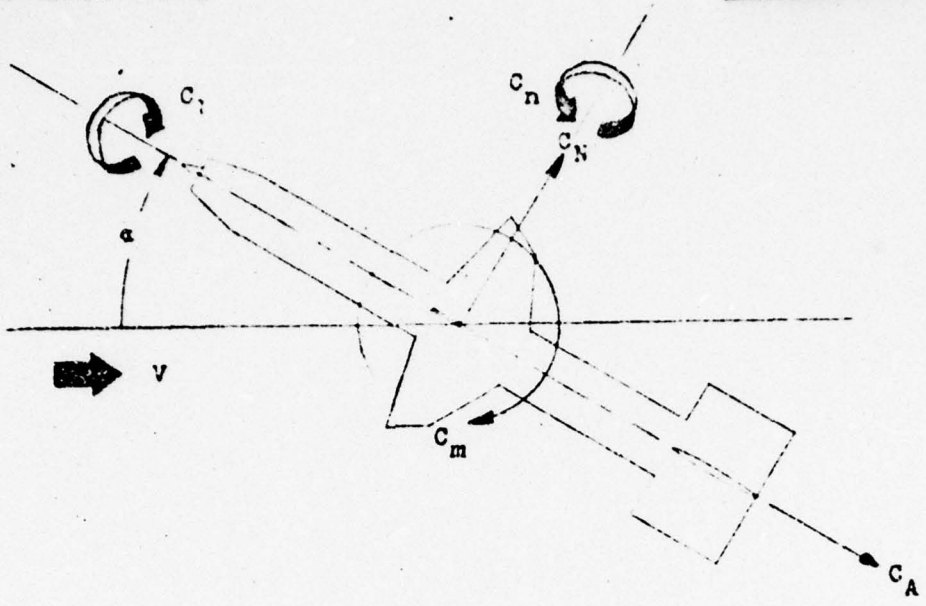

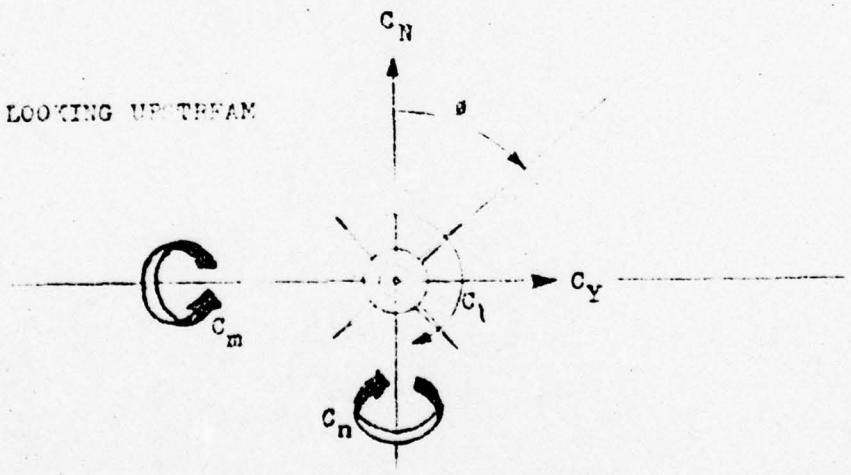

Figure I - Missle Axes Notation

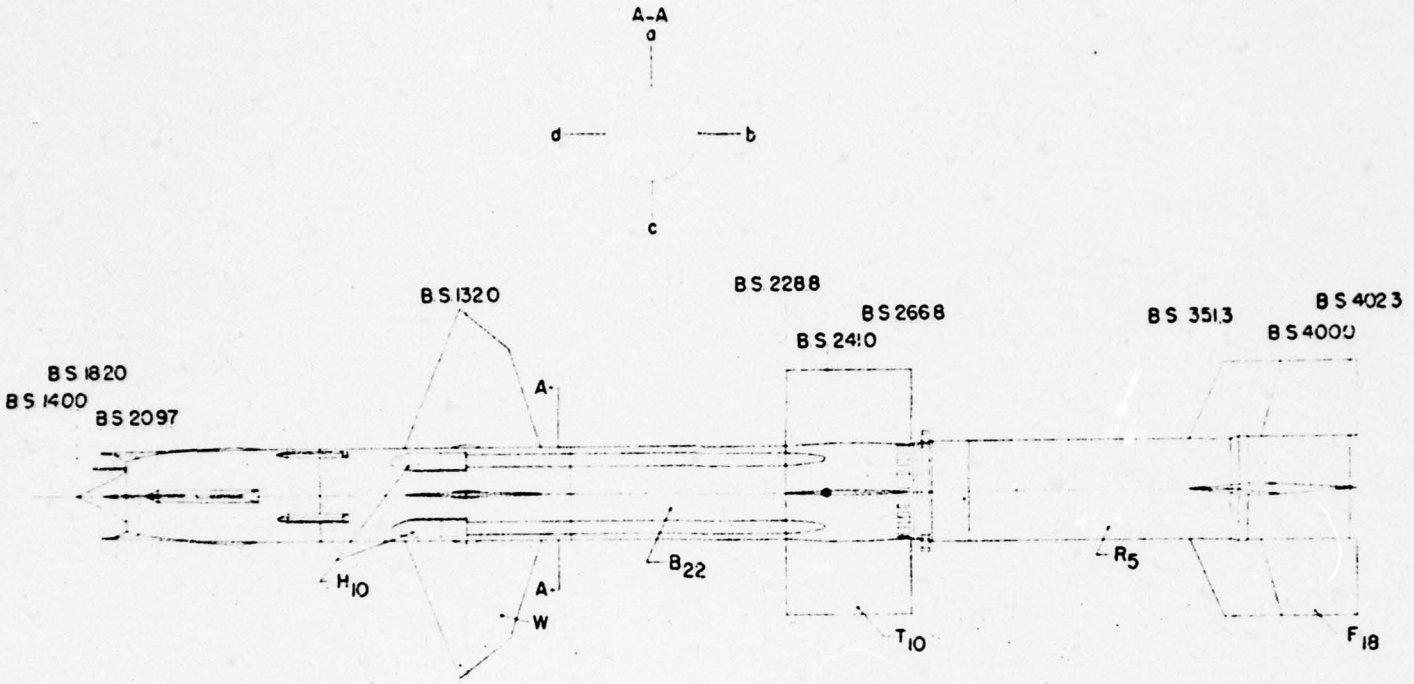

Figure 2

Figure 2 - Drawing of 1/15-Scale Model TALOS 6cl Missile With Pertinent Dimensions and Components Indicated

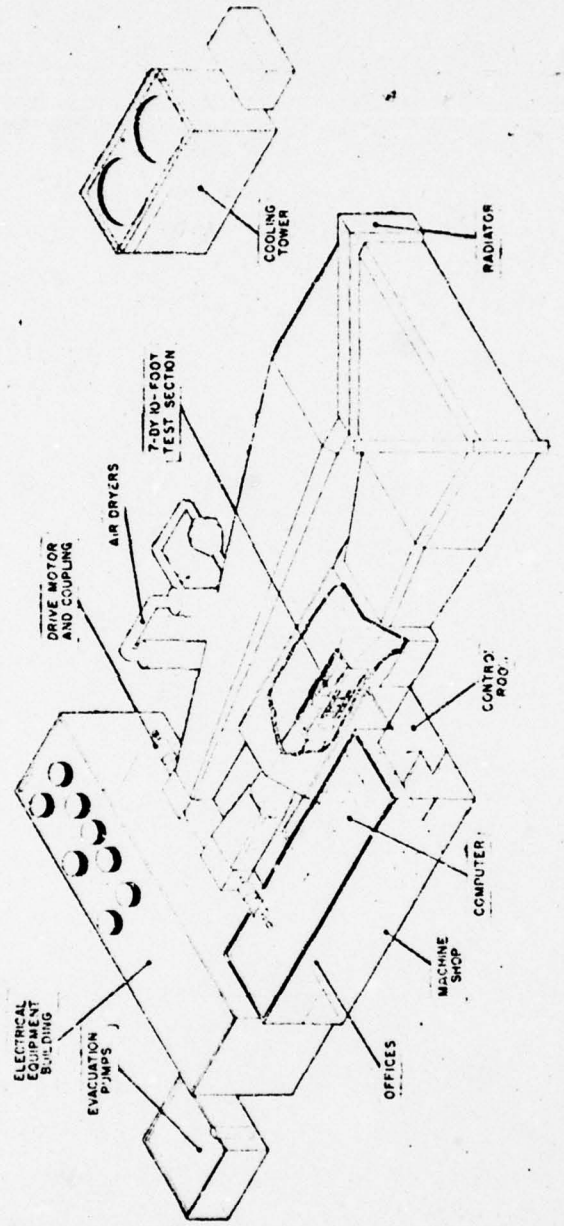

Figure 3 – Principal Components of The David Taylor Model Basin 7-by-10-Foot Transonic Wind Tunnel Facility

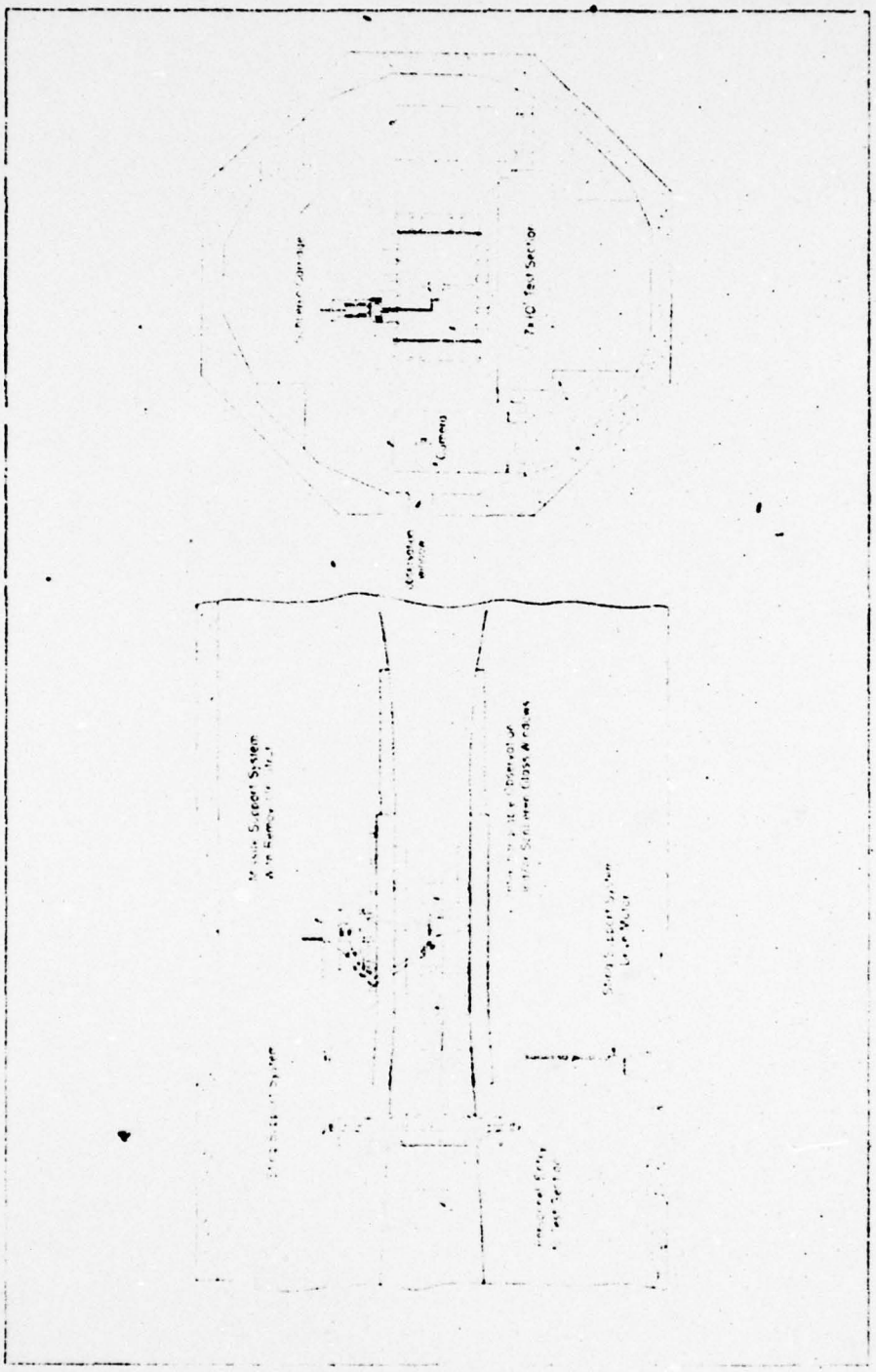

Figure 4

Figure 4 Details of the Test Section for the 7 by 10 Foot Transonic Wind Tunnel

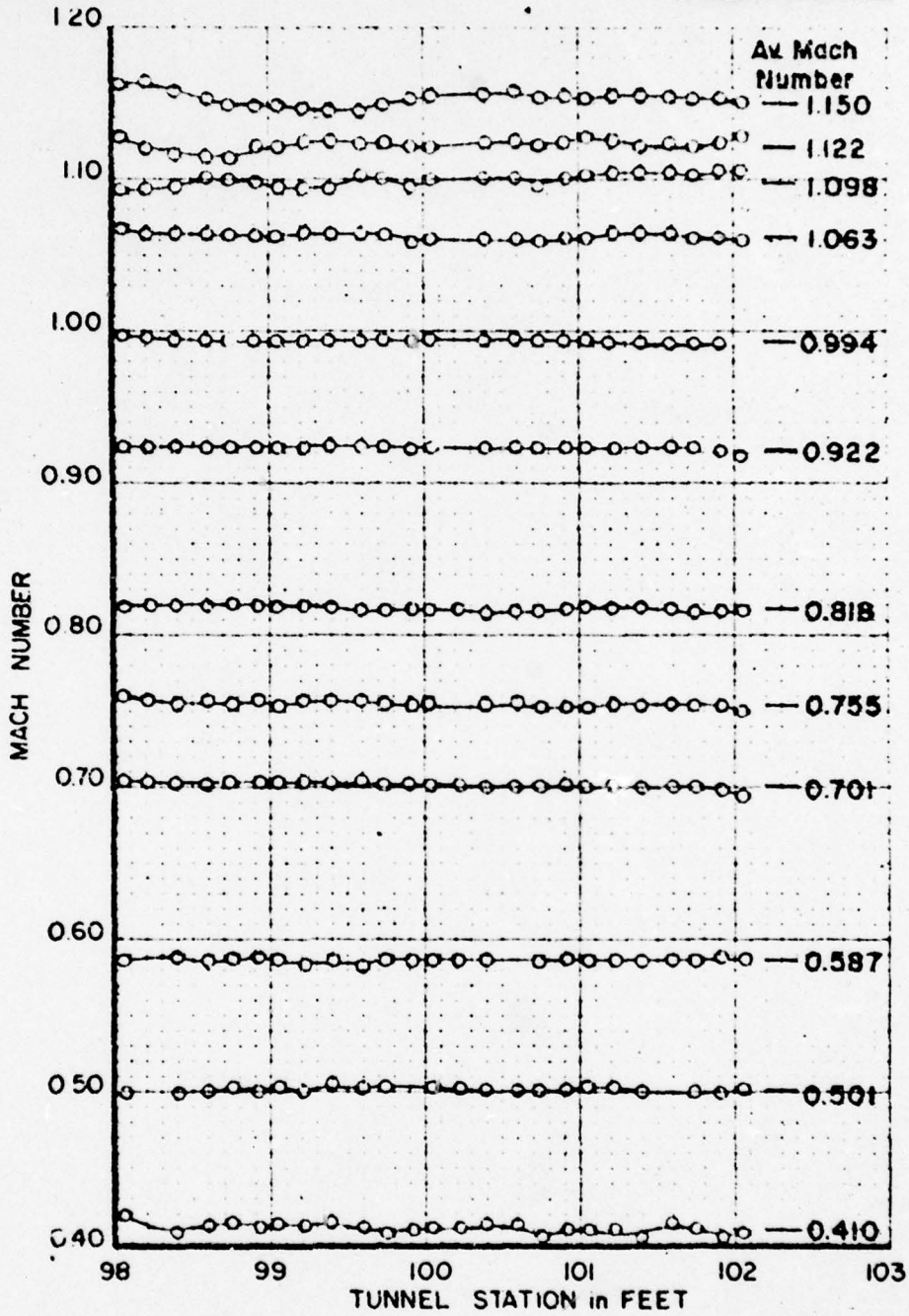

Figure 5 - Distribution of Mach Number in Model Region of Test Section

Figure 5

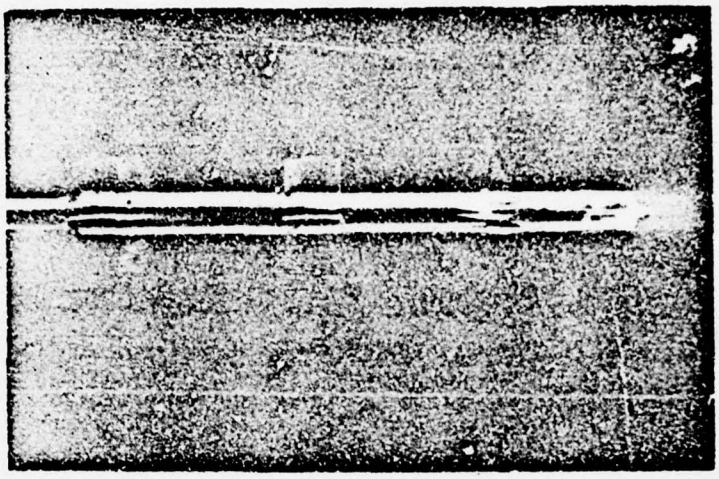

Configuration $B_{22}R_5H_{10}WT_{10}F_{18}$

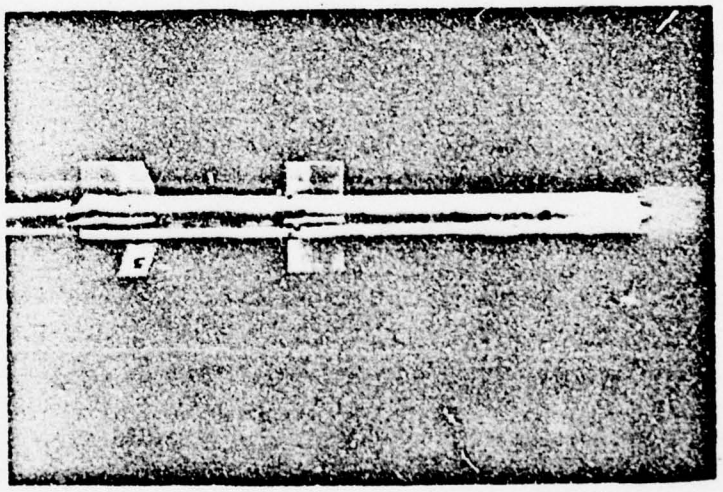

Configuration $B_{22}R_5H_{10}T_{10}F_{18}$

Figure 6 - Photographs of 1/15-Scale Model TALOS Model 601

PSD - 302,534 6 September 1963

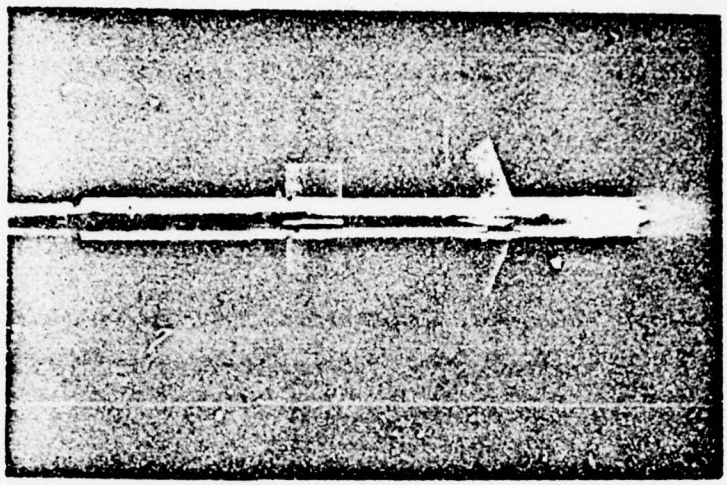

Configuration $B_{22}R_5H_{10}WT_{10}$

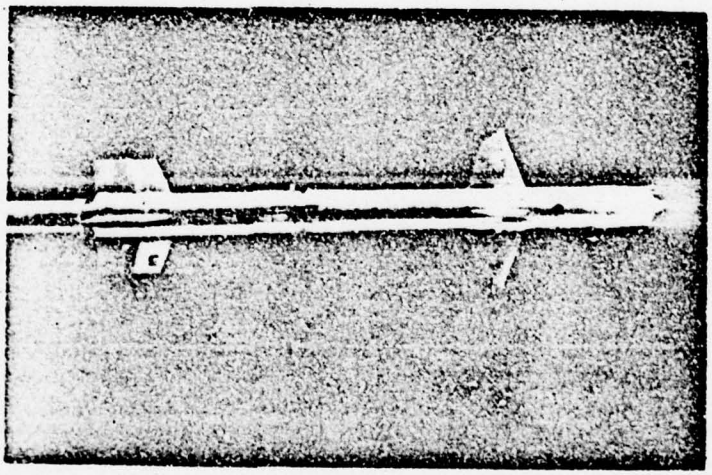

Configuration $B_{22}R_5H_{10}WF_{18}$

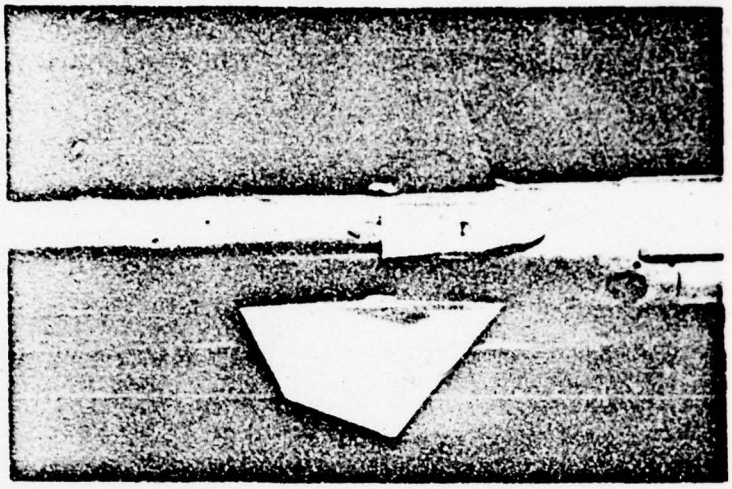

Close-Up Showing Missile Wings (W)
and Exhaust Louvers (H_{10})

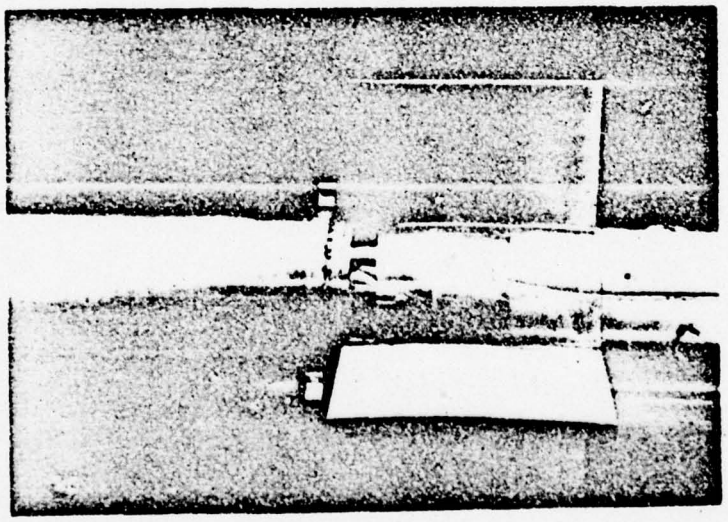

Missile Tail (T_{10})

Figure 7 - Photographs Showing Details of the Model

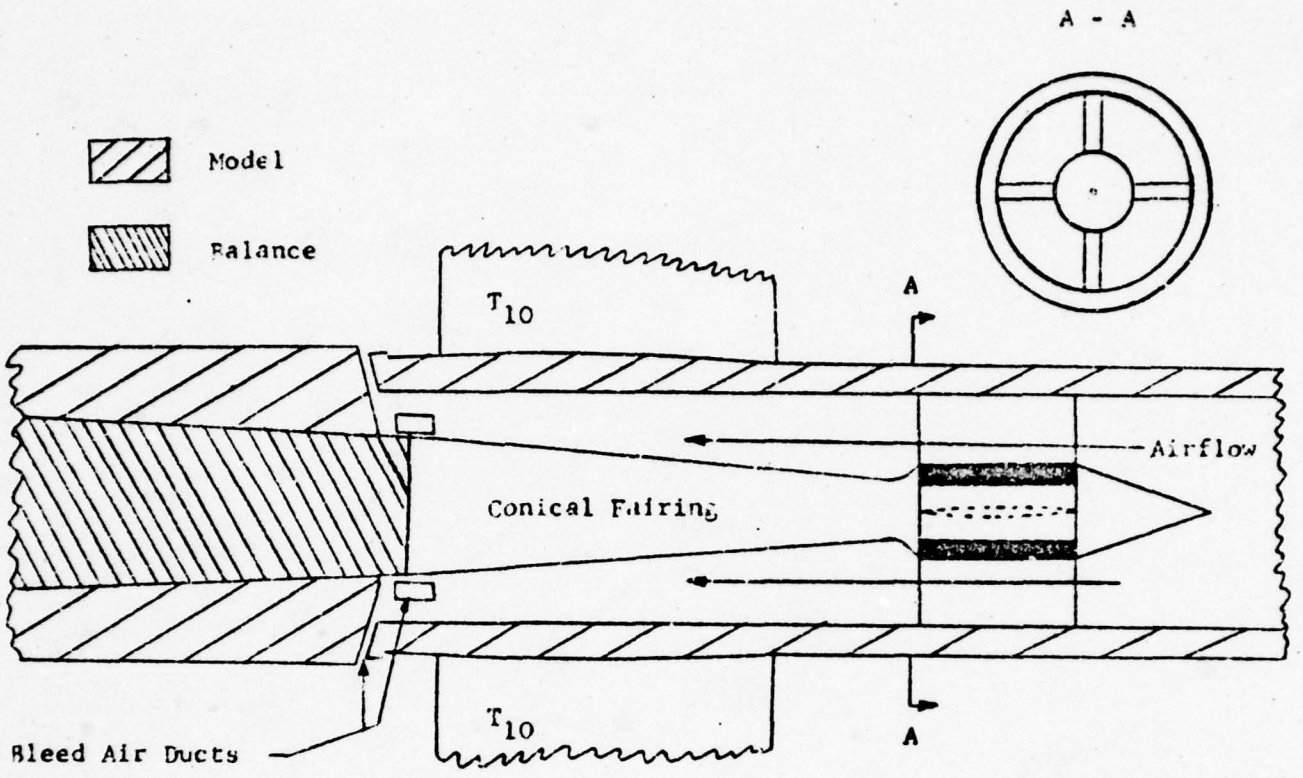

FIGURE 8

Figure 8 - Sketch Showing Details of the Internal Cross Strut and Conical Fairing for Ram Airflow

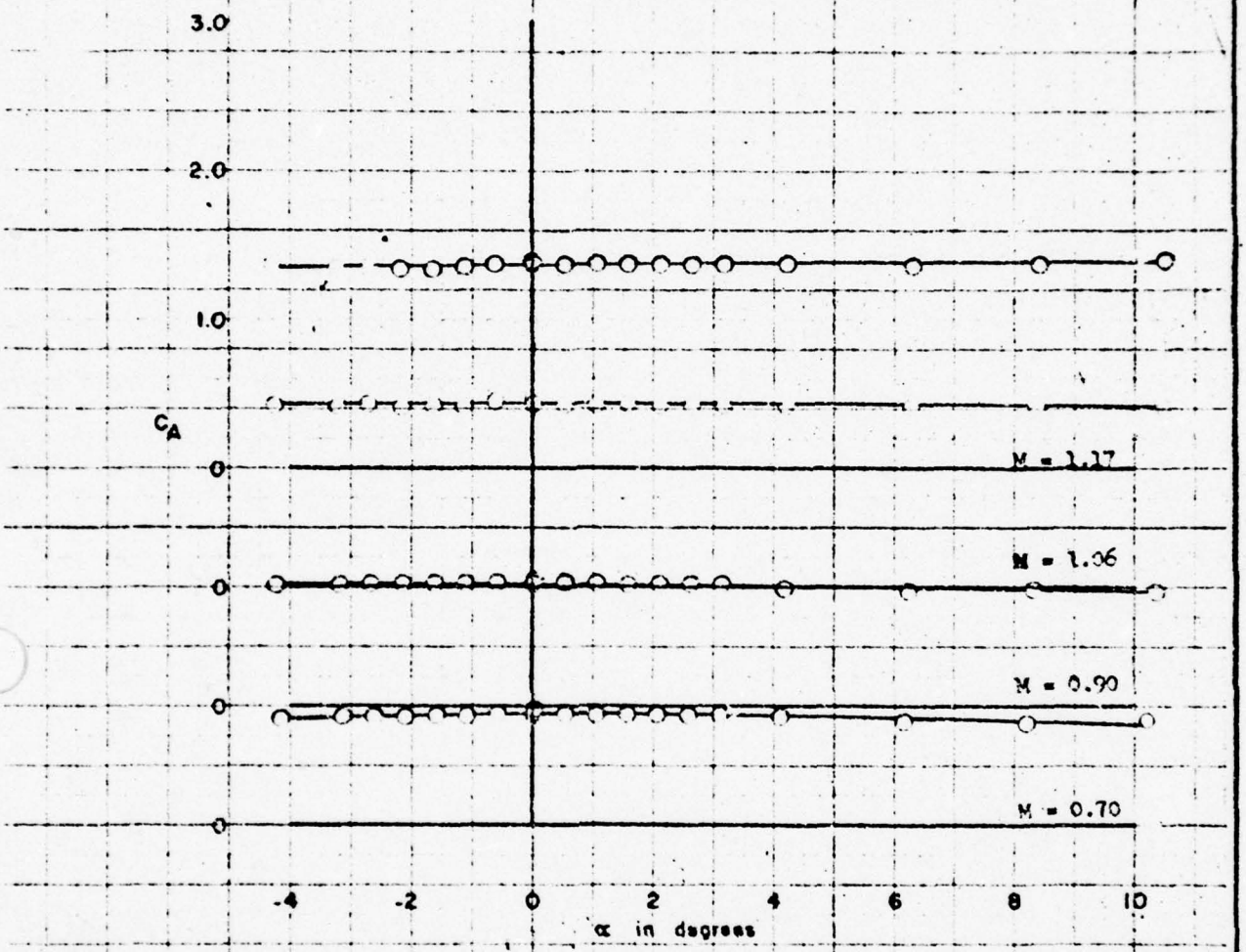

Figure 9 - Variation of the Aerodynamic Characteristics With Angle of Attack for Configuration $B_{22}R_5H_{10}W$

(a) ϕ=-45°; i=i'=0°; δ=δ'=0°

FIGURE 9a

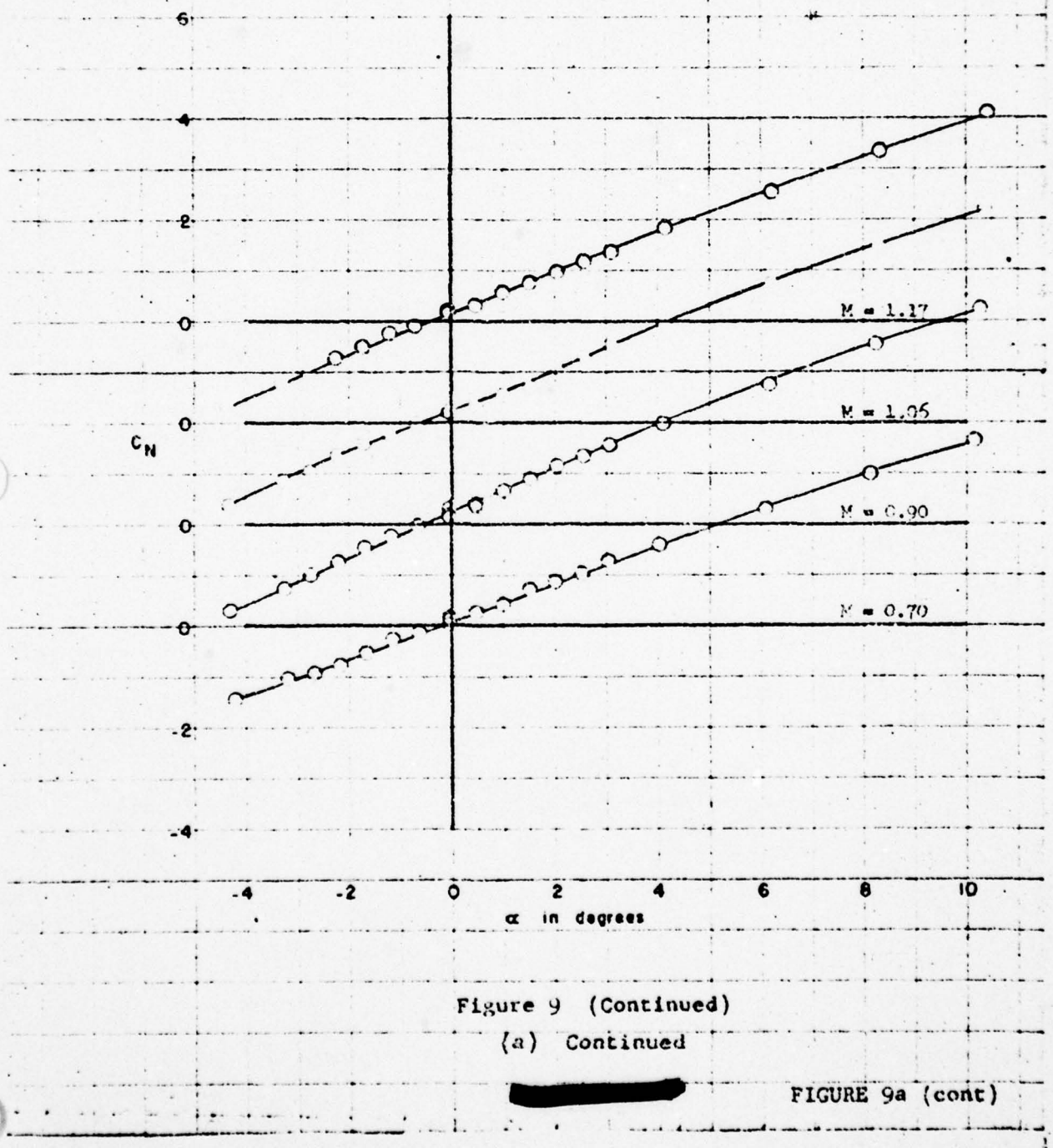

Figure 9 (Continued)

(a) Continued

[redacted] FIGURE 9a (cont)

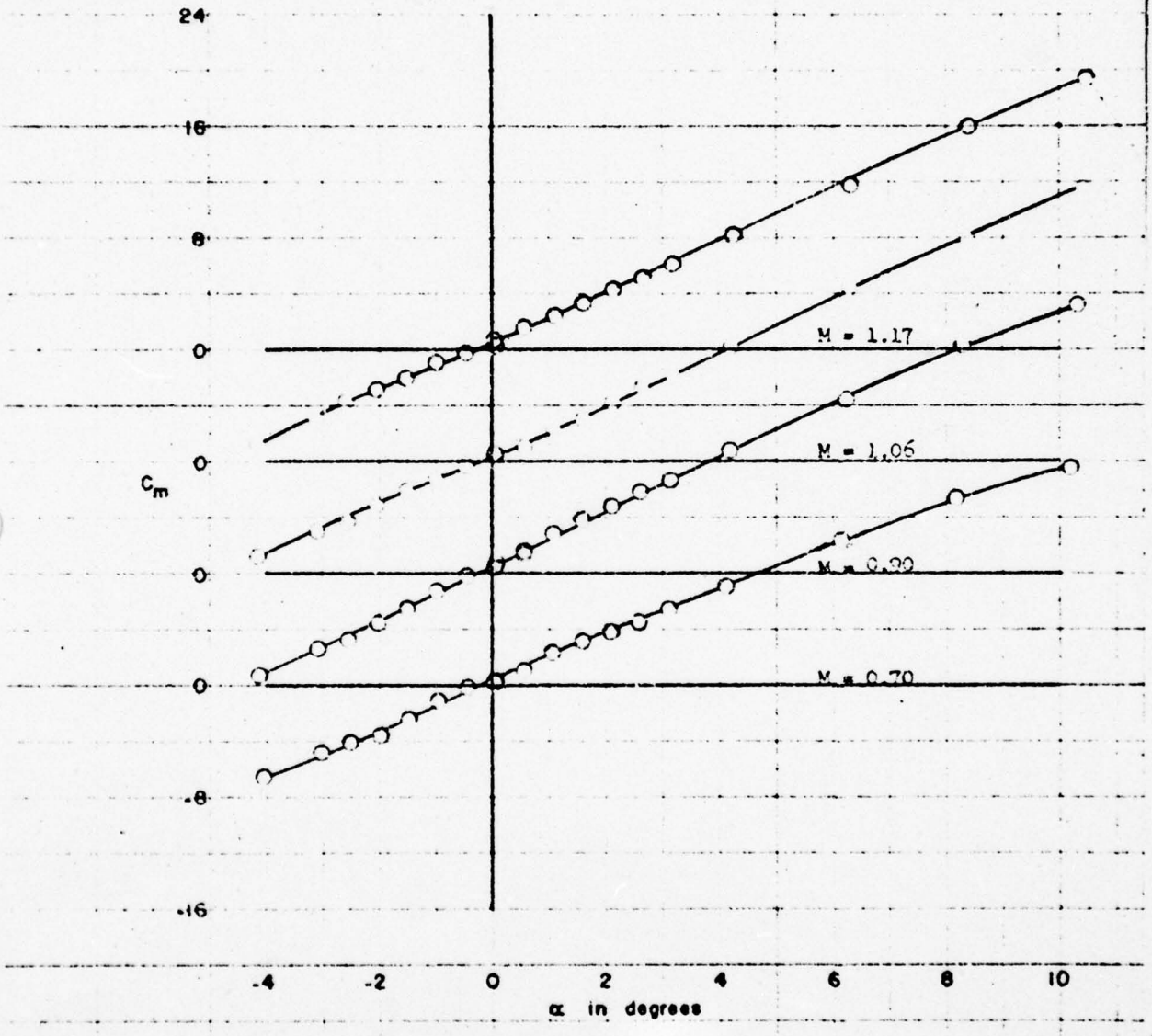

Figure 9 (Continued)

(a) Continued

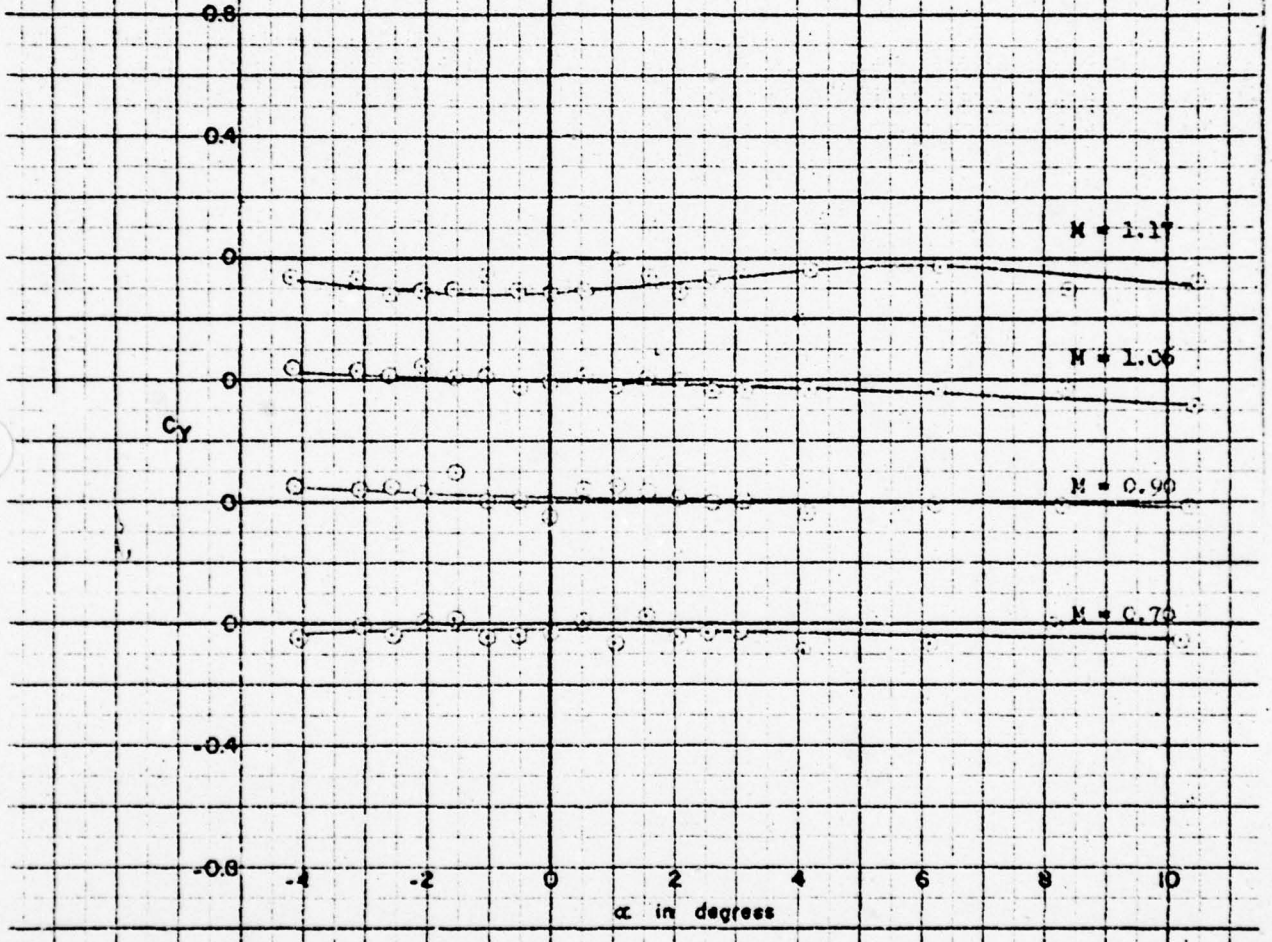

Figure 9 (Continued)

(a) Continued

[redacted]

FIGURE 9a (cont)

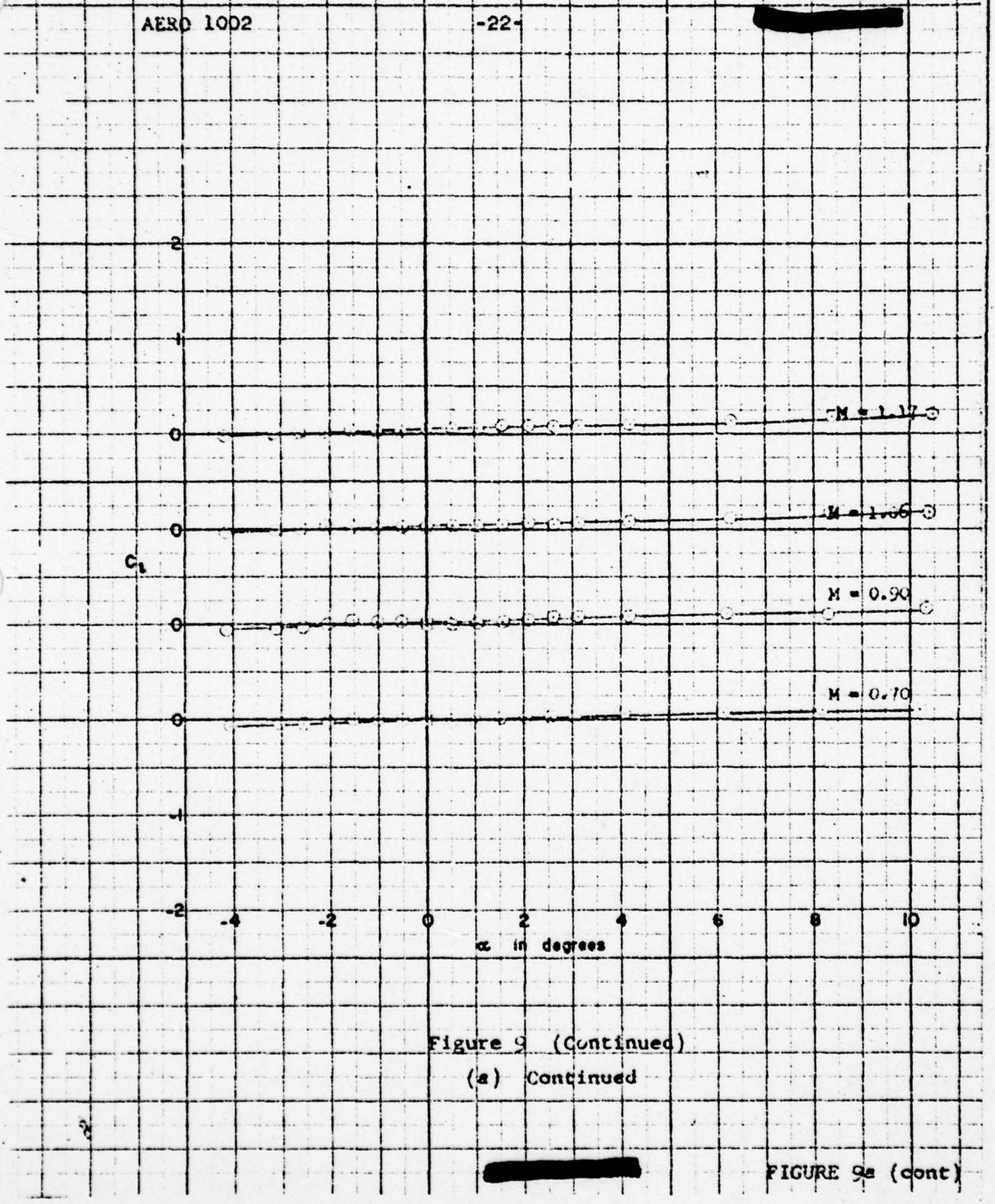

Figure 9 (Continued)

(e) Continued

FIGURE 9e (cont)

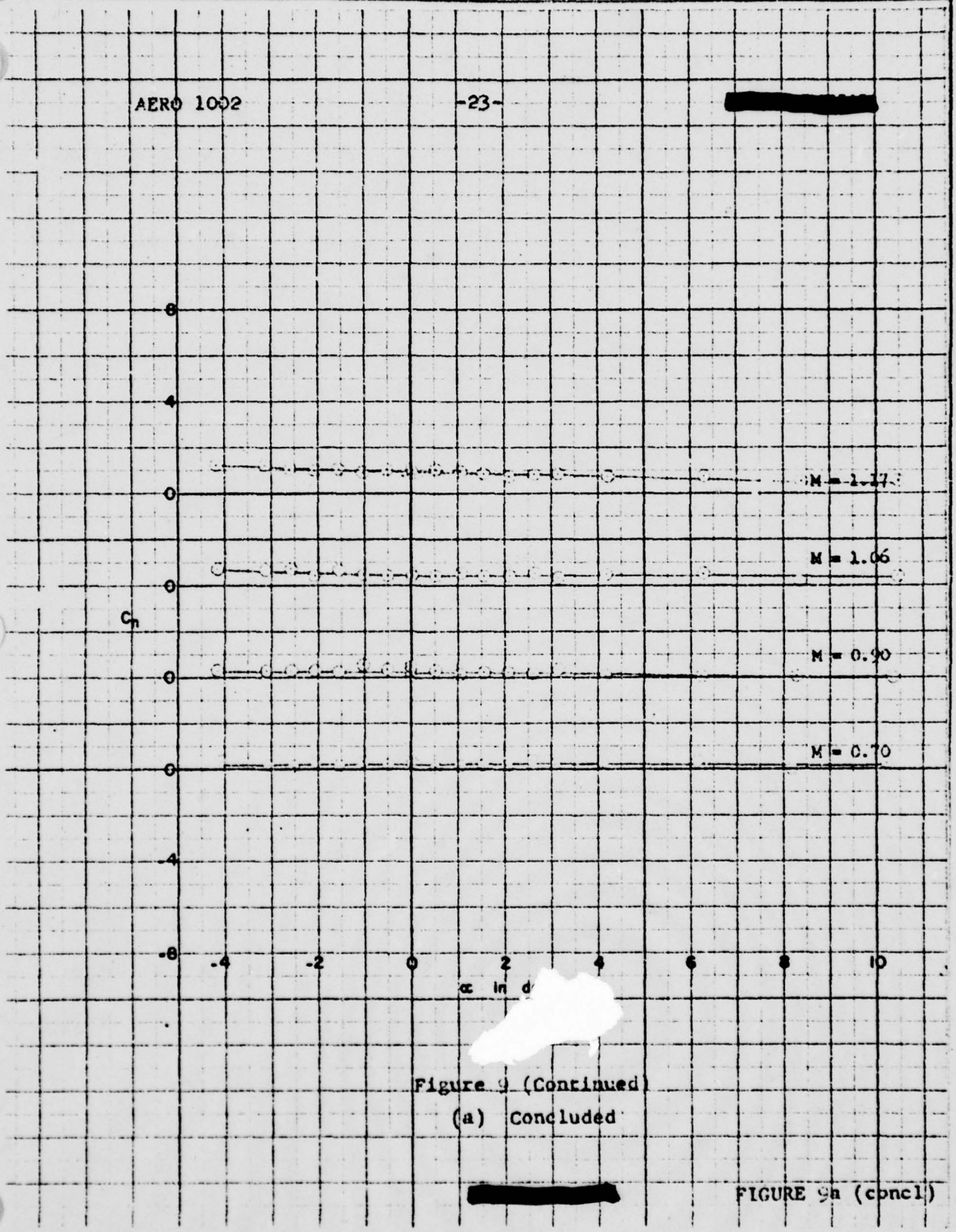

Figure 9 (Continued)
(a) Concluded

[redacted]

FIGURE 9a (concl)

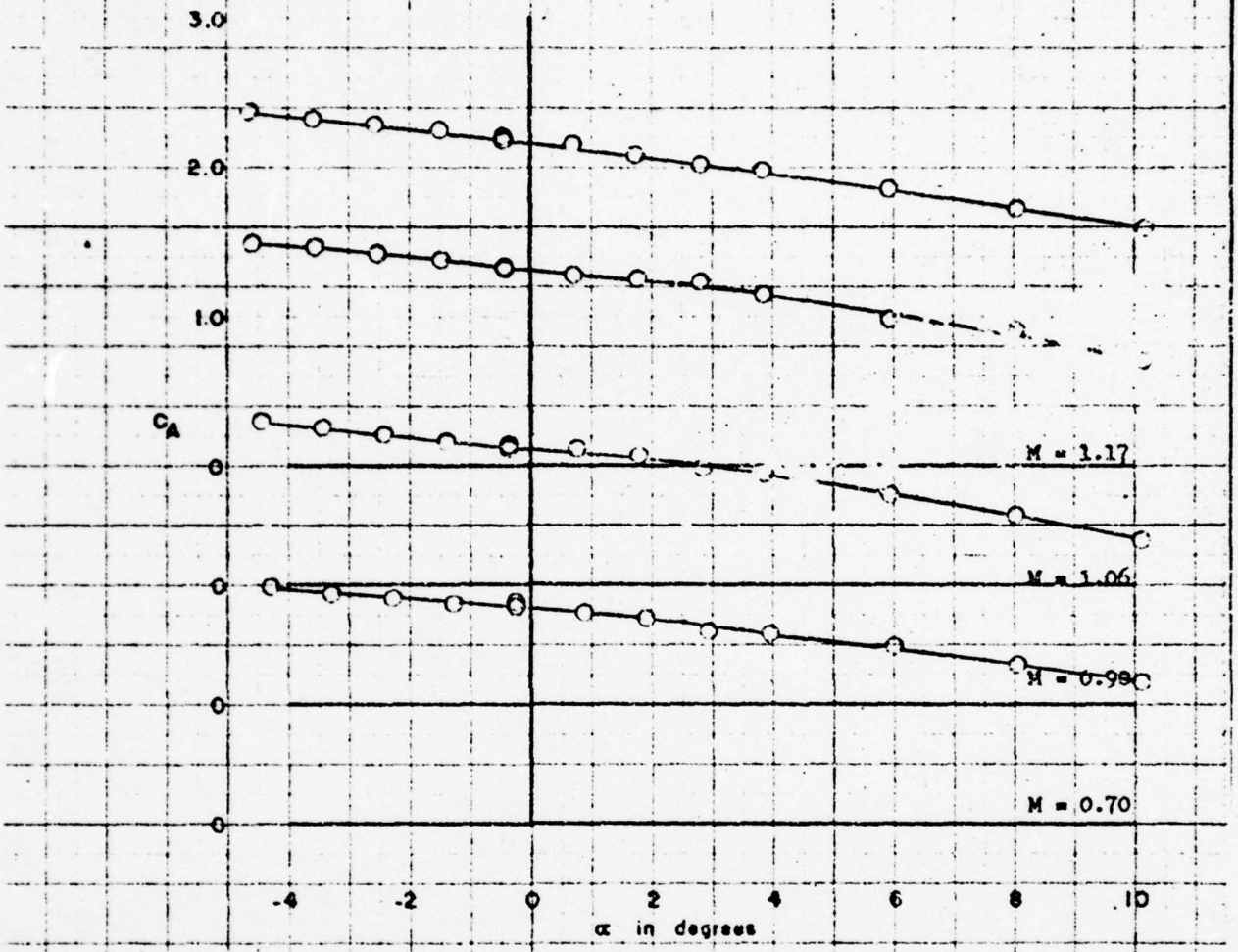

Figure 9 (Continued)

(b) ϕ=-45°; i=i'=-10°; δ=δ'=0°

[redacted]

FIGURE 9b

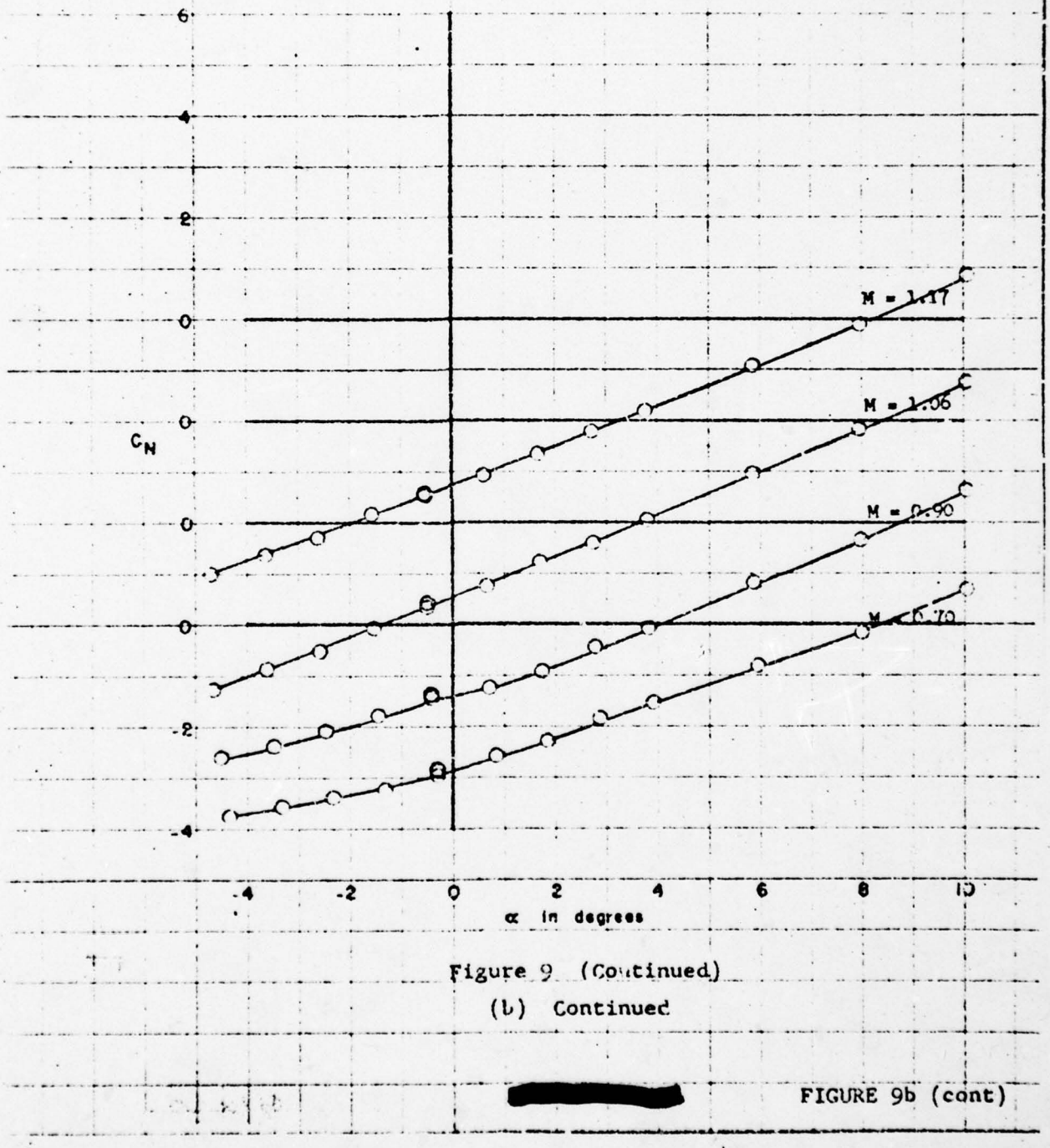

Figure 9 (Continued)

(b) Continued

[redacted]

FIGURE 9b (cont)

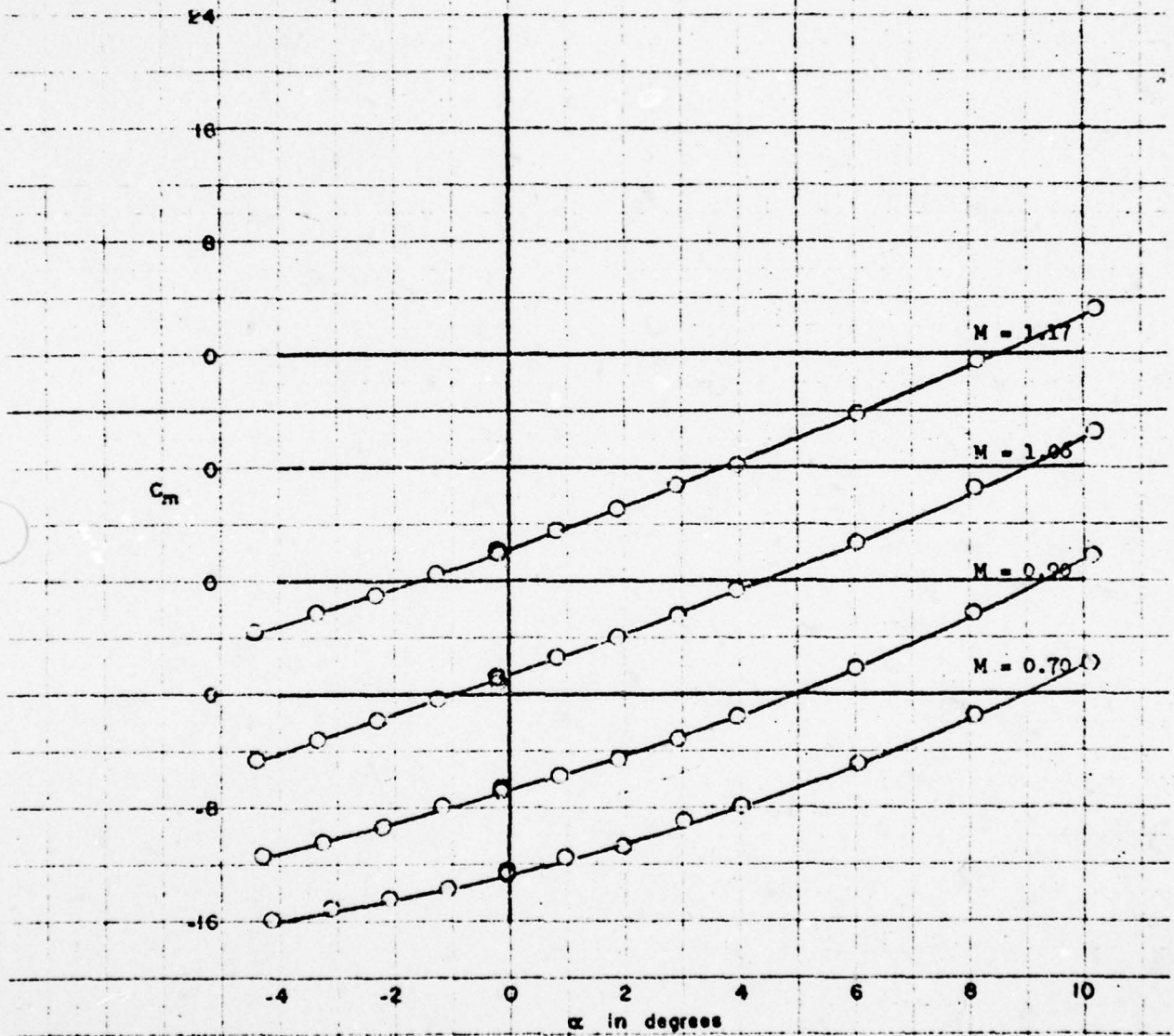

Figure 9 (Continued)

(b) Concluded

[redacted]

FIGURE 9b (concl)

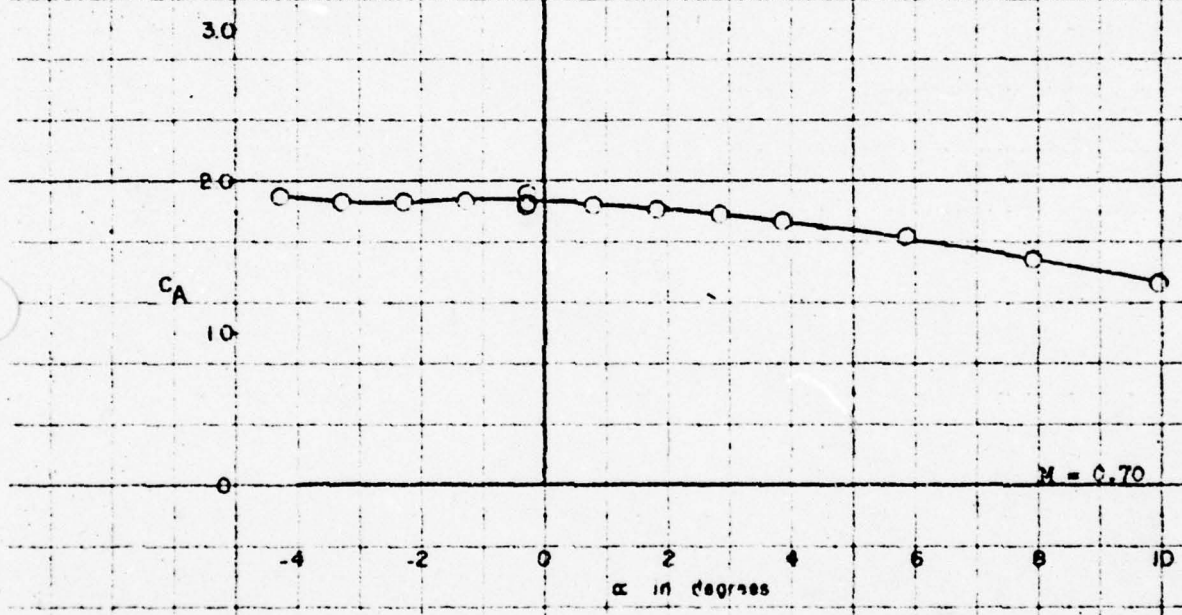

Figure 9 (Continued)

(c) ϕ=-45°; i=i'=-15°; δ=δ'=0°

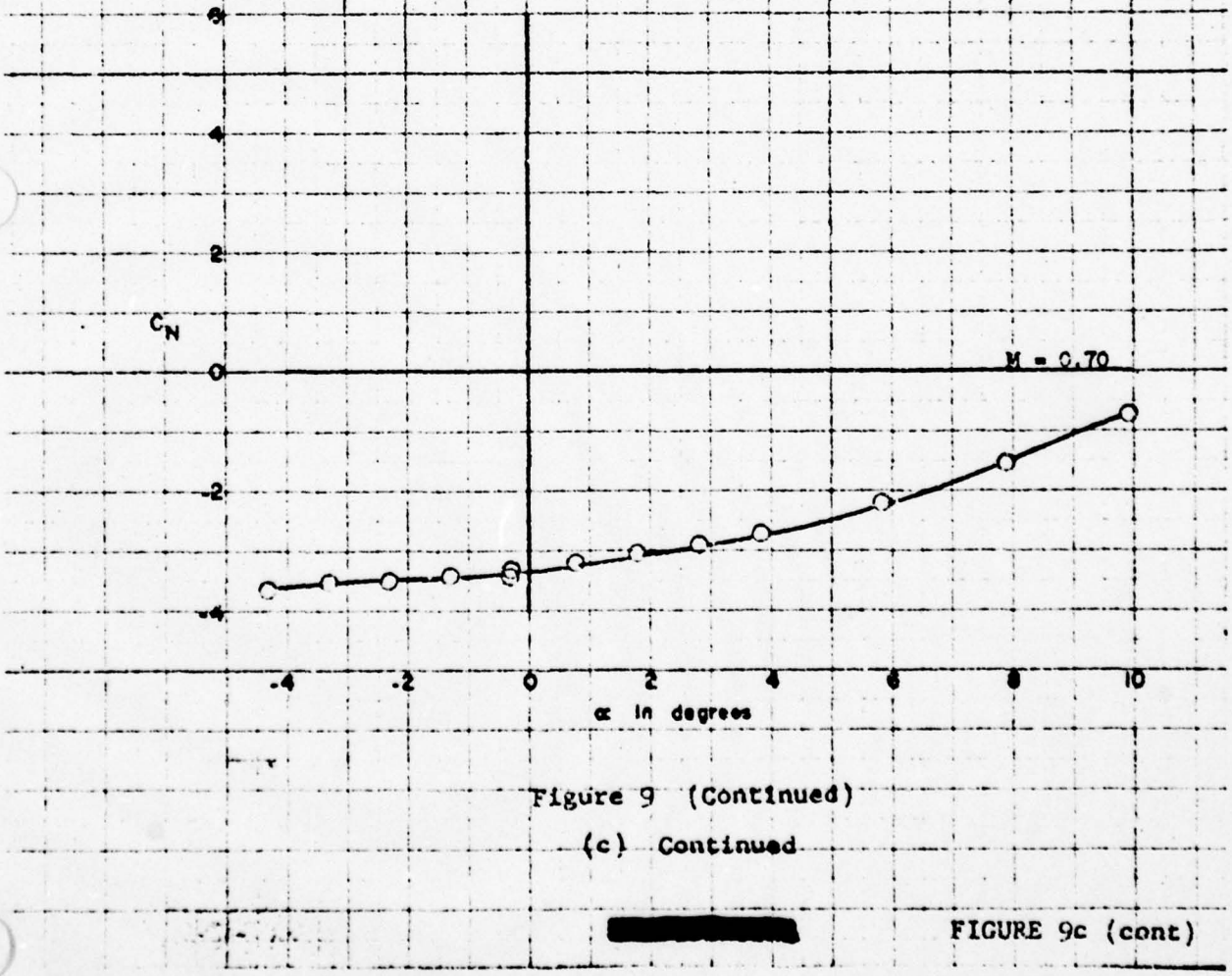

Figure 9 (Continued)

(c) Continued

FIGURE 9c (cont)

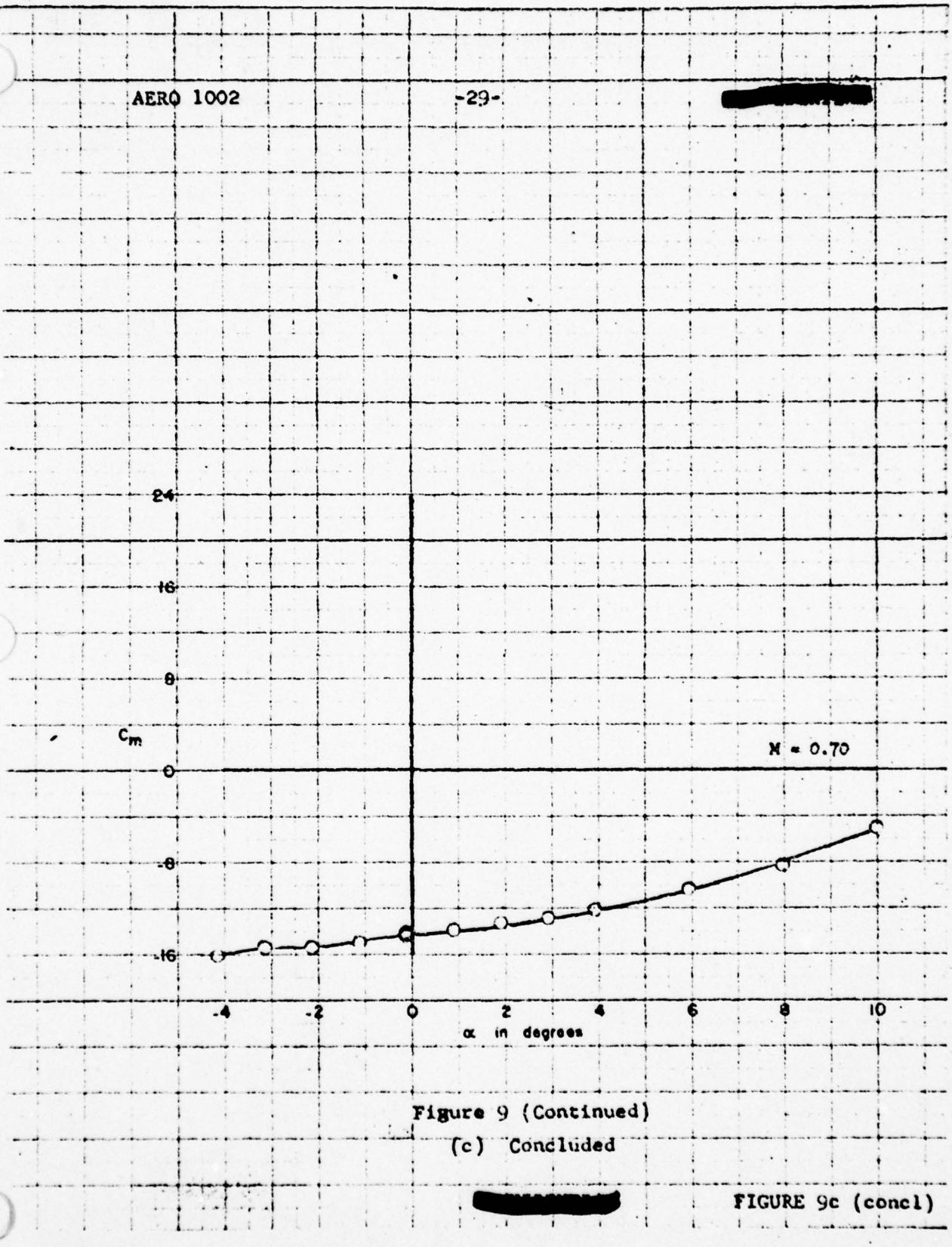

Figure 9 (Continued)

(c) Concluded

[redacted]

FIGURE 9c (concl)

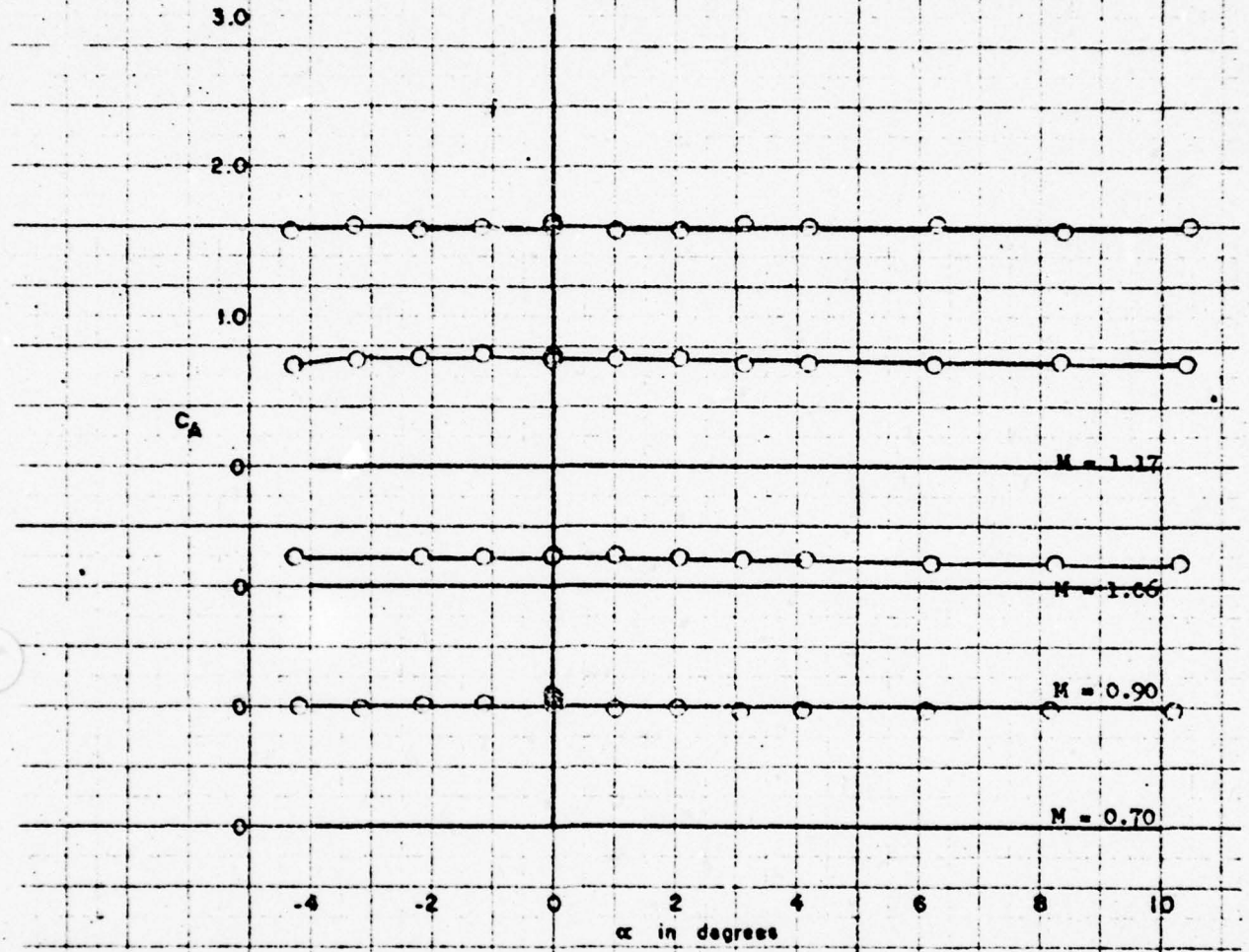

Figure 9 (Continued)

(d) ϕ=-45°; i=i'=0°; δ=δ'=5°

FIGURE 9d

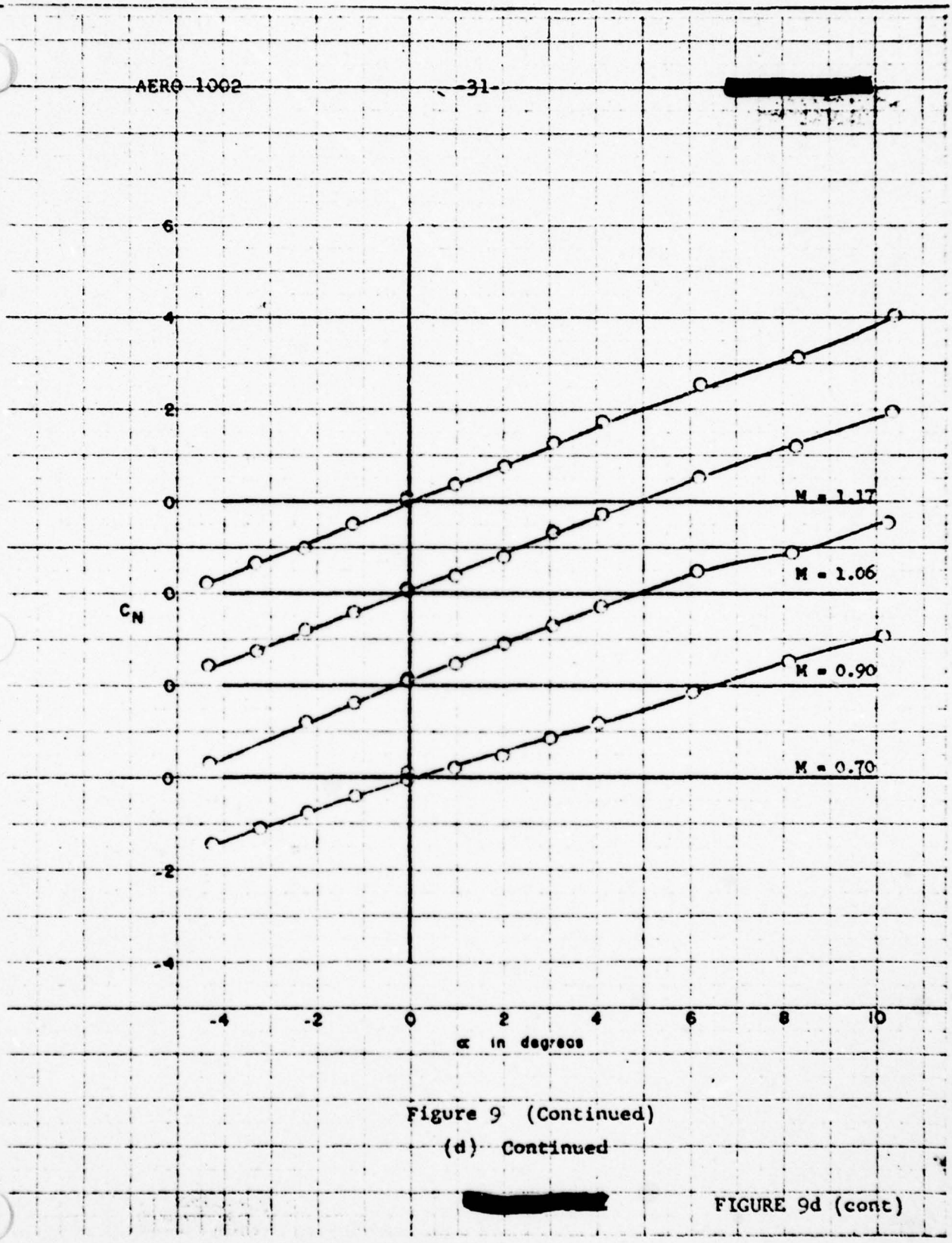

Figure 9 (Continued)

(d) Continued

FIGURE 9d (cont)

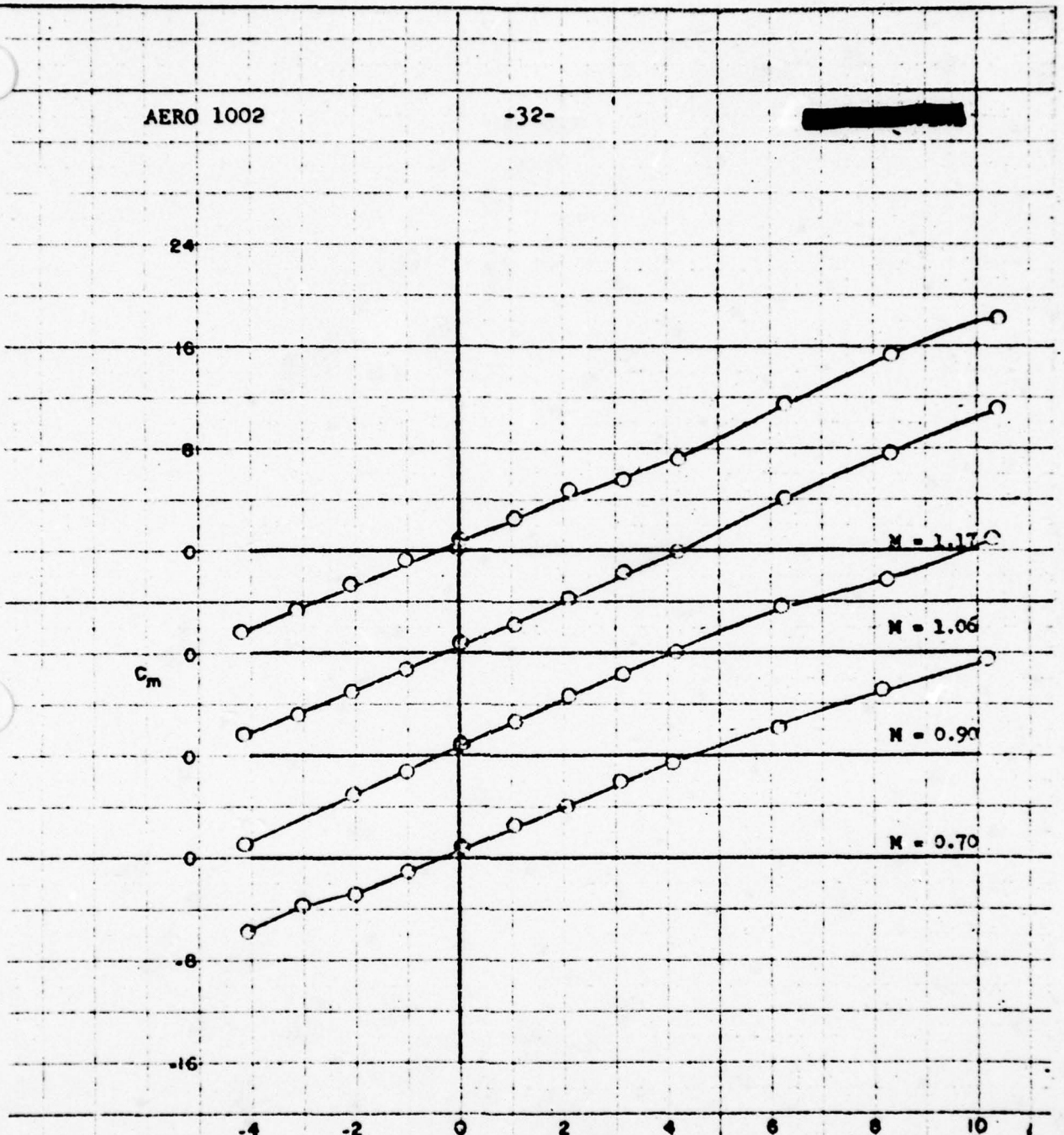

Figure 9 (Continued)

(d) Continued

[redacted]

FIGURE 9d (cont)

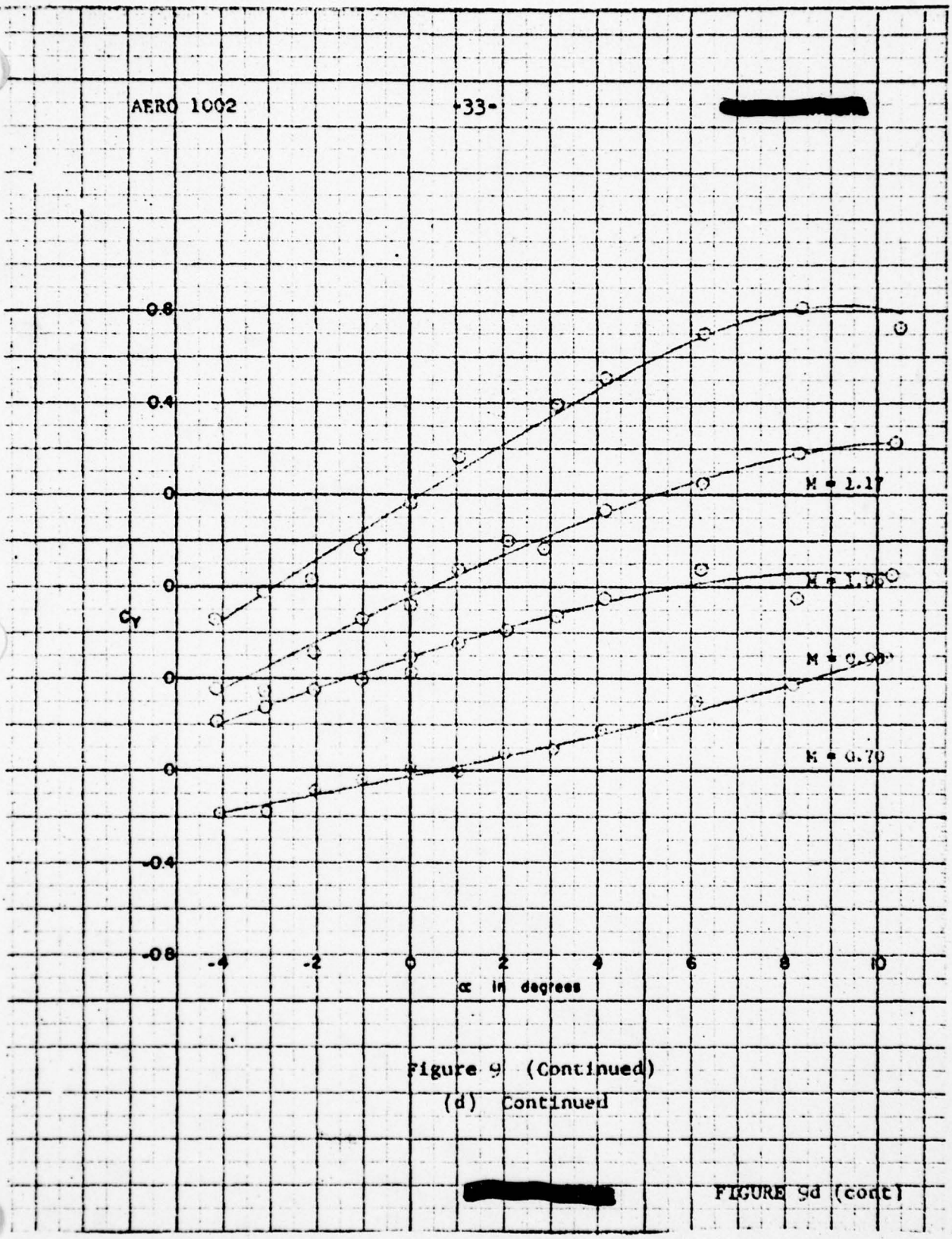

Figure 9 (Continued)

(d) Continued

[redacted]

FIGURE 9d (cont)

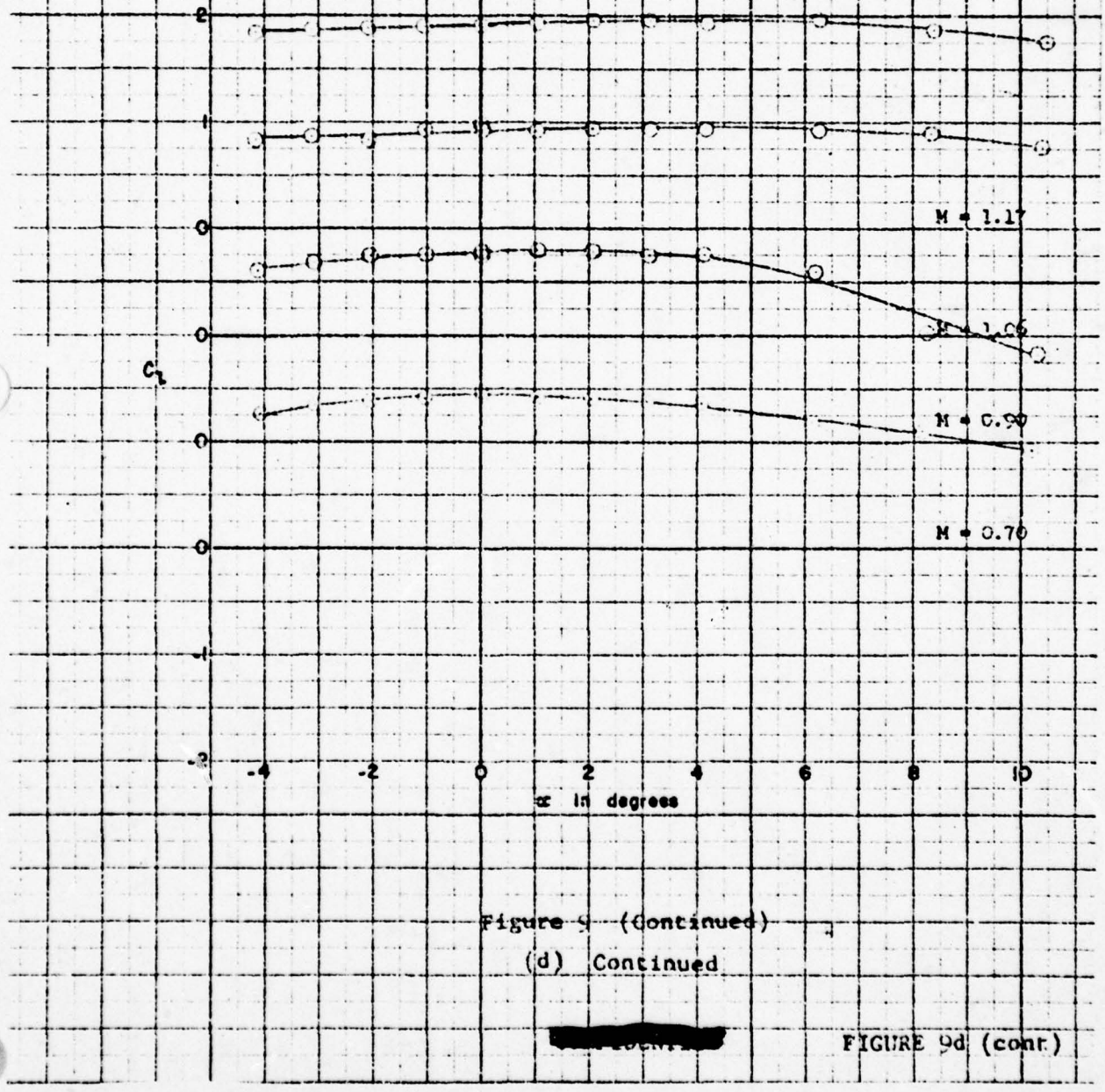

Figure 9 (Continued)

(d) Continued

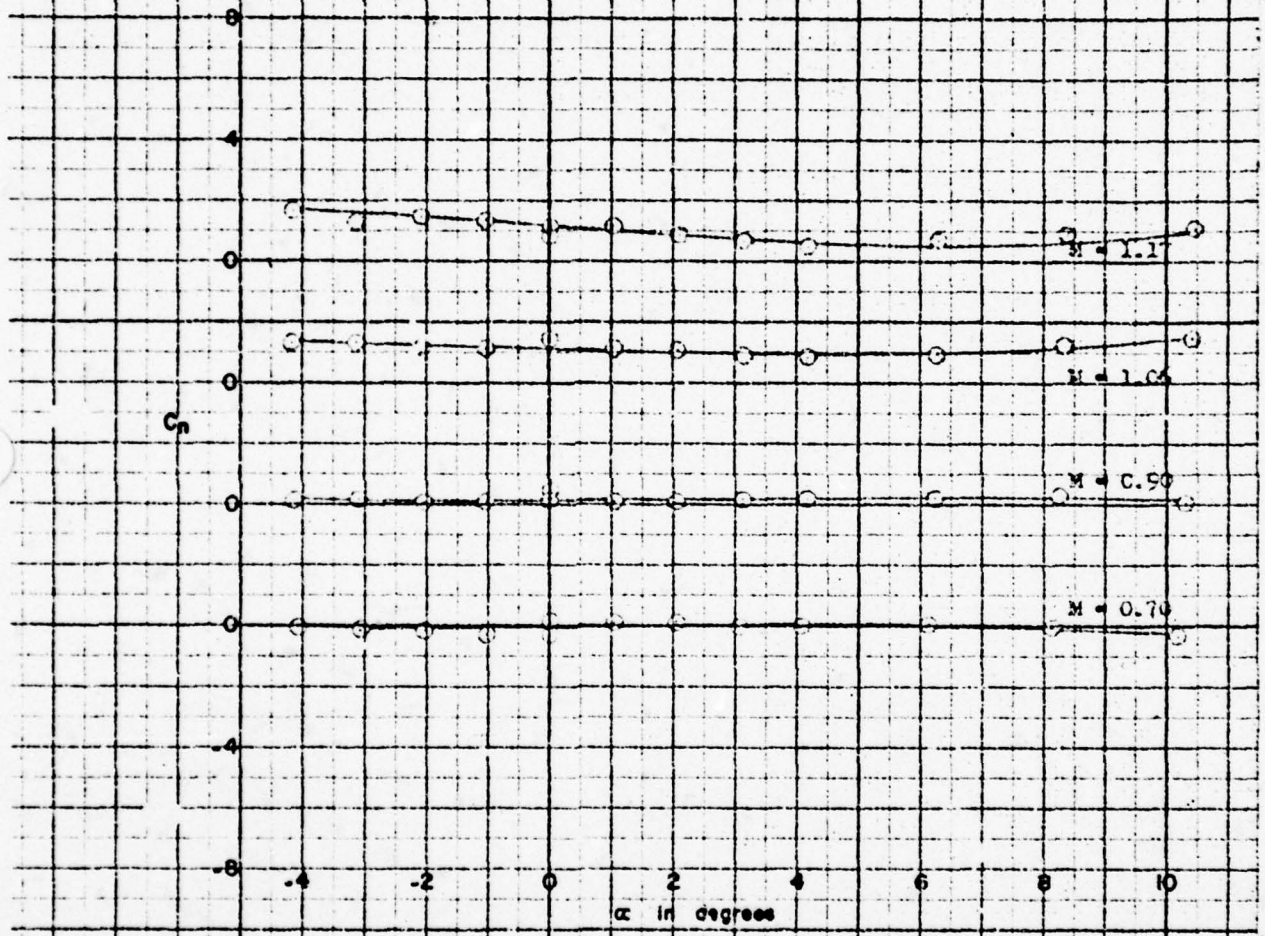

Figure 9 (Continued)
(d) Concluded

FIGURE 9d (concl)

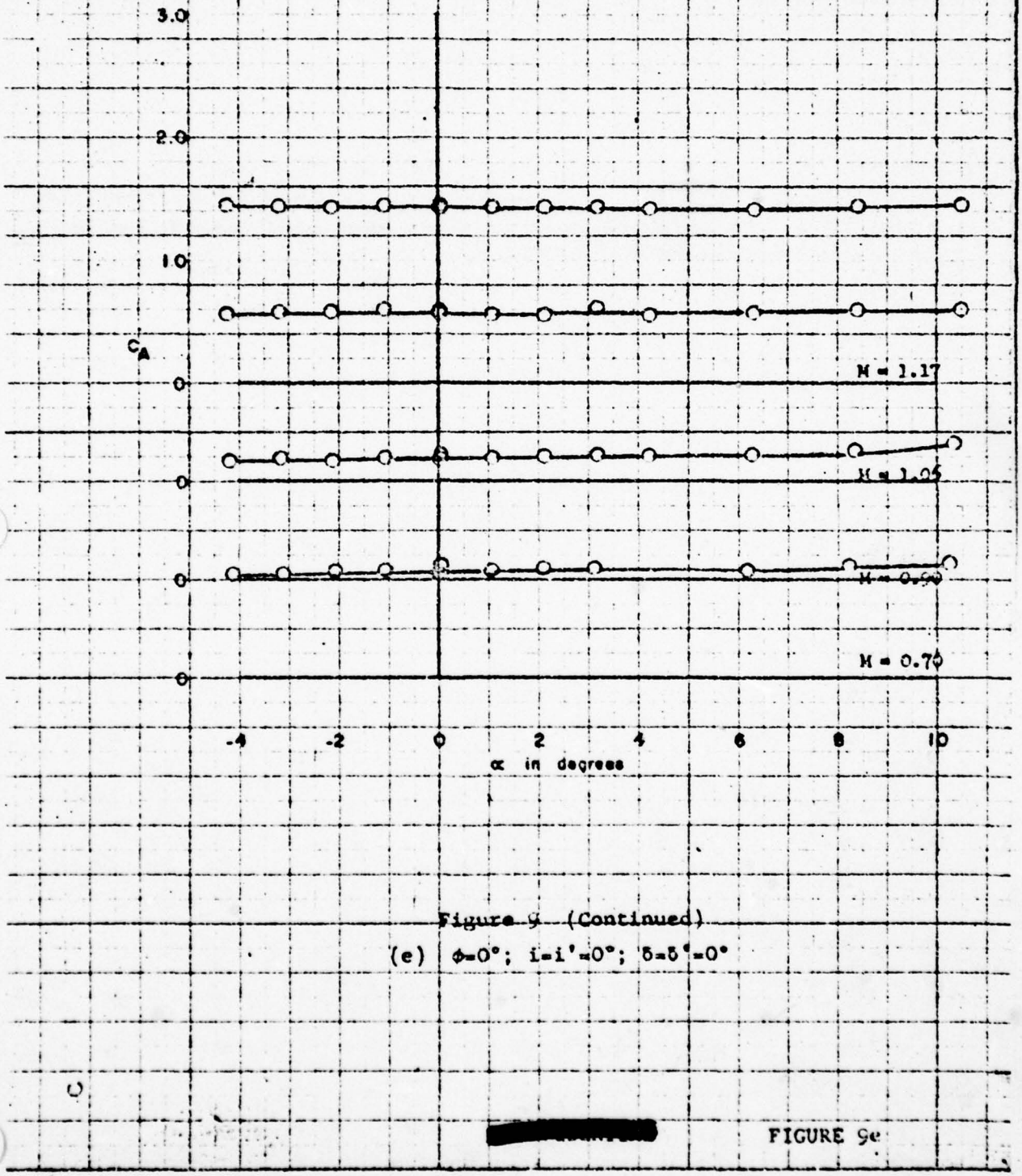

Figure 9 (Continued)

(e) $\phi=0°$; $i=i'=0°$; $\delta=\delta'=0°$

FIGURE 9e

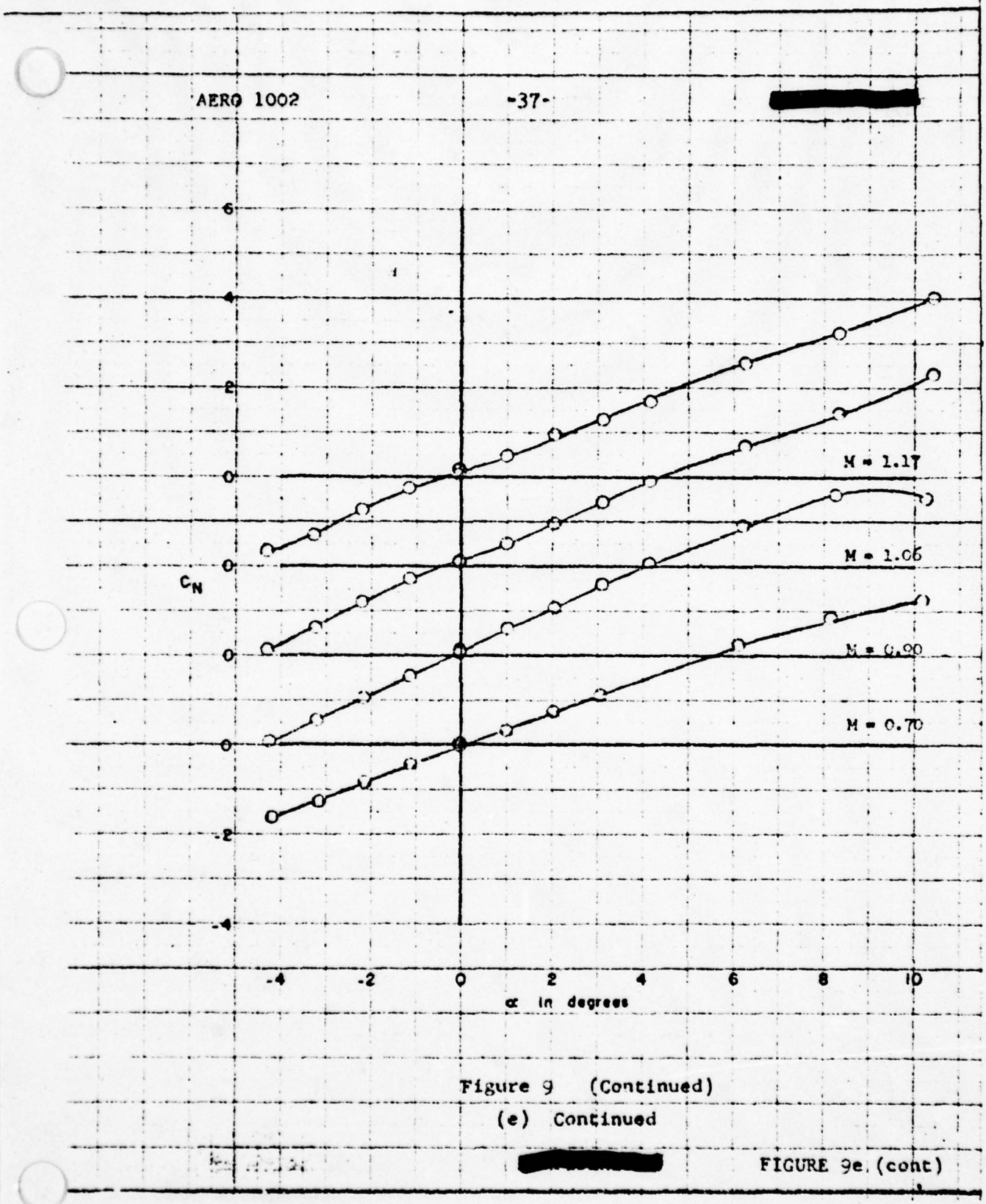

Figure 9 (Continued)

(e) Continued

[redacted]

FIGURE 9e. (cont)

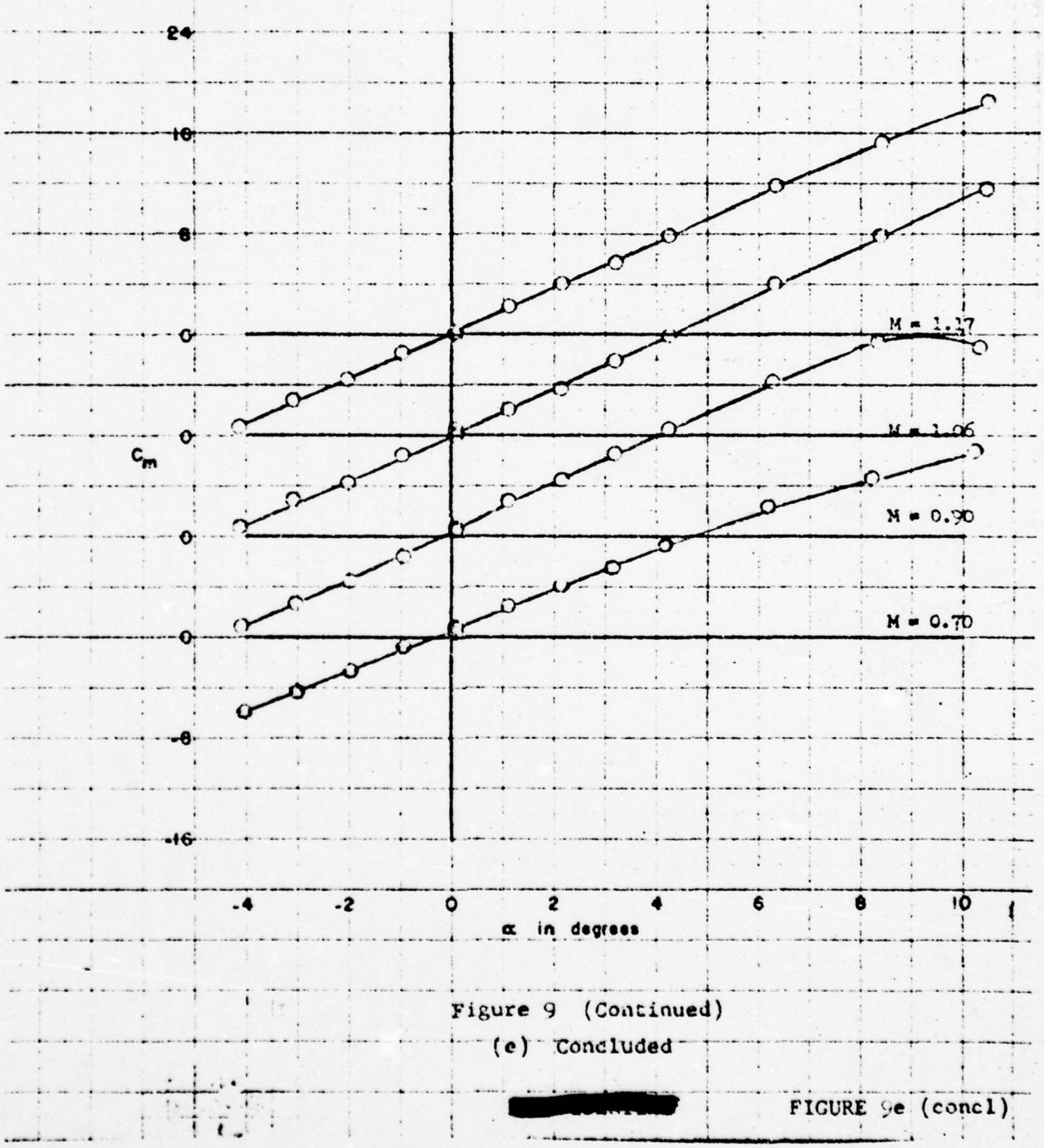

Figure 9 (Continued)

(e) Concluded

[redacted] FIGURE 9e (concl)

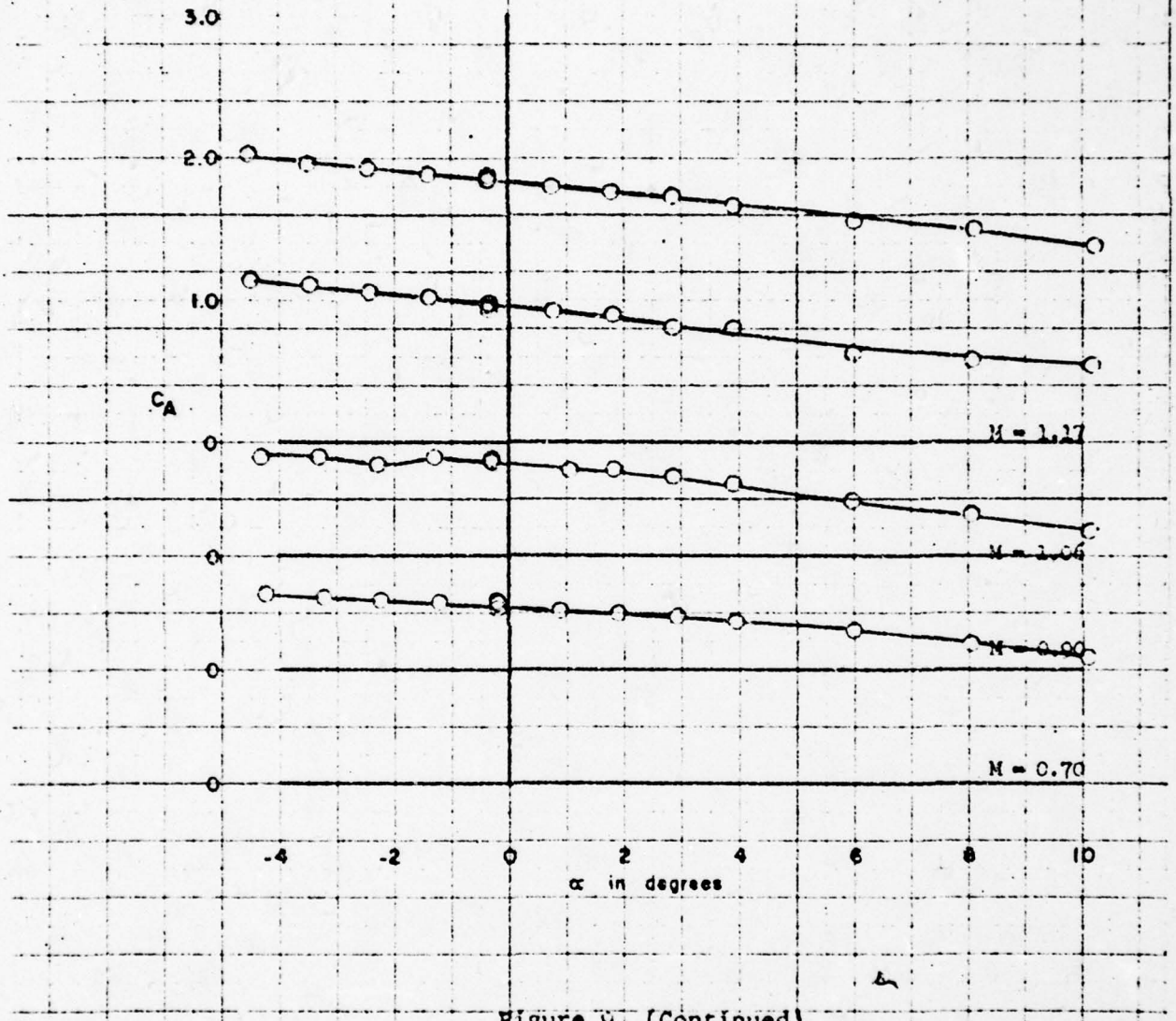

Figure 9 (Continued)

(f) ϕ=0°; i=-10°, i'=0°; δ=δ'=0°

FIGURE 9f

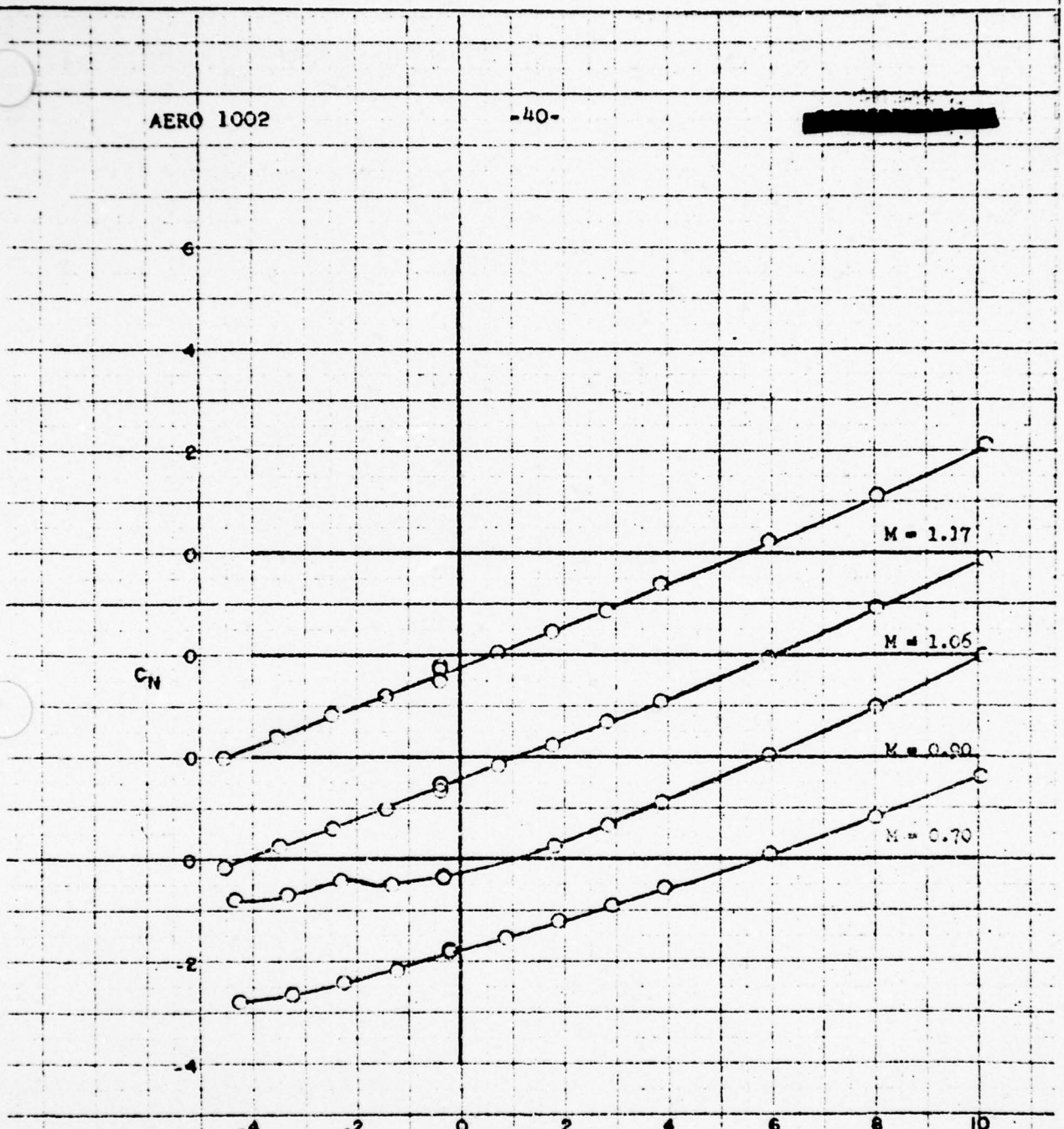

Figure 9 (Continued)

(f) Continued

[redacted]

FIGURE 9f (cont)

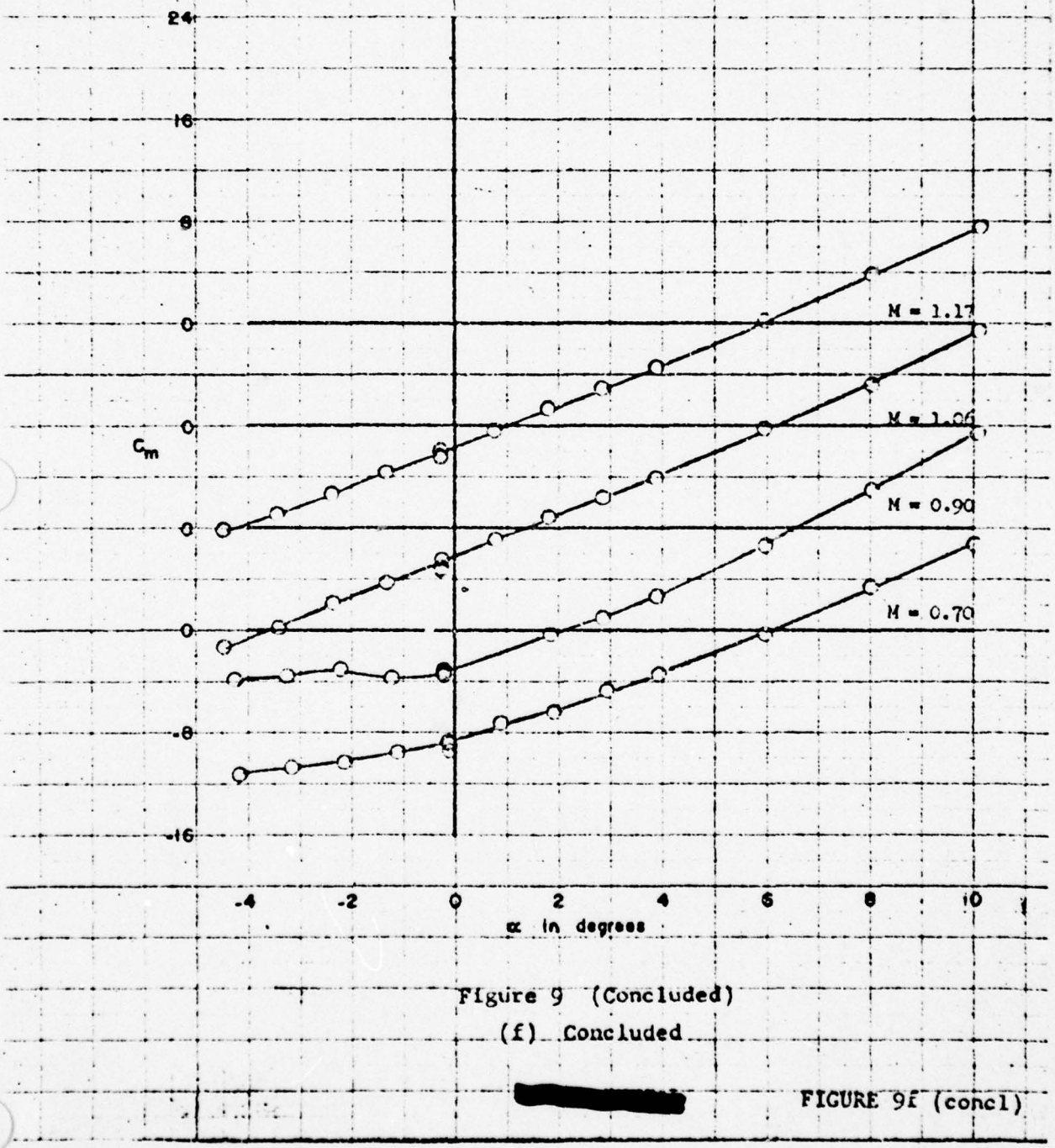

Figure 9 (Concluded)

(f) Concluded

[redacted]

FIGURE 9f (concl)

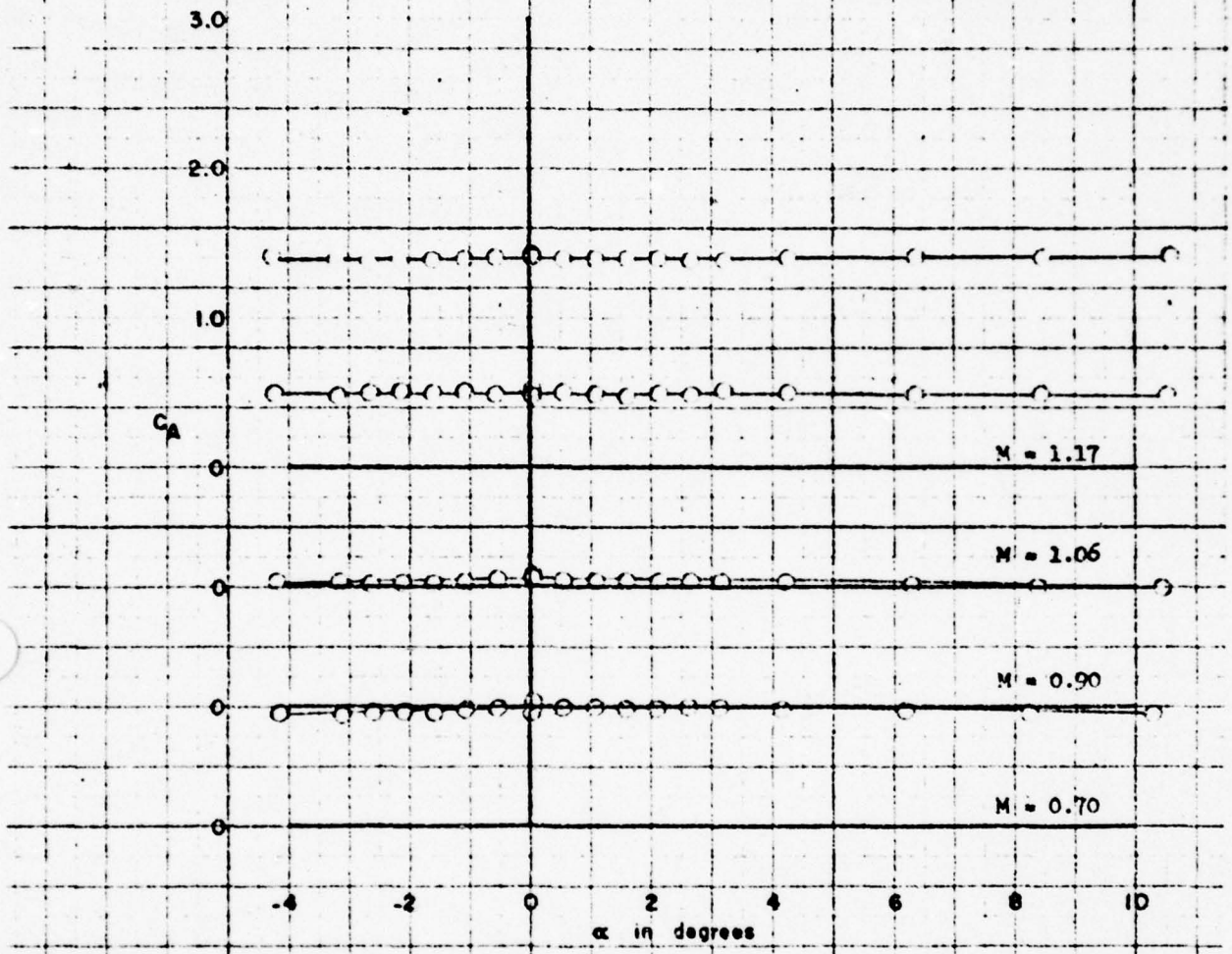

Figure 10 - Variation of the Aerodynamic Characteristics With Angle of Attack for Configuration $B_{22}R_5H_{10}WT_{10}$

(a) $\phi = -5°$; $i = i' = 0°$; $\delta = \delta' = 0°$

FIGURE 10a

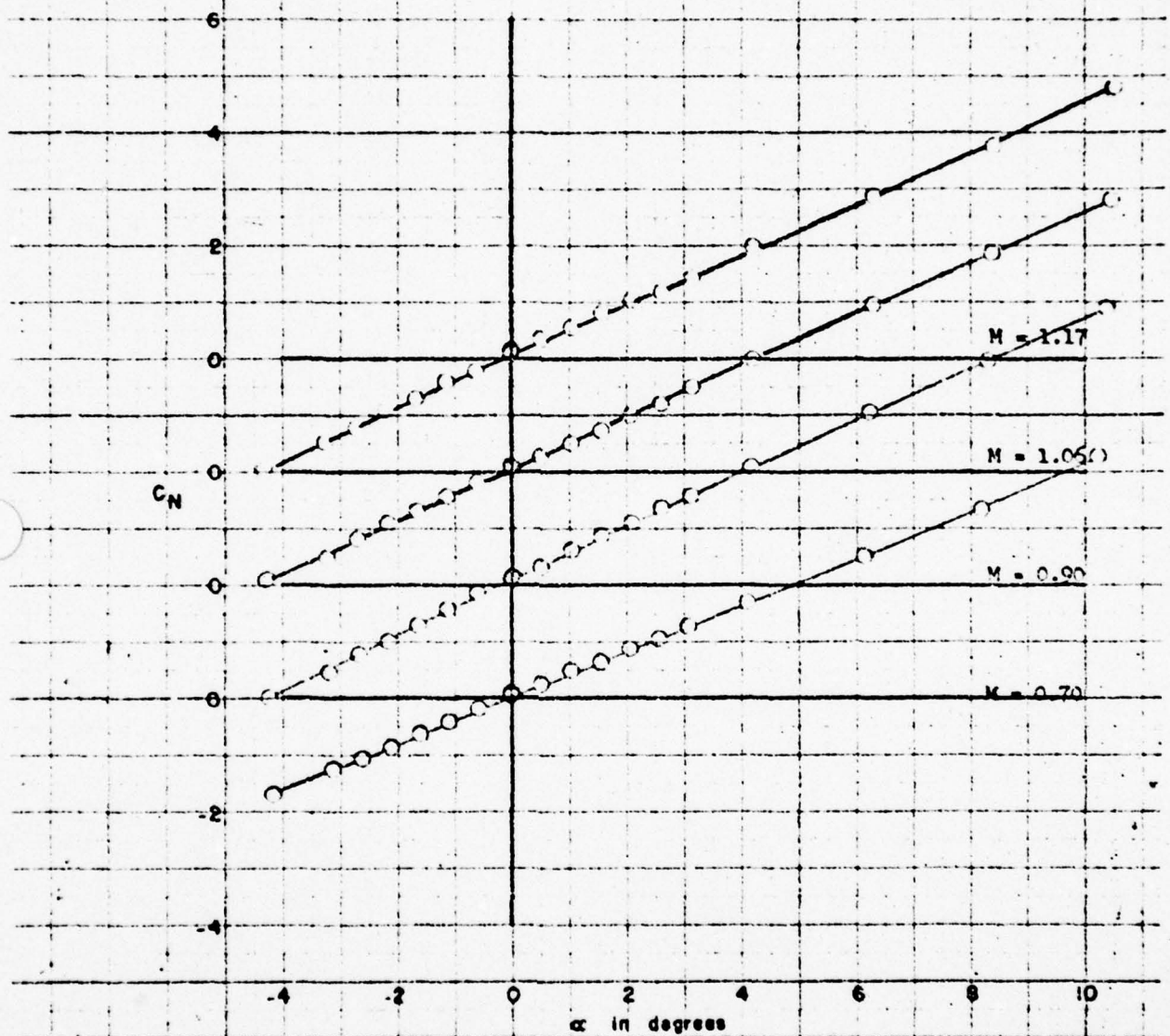

Figure 10 (Continued)

(a) Continued

[redacted]

FIGURE 10a (cont)

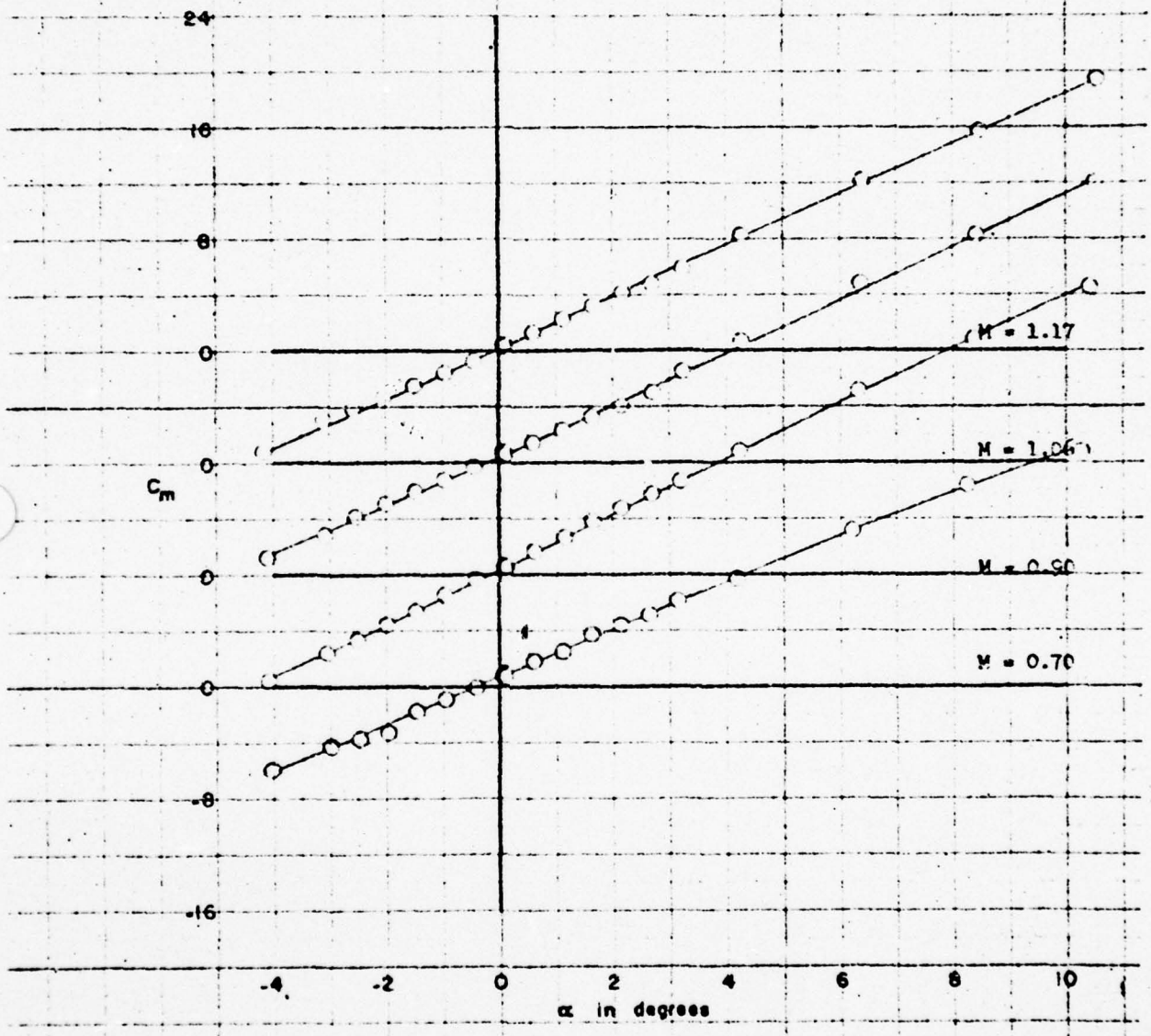

Figure 10 (Continued)

(a) Continued

[redacted]

FIGURE 10a (cont)

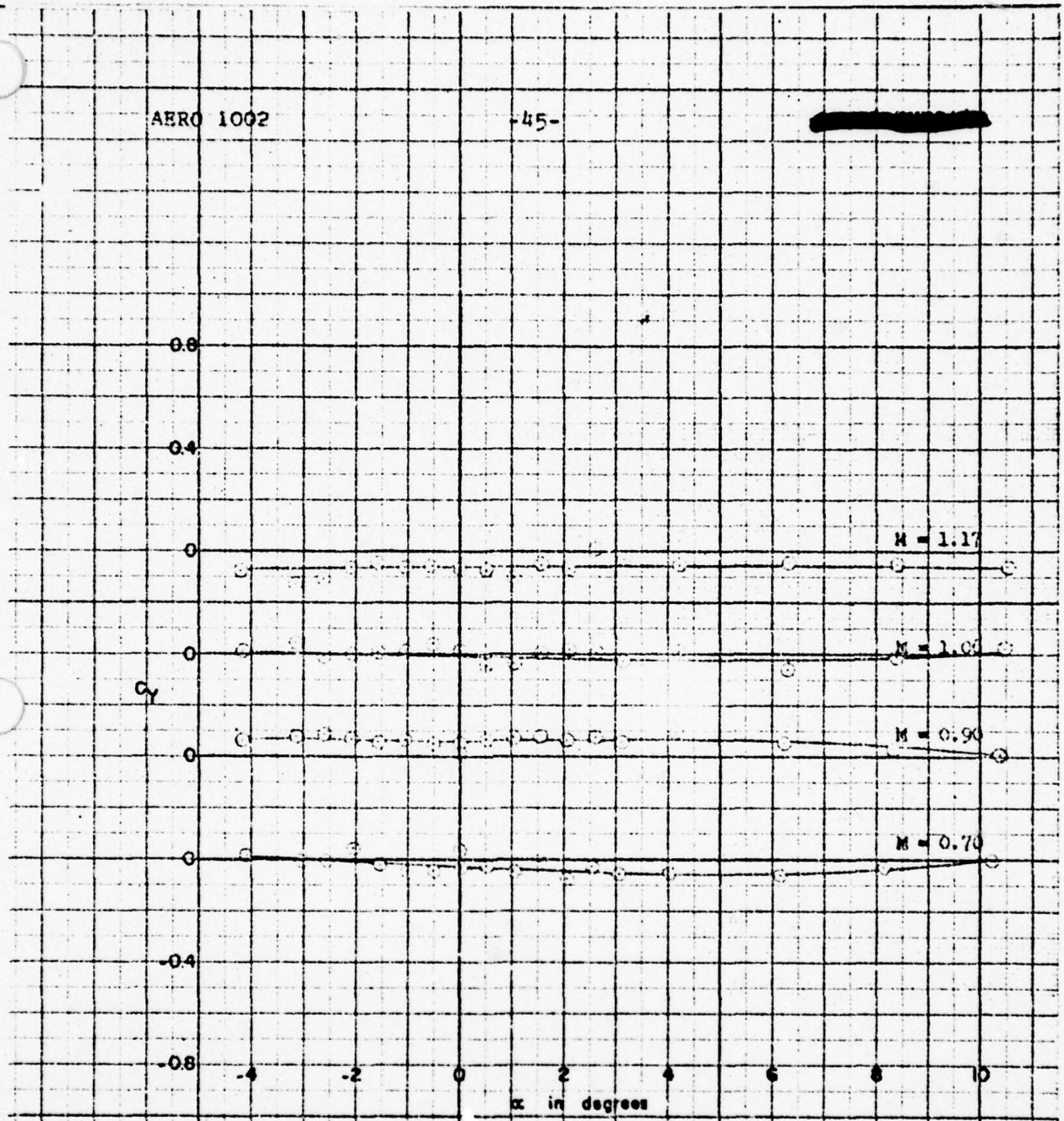

Figure 10 (Continued)

(d) Continued

[redacted]

FIGURE 10a (cont)

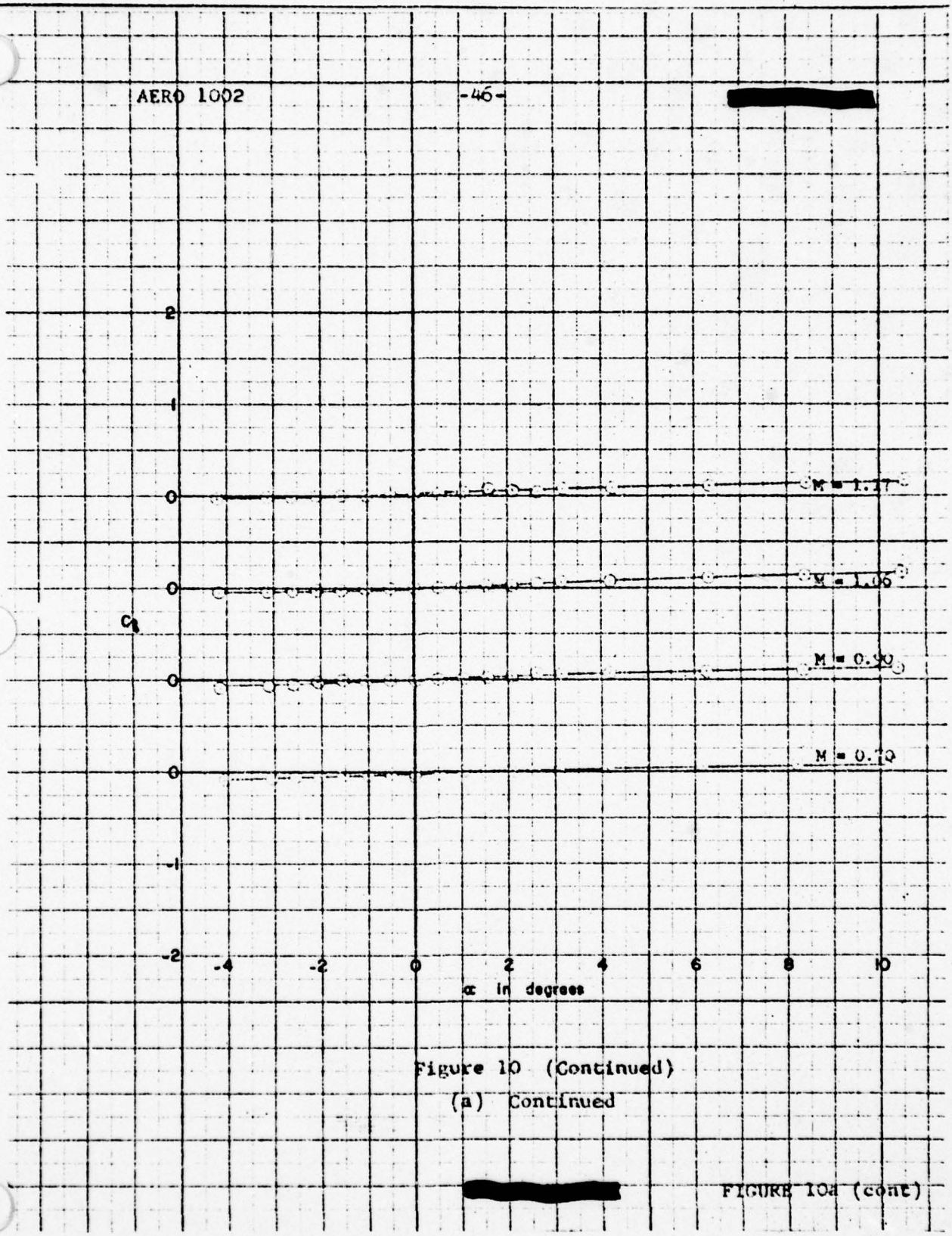

Figure 10 (Continued)
(a) Continued

[redacted]

FIGURE 10a (cont)

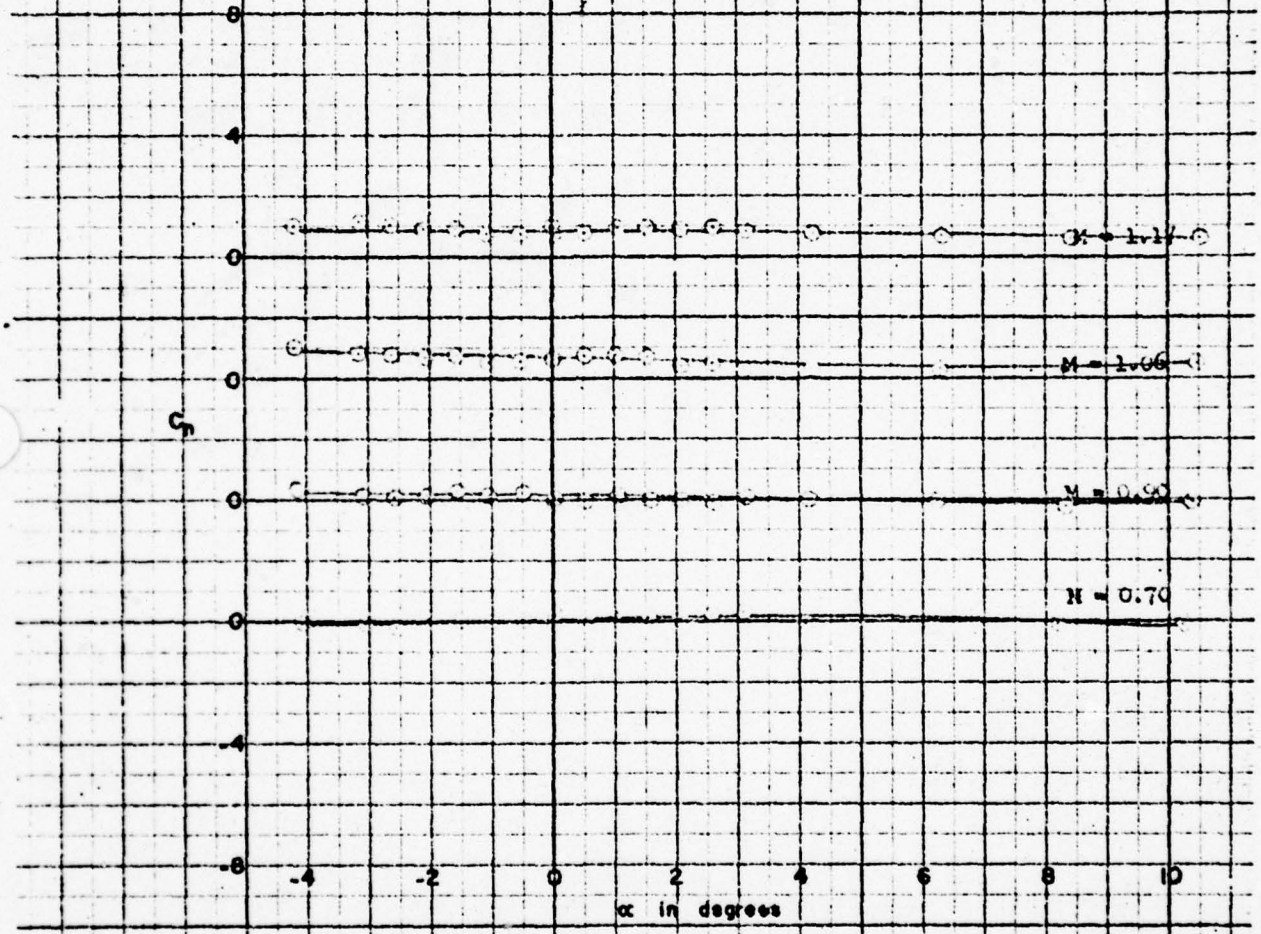

Figure 10 (Continued)

(a) Concluded

[redacted] FIGURE 10a (concl)

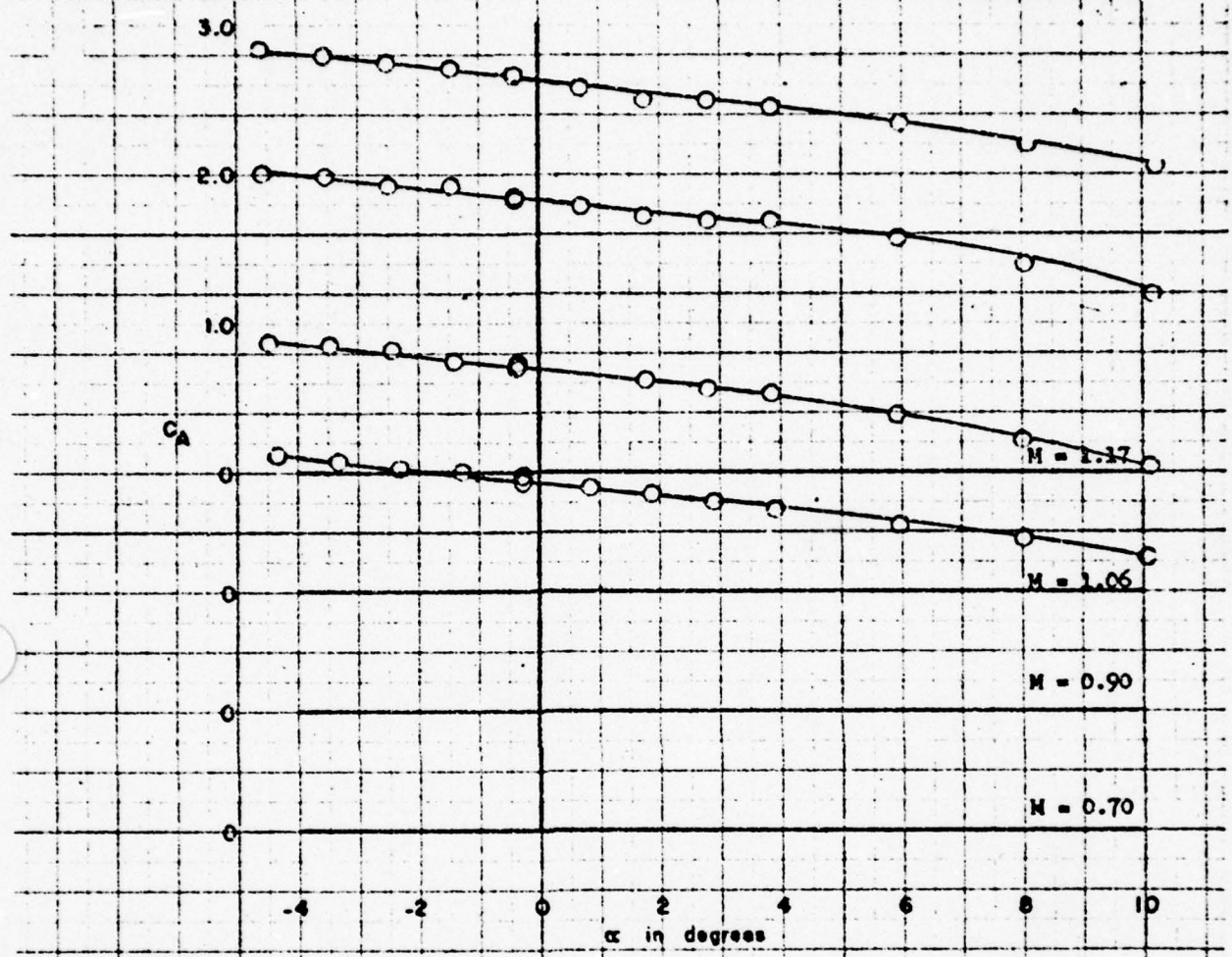

Figure 10 – (Continued)

(b) ϕ=-45°; i=i'=-10°; δ=δ'=0°

[redacted]

FIGURE 10b

[redacted]

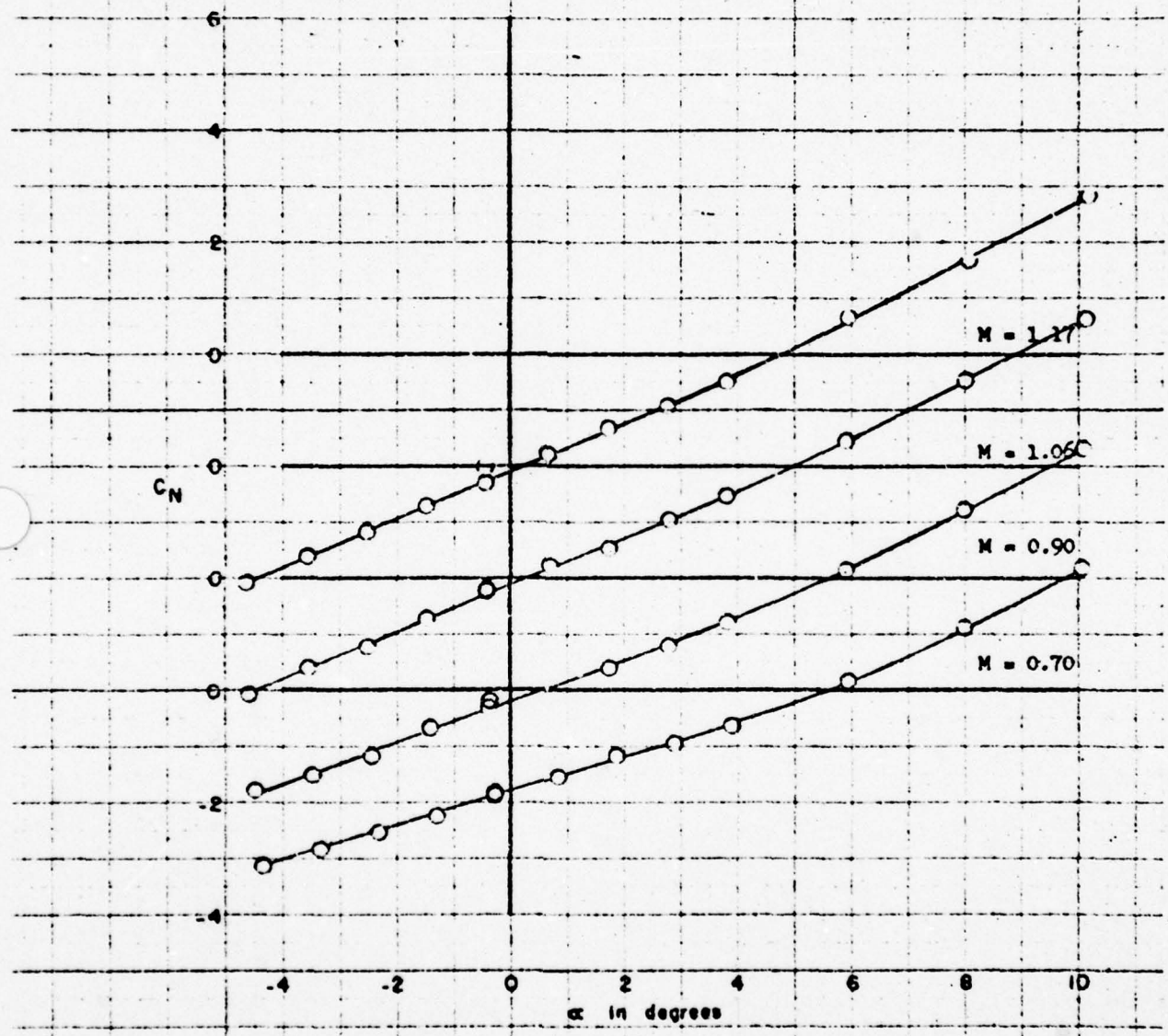

Figure 10 (Continued)

(b) Continued

[redacted]

FIGURE 10b (cont)

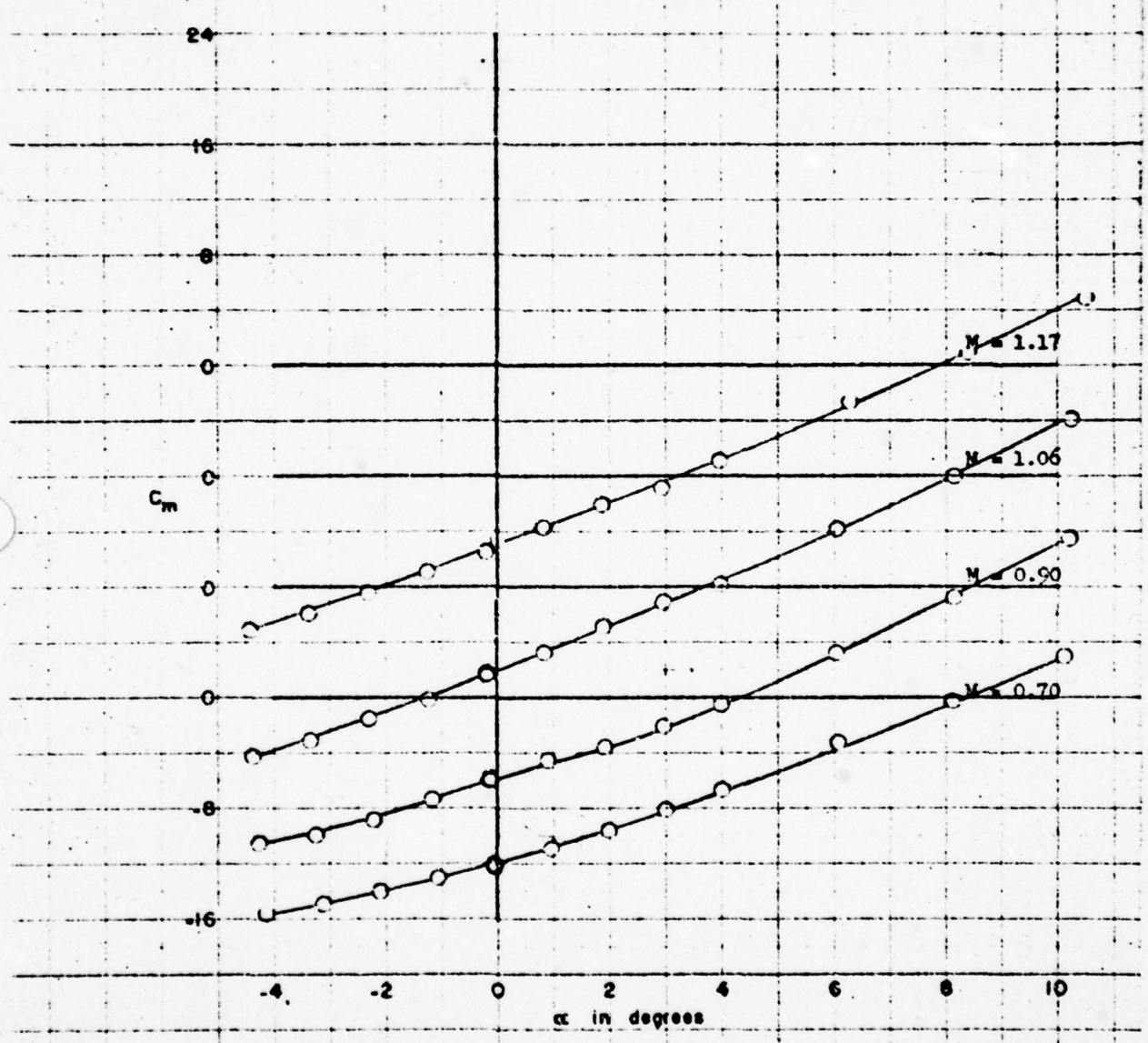

Figure 10 (Continued)
(b) Concluded

FIGURE 10b (concl)

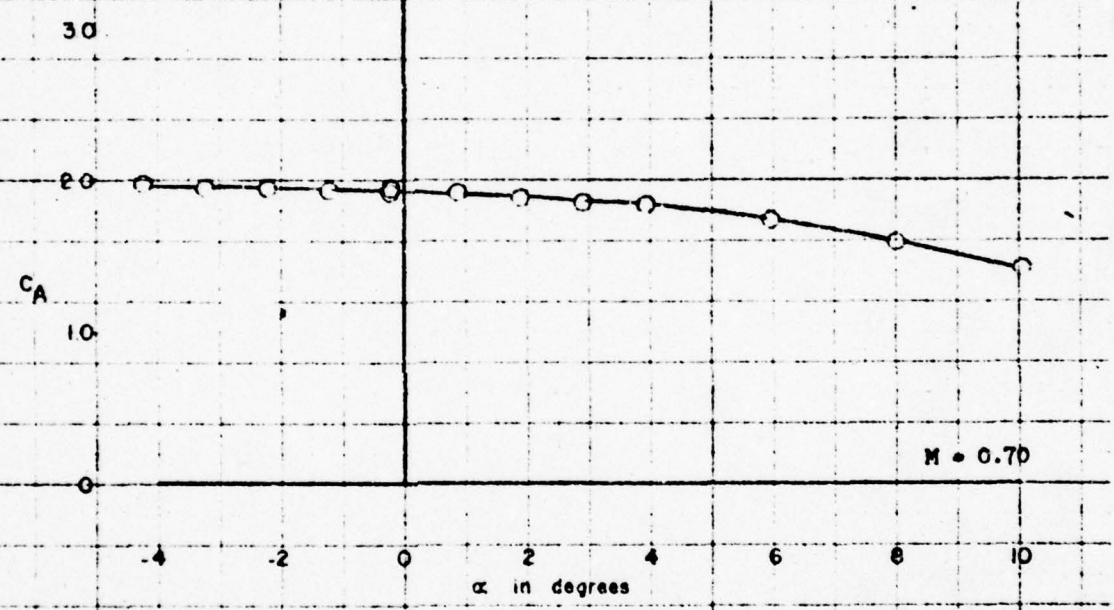

Figure 10 (Continued)

(c) ϕ=-45°; i=i'=-15°; δ=δ'=0°

[redacted] FIGURE 10c

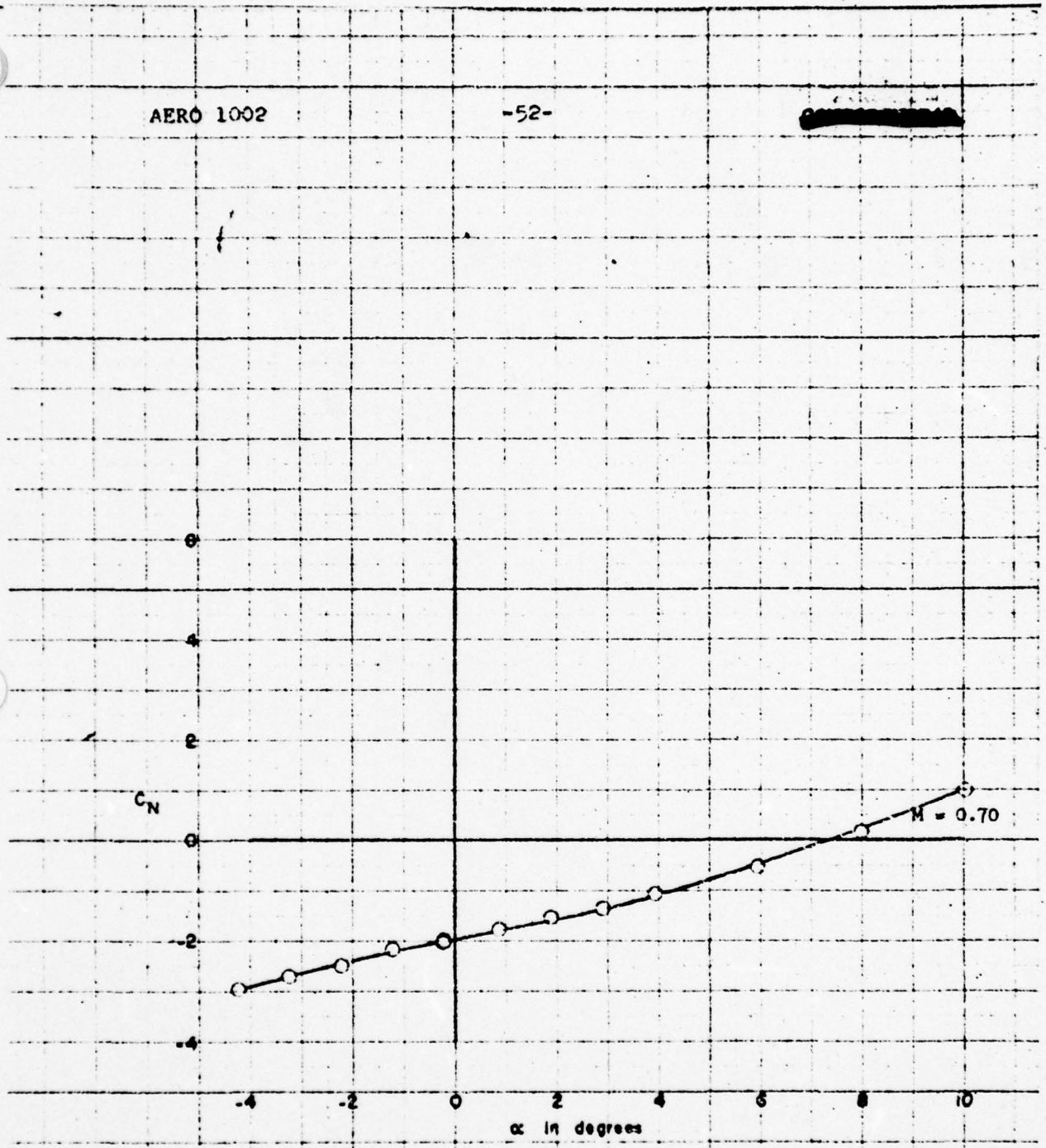

Figure 10 (Continued)

(c) Continued

[redacted]

FIGURE 10c (cont)

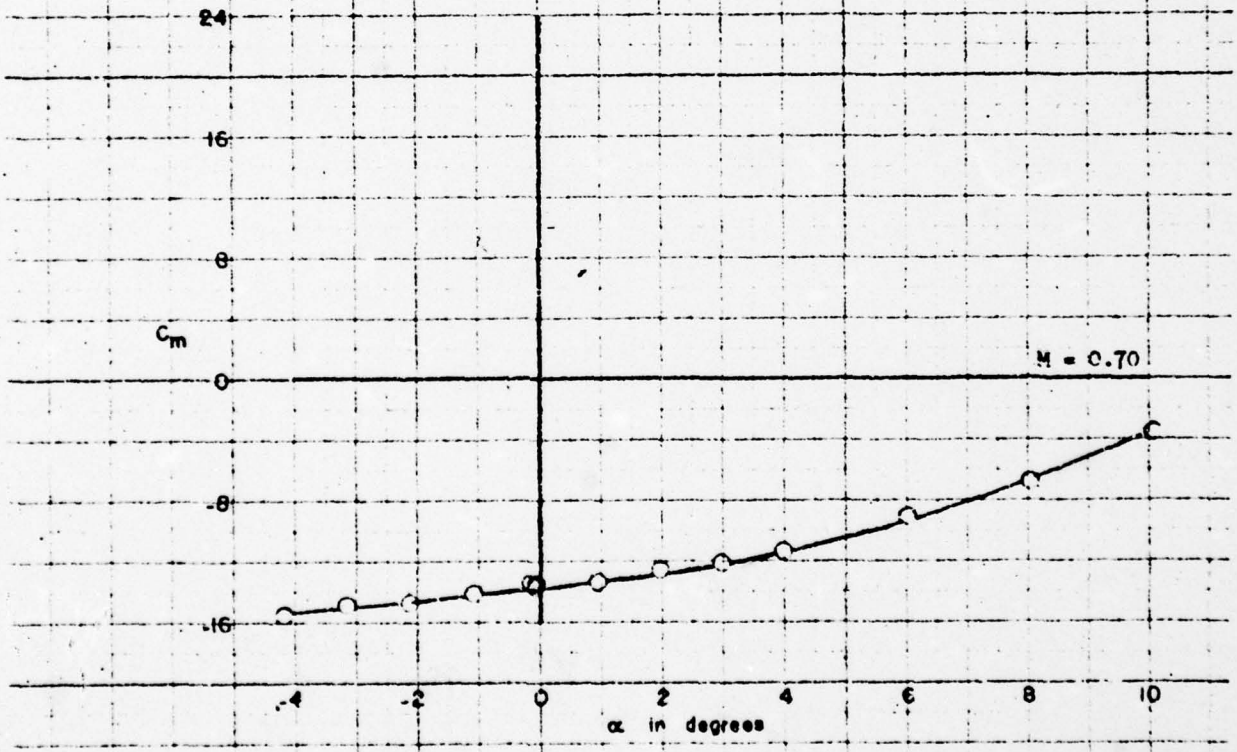

Figure 10 (Continued)

(c) Concluded

FIGURE 10c (concl)

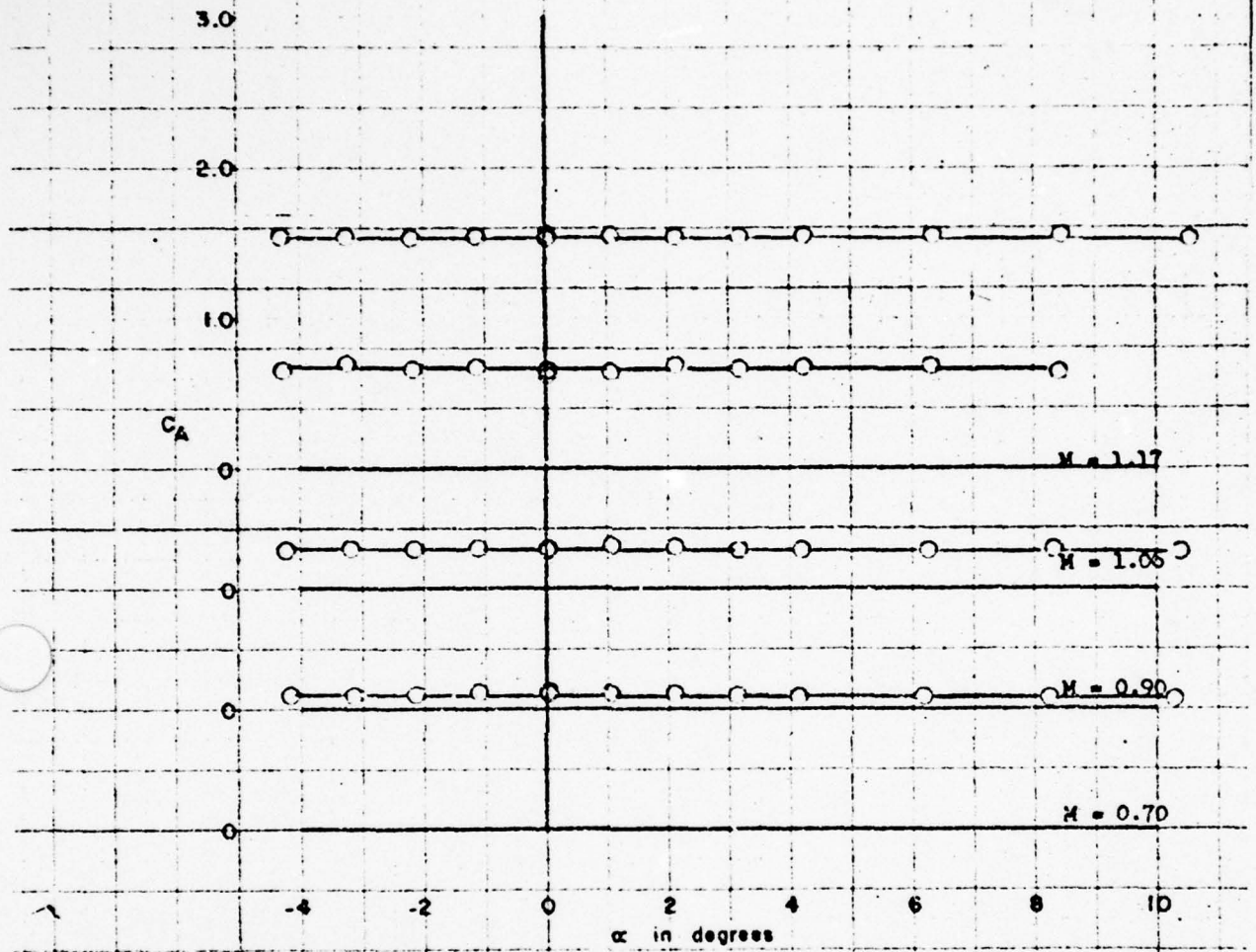

Figure 10 (Continued)

(d) $\delta=-45°$; $i=i'=0°$; $\delta=\delta'=5°$

[redacted]

FIGURE 10d

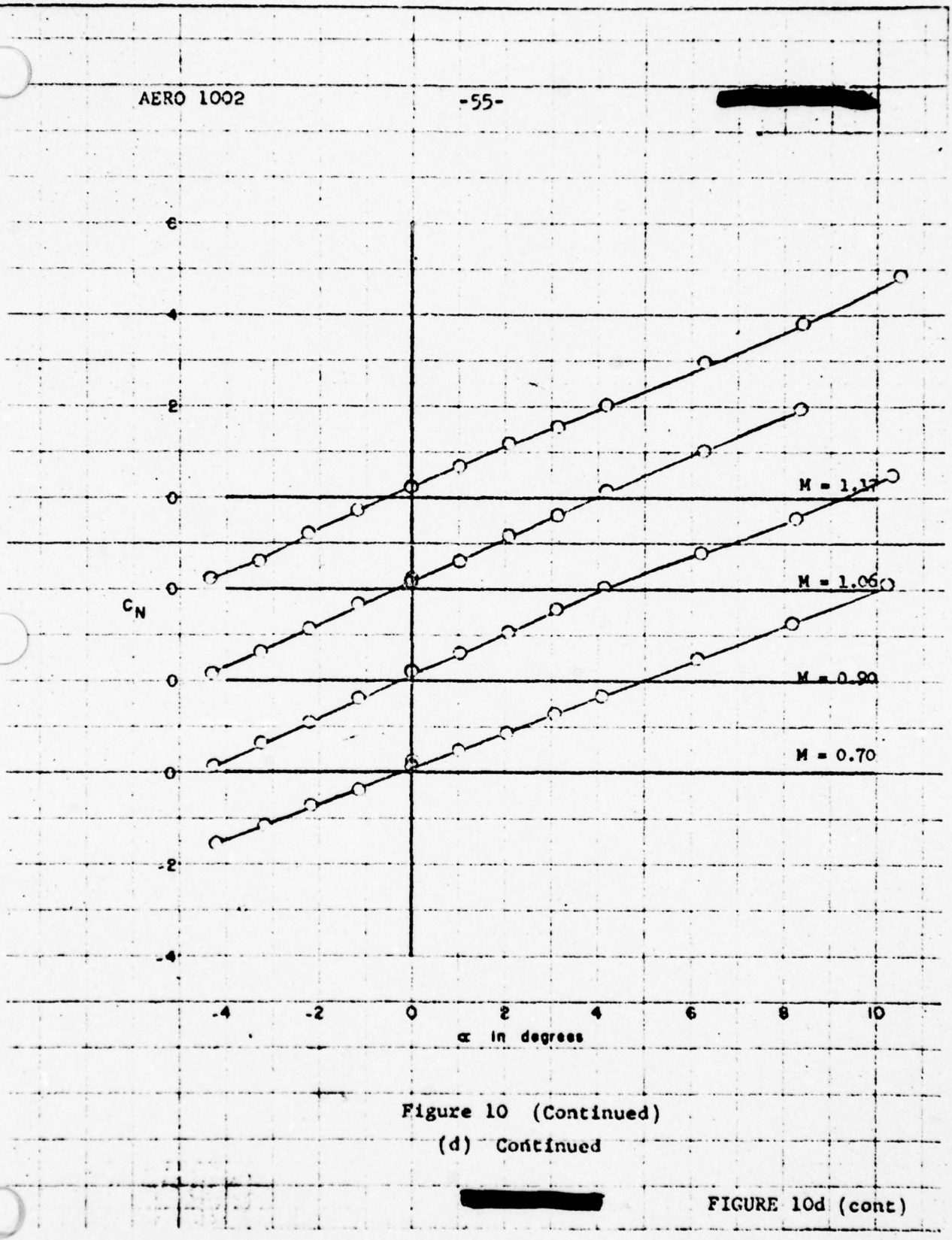

Figure 10 (Continued)

(d) Continued

FIGURE 10d (cont)

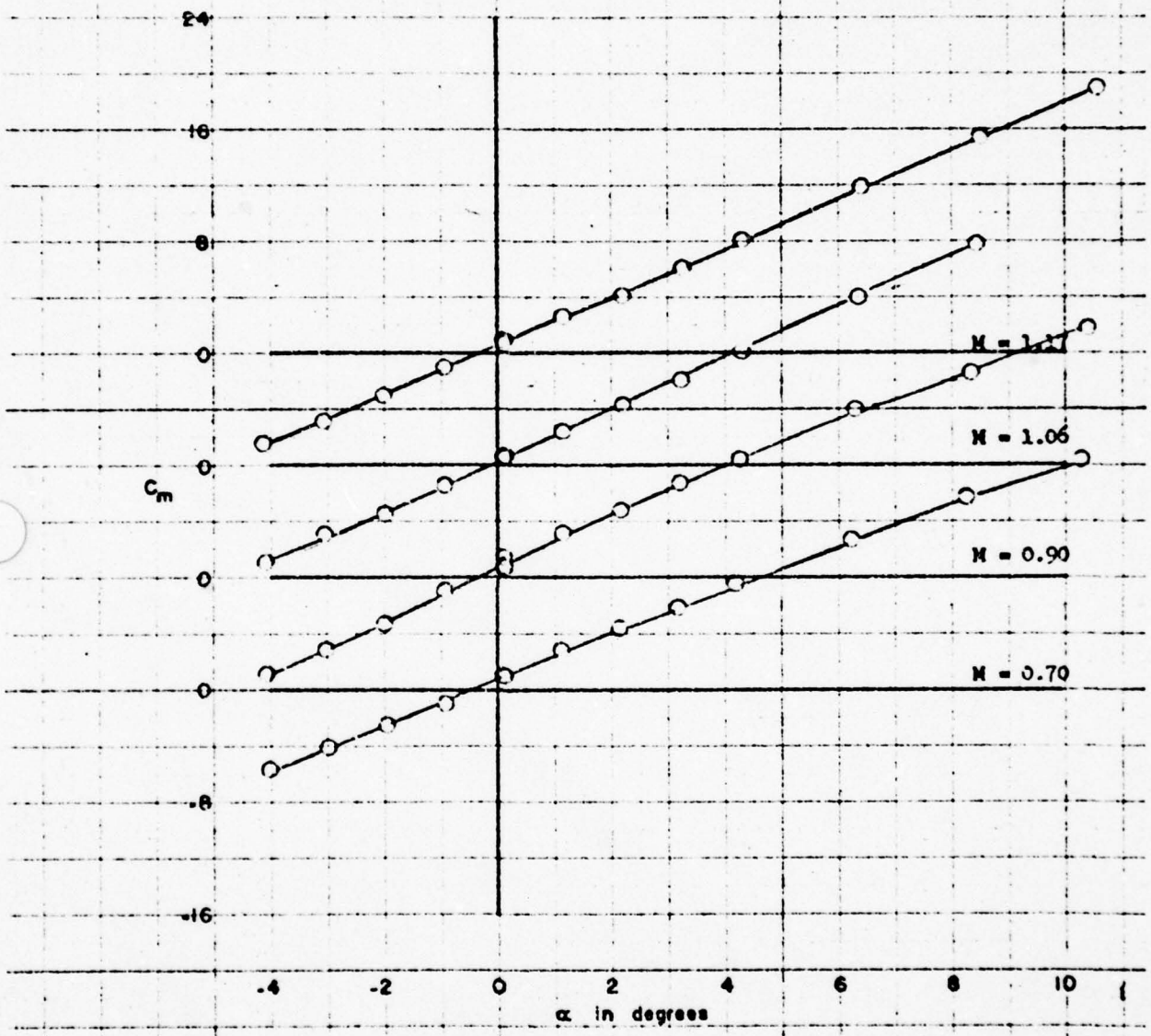

Figure 10 (Continued)

(d) Continued

[redacted]

FIGURE 10d (cont)

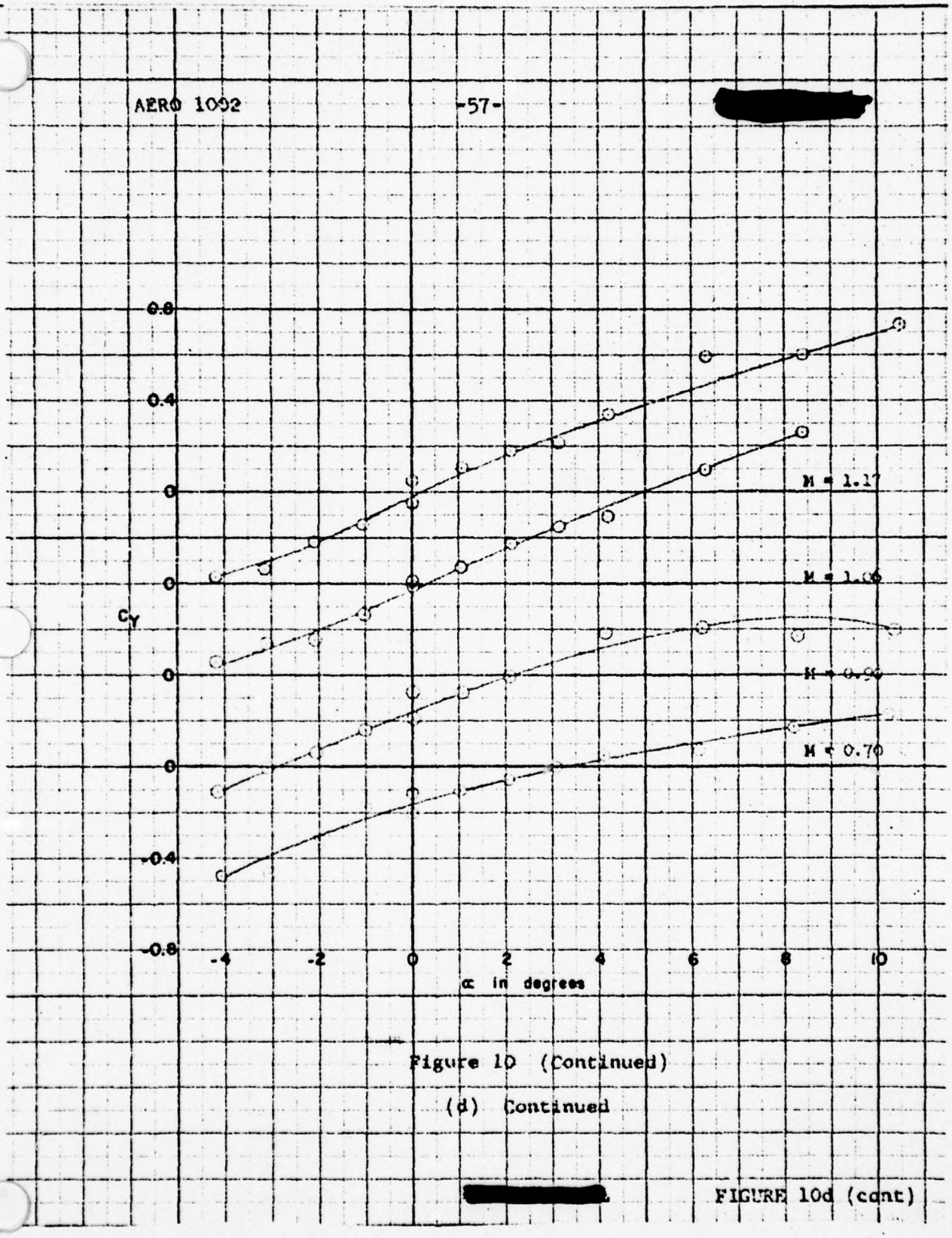

Figure 10 (Continued)

(d) Continued

[redacted]

FIGURE 10d (cont)

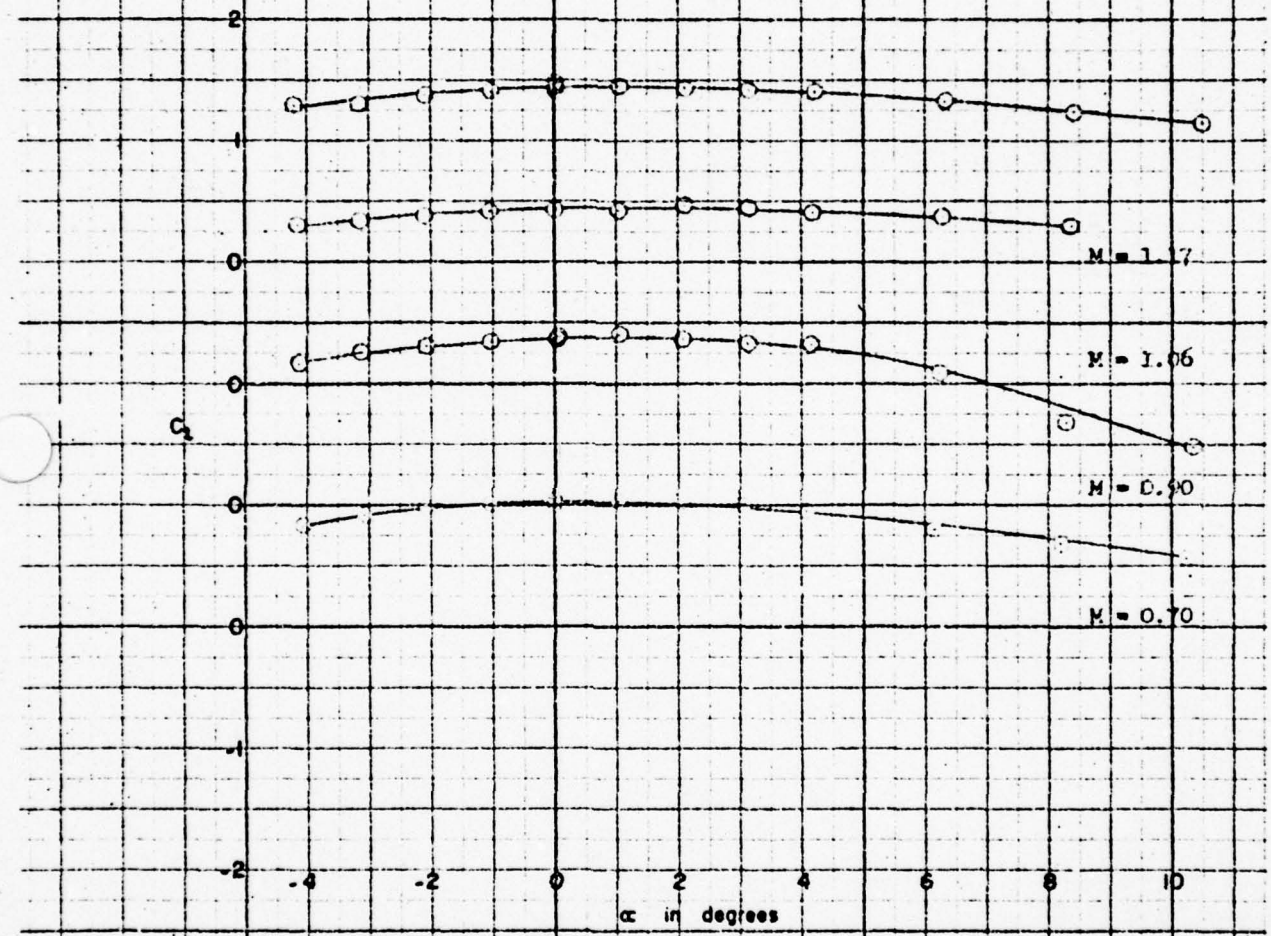

Figure 10 (Continued)

(d) Continued)

[redacted]

FIGURE 10d (cont)

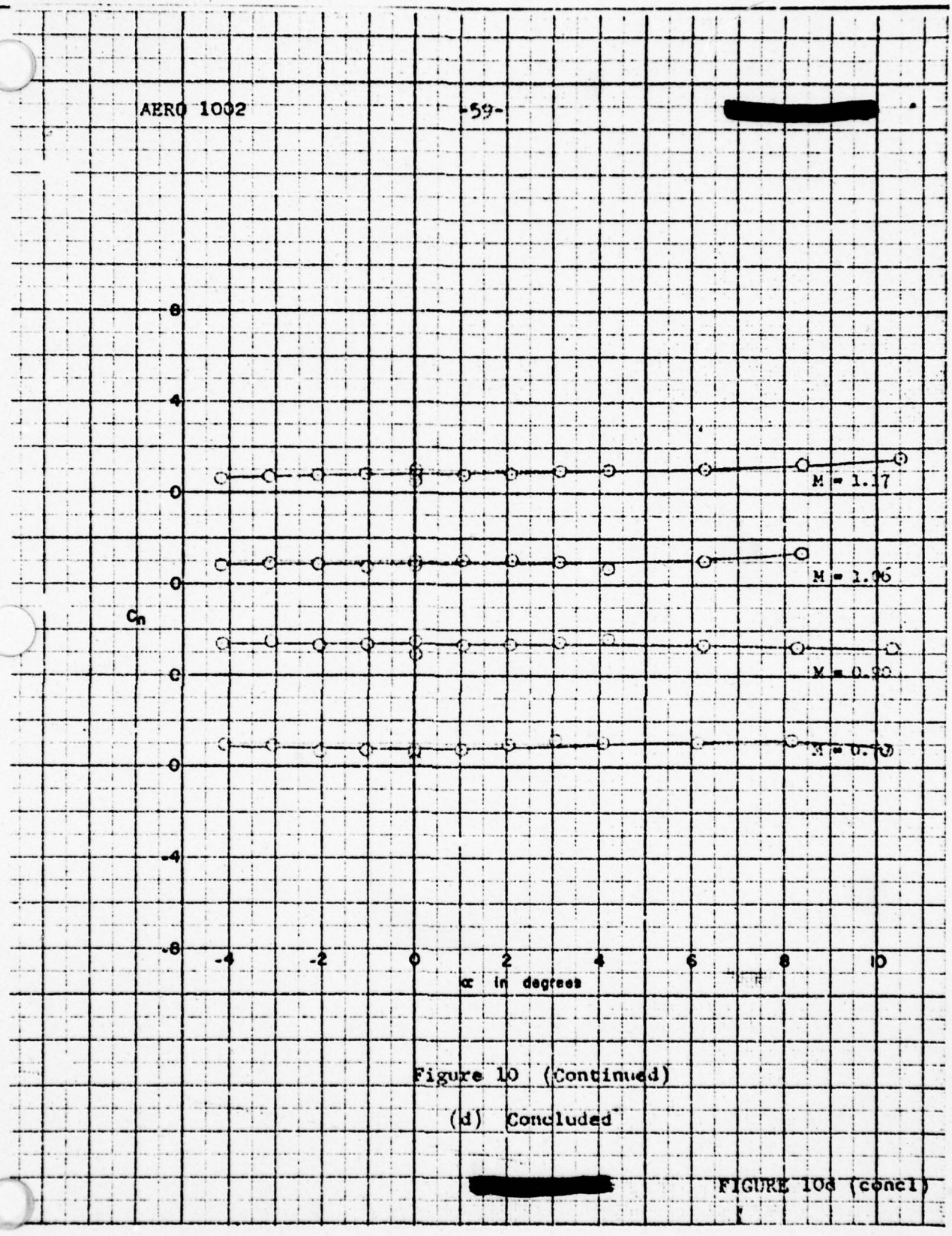

Figure 10 (Continued)

(d) Concluded

[redacted]

FIGURE 10d (concl)

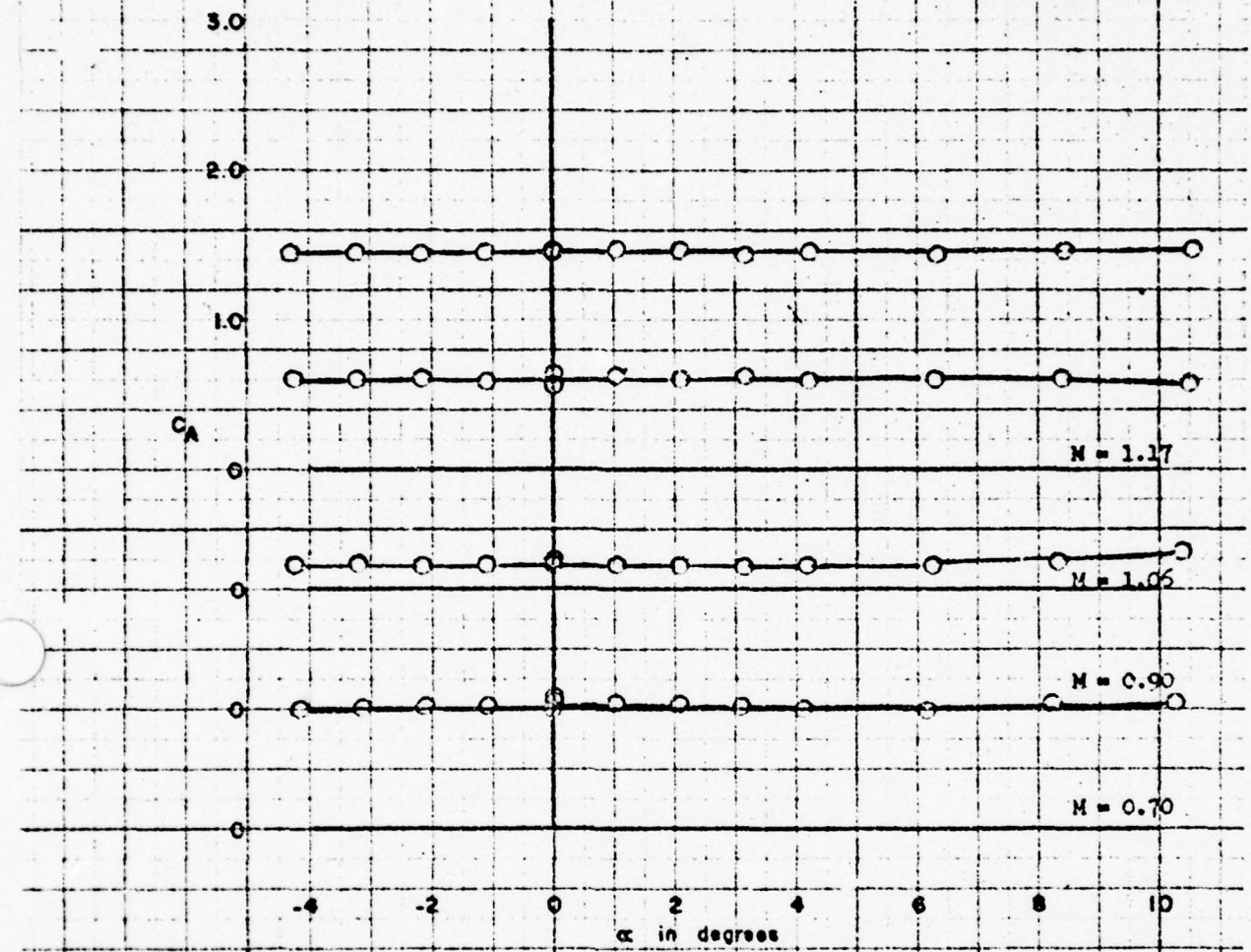

Figure 10 (Continued)

(e) $\phi=0°$; $i=i'=0°$; $\delta=\delta'=0°$

[redacted] FIGURE 10e

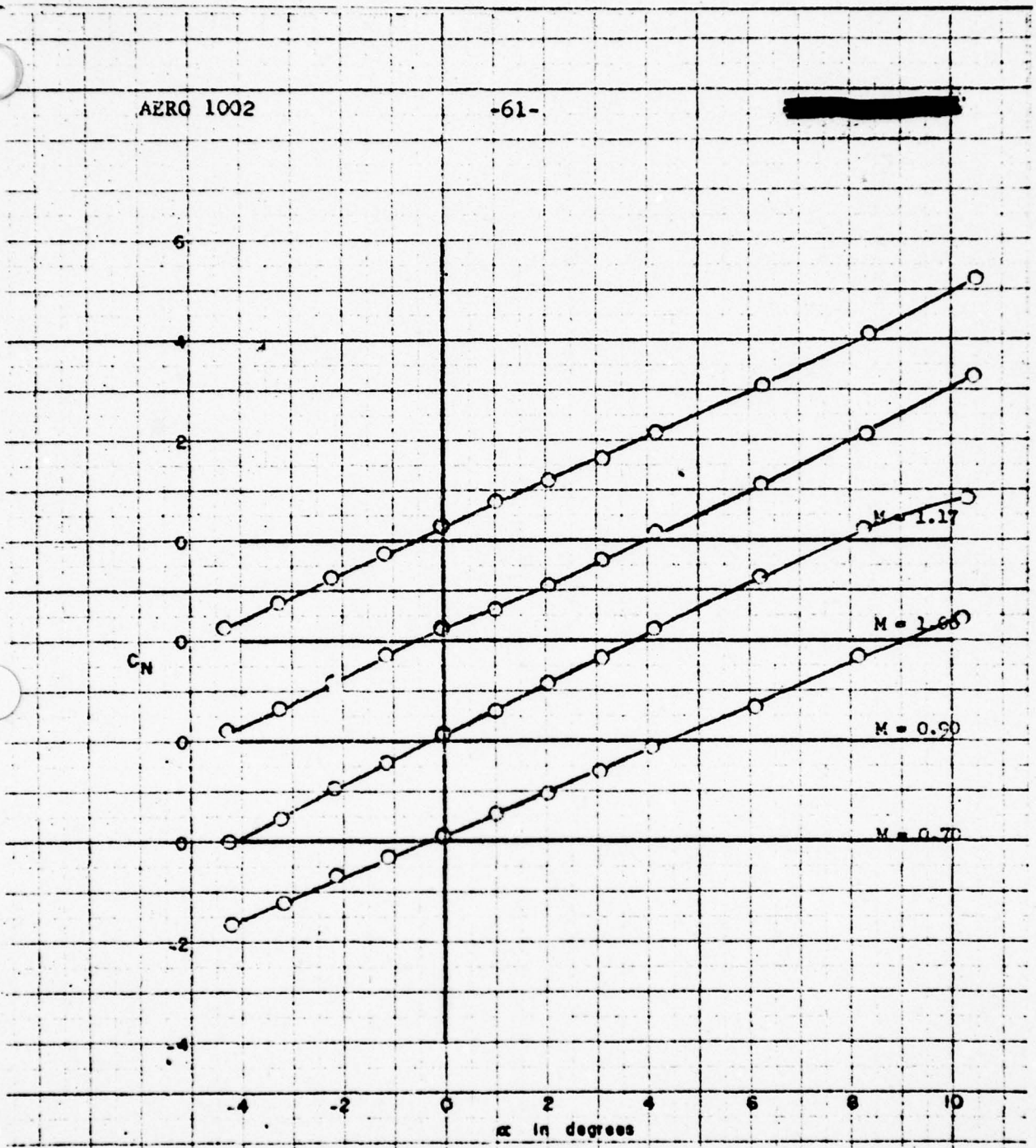

Figure 10 (Continued)

(e) Continued

[redacted]

FIGURE 10e (cont)

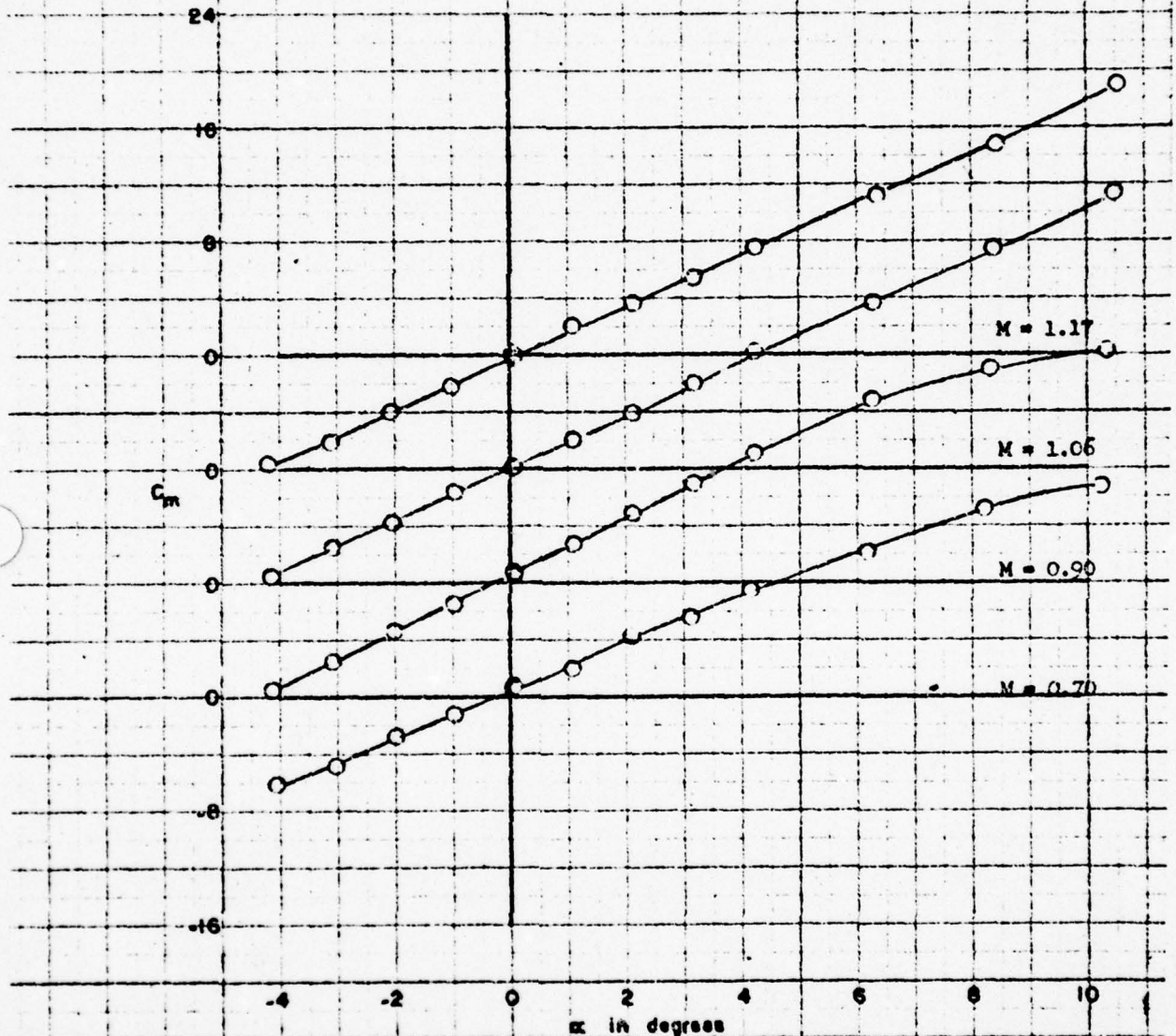

Figure 10 (Continued)

(e) Concluded

[redacted]

FIGURE 10e (concl)

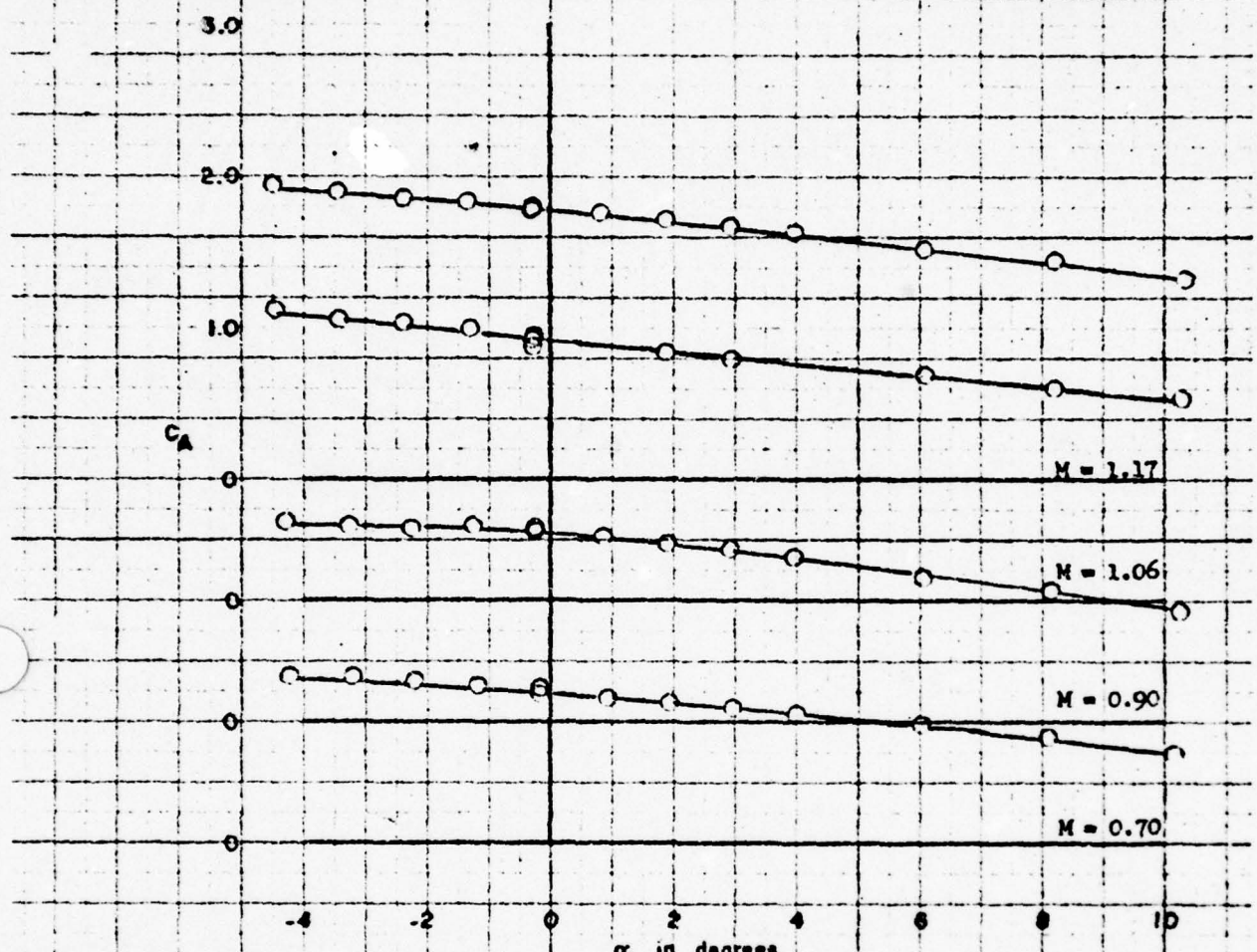

Figure 10 (Continued)

(f) ϕ=0°; i -10°, i'=0°; δ-δ'=0°

FIGURE 10f

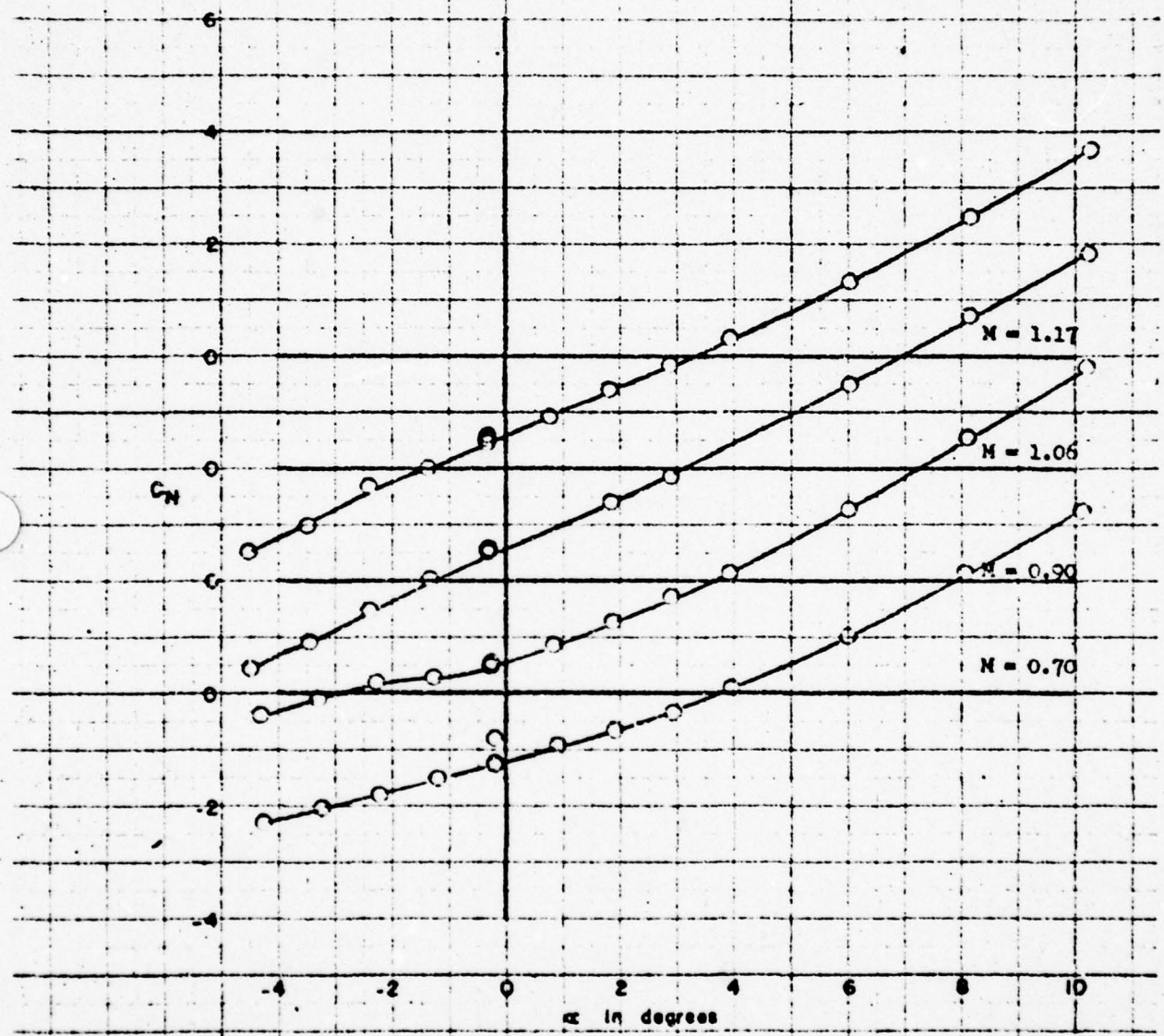

Figure 10 (Continued)

(f) Continued

[redacted]

FIGURE 10f (cont)

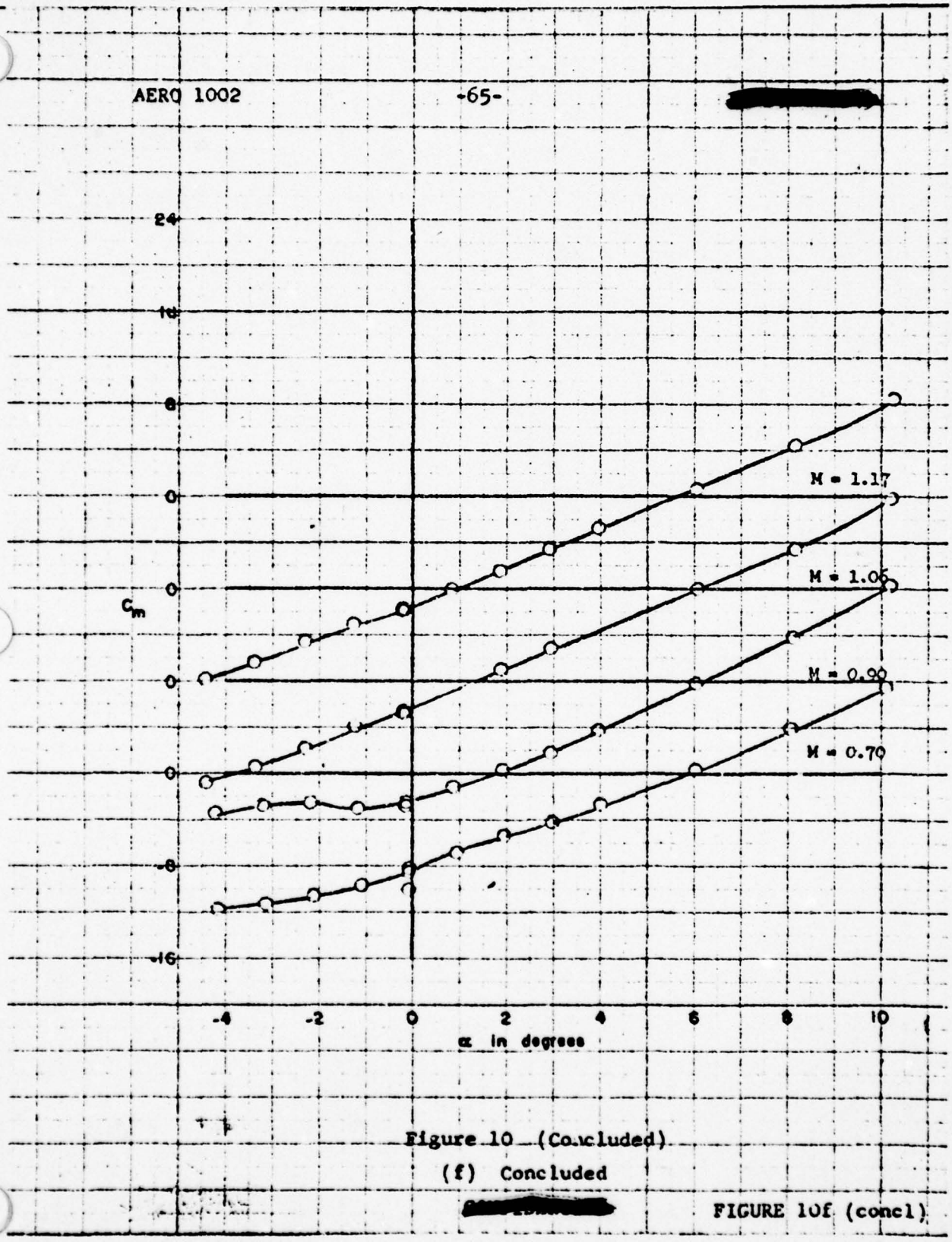

Figure 10 (Concluded)

(f) Concluded

[redacted]

FIGURE 10f (concl)

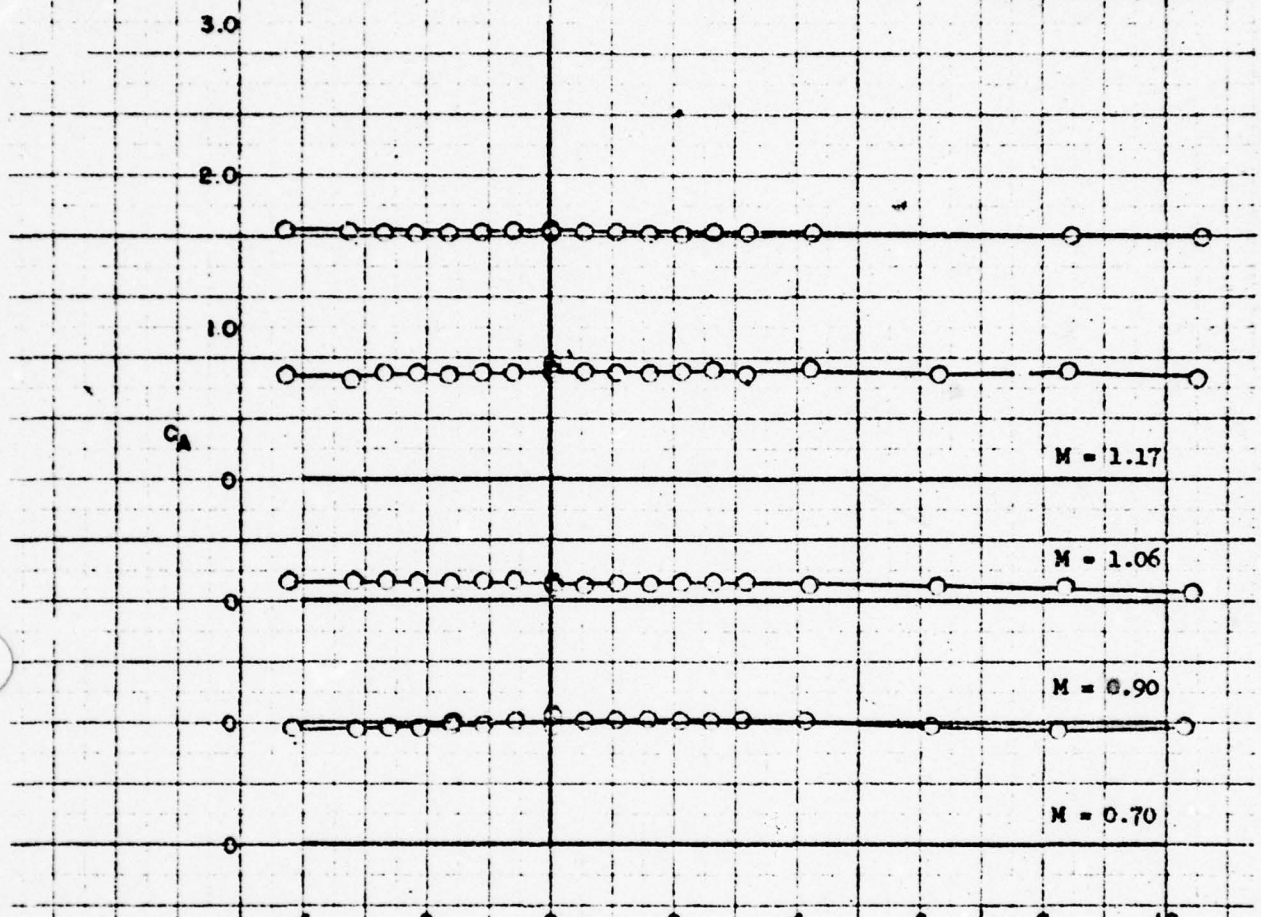

Figure 11 - Variation of the Aerodynamic Characteristics With Angle of Attack for Configuration $B_{22}R_5H_{10}WT_{10}F_{18}$

(a) ϕ=-45°; i=i'=0°; δ=δ'=0°

FIGURE 11a

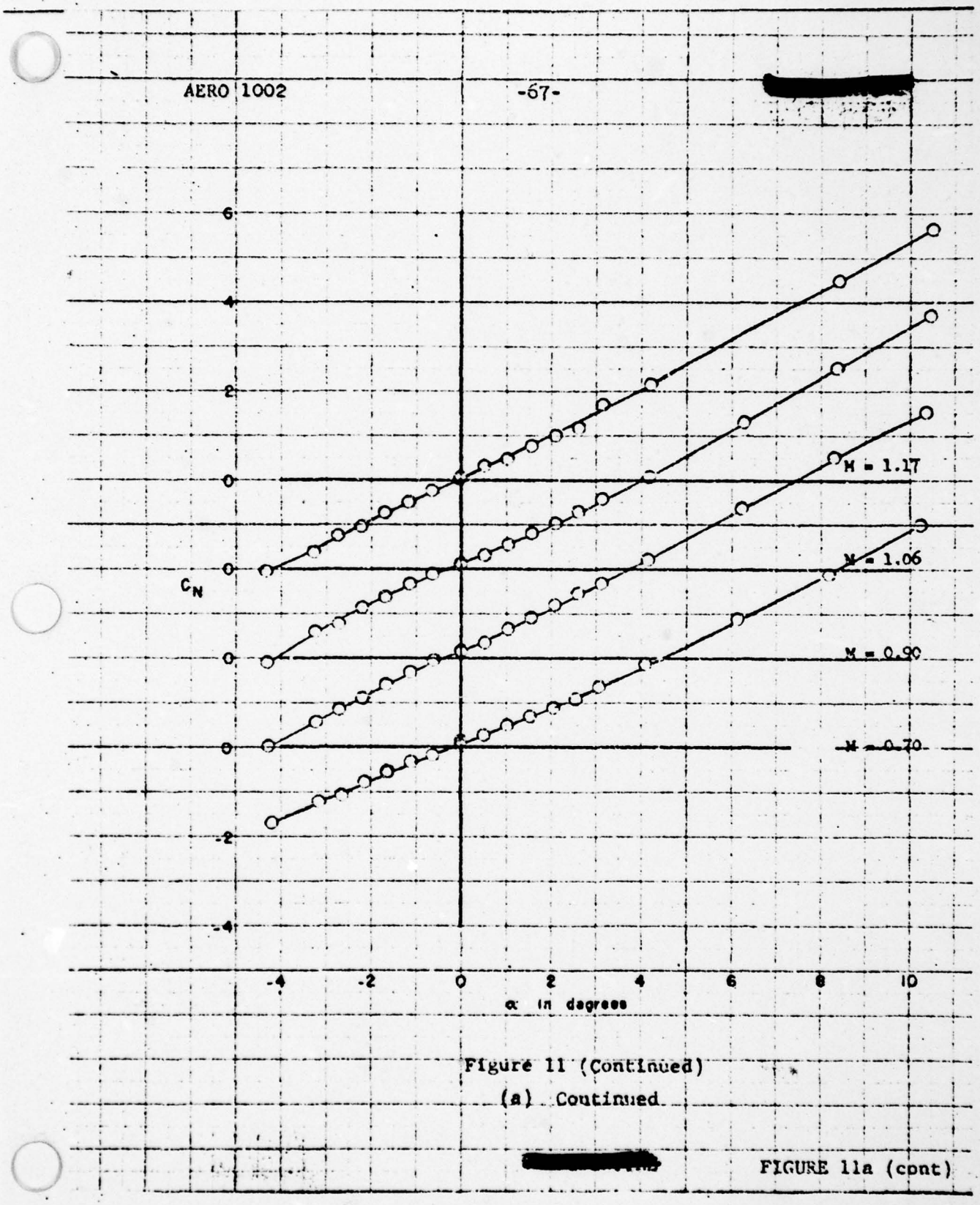

Figure 11 (Continued)

(a) Continued

FIGURE 11a (cont)

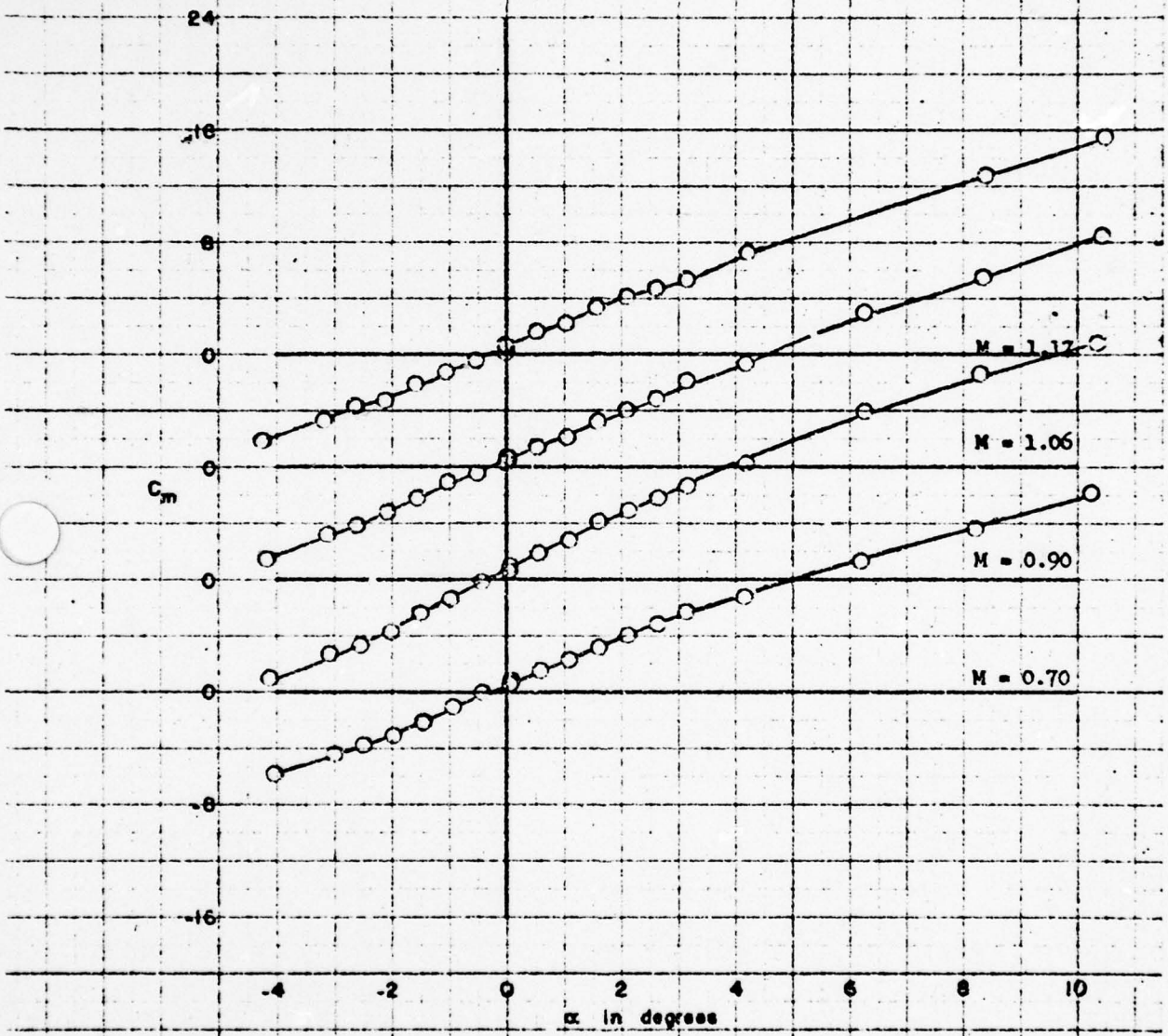

Figure 11 (Continued)

(a) Continued

[redacted]

FIGURE 11a (cont)

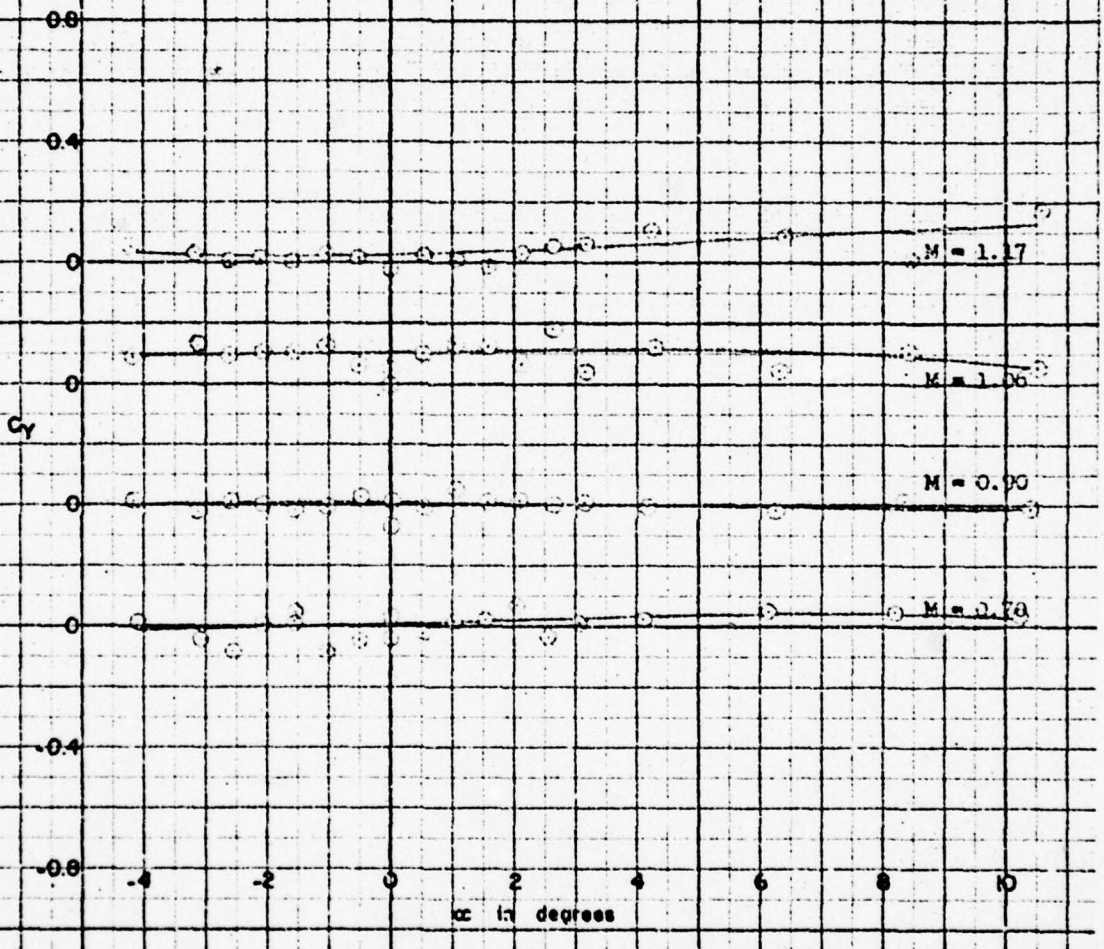

Figure 11 (Continued)

(a) Continued

[redacted]

FIGURE 11a (cont)

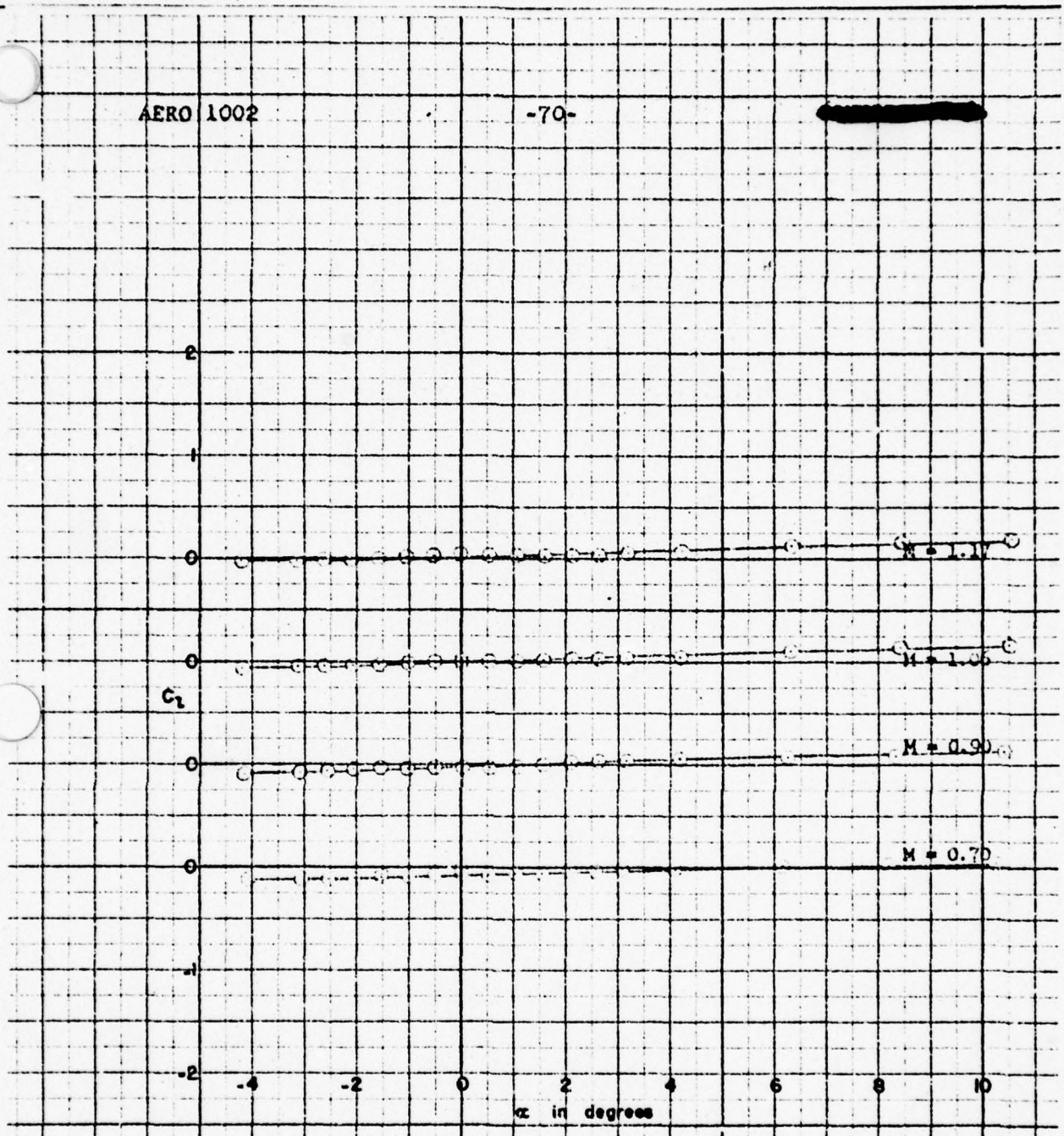

Figure 11 (Continued)
(a) Continued

[redacted]

FIGURE 11a (cont)

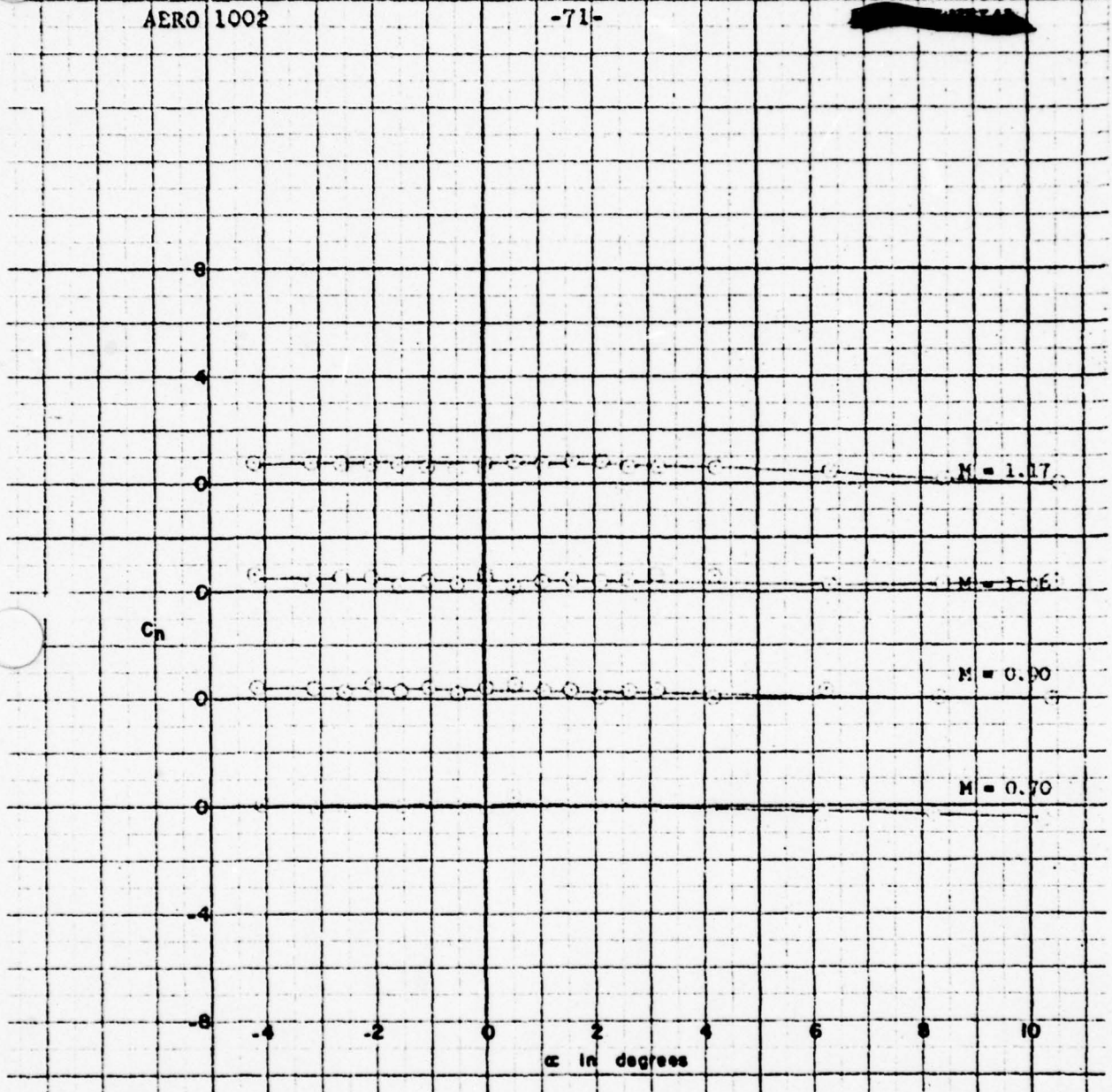

Figure 11 (Continued)
(a) Concluded

[redacted]

FIGURE 11a (concl)

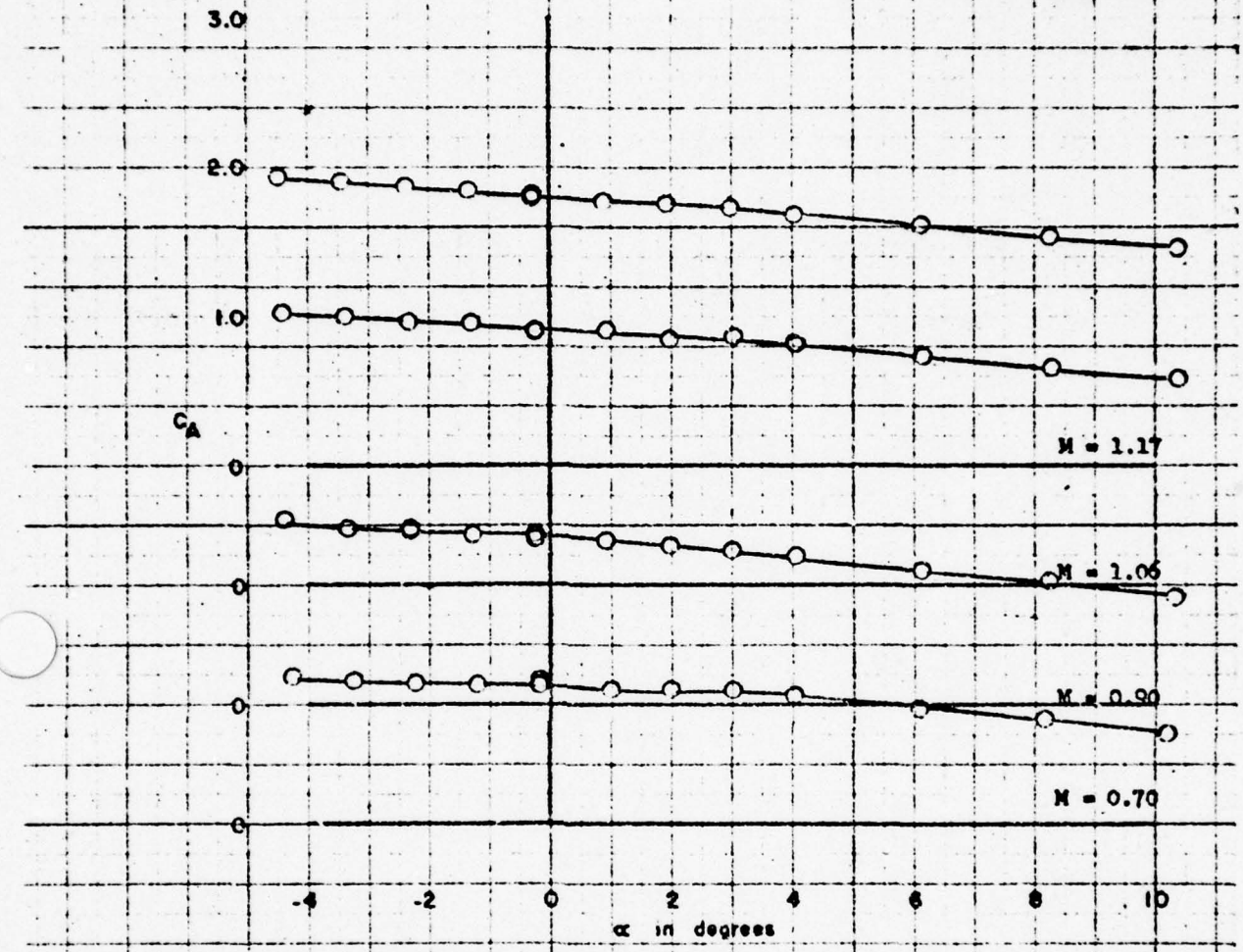

Figure 11 (Continued)

(b) $\phi = -45°$; $i = i' = -5°$; $\delta = \delta' = 0°$

FIGURE 11b

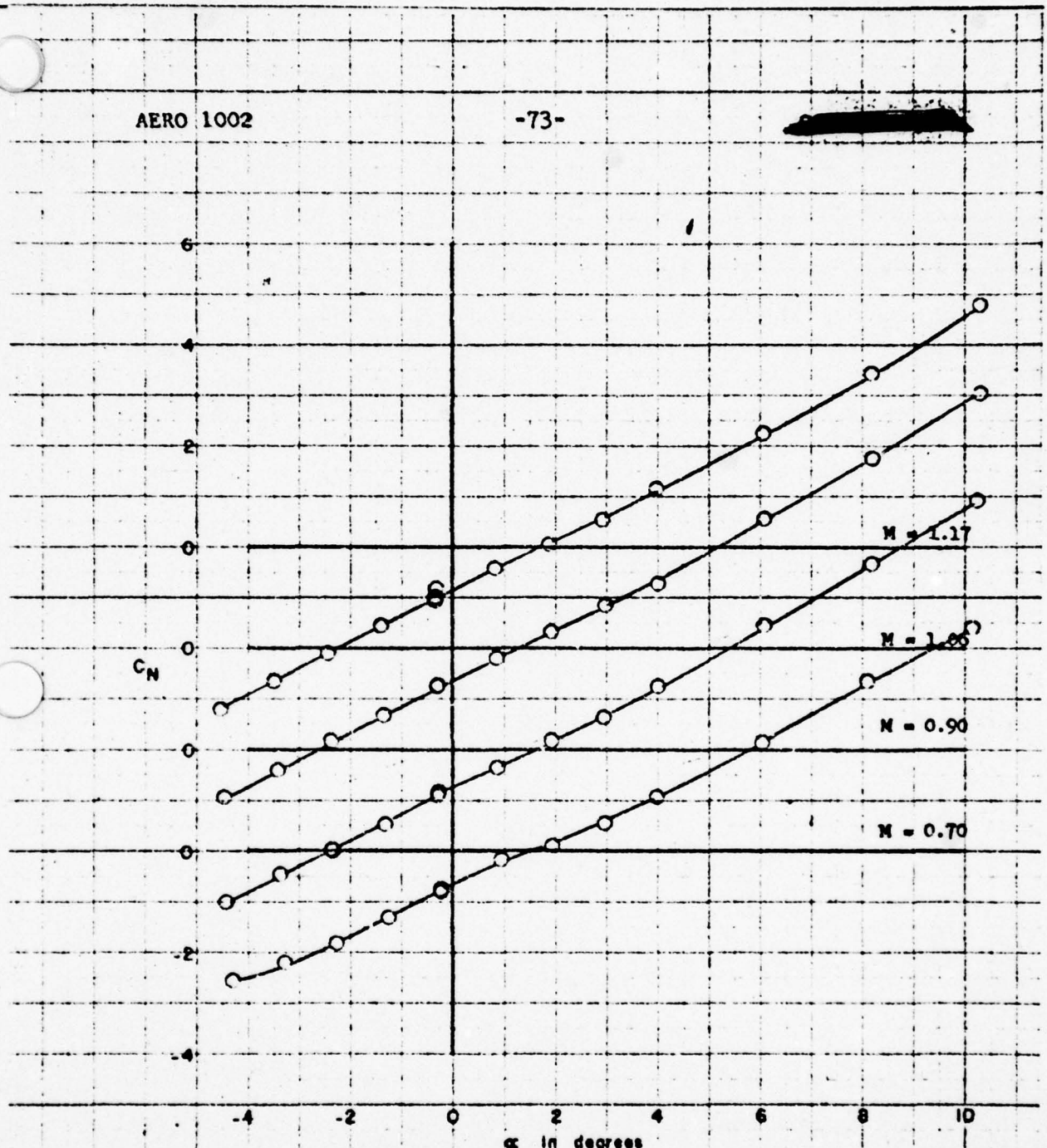

Figure 11 (Continued)

(b) Continued

[redacted] FIGURE 11b (cont)

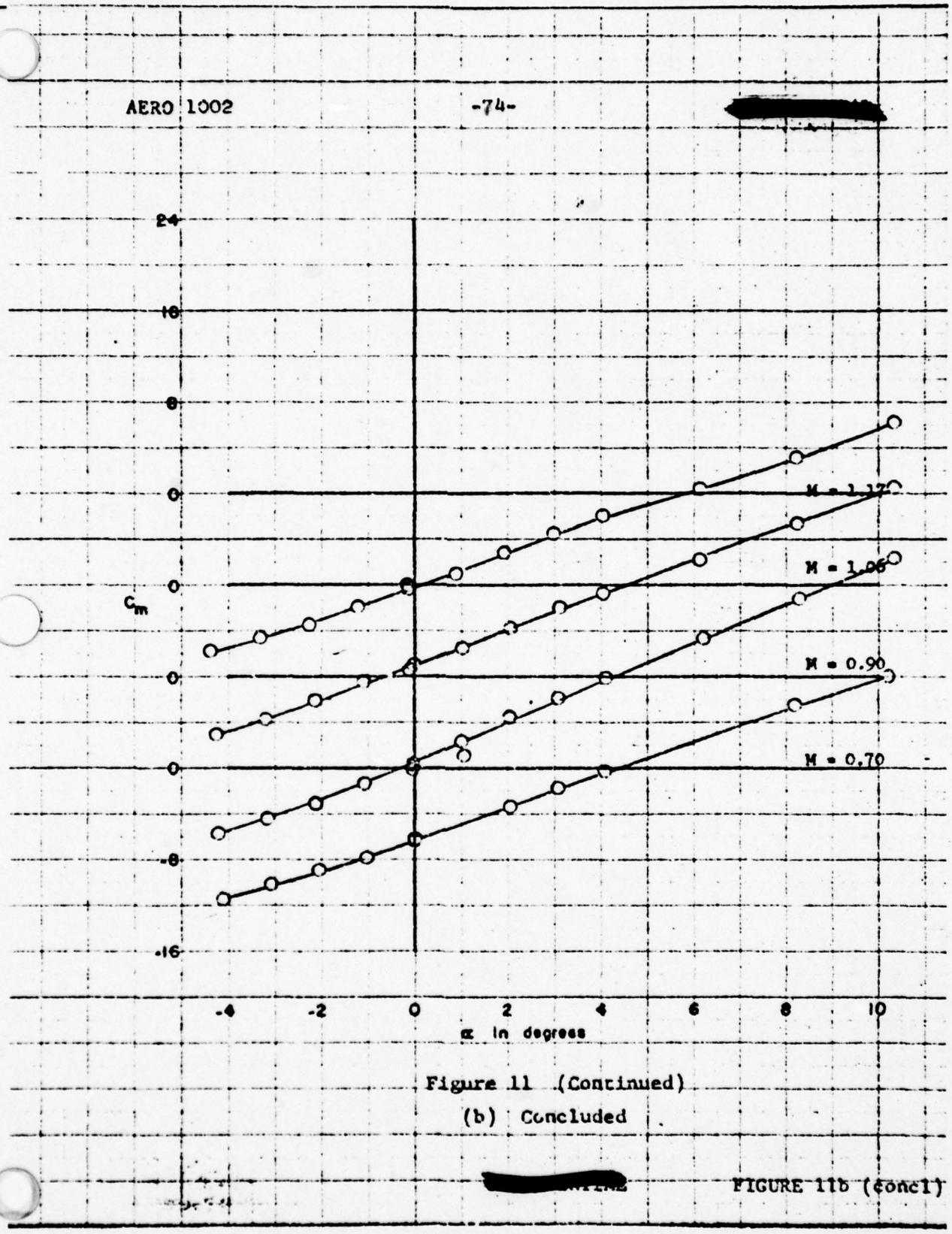

Figure 11 (Continued)
(b) Concluded

[redacted]

FIGURE 11b (Concl)

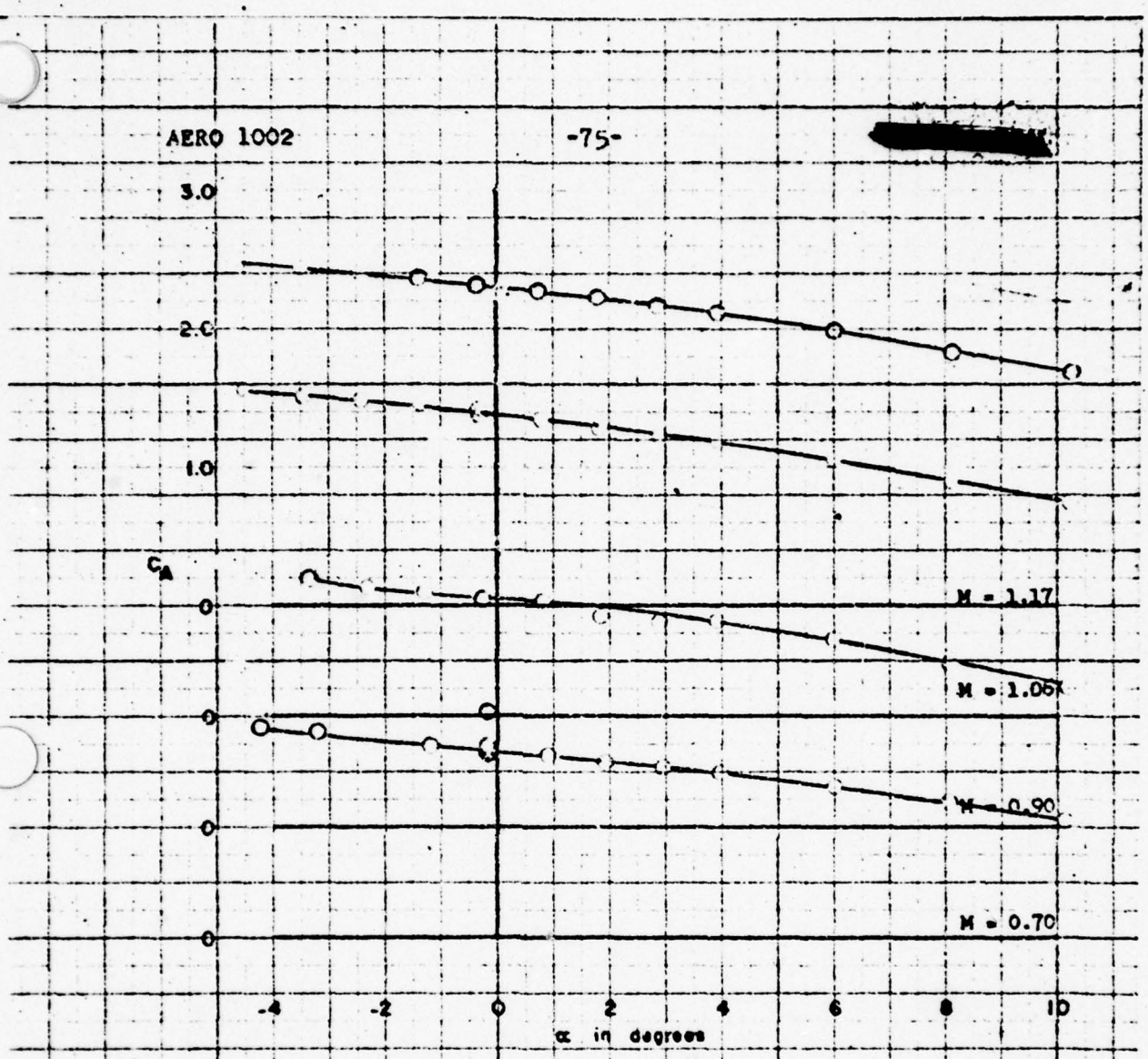

Figure 11 (Continued)

(c) $\phi = -45°$; $i = i' = -10°$; $\delta = \delta' = 0°$

FIGURE 11c

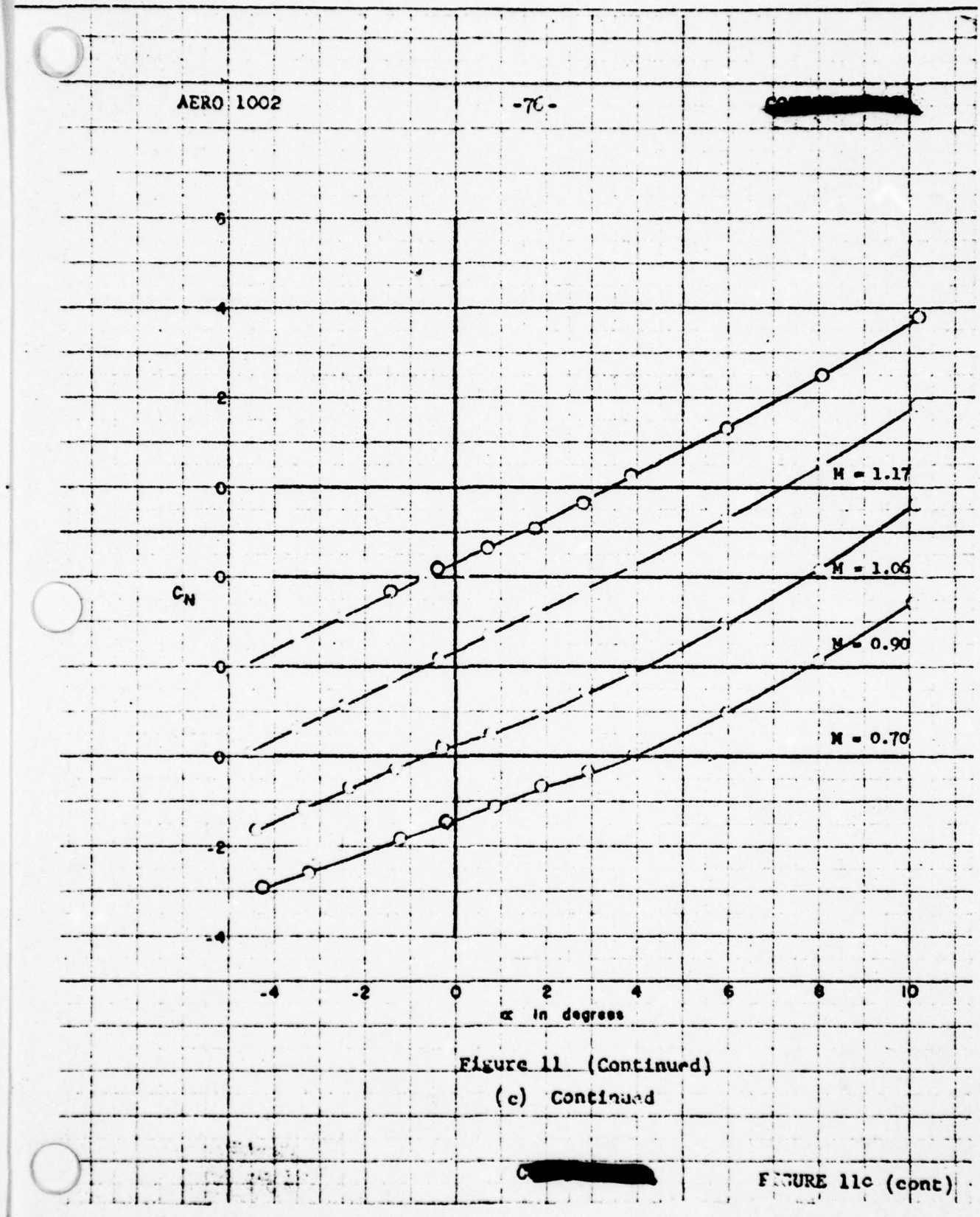

Figure 11 (Continued)

(c) Continued

FIGURE 11c (cont)

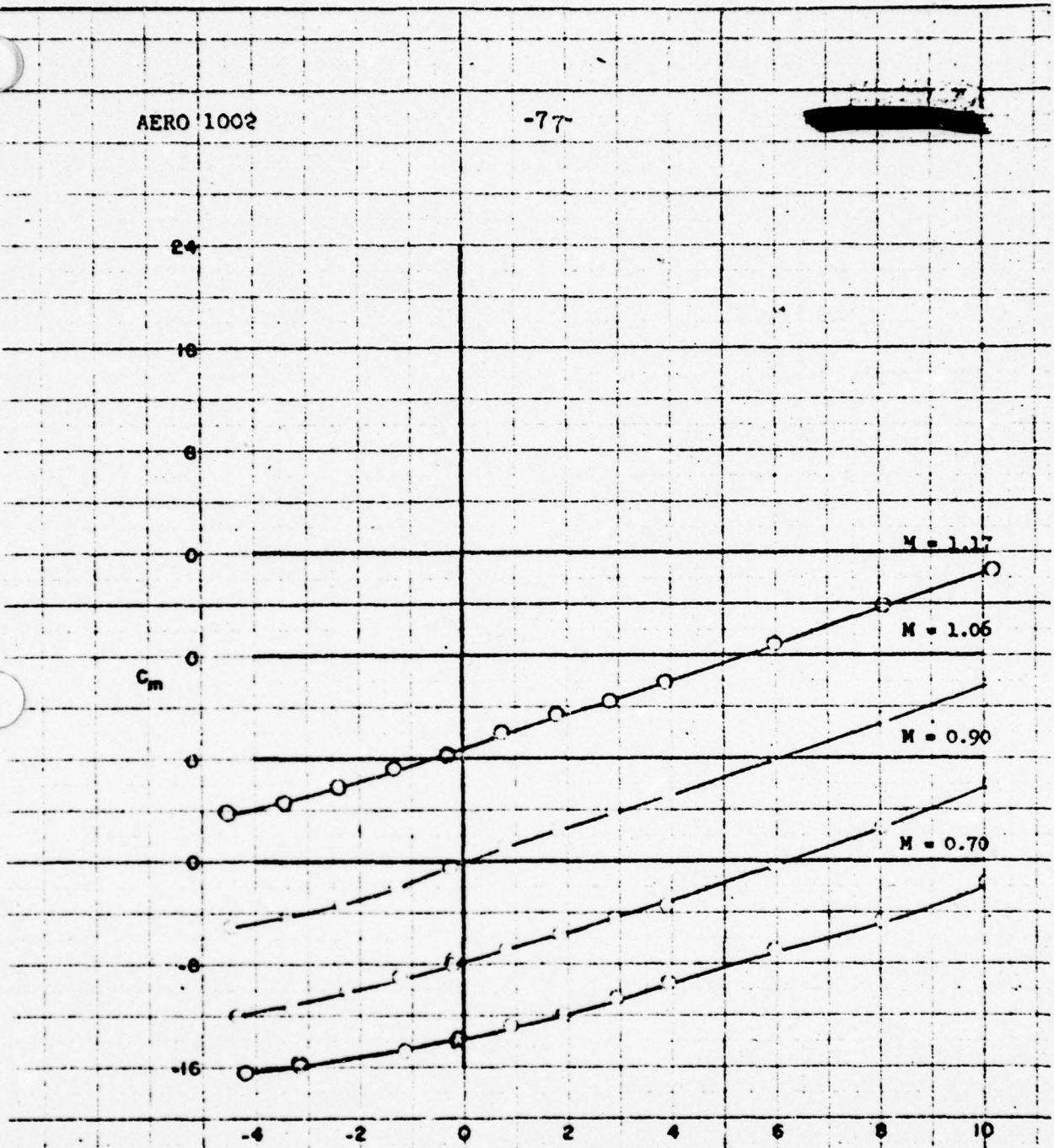

Figure 11 (Continued)

(c) Concluded

[redacted]

FIGURE 11c (concl

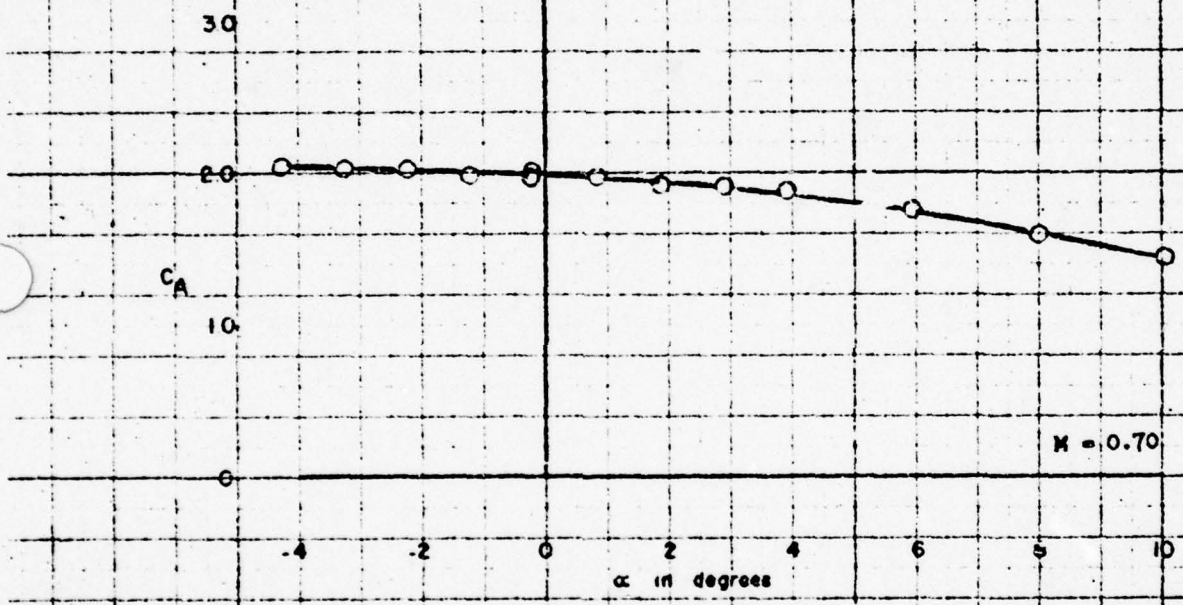

Figure 11 (Continued)

(d) $\phi = -45°$; $i = i' = -15°$; $\delta = \delta' = 0°$

[redacted]

FIGURE 11d

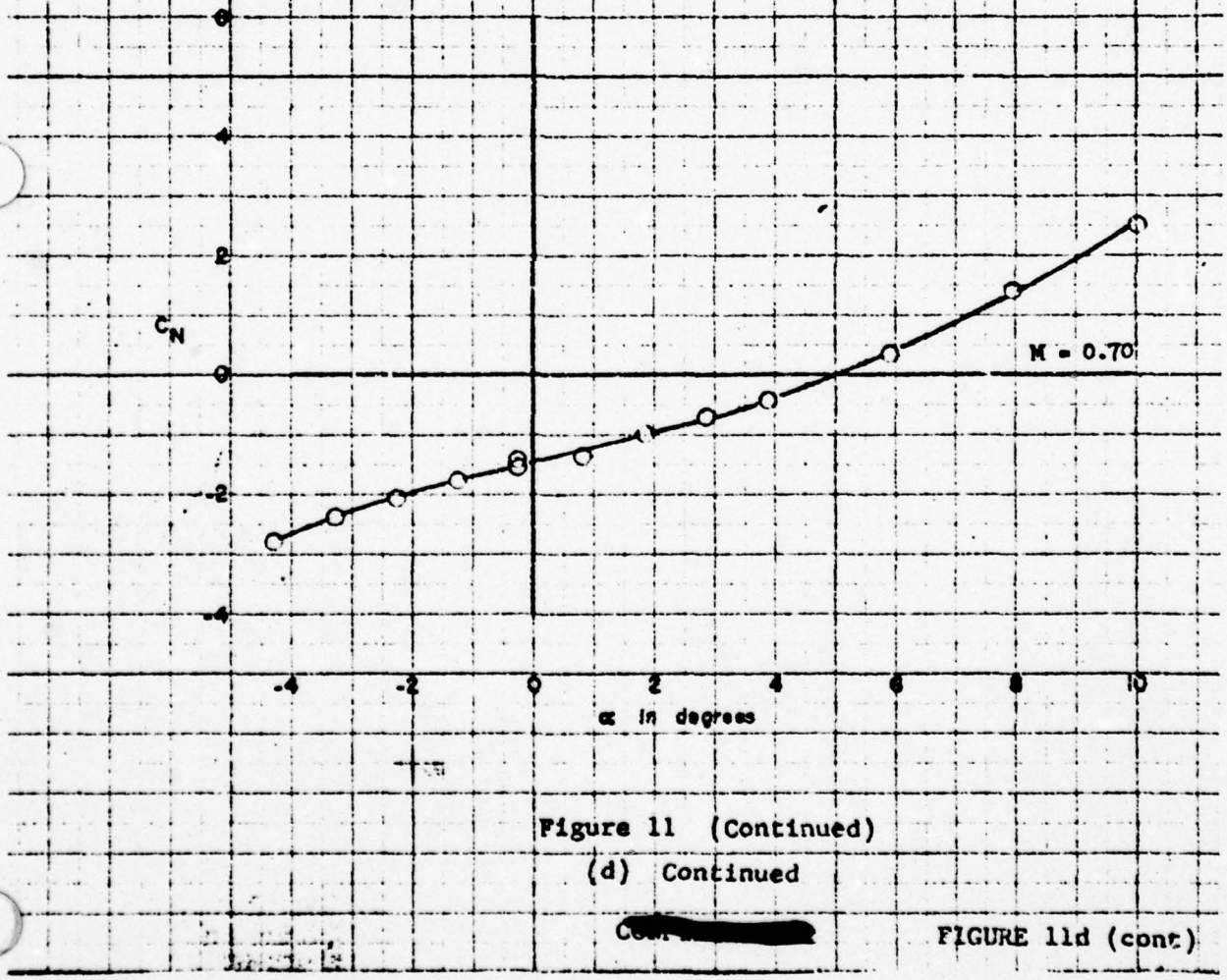

Figure 11 (Continued)

(d) Continued

[redacted]

FIGURE 11d (cont)

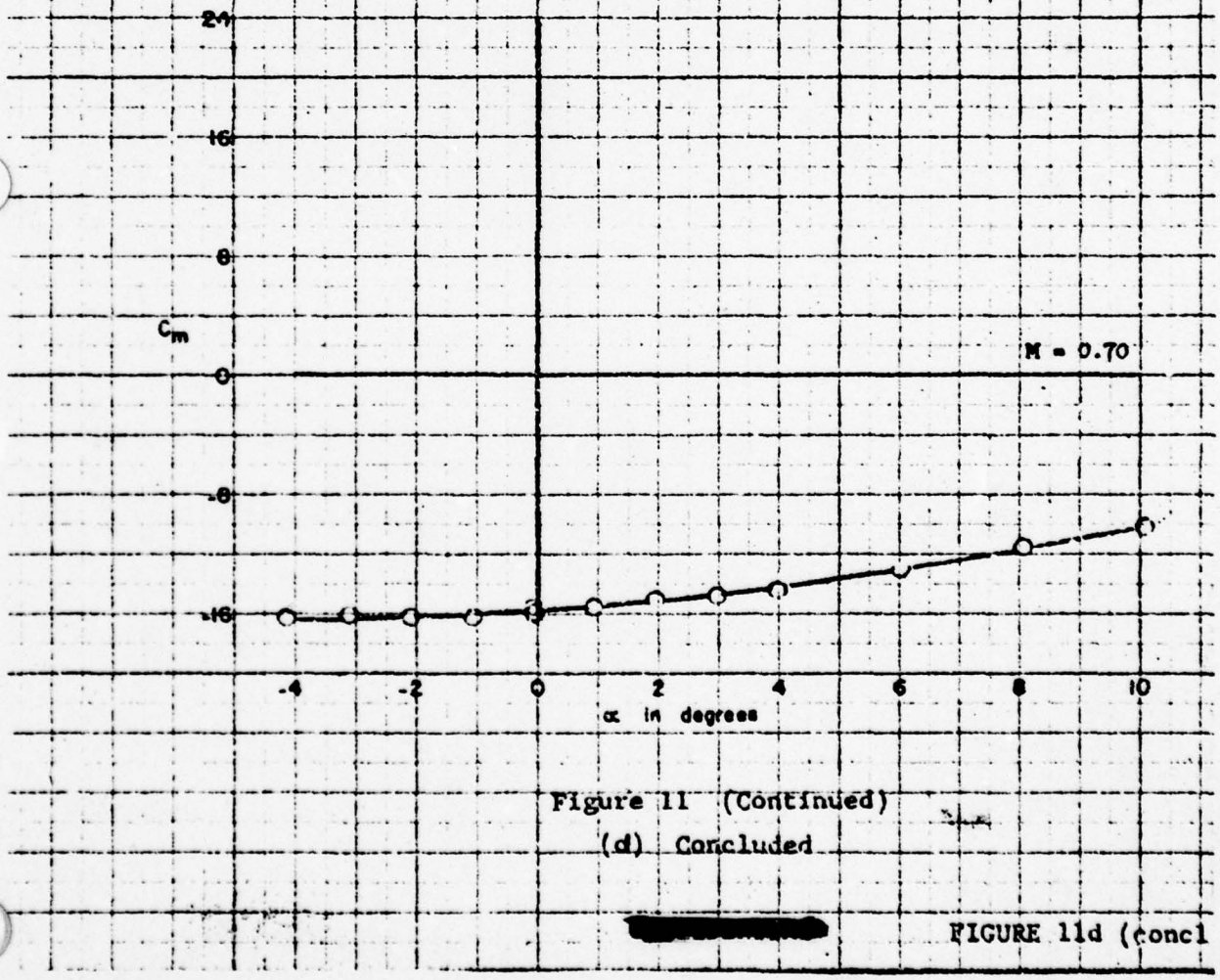

Figure 11 (Continued)
(d) Concluded

FIGURE 11d (concl

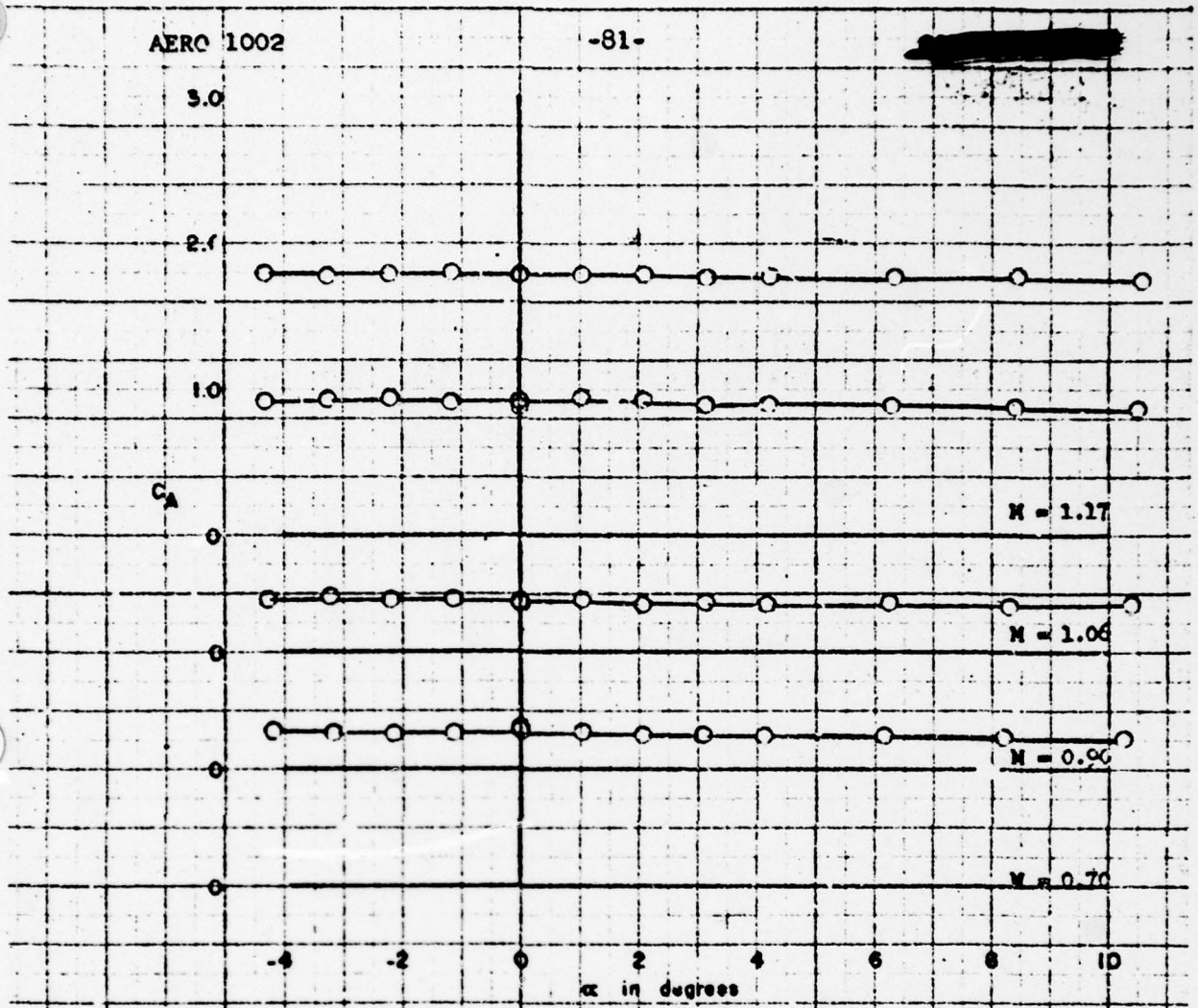

Figure 11 (Continued)

(e) ϕ=-45°; i=i'=0°; δ=δ'=5°

FIGURE 11e

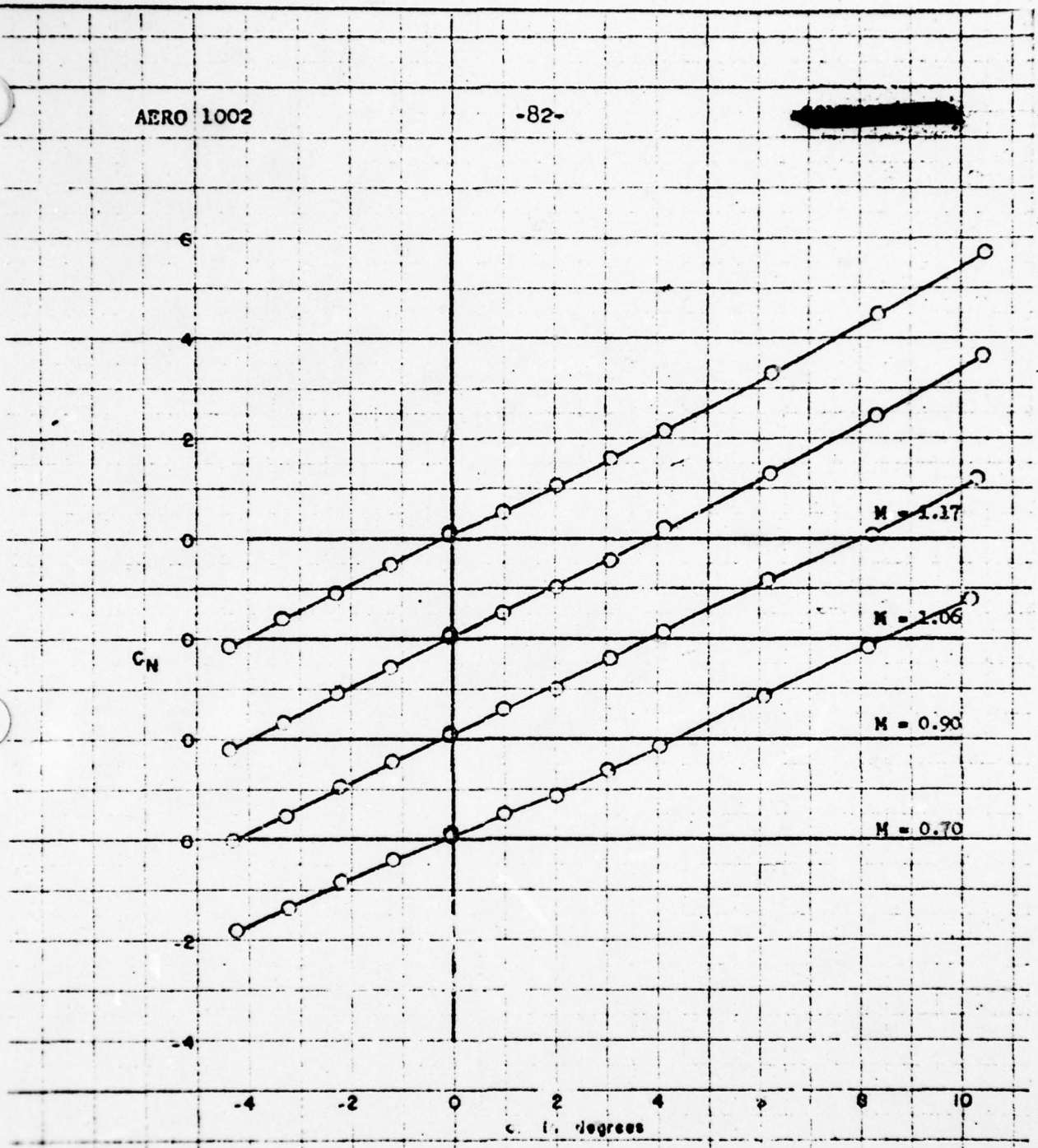

Figure 11 (Continued

(e) Continued

[redacted]

FIGURE 11e (cont)

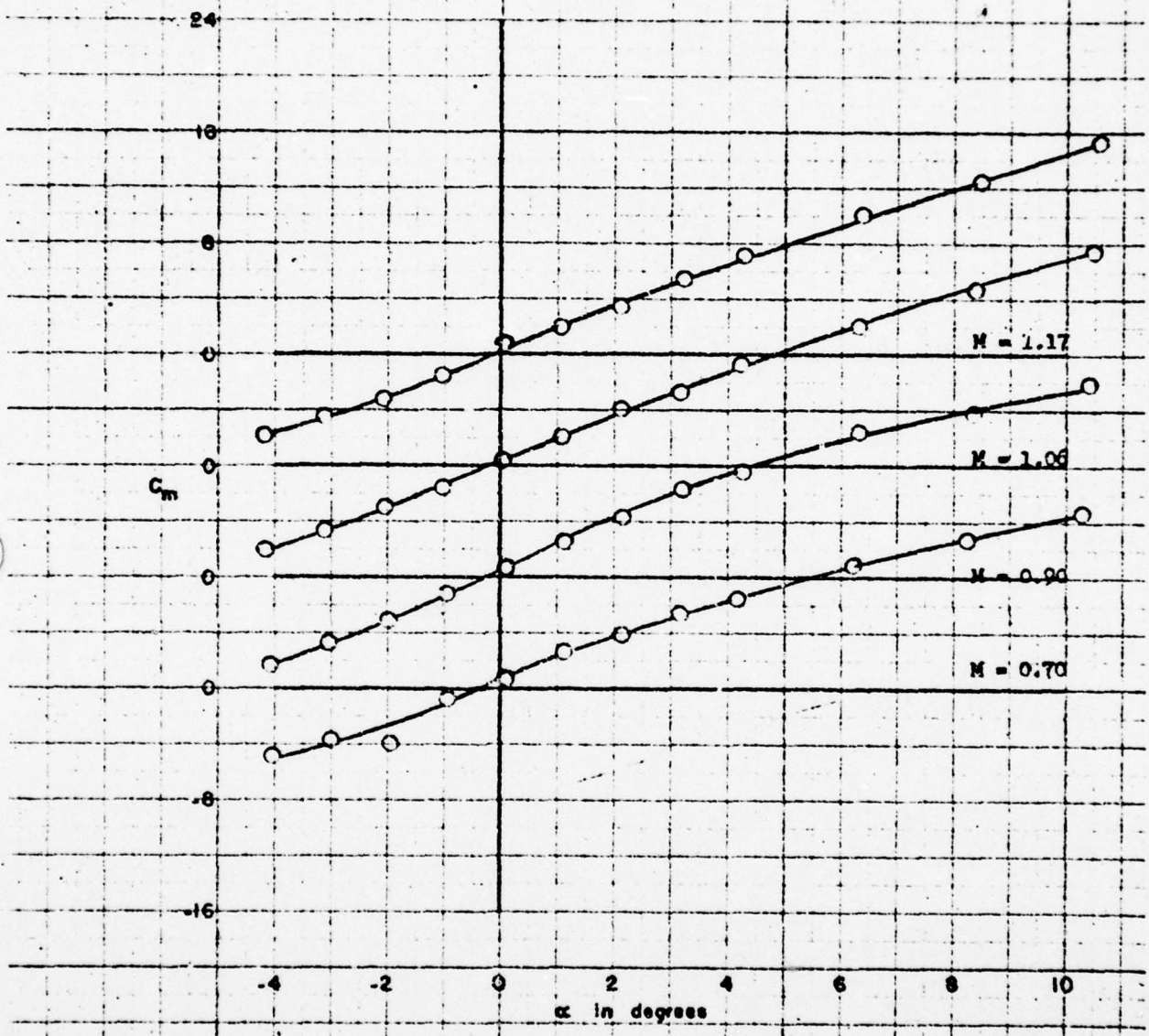

Figure 11 (Continued)

(e) Continued

[redacted] FIGURE 11e (cont)

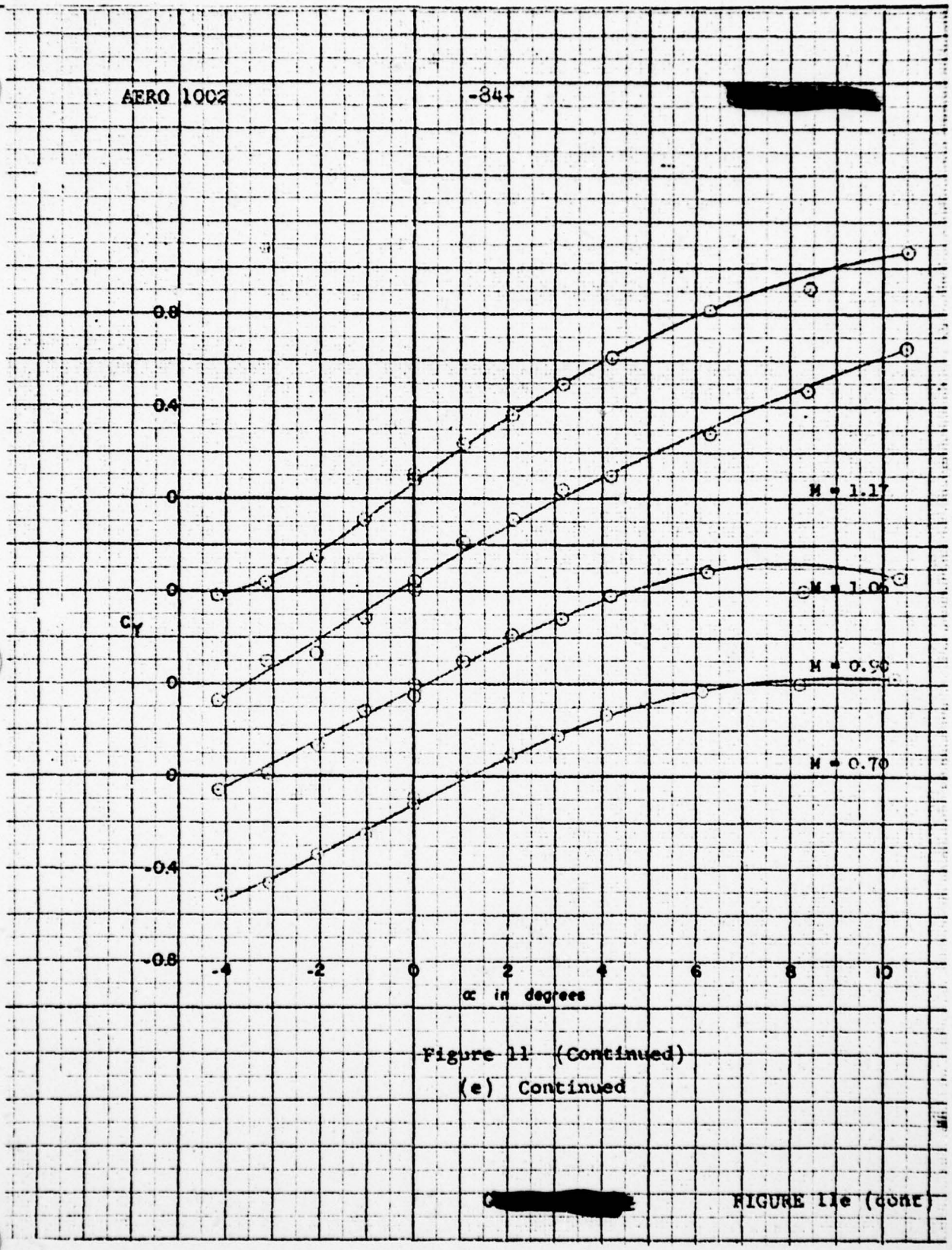

Figure 11 (Continued)

(e) Continued

[redacted]

FIGURE 11e (CONT)

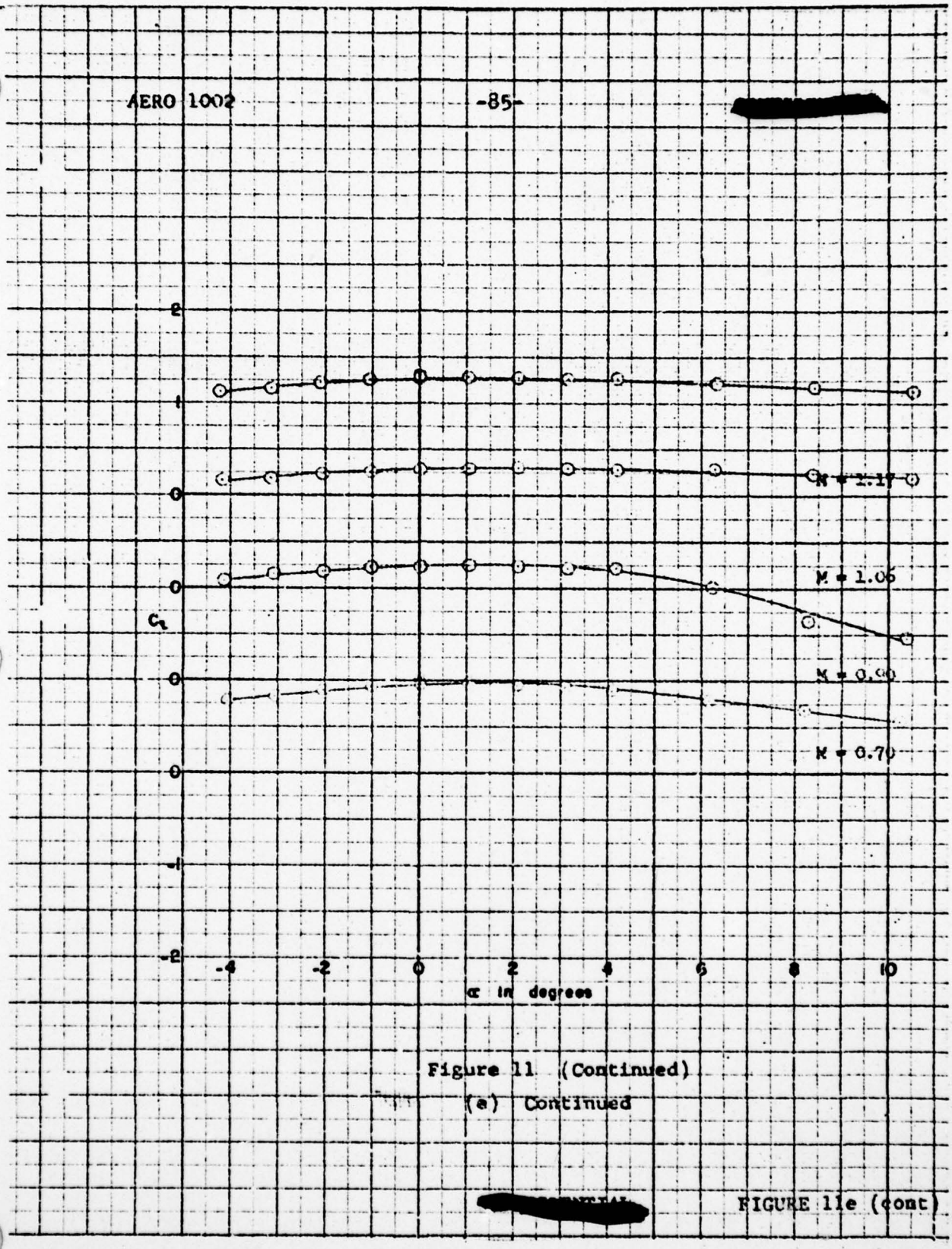

Figure 11 (Continued)
(e) Continued

[redacted]

FIGURE 11e (cont)

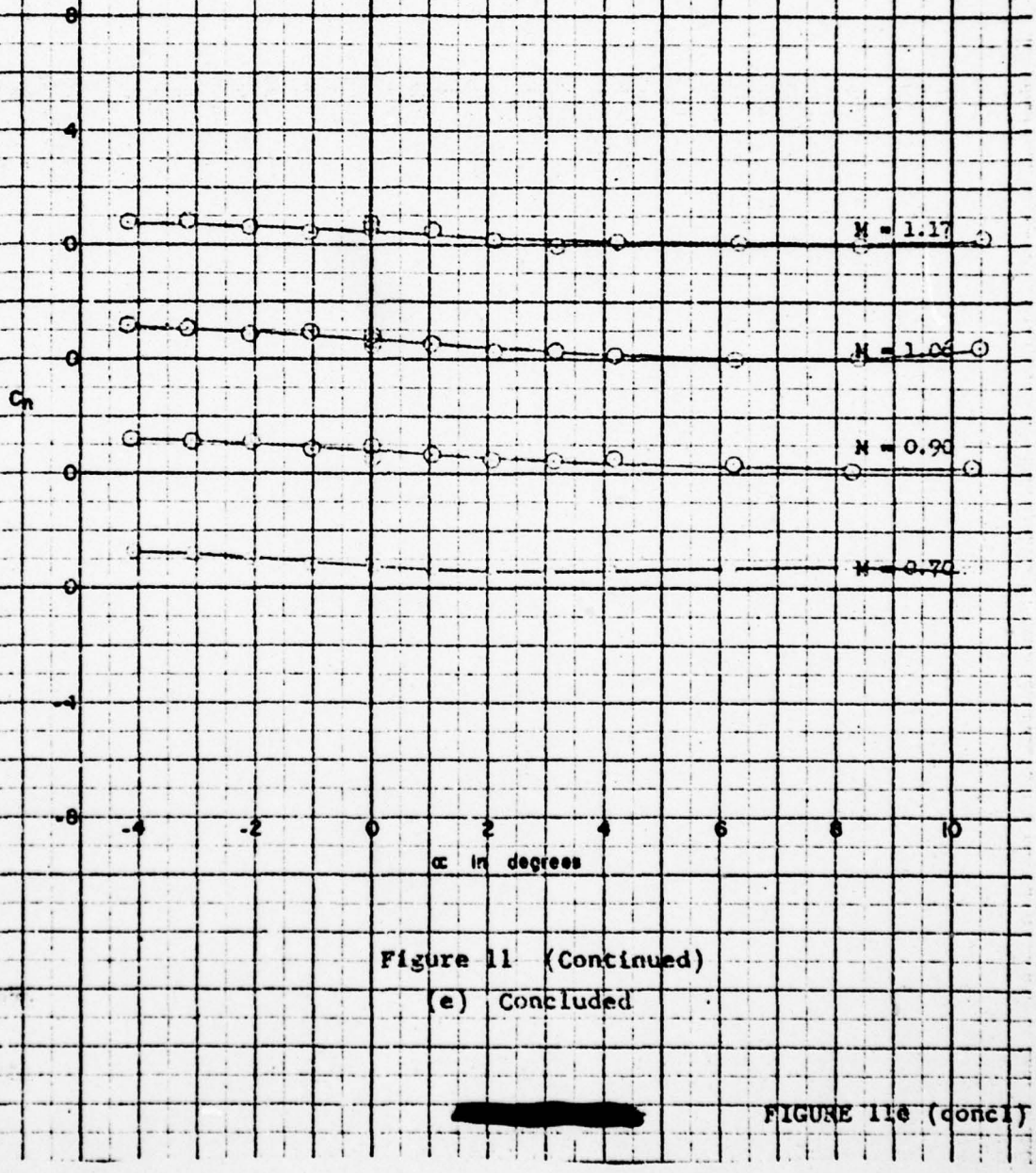

Figure 11 (Continued)
(e) Concluded

[redacted]

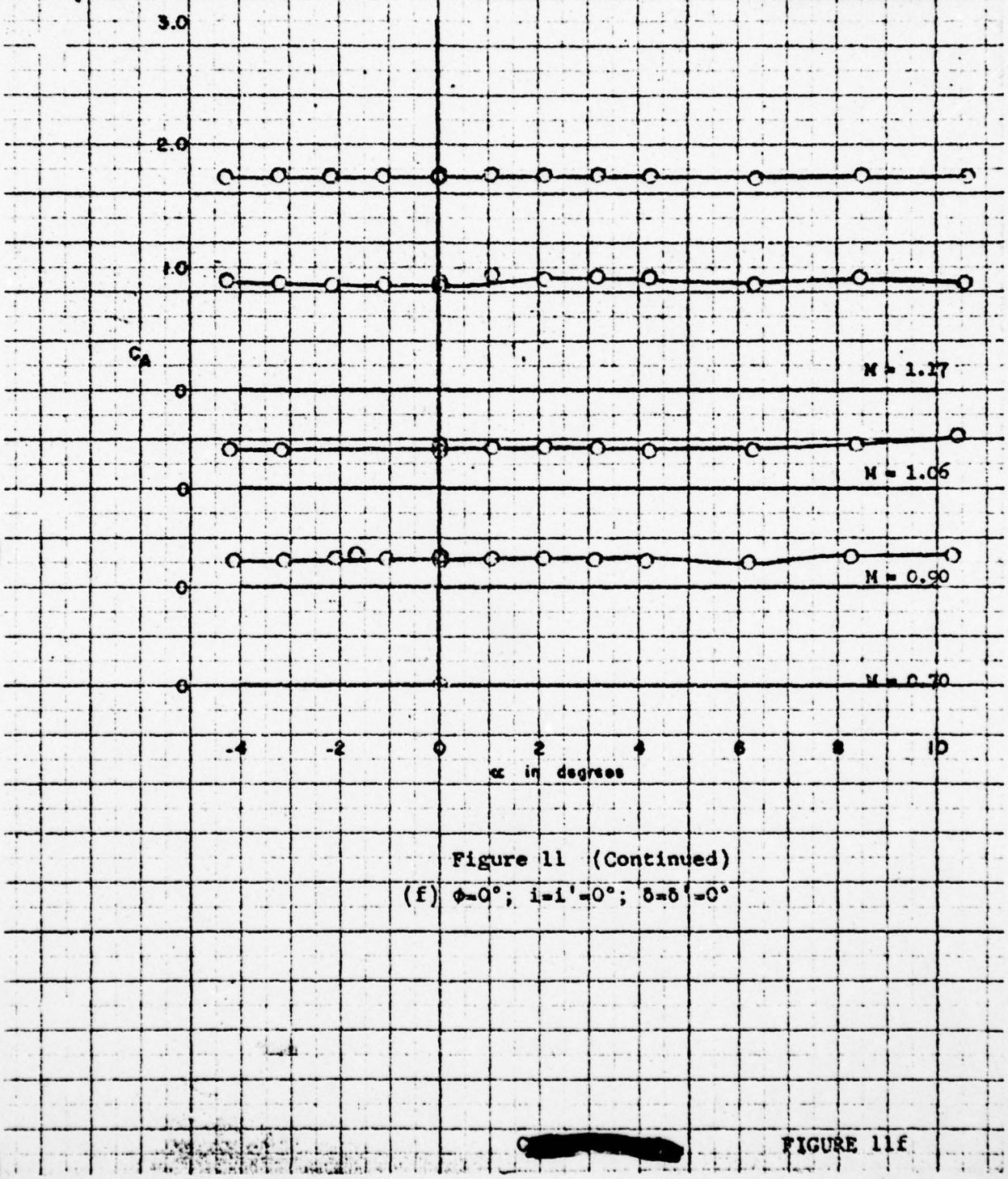

Figure 11 (Continued)

(f) $\phi=0°$; $i=i'=0°$; $\delta=\delta'=0°$

[redacted]

FIGURE 11f

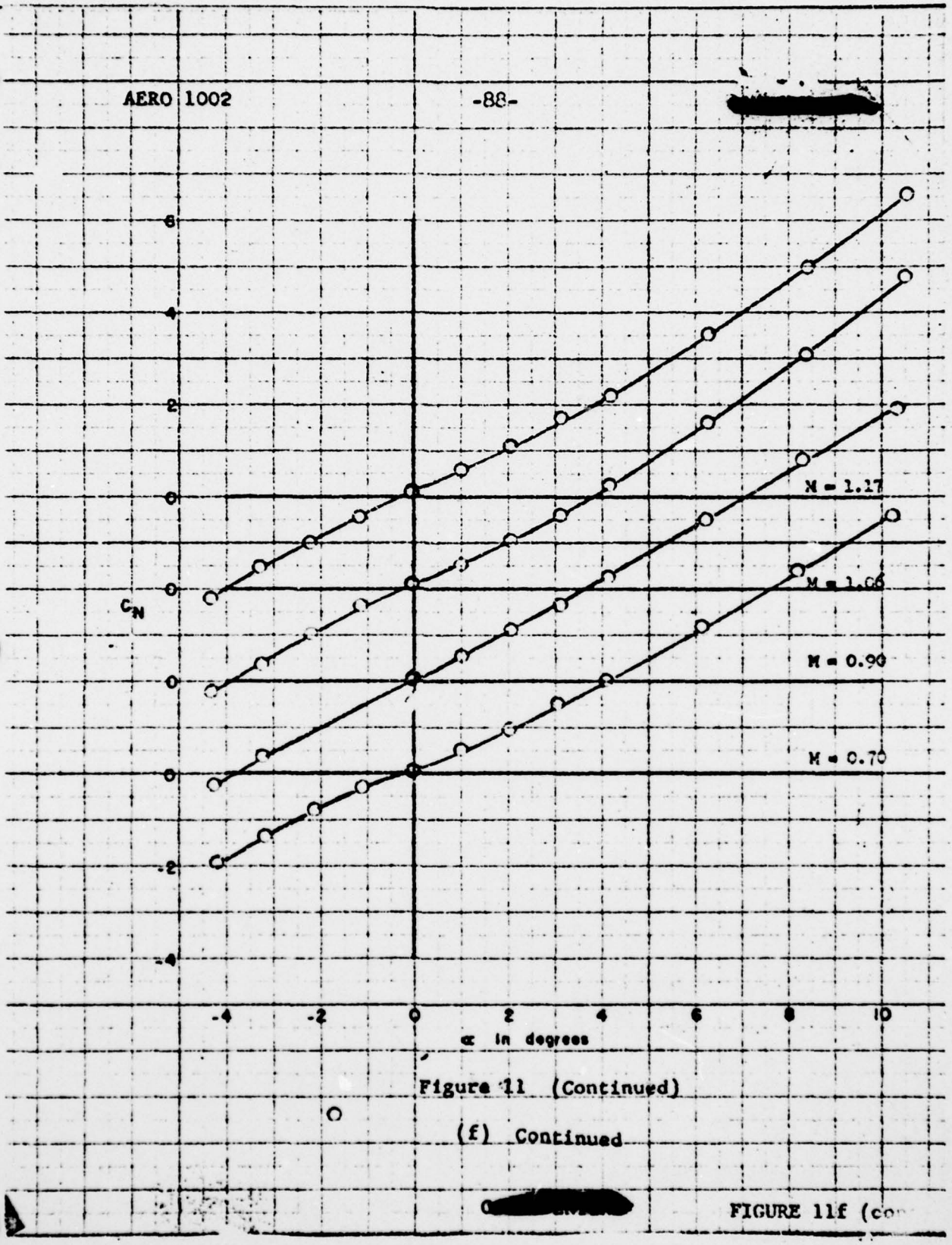

Figure 11 (Continued)

(f) Continued

[redacted]

FIGURE 11f (co

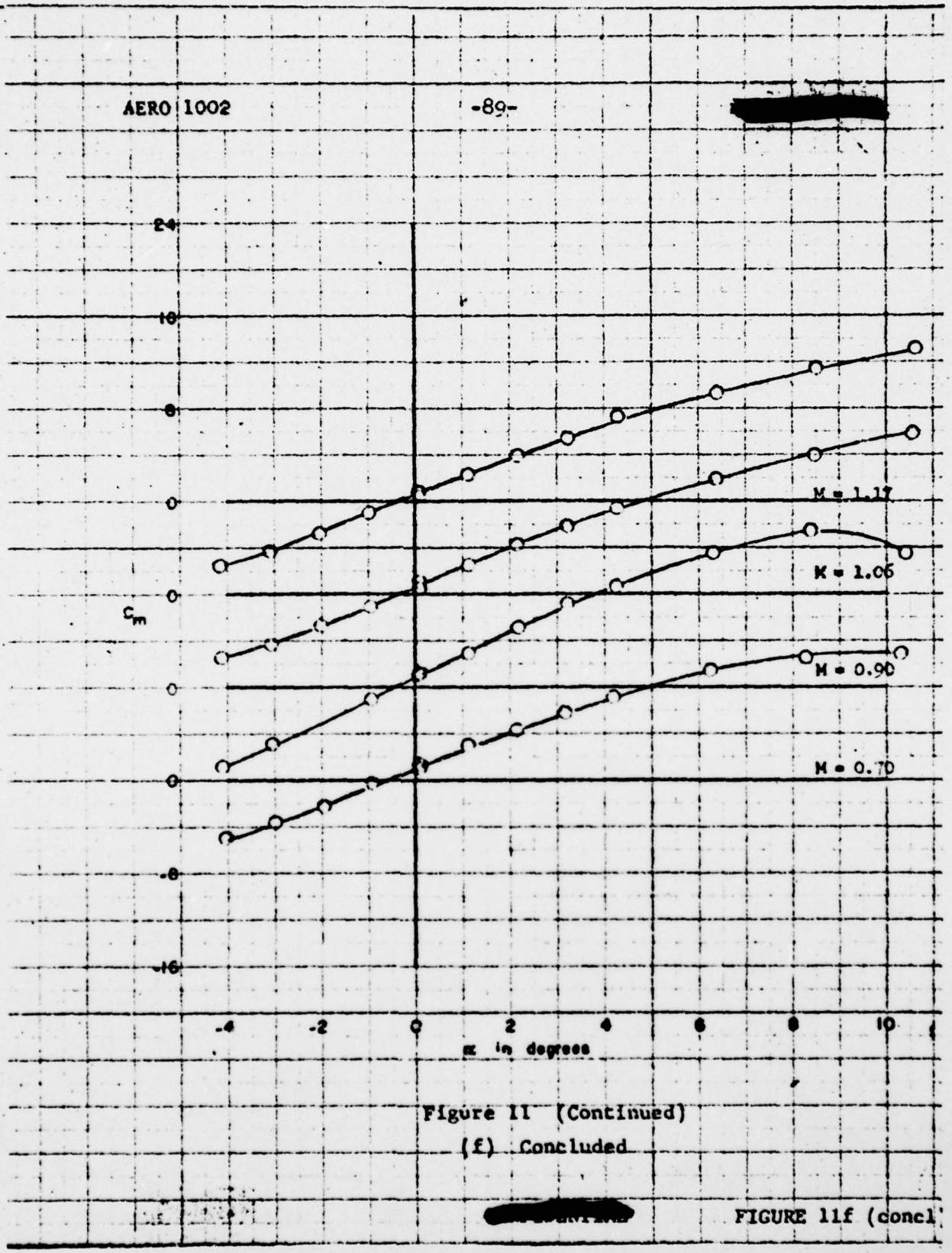

Figure 11 (Continued)

(f) Concluded

[redacted]

FIGURE 11f (concl

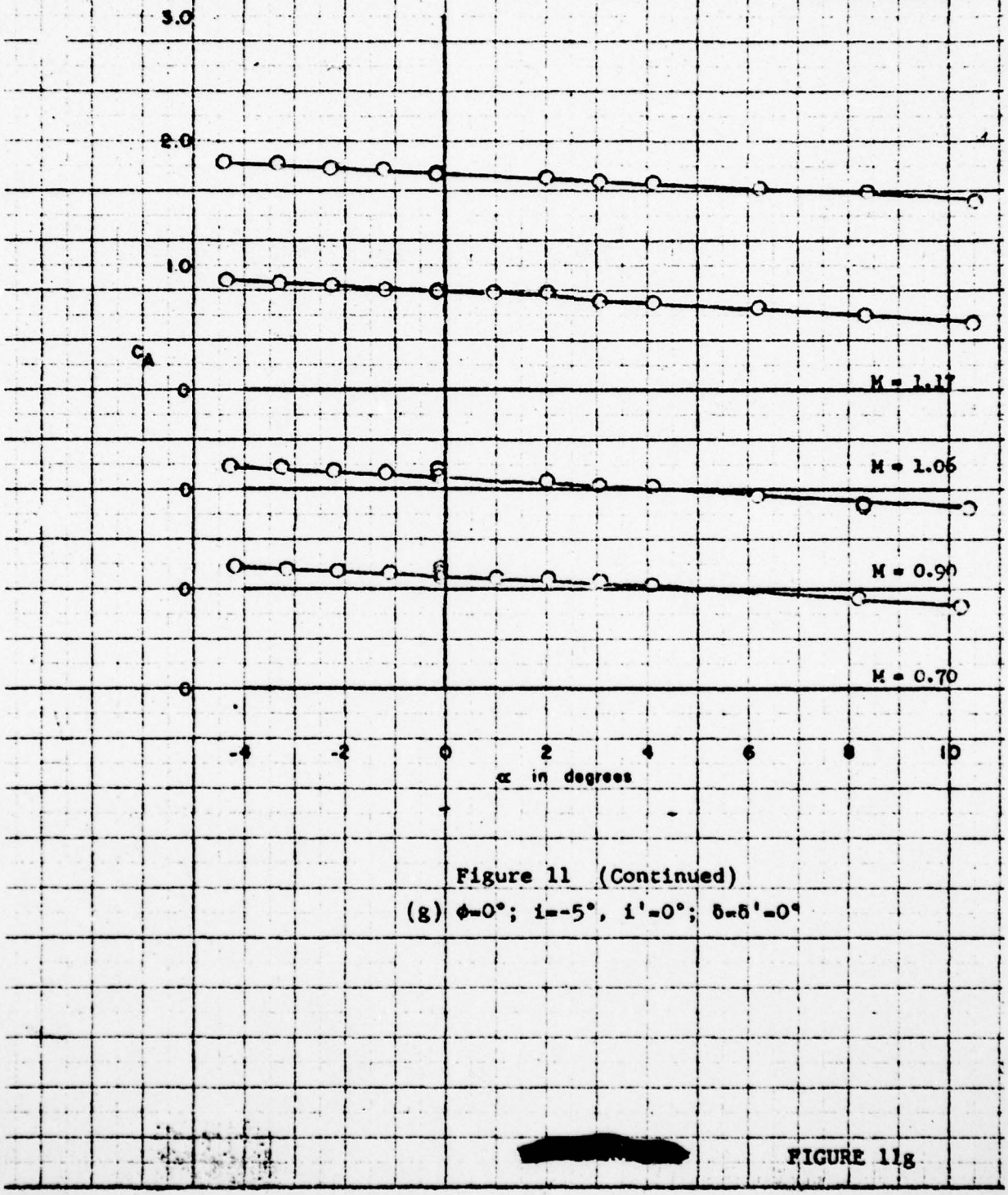

Figure 11 (Continued)

(g) ϕ=0°; i=-5°, i'=0°; δ=δ'=0°

FIGURE 11g

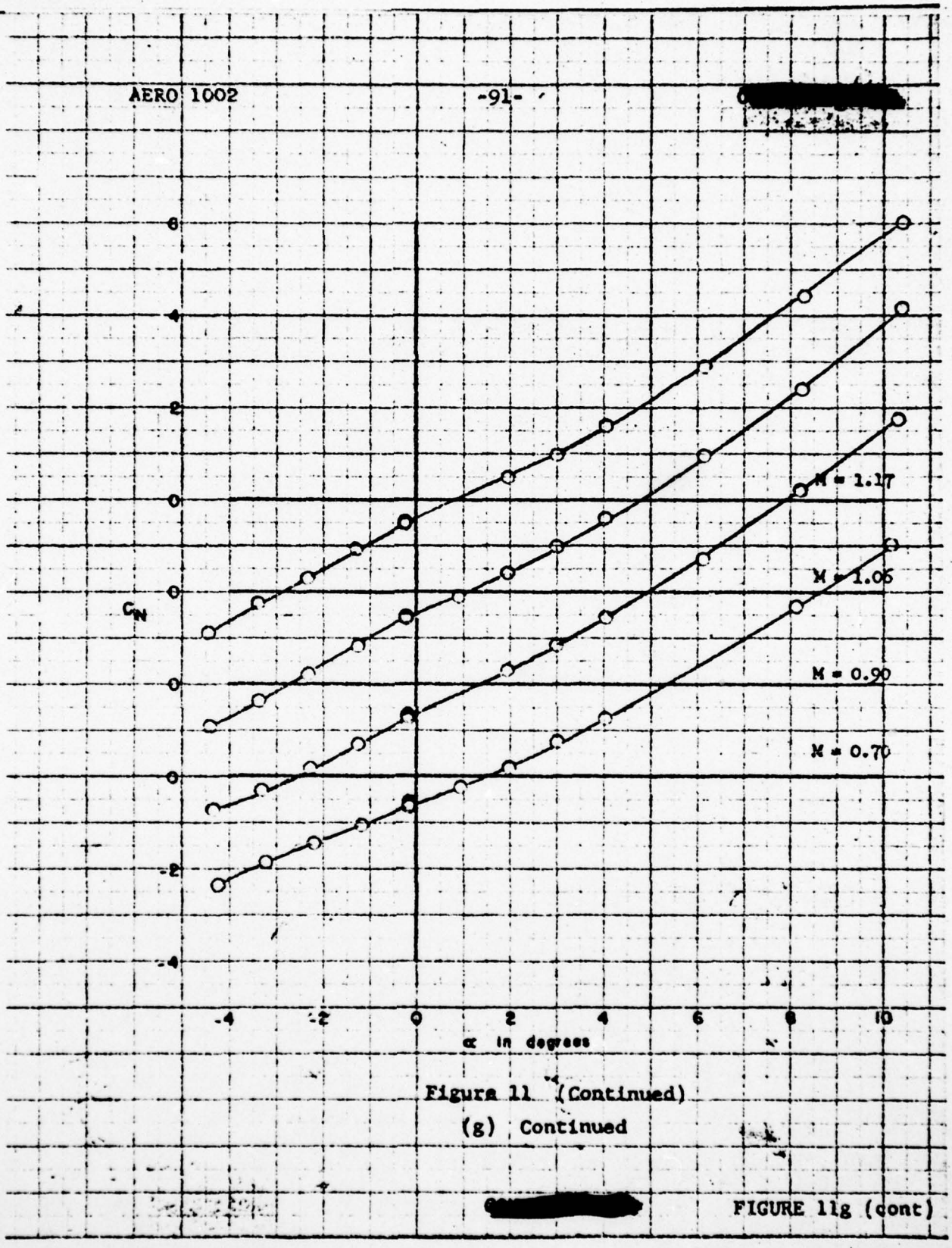

Figure 11 (Continued)

(g) Continued

[redacted]

FIGURE 11g (cont)

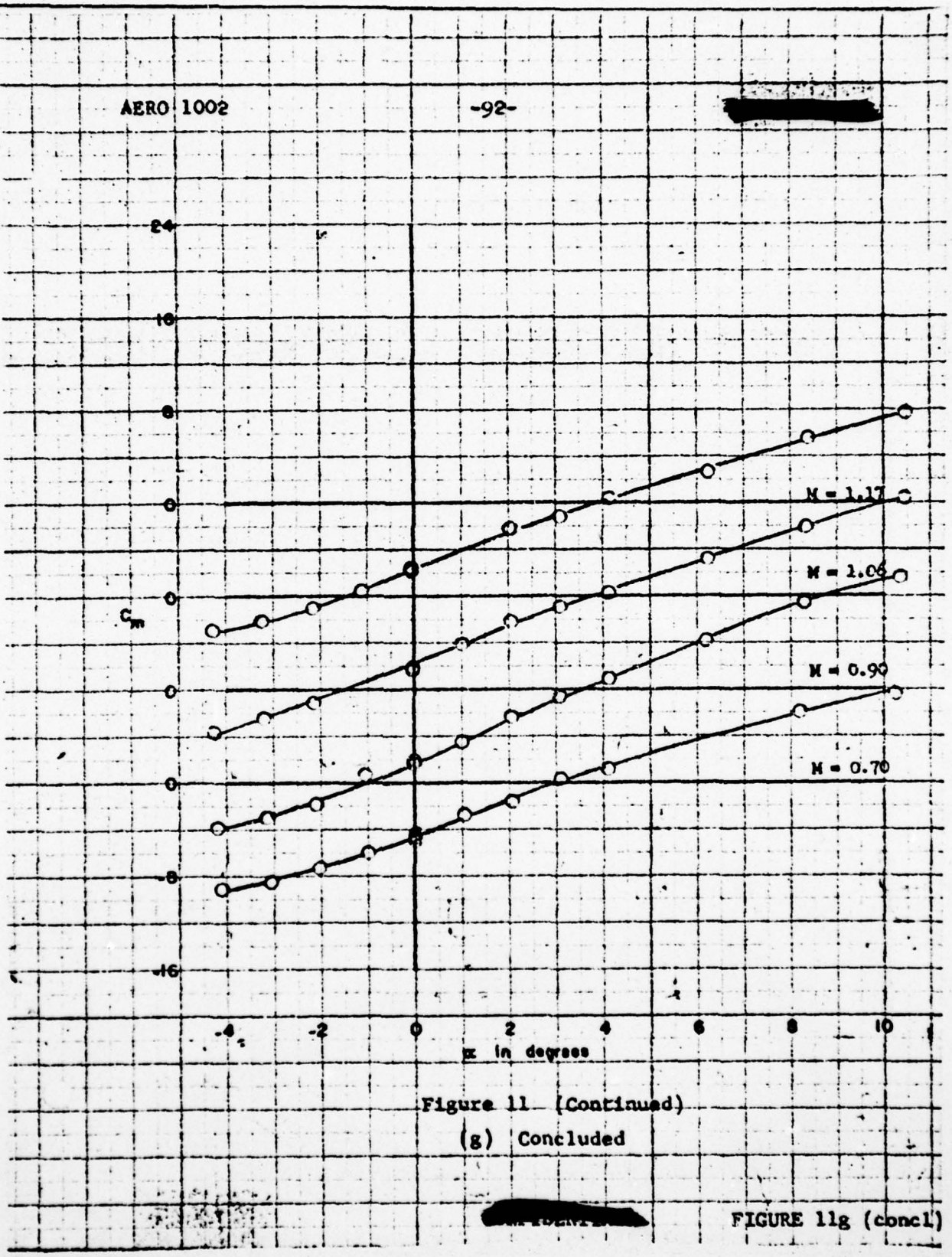

Figure 11 (Continued)

(g) Concluded

[redacted]

FIGURE 11g (concl)

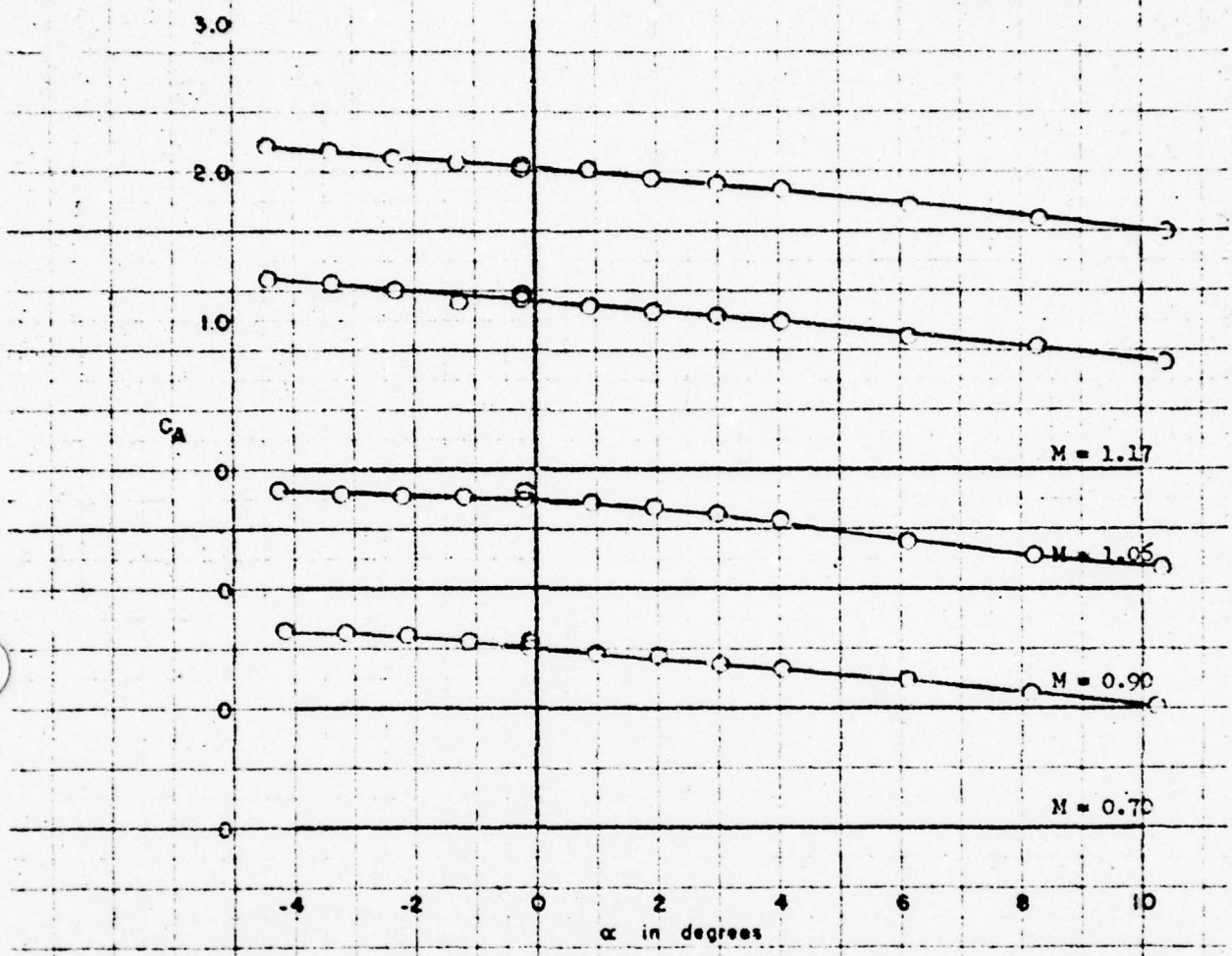

Figure 11 (Continued)

(h) ϕ=0°; i=-10°, i'=0°' δ=δ'=0°

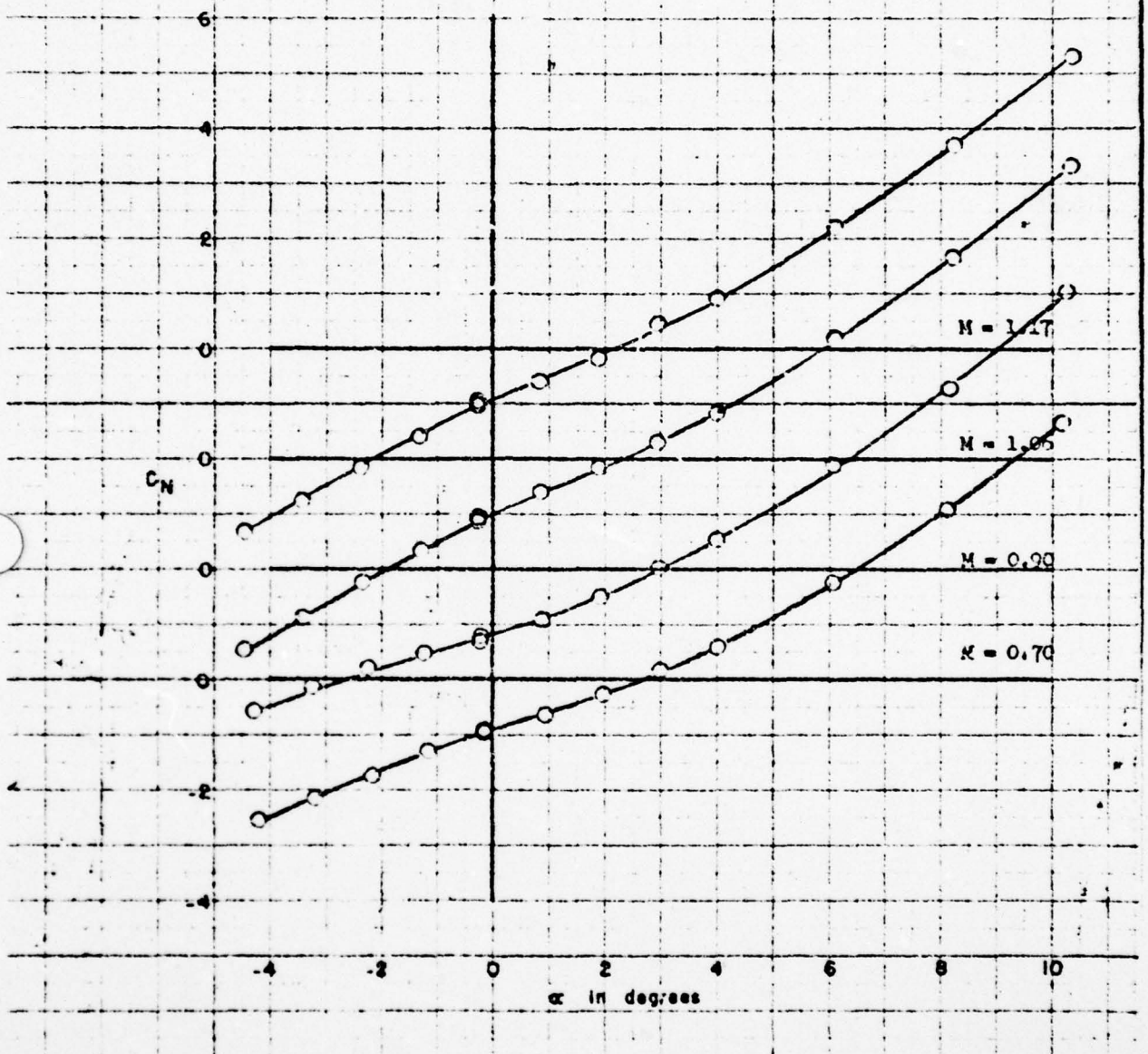

Figure 11 (Continued)

(h) Continued

FIGURE 11h (cont)

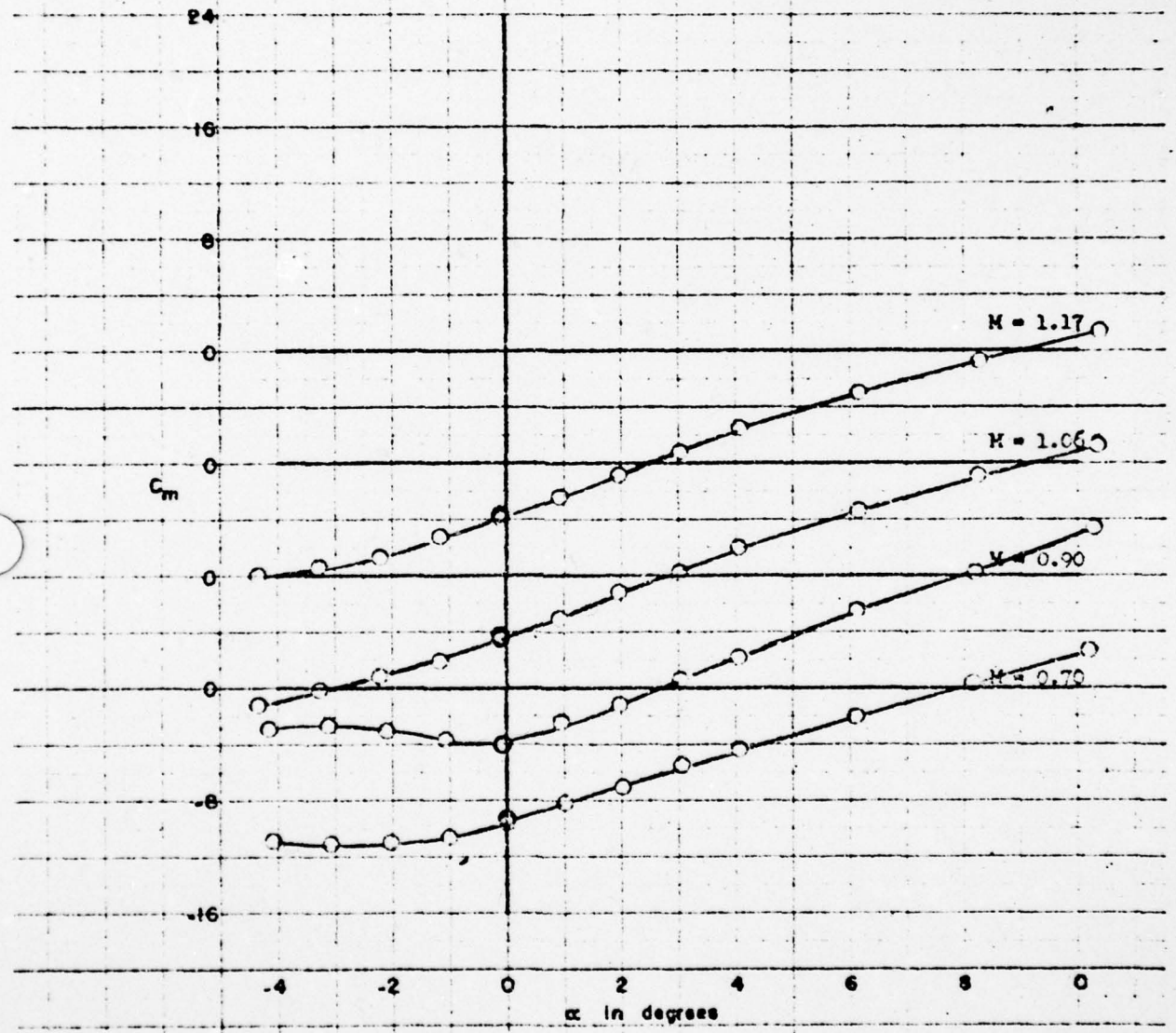

Figure 11 (Concluded)

(h) Concluded

[redacted]

FIGURE 11h (concl)

AD-A062 289 DAVID TAYLOR MODEL BASIN WASHINGTON D C AERODYNAMICS LAB F/G 16/4.2
TRANSONIC WIND-TUNNEL TESTS OF A 1/15-SCALE MODEL OF THE TALOS --ETC(U)
MAR 61 M E MCDONALD

UNCLASSIFIED AERO-1002 NL

2 OF 3
ADA
062289

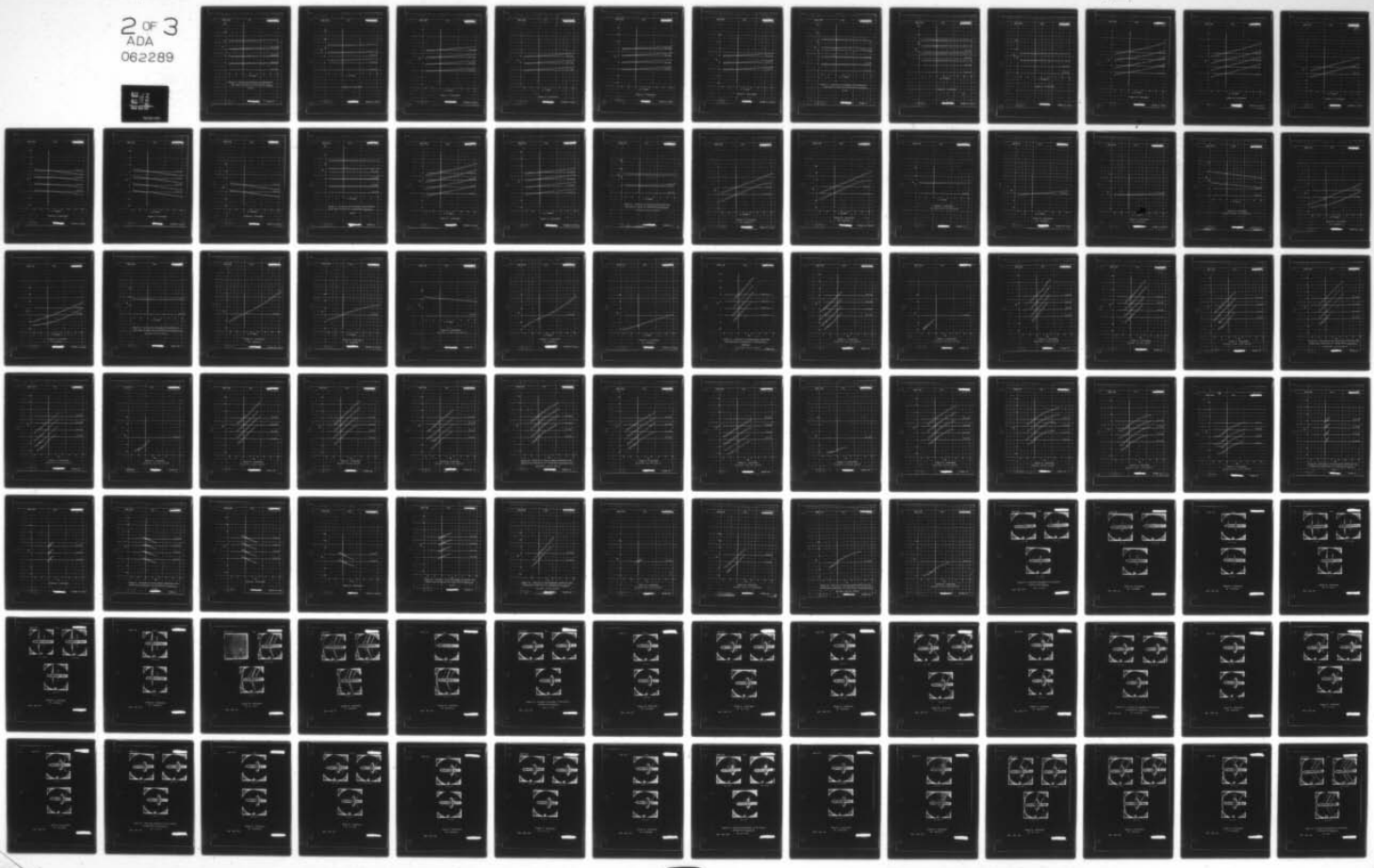

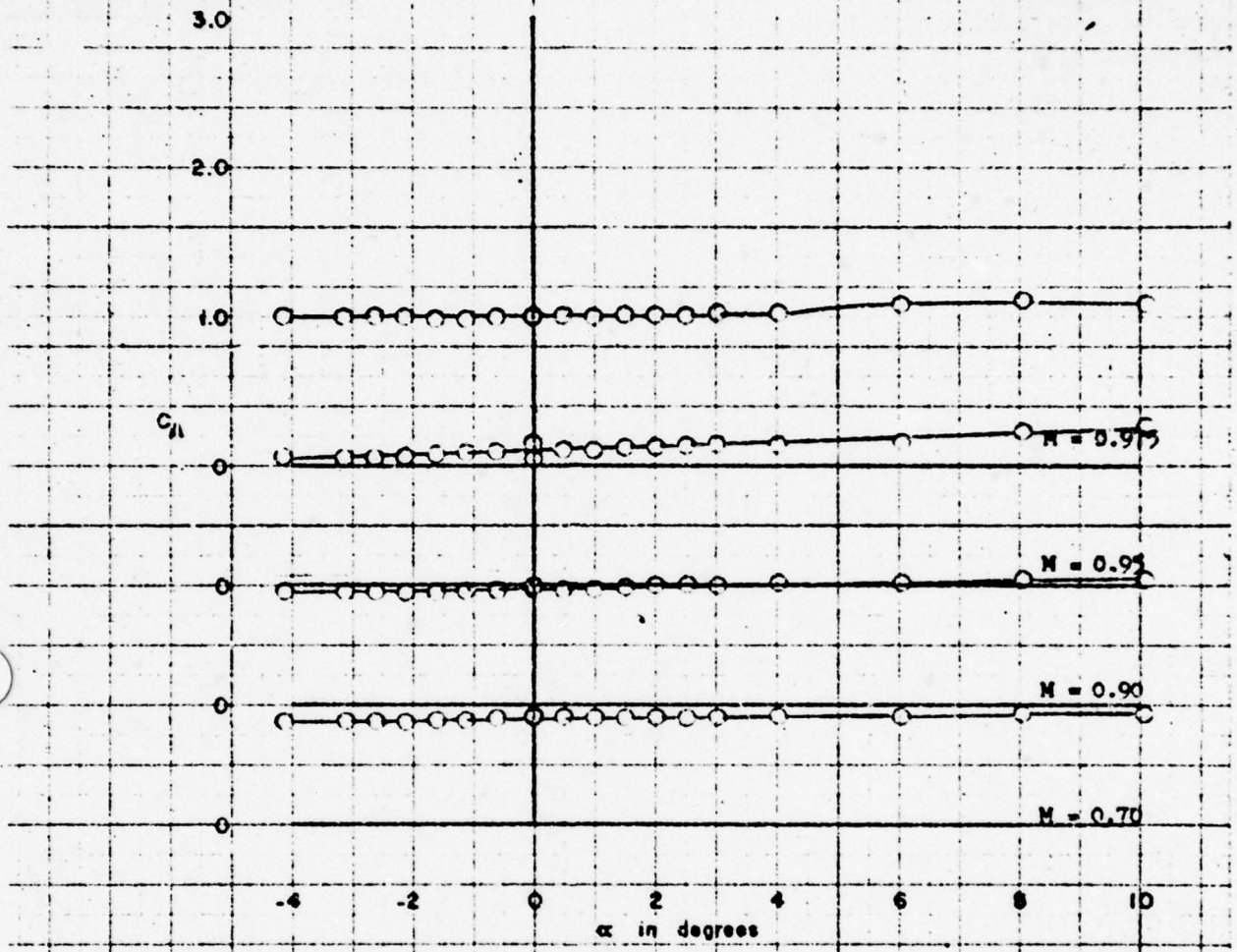

Figure 12 - Variation of Aerodynamic Characteristics With Angle of Attack for Configuration $B_{22}R_5H_{10}$

$\phi = -45°$

[redacted] FIGURE 12

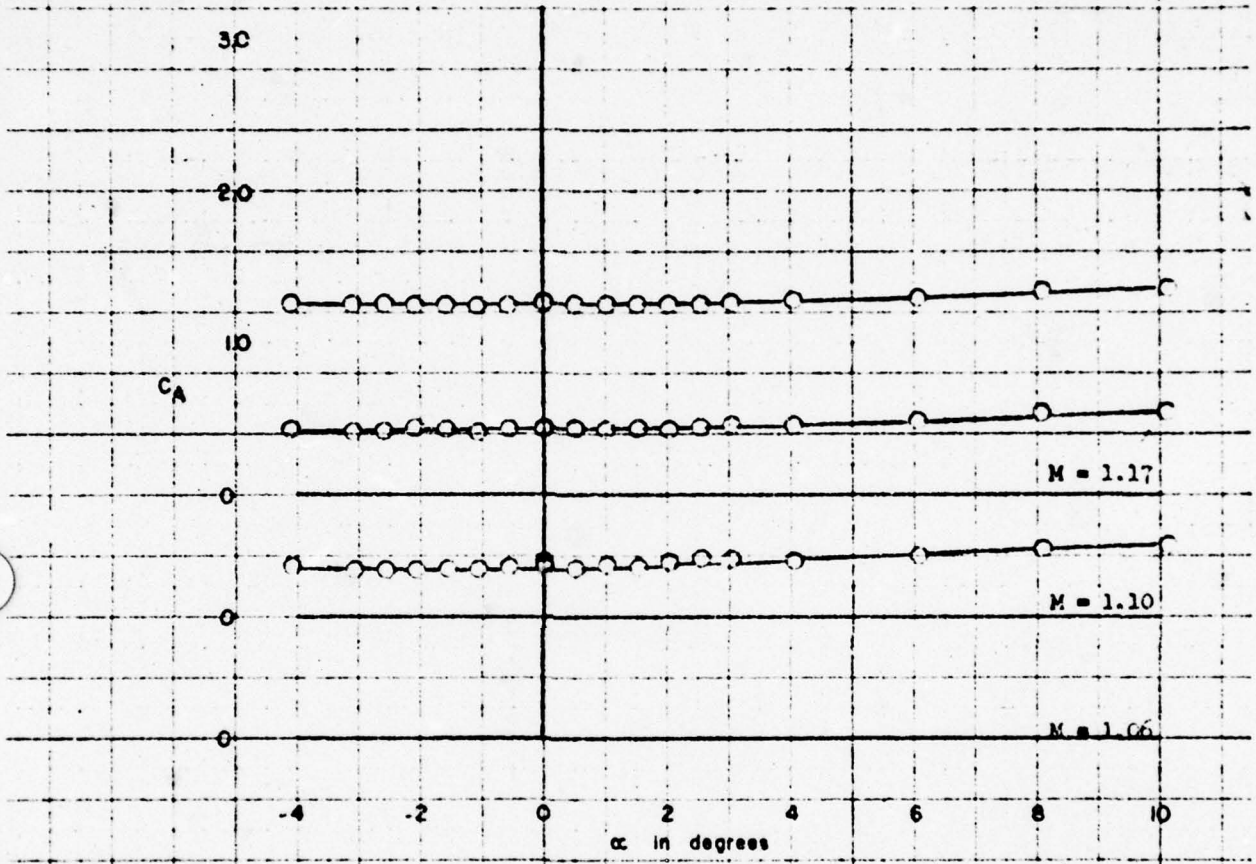

Figure 12 (Continued)

[redacted] FIGURE 12 (cont)

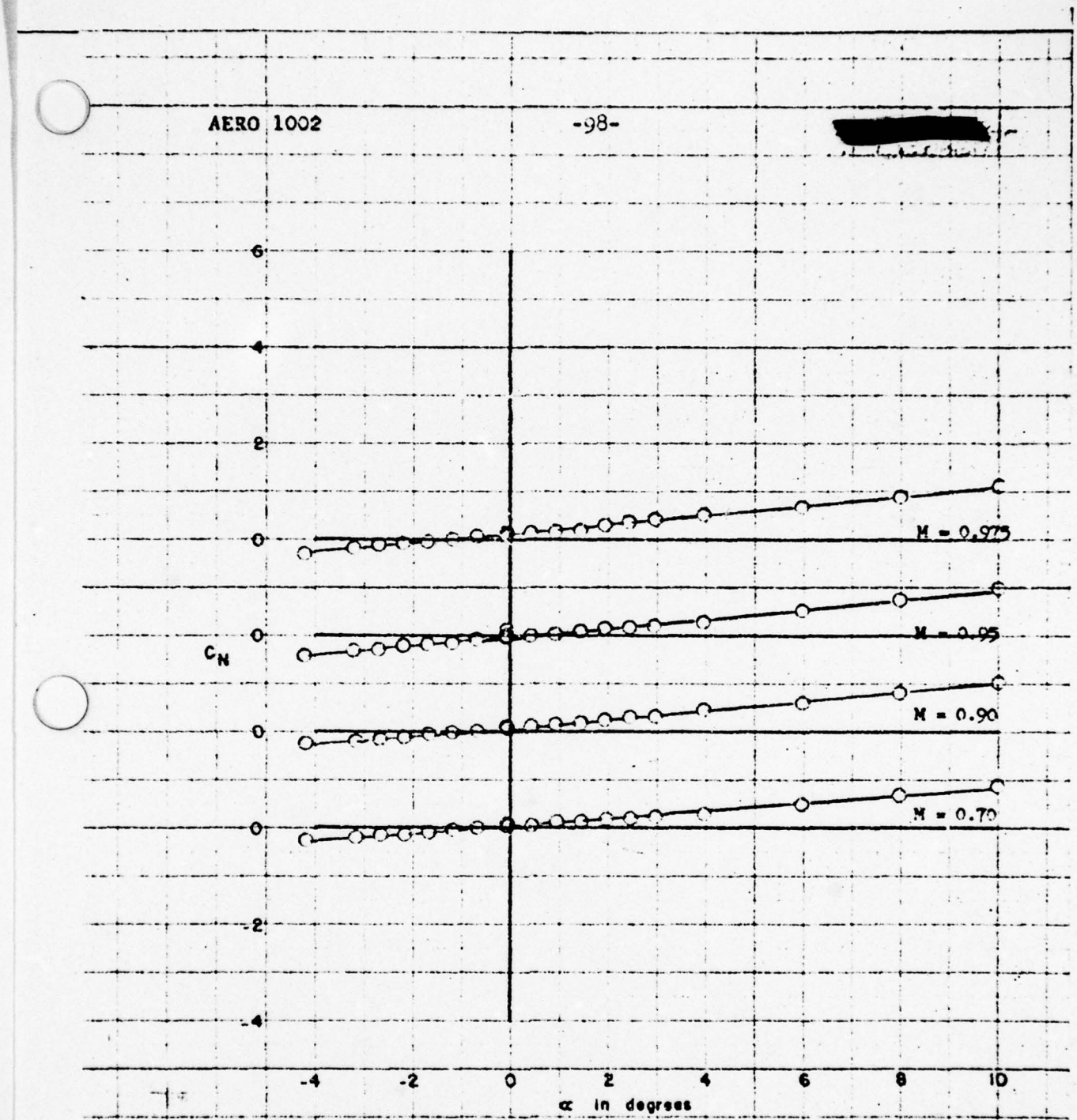

Figure 12 (Continued)

[redacted] FIGURE 12 (cont)

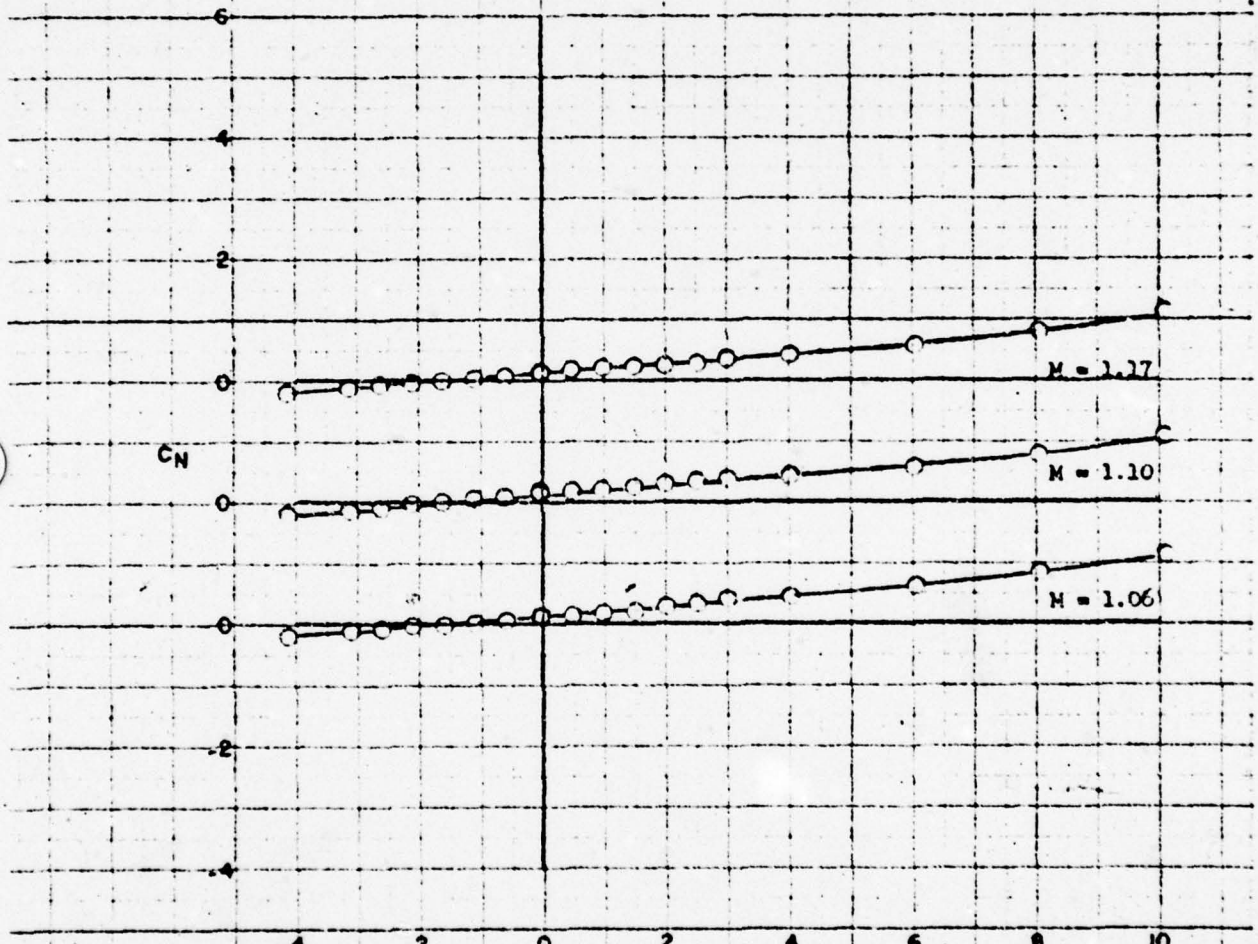

Figure 12 (Continued)

[redacted] FIGURE 12 (cont)

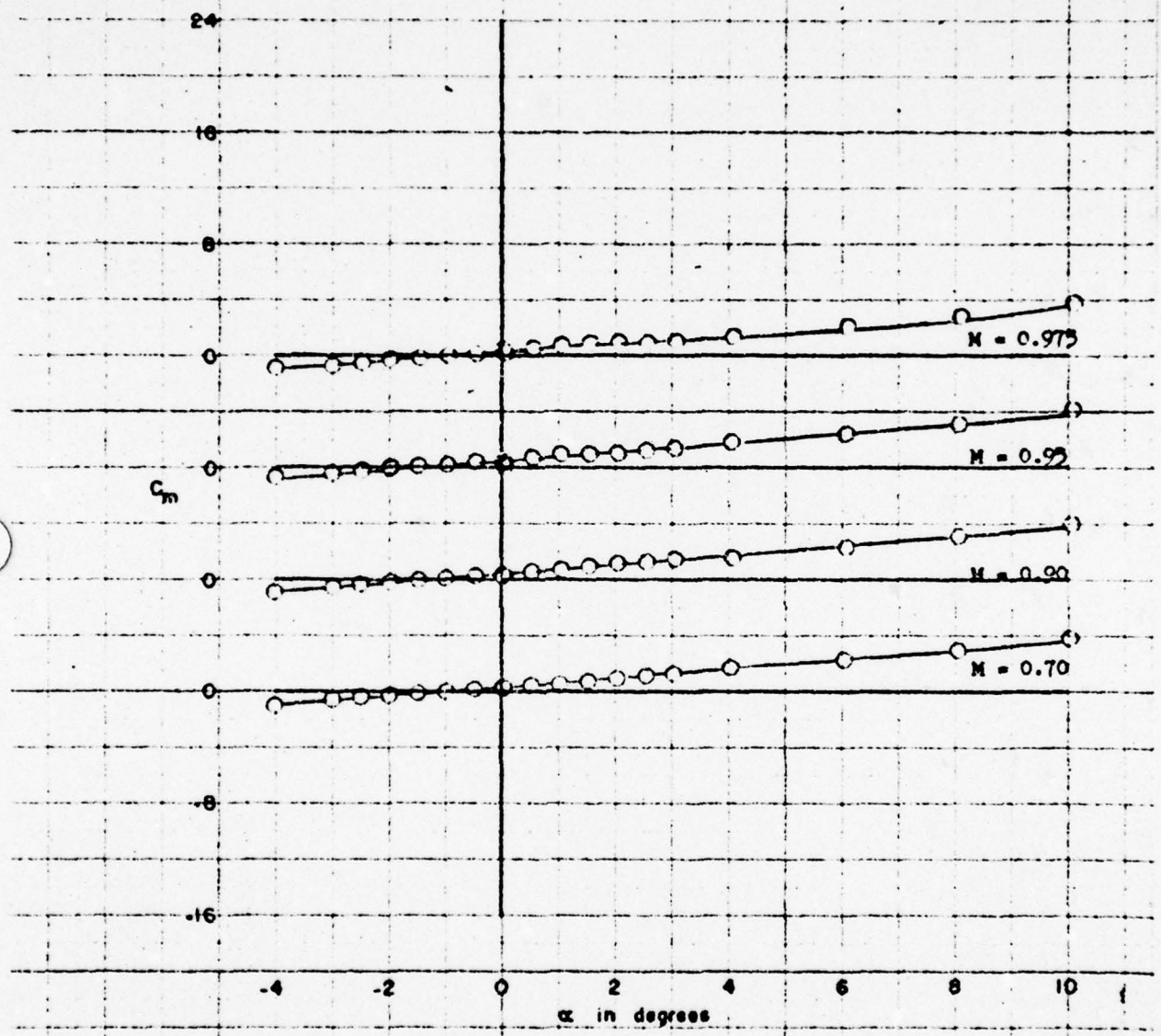

Figure 12 (Continued)

[redacted] FIGURE 12 (cont)

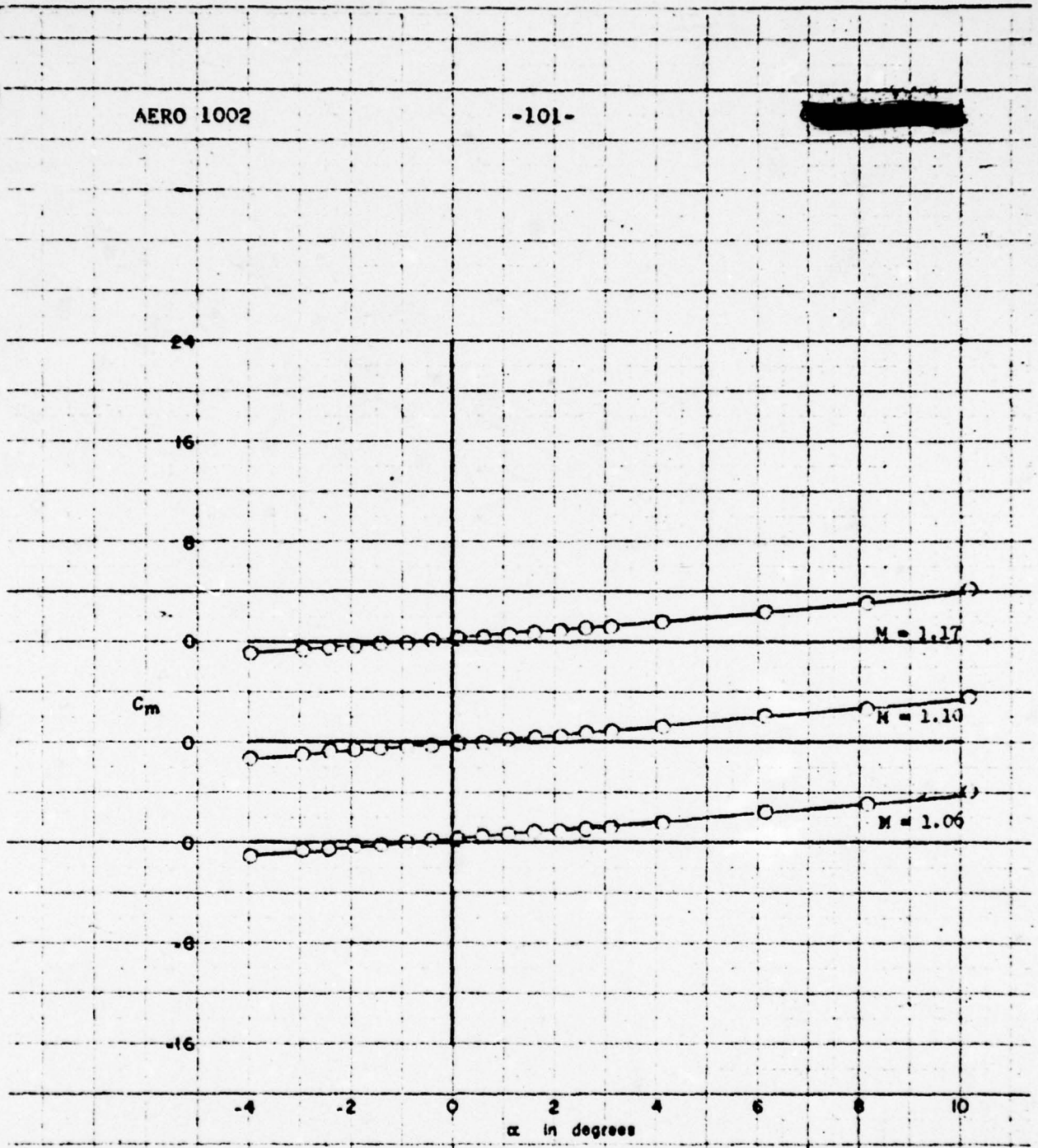

Figure 12 (Concluded)

FIGURE 12 (concl)

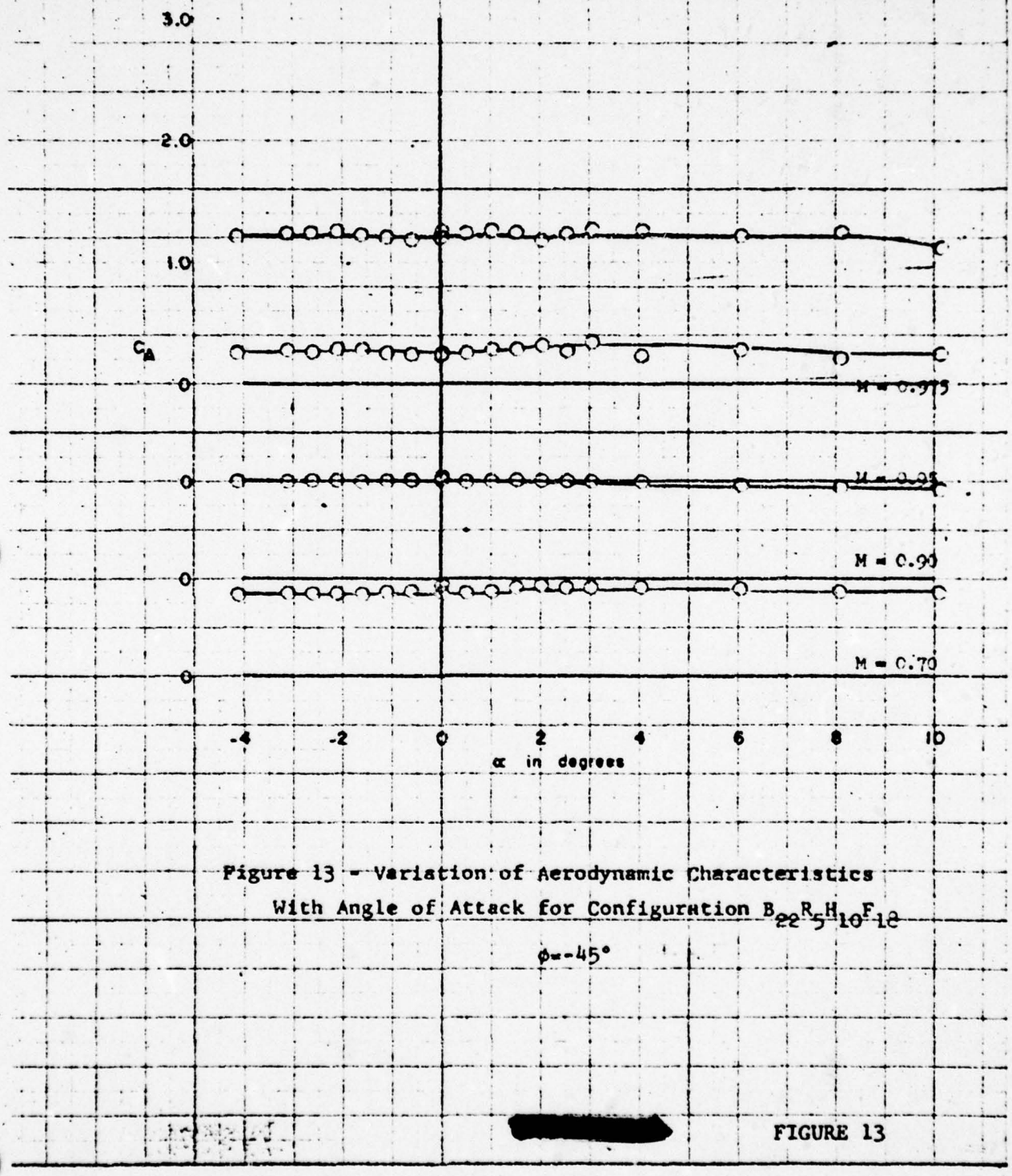

Figure 13 - Variation of Aerodynamic Characteristics With Angle of Attack for Configuration $B_{22}R_5H_{10}F_{18}$

ϕ=-45°

FIGURE 13

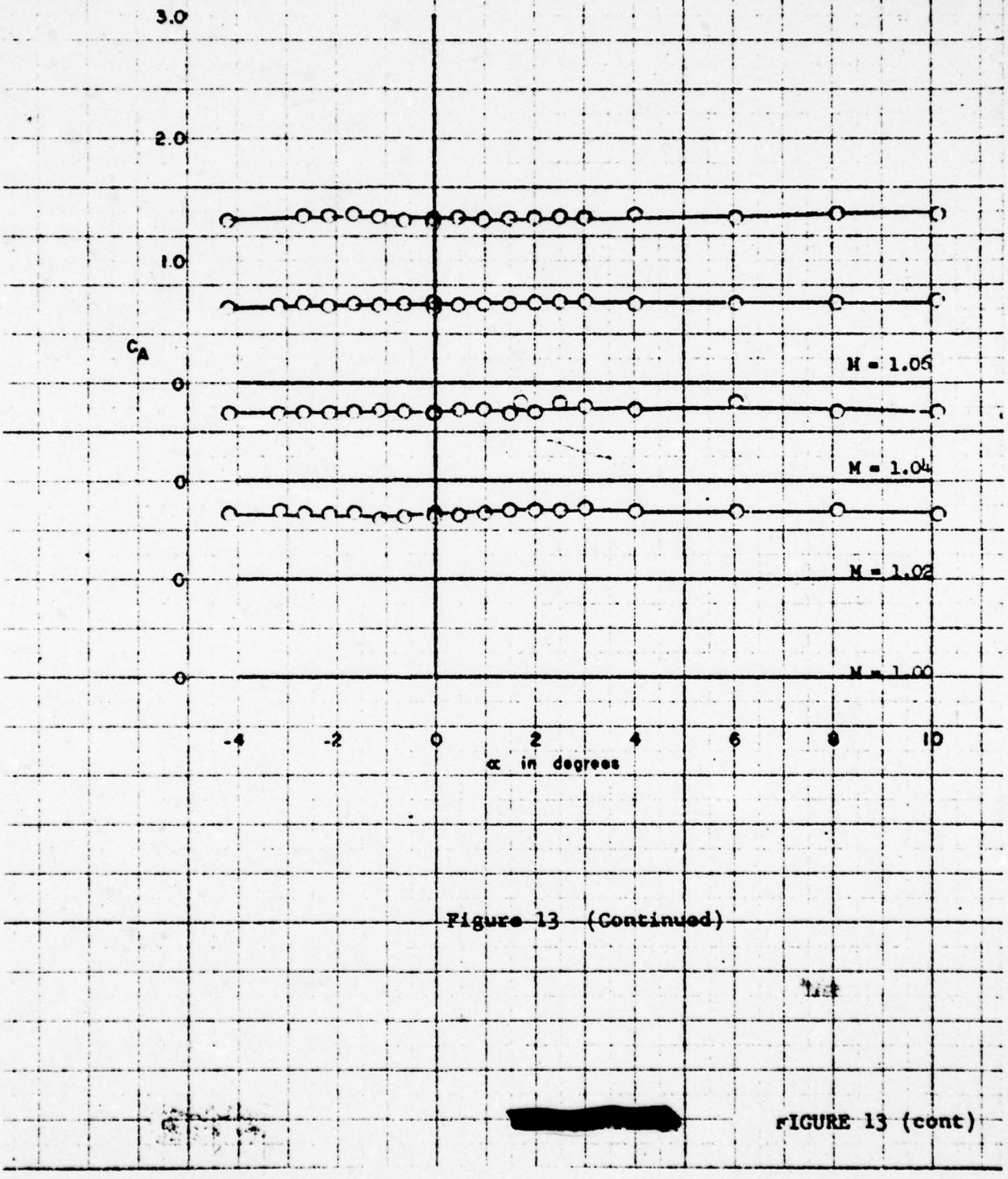

Figure 13 (Continued)

[redacted]

FIGURE 13 (cont)

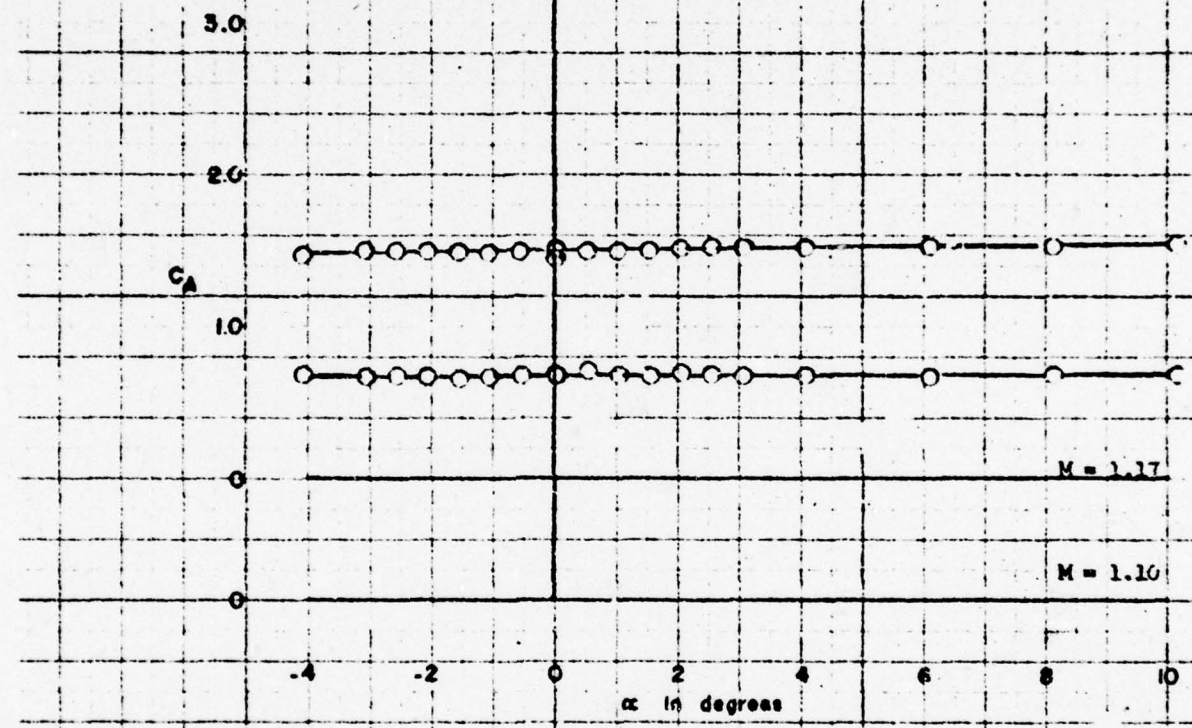

Figure 13 (Continued)

[redacted]

FIGURE 13 (cont)

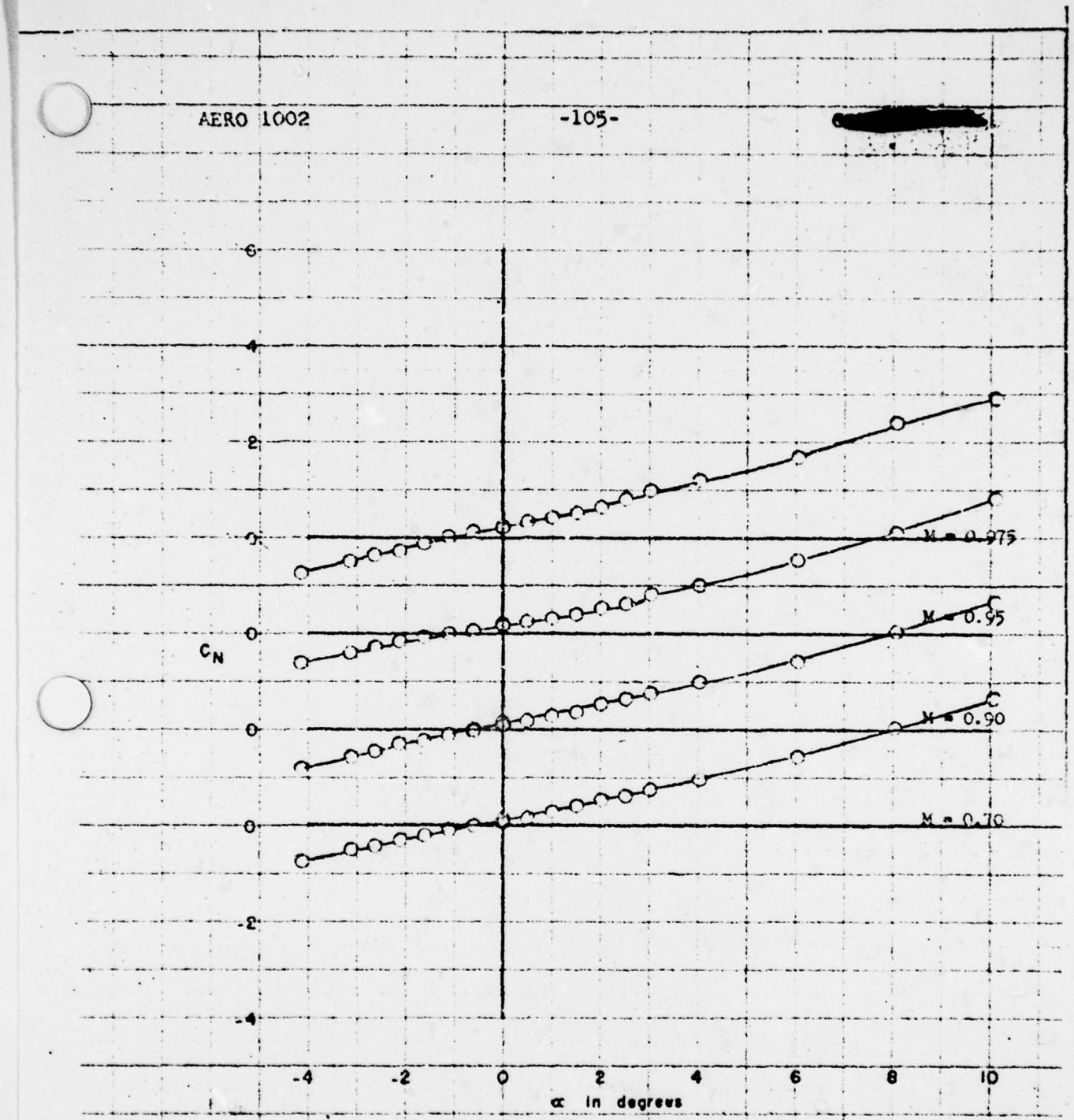

Figure 13 (Continued)

[redacted] FIGURE 13 (cont)

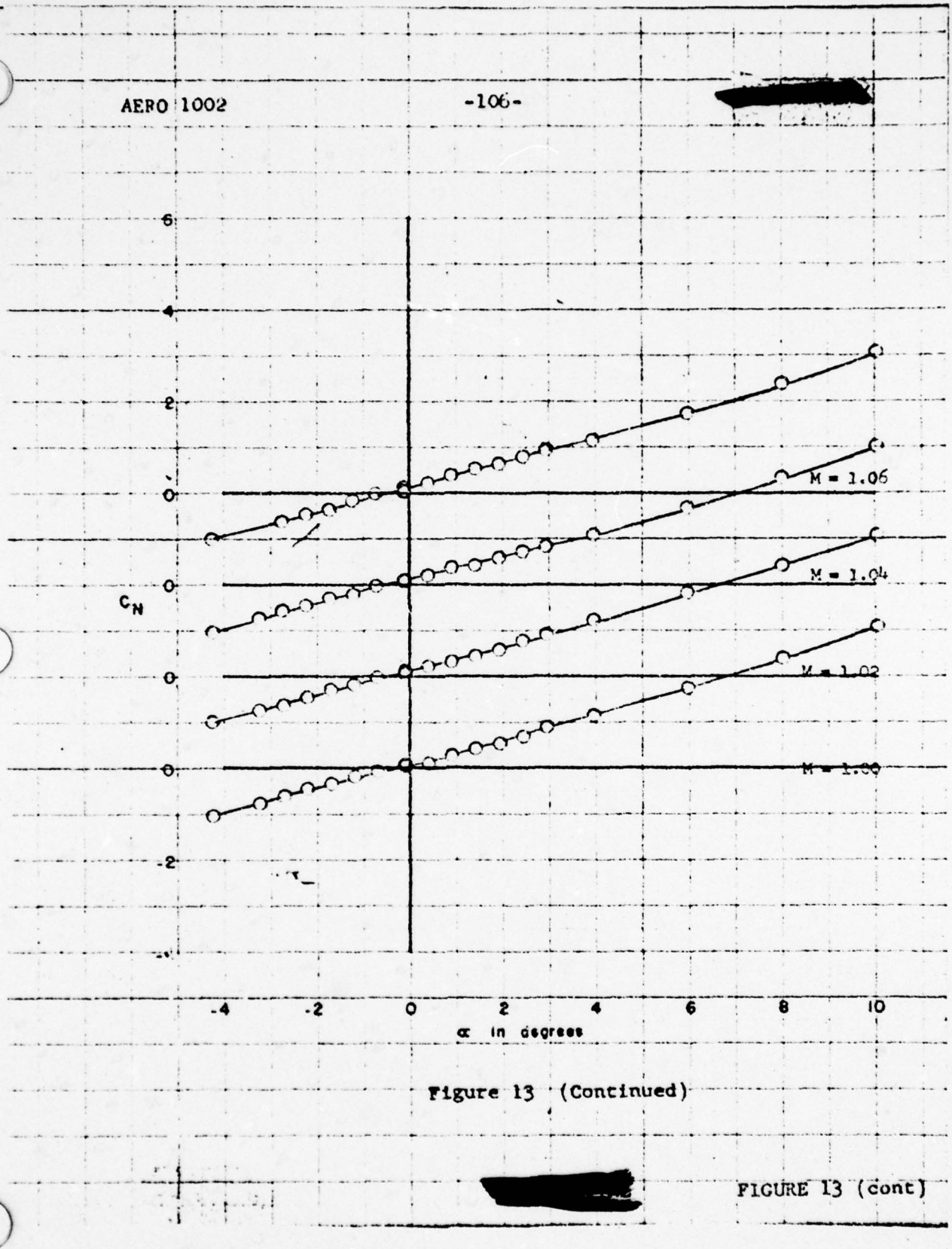

Figure 13 (Continued)

FIGURE 13 (cont)

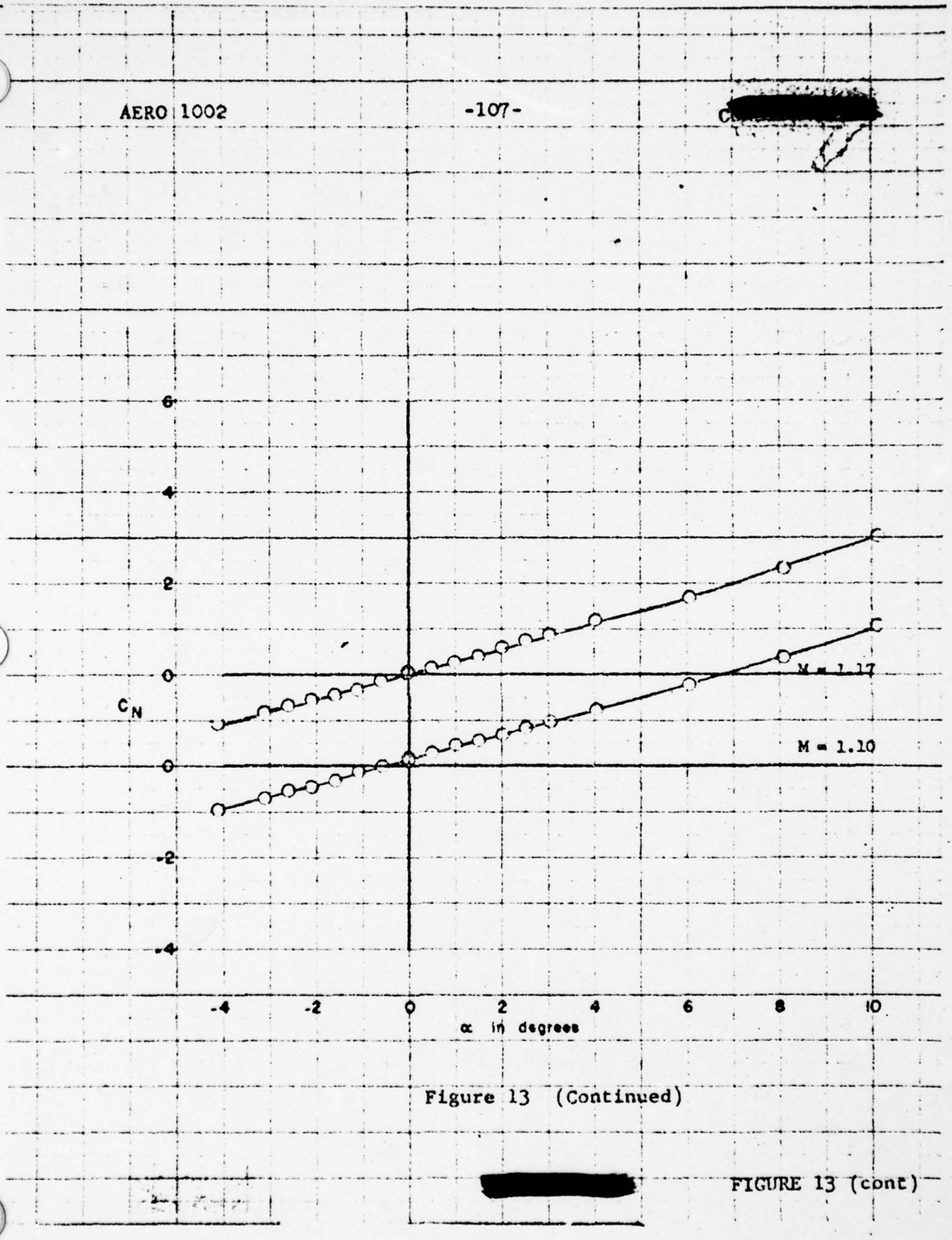

Figure 13 (Continued)

FIGURE 13 (cont)

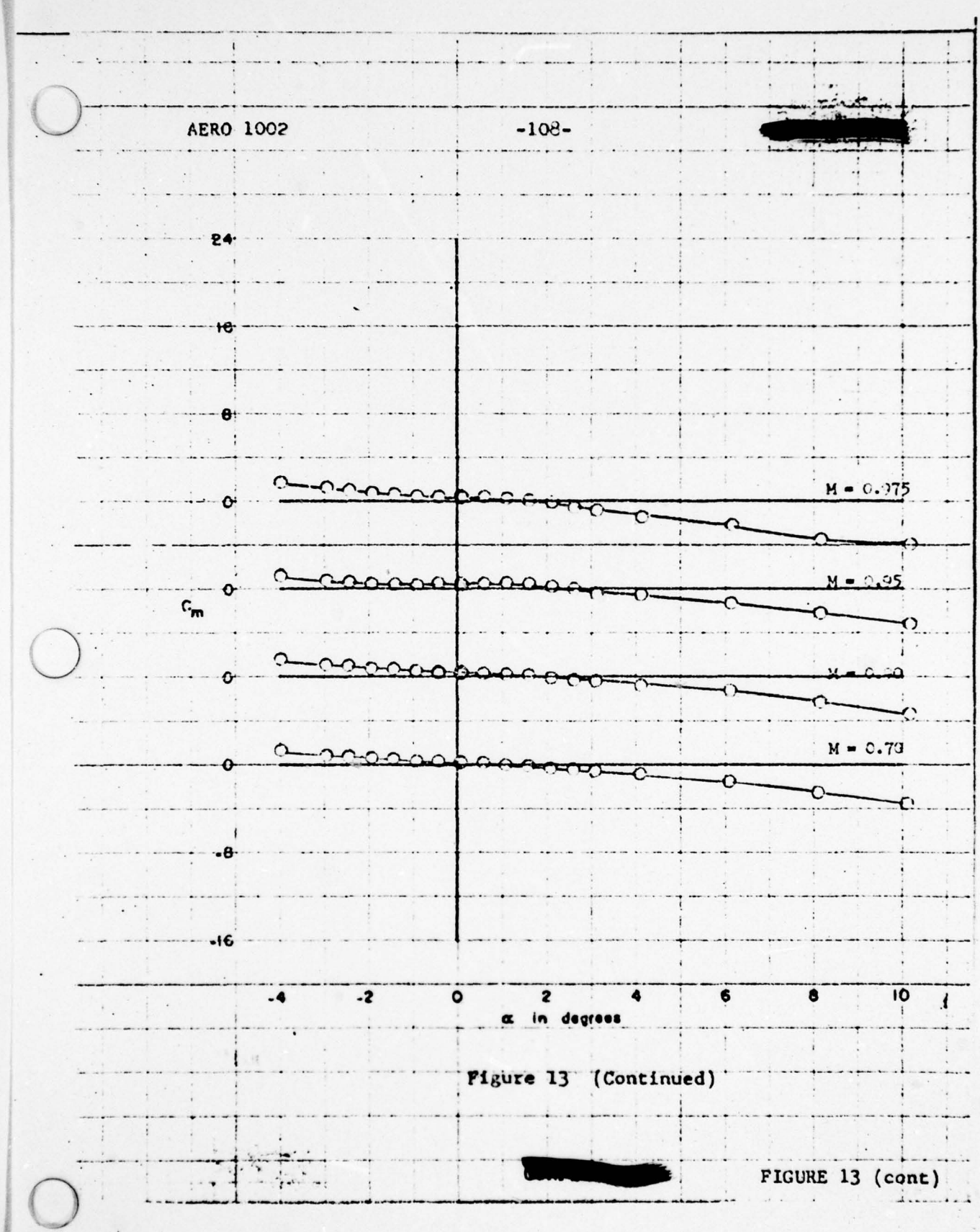

Figure 13 (Continued)

[redacted]

FIGURE 13 (cont)

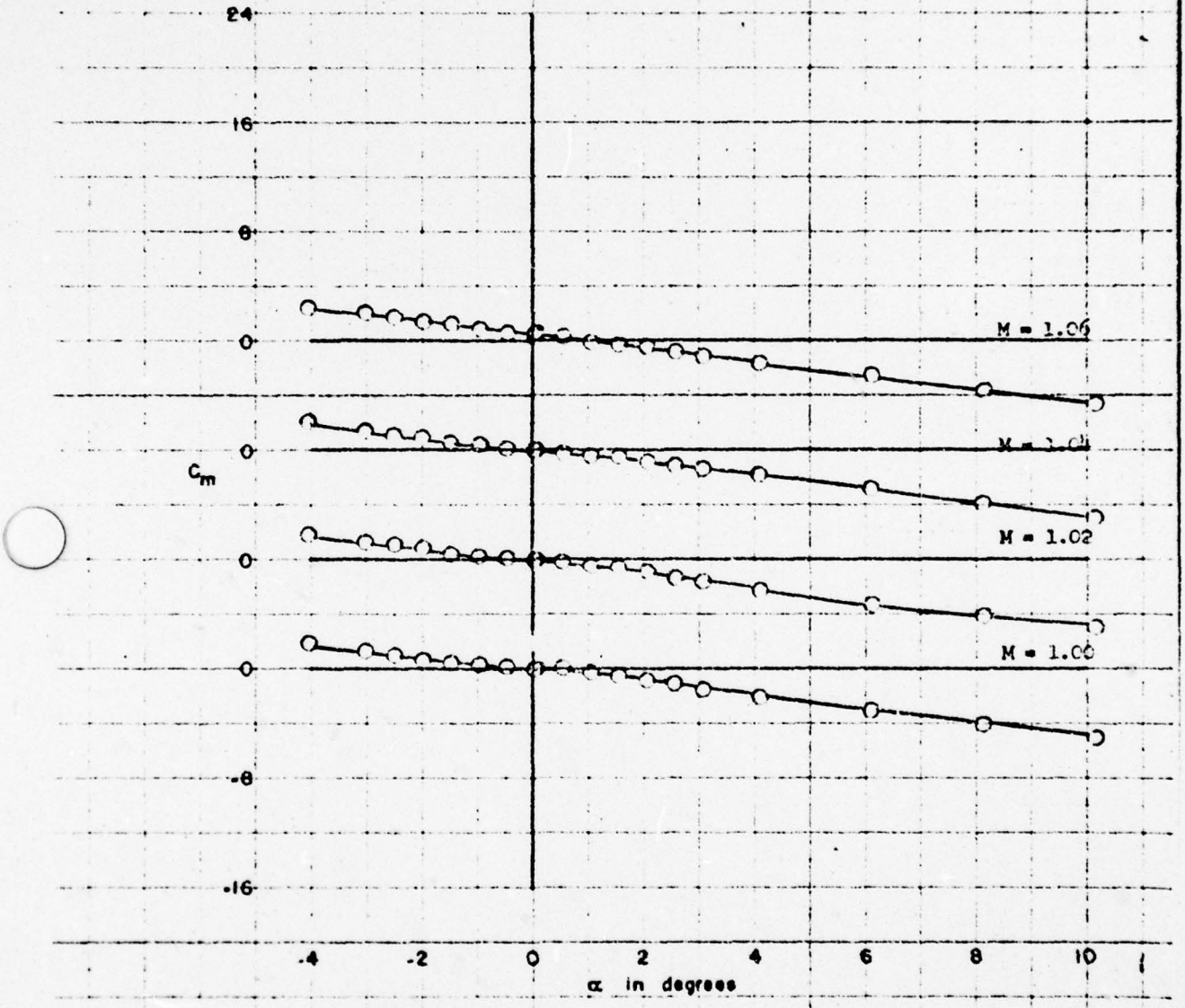

Figure 13 (Continued)

[redacted]

FIGURE 13 (cont)

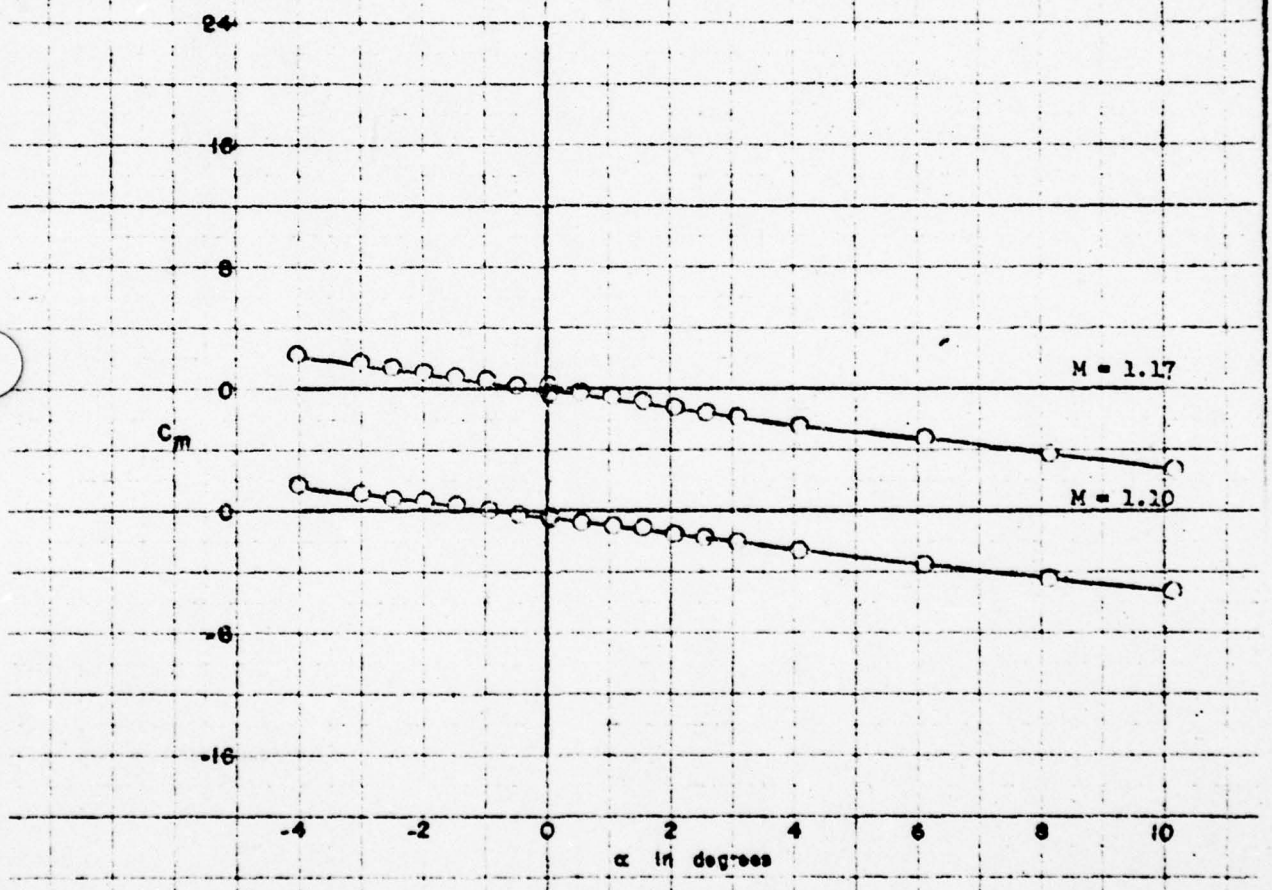

Figure 13 (Concluded)

[redacted] FIGURE 13 (concl)

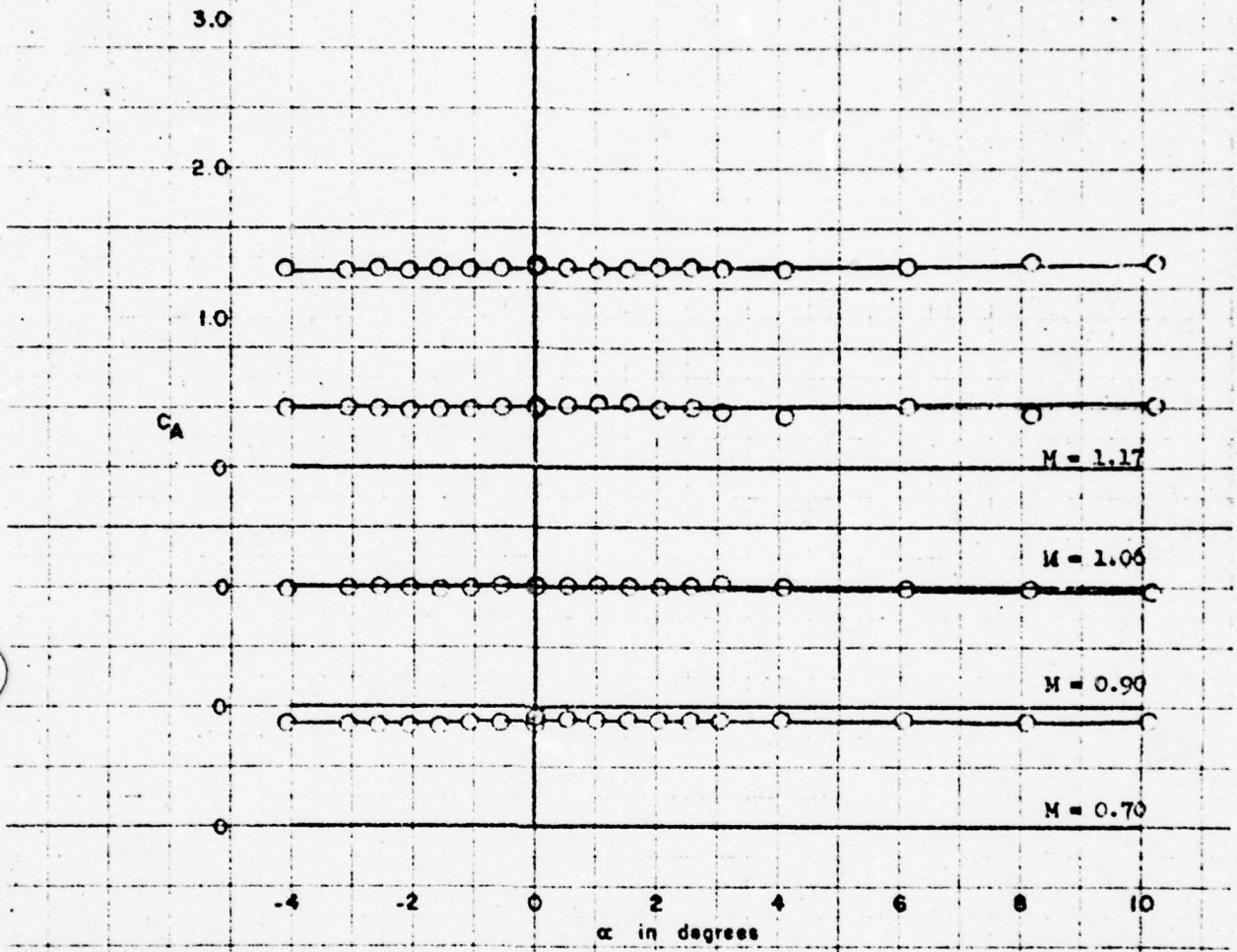

Figure 14 - Variations of Aerodynamic Characteristics With Angle of Attack for Configuration $B_{22}R_5H_{10}T_{10}$

$\phi = -45°$

FIGURE 14

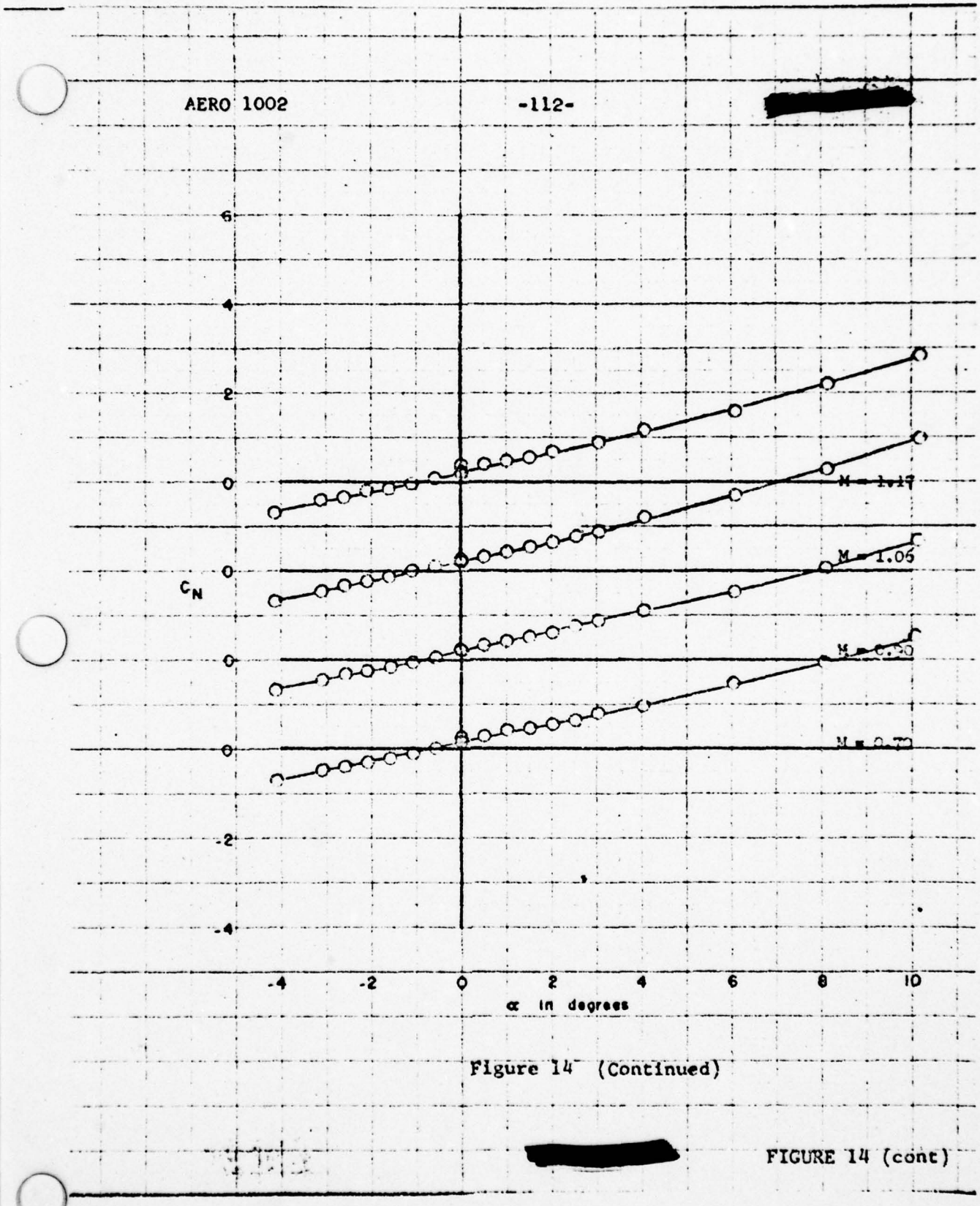

Figure 14 (Continued)

FIGURE 14 (cont)

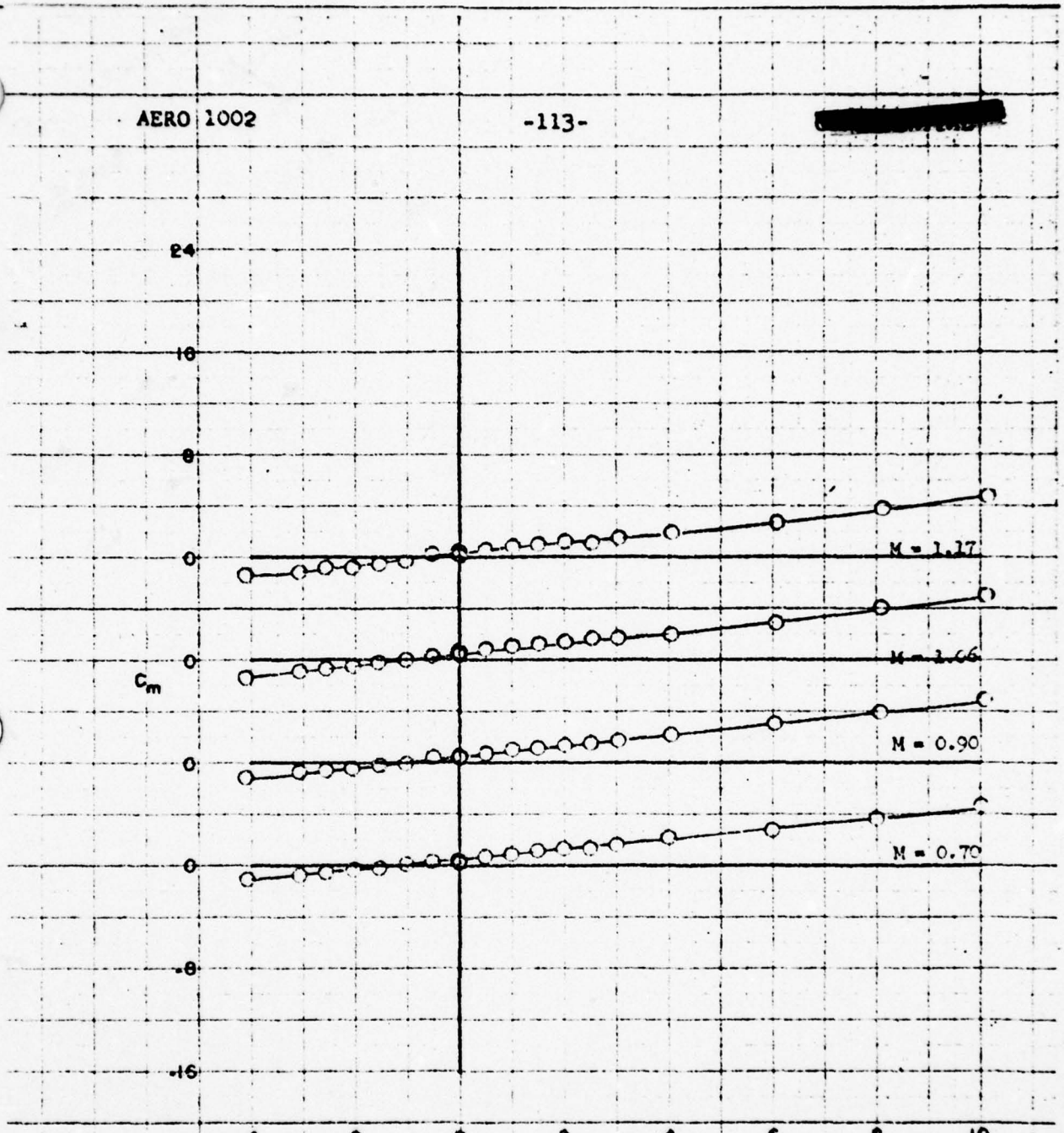

Figure 14 (Concluded)

FIGURE 14 (concl)

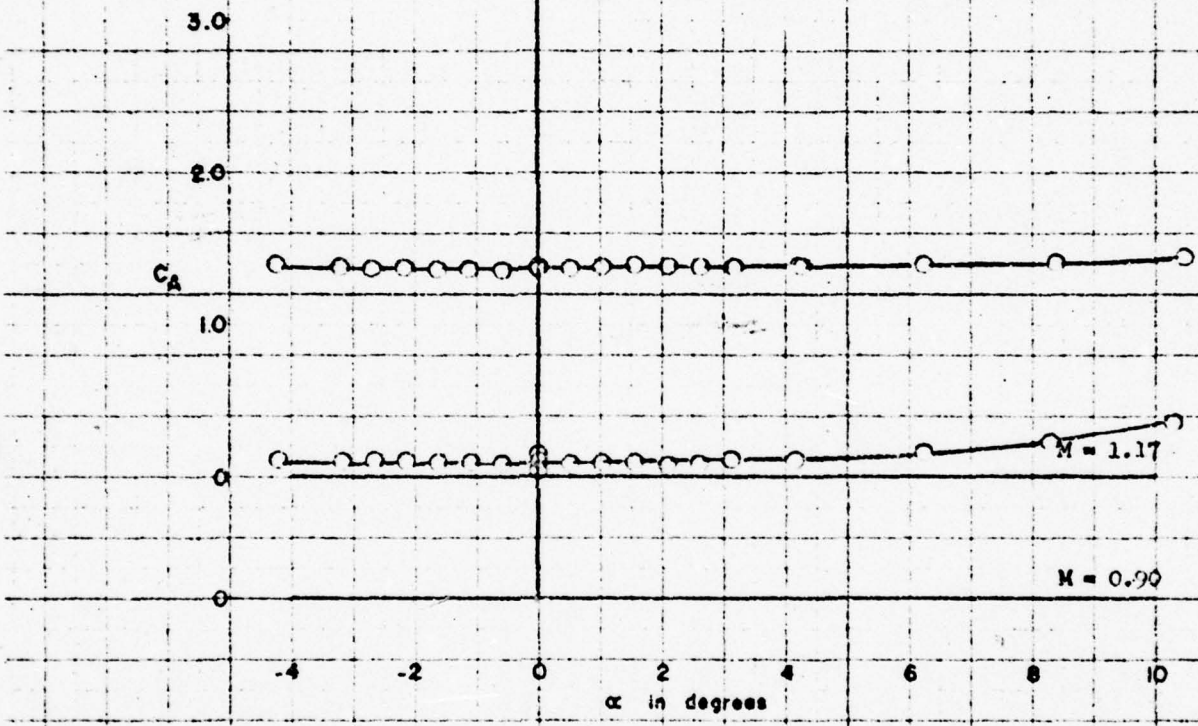

Figure 15 - Variation of Aerodynamic Characteristics With Angle of Attack for Configuration $B_{22}R_5H_{10}WC$

(a) ϕ=0°; i=i'=0°; δ=δ'=0°

[redacted]

FIGURE 15a

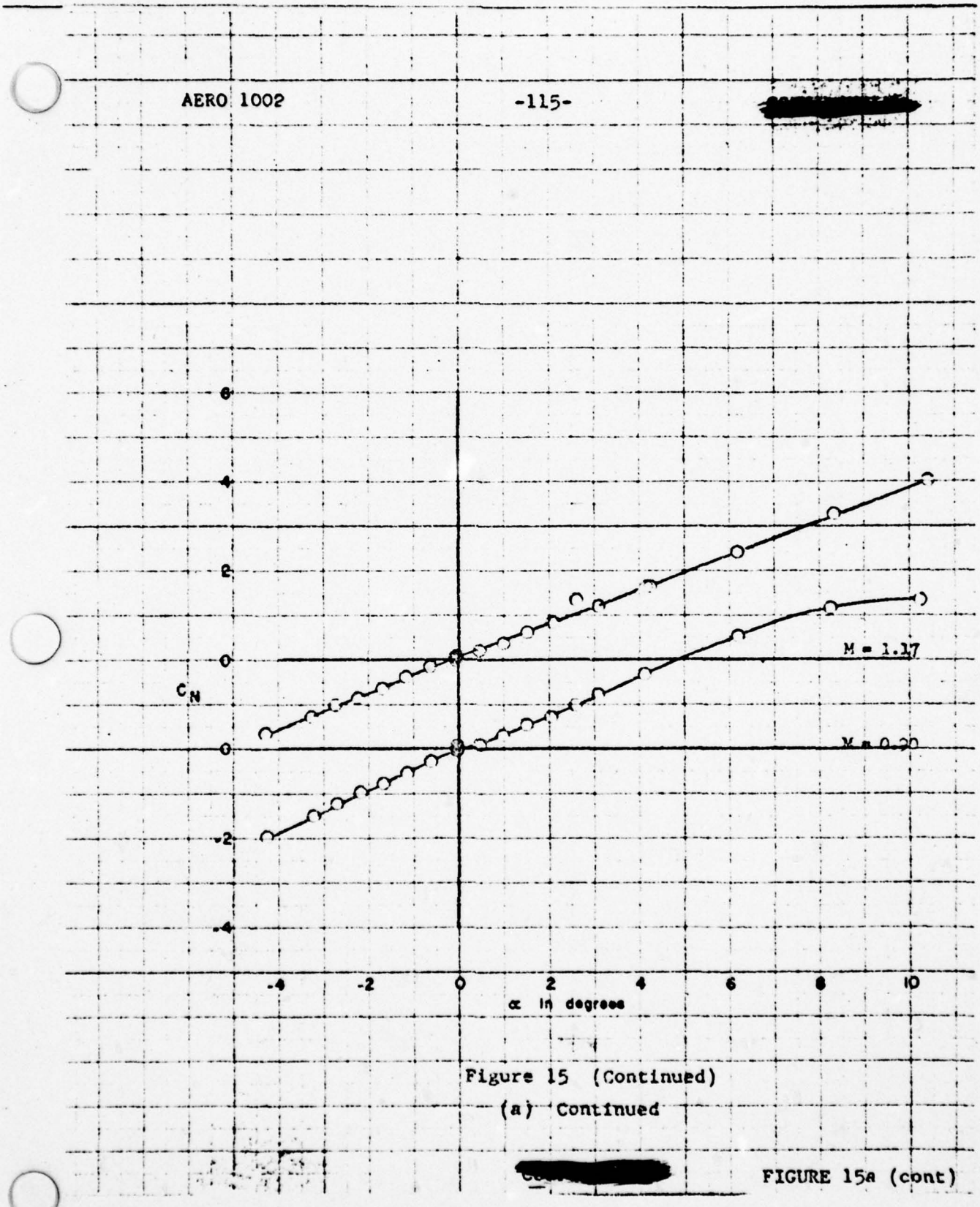

Figure 15 (Continued)

(a) Continued

[redacted]

FIGURE 15a (cont)

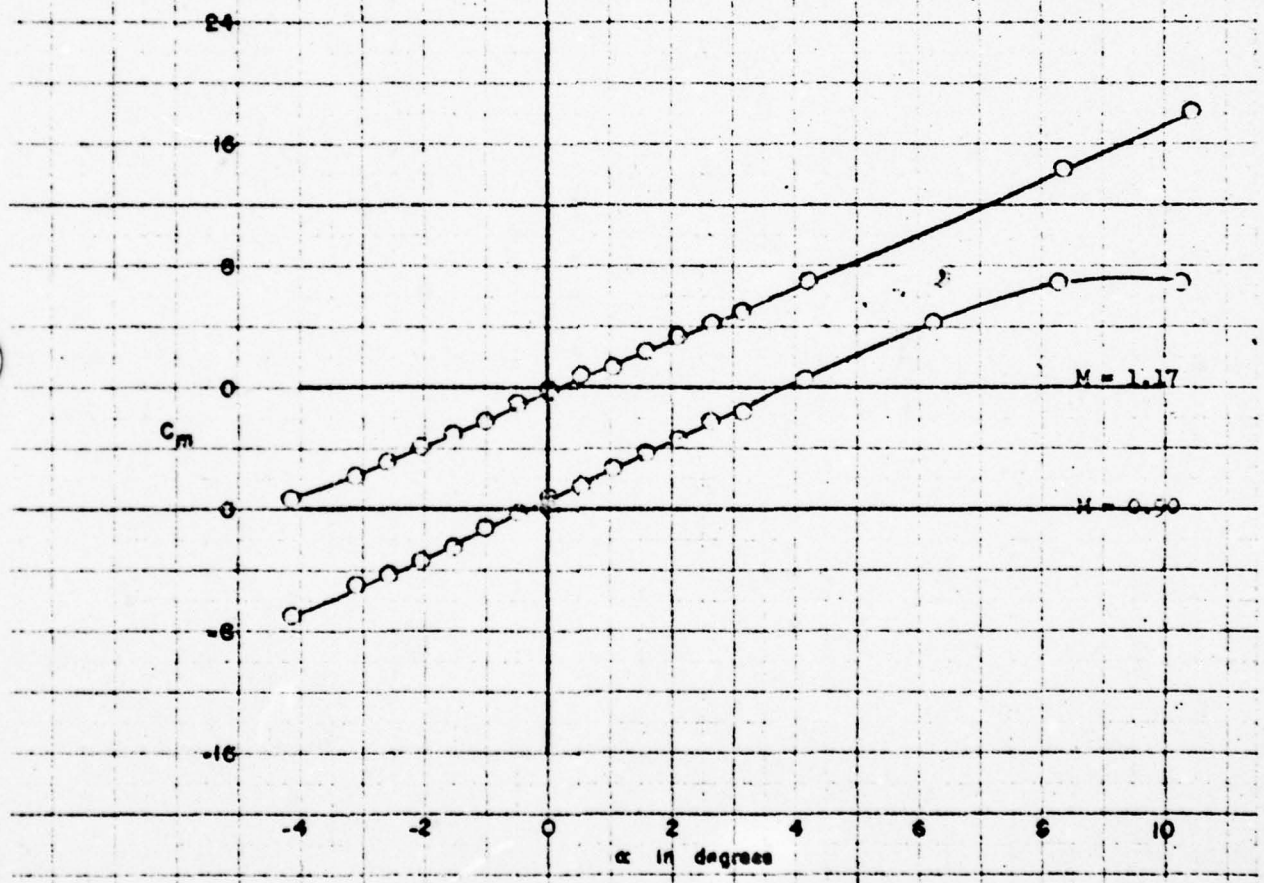

Figure 15 (Continued)

(a) Concluded

[redacted]

FIGURE 15a (concl)

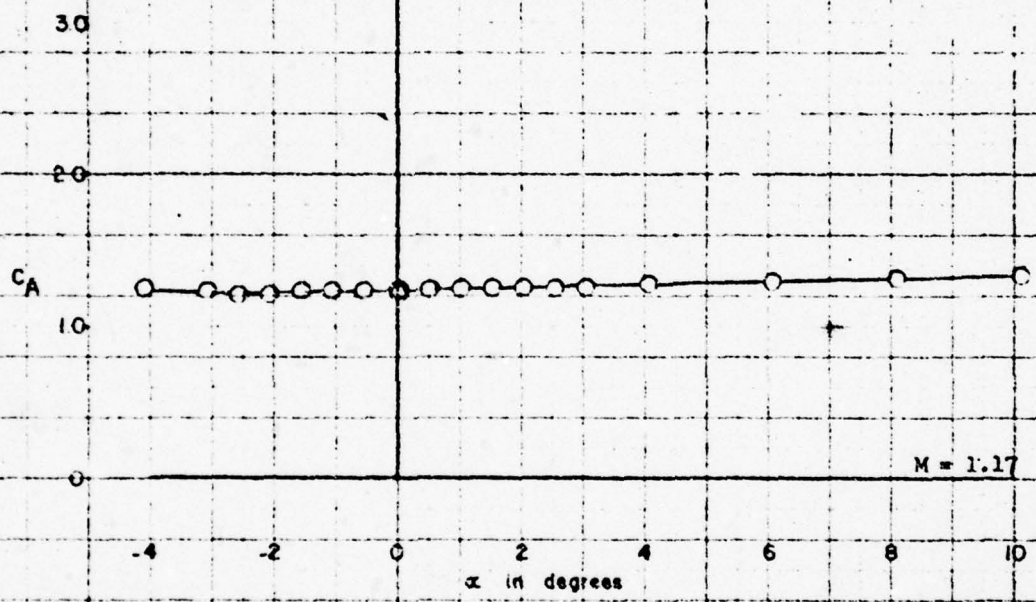

Figure 15 (Continued)

(b) $\phi=0°$; $i=-5°$, $i'=0°$; $\delta=\delta'=0°$

[redacted]

FIGURE 15b

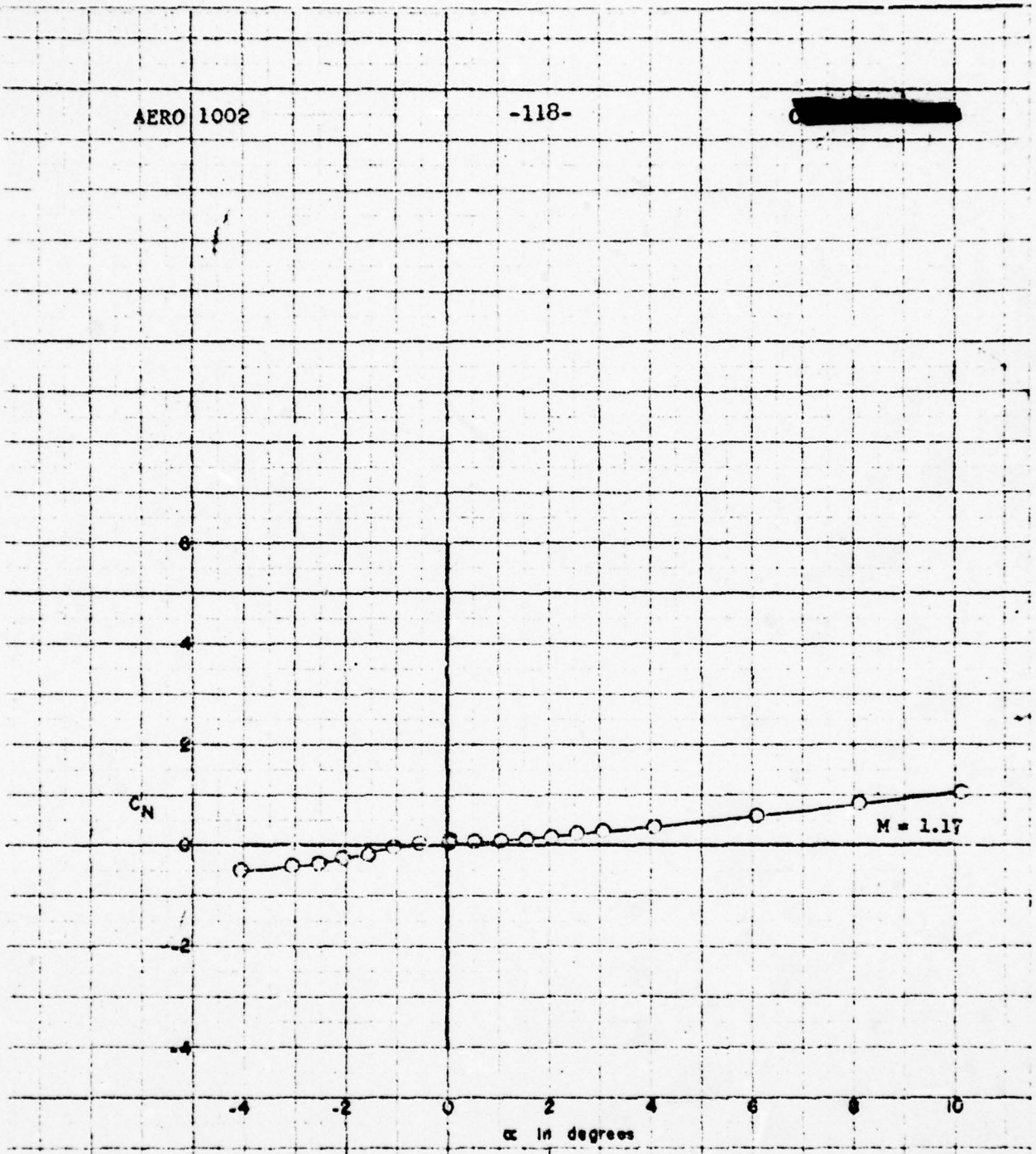

Figure 15 (Continued)

(b) Continued

[redacted]

FIGURE 15b (cont)

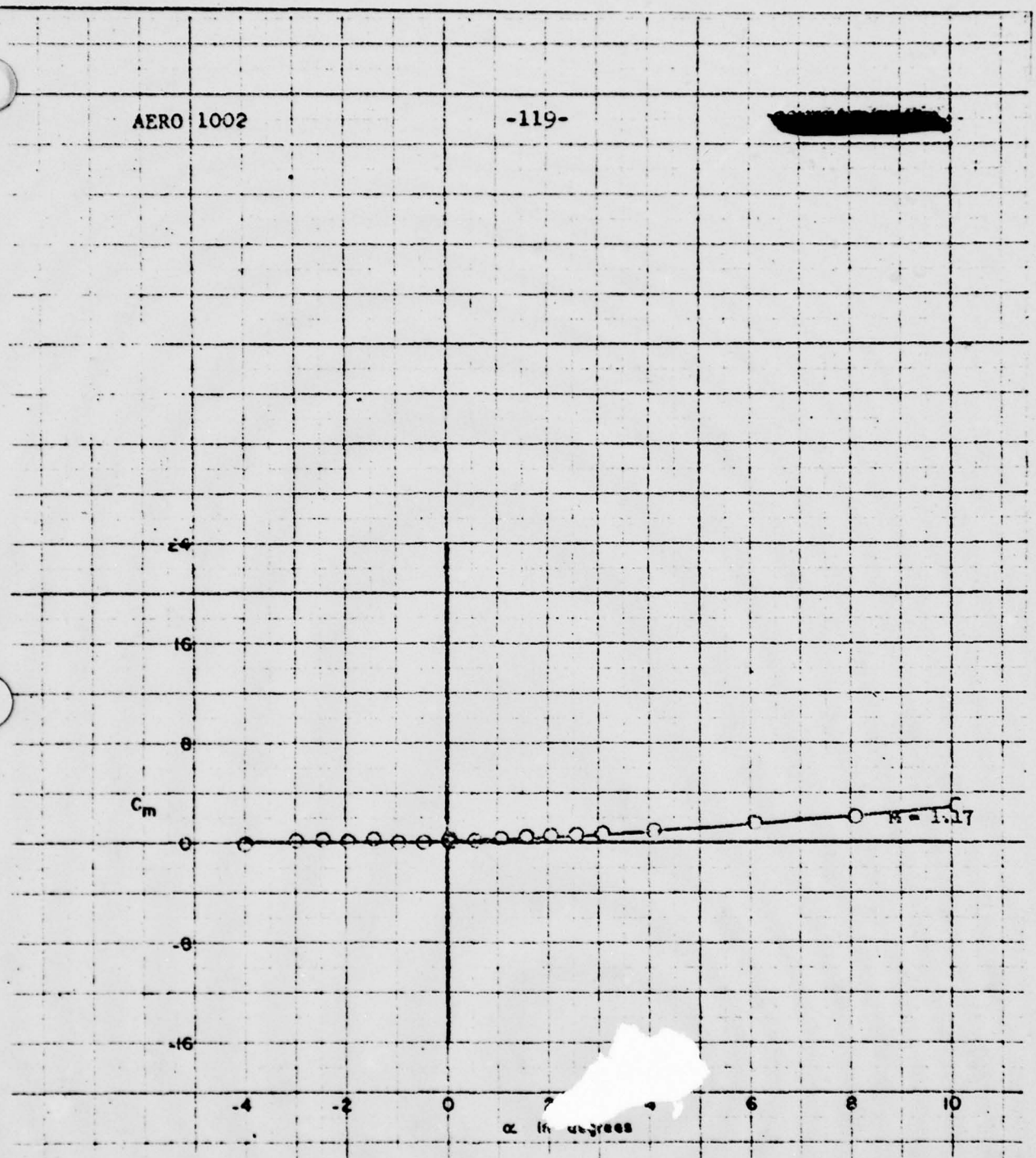

Figure 15 (Continued)

(b) Concluded

FIGURE 15b (concl

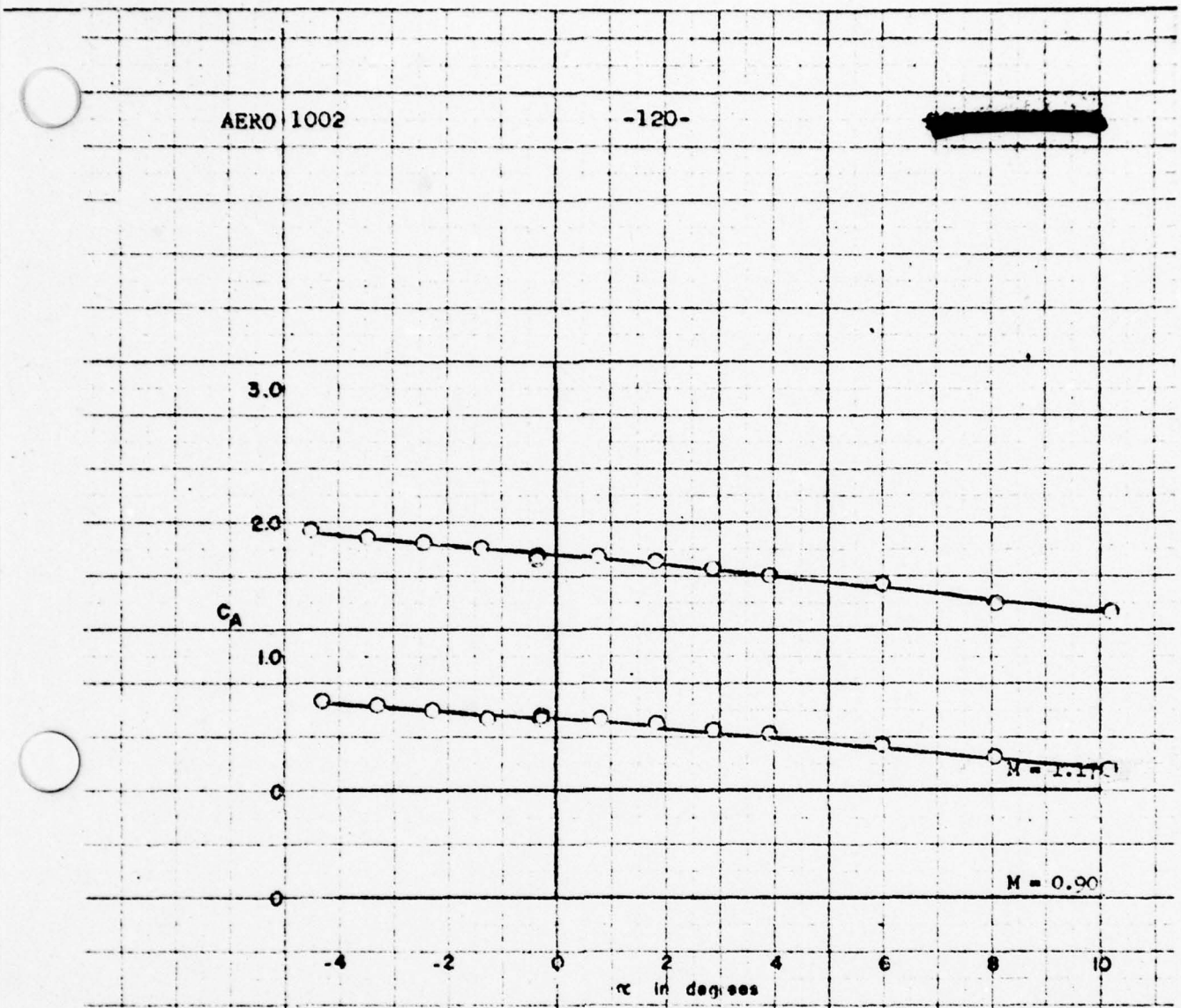

Figure 15 (Continued)

(c) $\phi=0°$; $i=-10°$, $i'=0°$; $\delta=\delta'=0°$

[redacted] FIGURE 15(c)

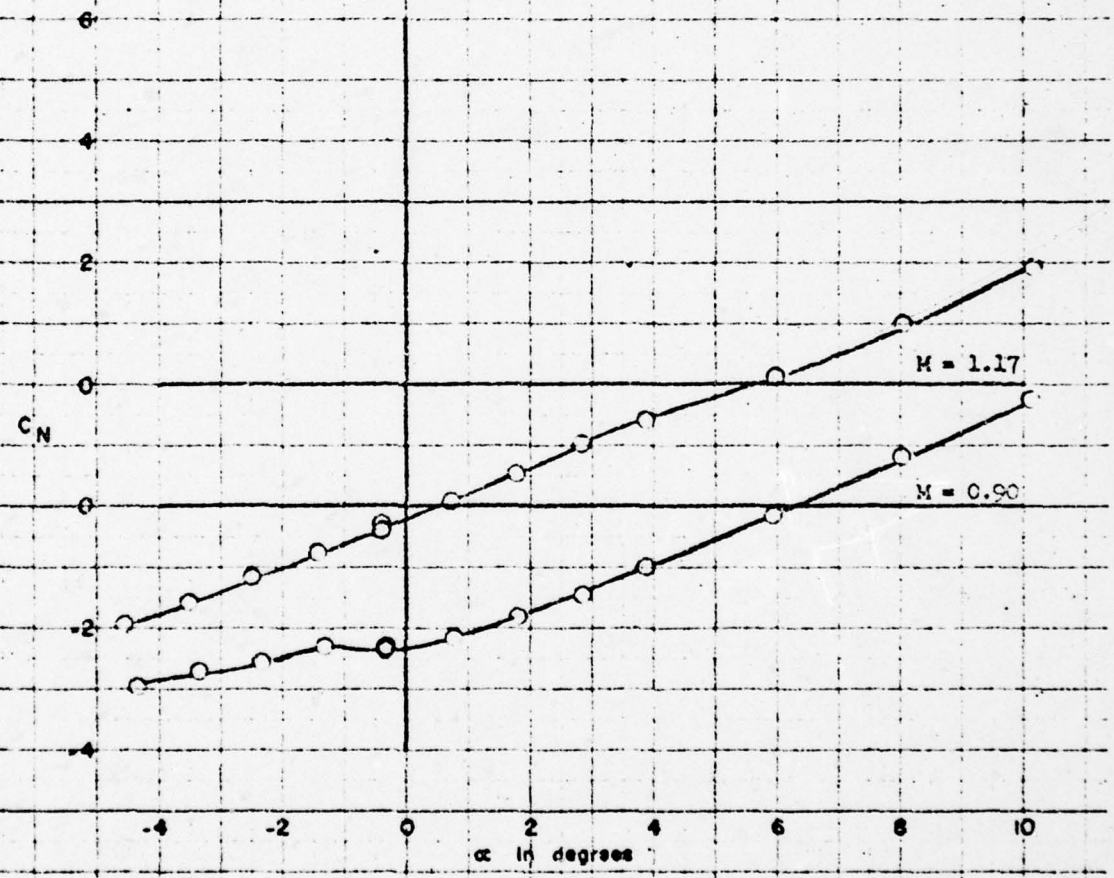

Figure 15 (Continued)

(c) Continued

FIGURE 15c (cont)

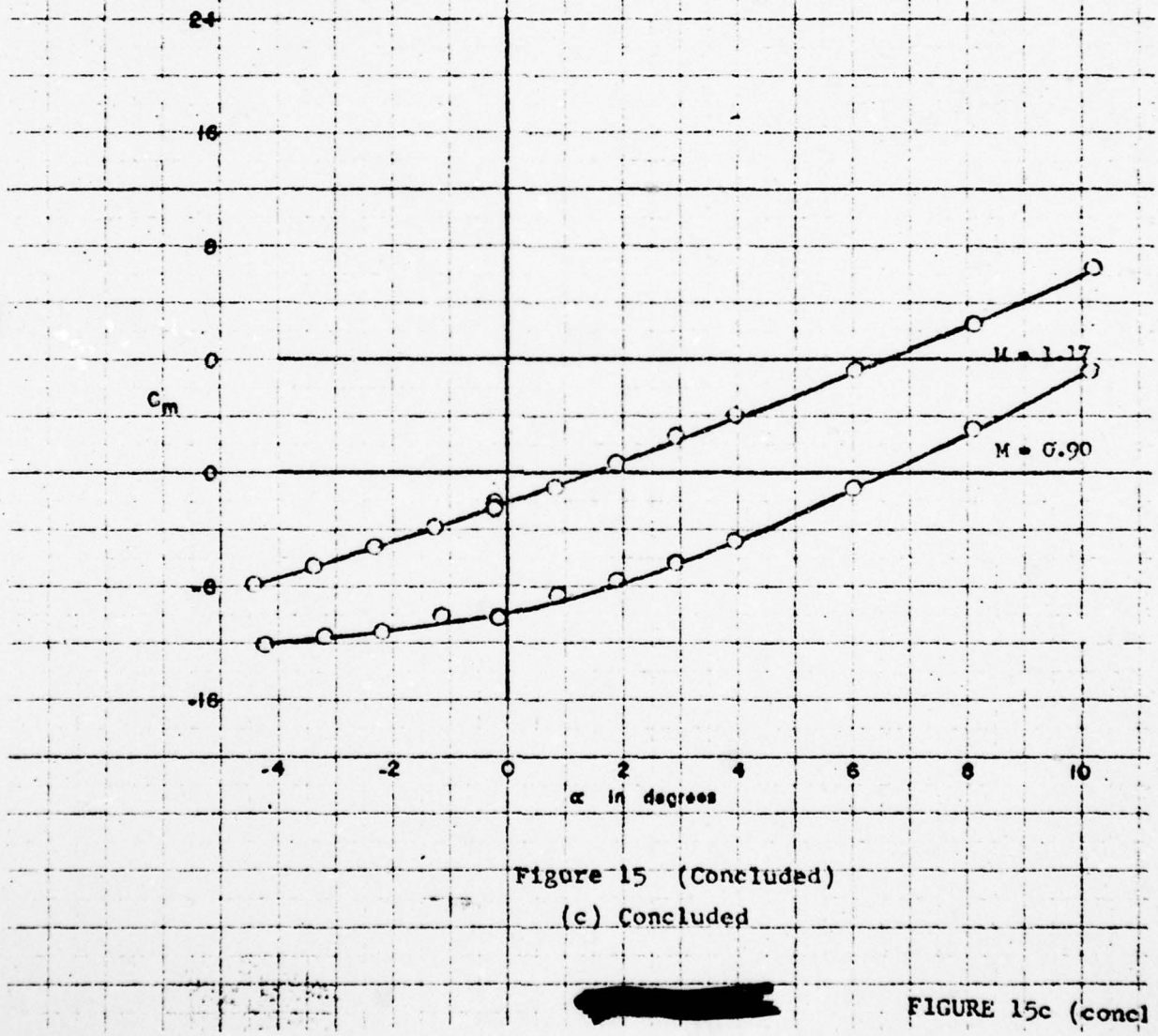

Figure 15 (Concluded)

(c) Concluded

[redacted]

FIGURE 15c (concl

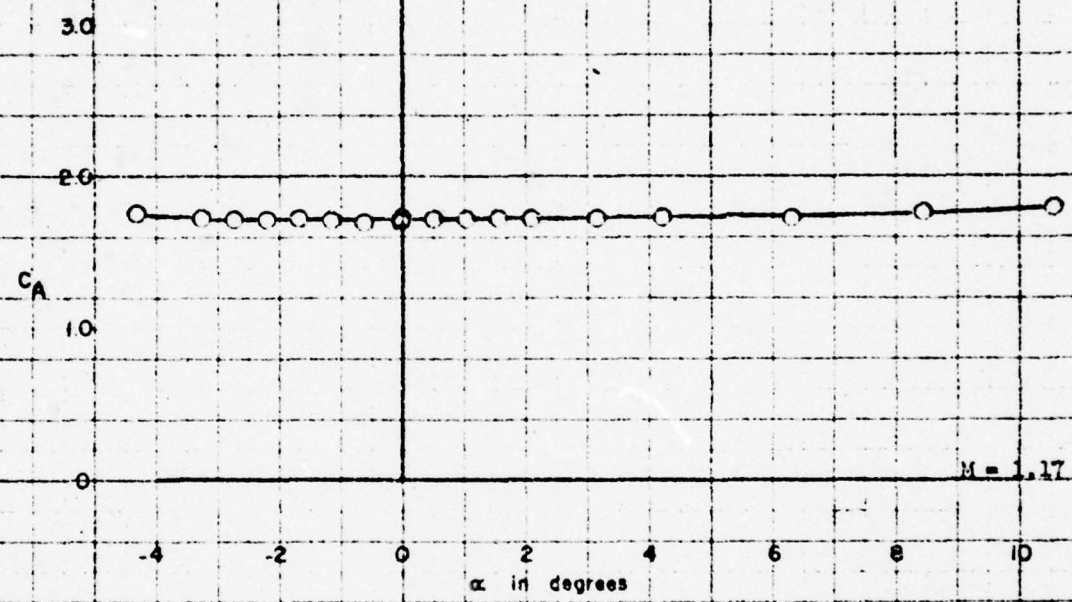

Figure 16 - Variation of Aerodynamic Characteristics With Angle of Attack for Configuration $B_{22}R_5H_{10}{}^{W}T_{1C}F_{18}{}^{C}$

(a) $\phi=0°$; $i=i'=0°$; $\delta=\delta'=0°$

[redacted] FIGURE 16a

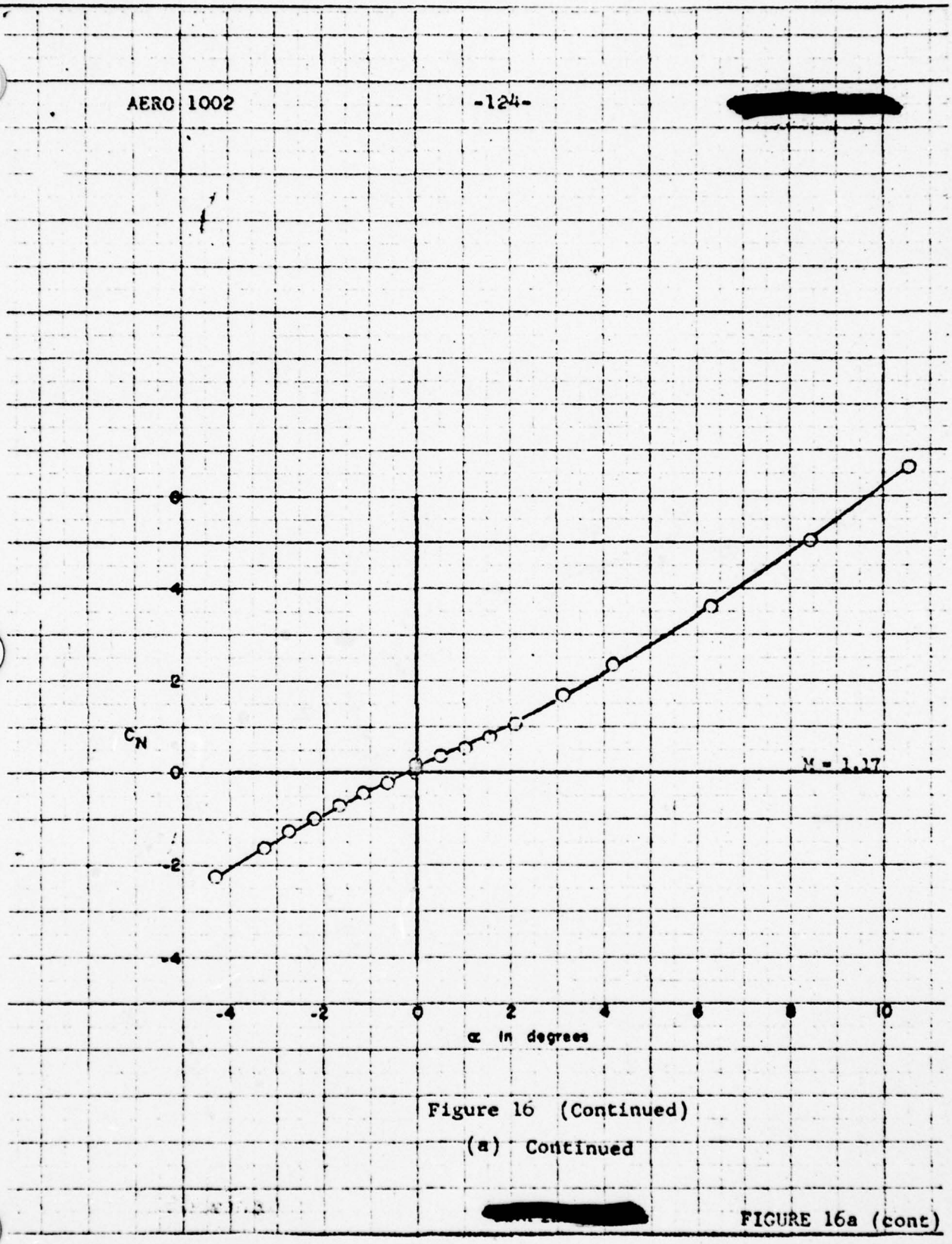

Figure 16 (Continued)

(a) Continued

FIGURE 16a (cont)

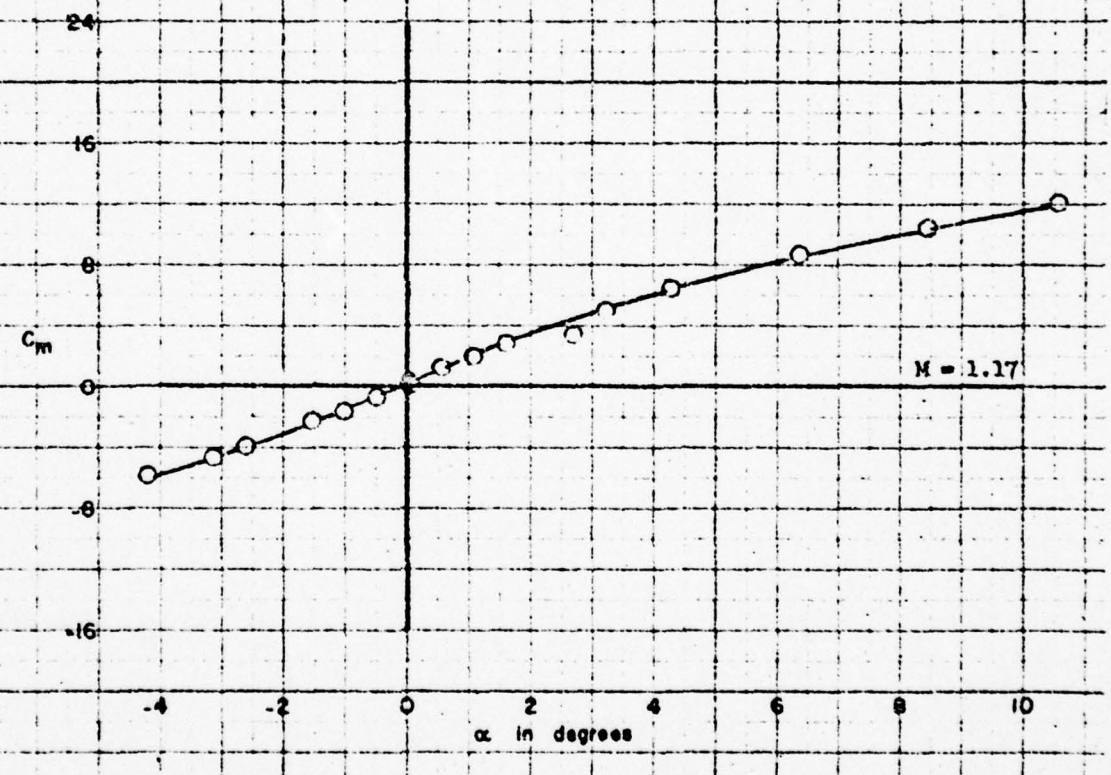

Figure 16 (Continued)

(a) Concluded

FIGURE 16a (concl.)

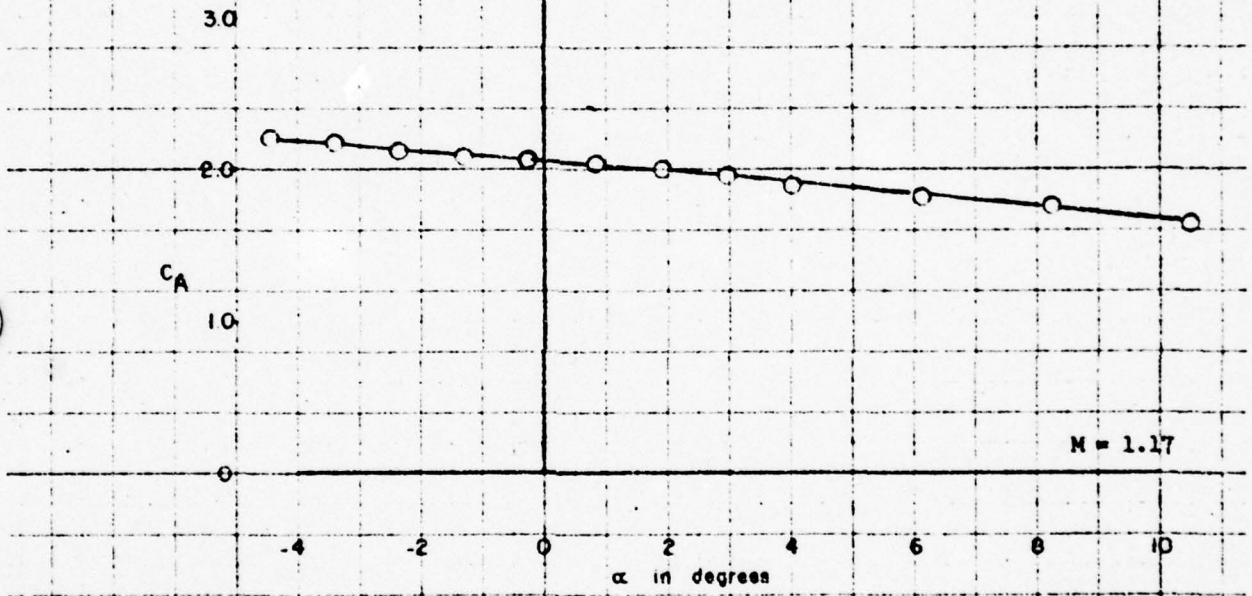

Figure 16 (Continued)

(b) ϕ=0°; i=-10°, i'=0°; δ=δ'=0°

FIGURE 16b

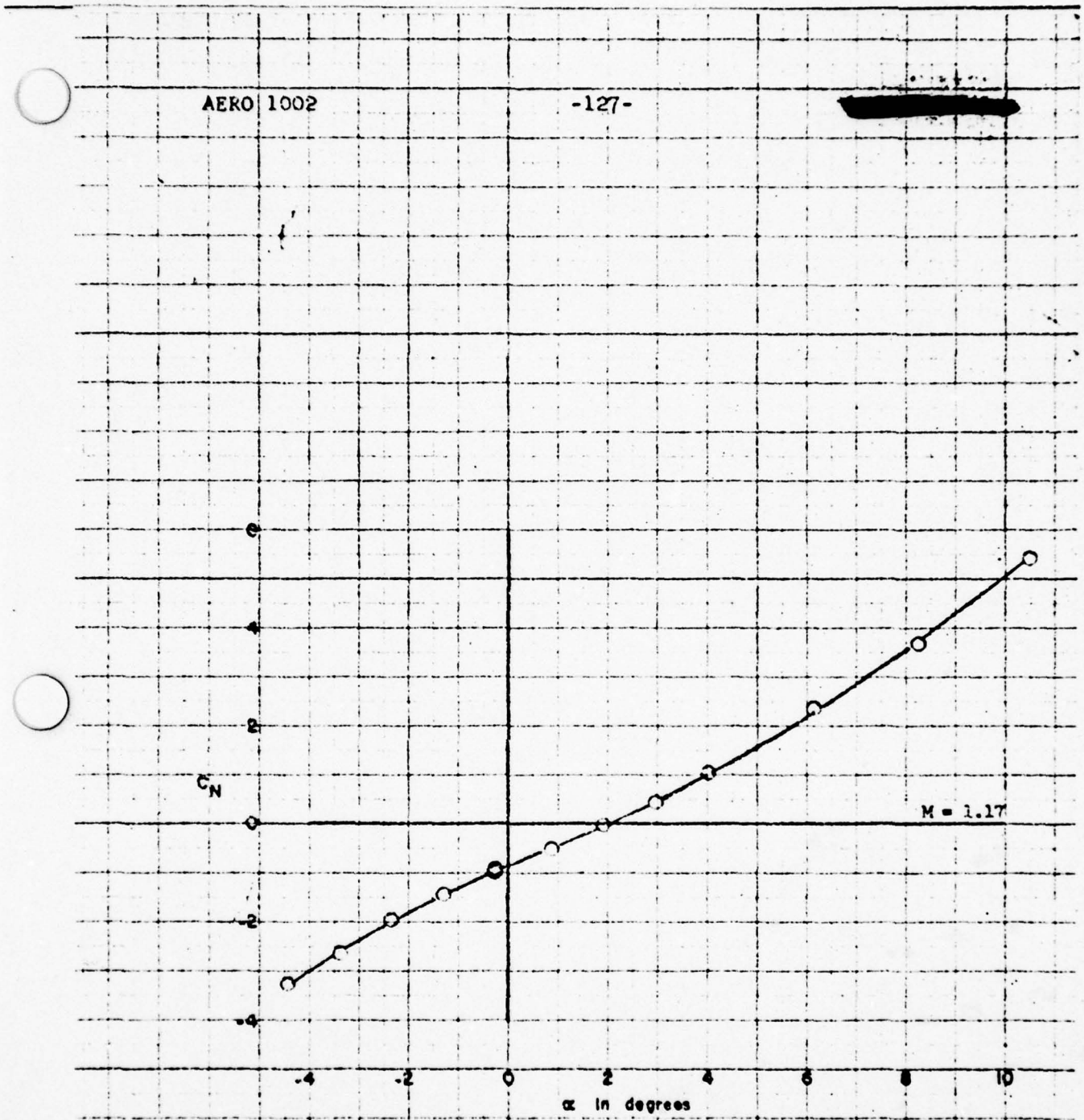

Figure 16 (Continued)

(b) Continued

[redacted]

FIGURE 16b (cont)

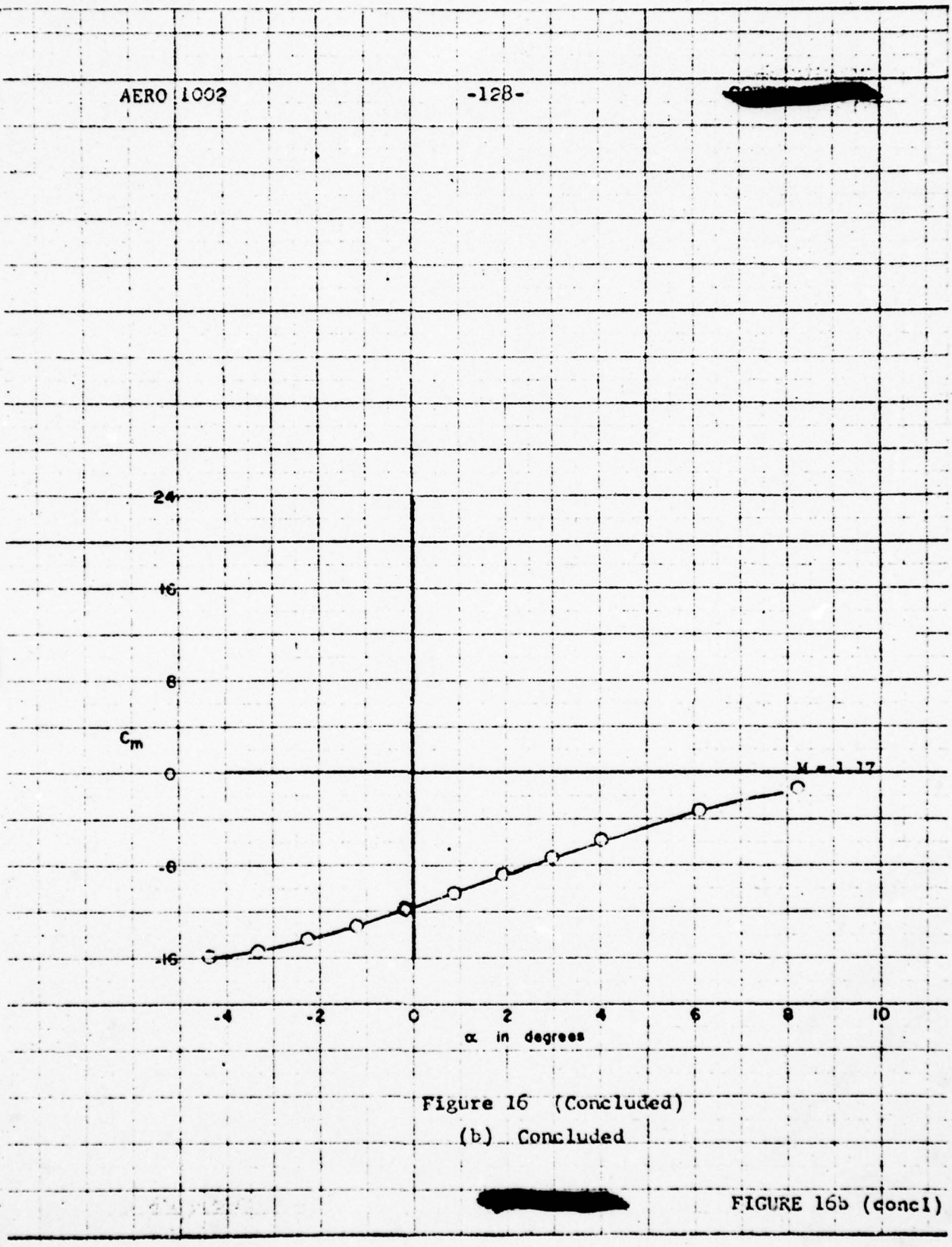

Figure 16 (Concluded)

(b) Concluded

FIGURE 16b (concl)

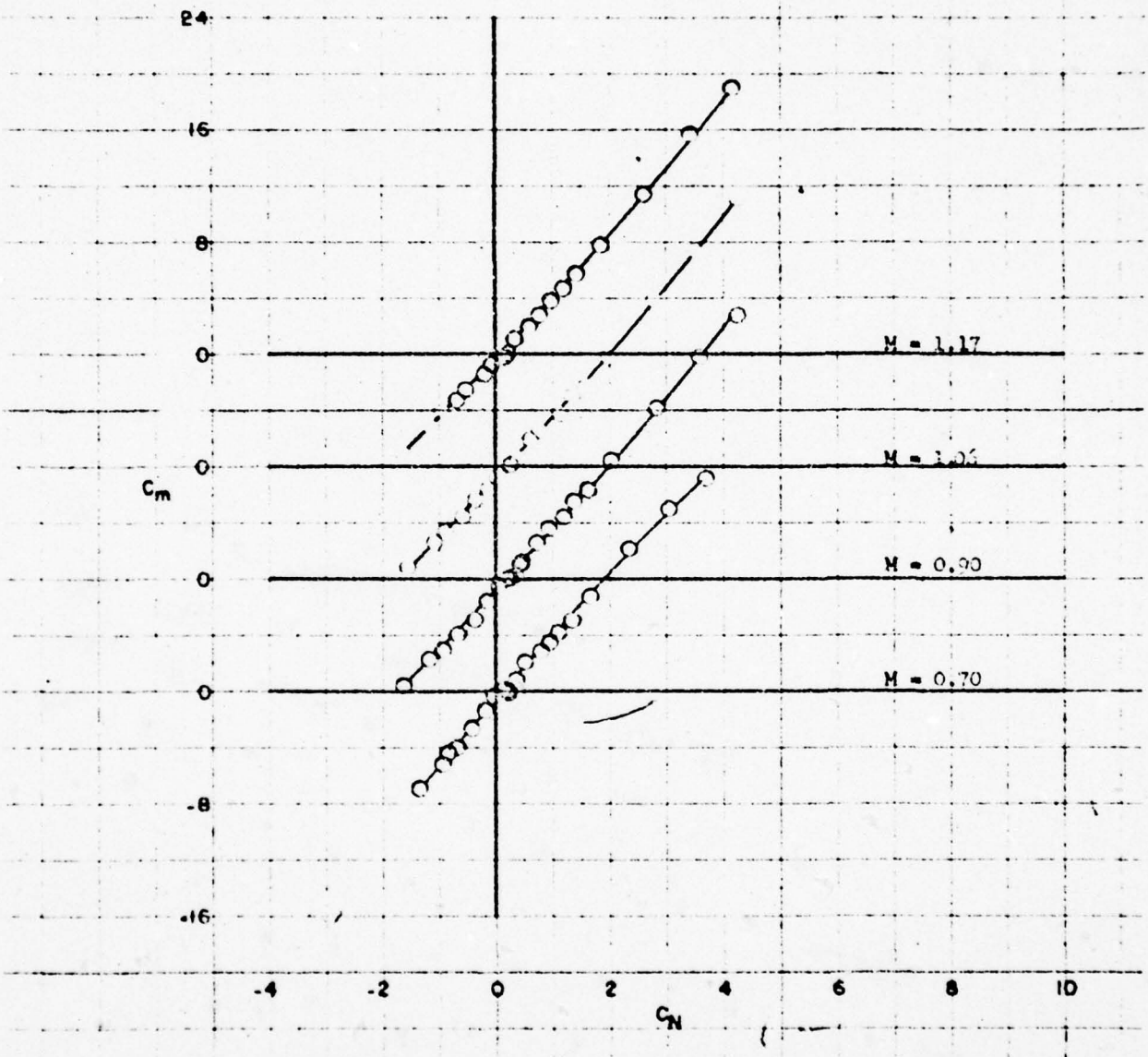

Figure 17 - Variation of Pitching-Moment Coefficient With Normal-Force Coefficient for Configuration $B_{22}R_5H_{10}W$

(a) ϕ=-45°; i=i'=0°; δ=δ'=0°

FIGURE 17a

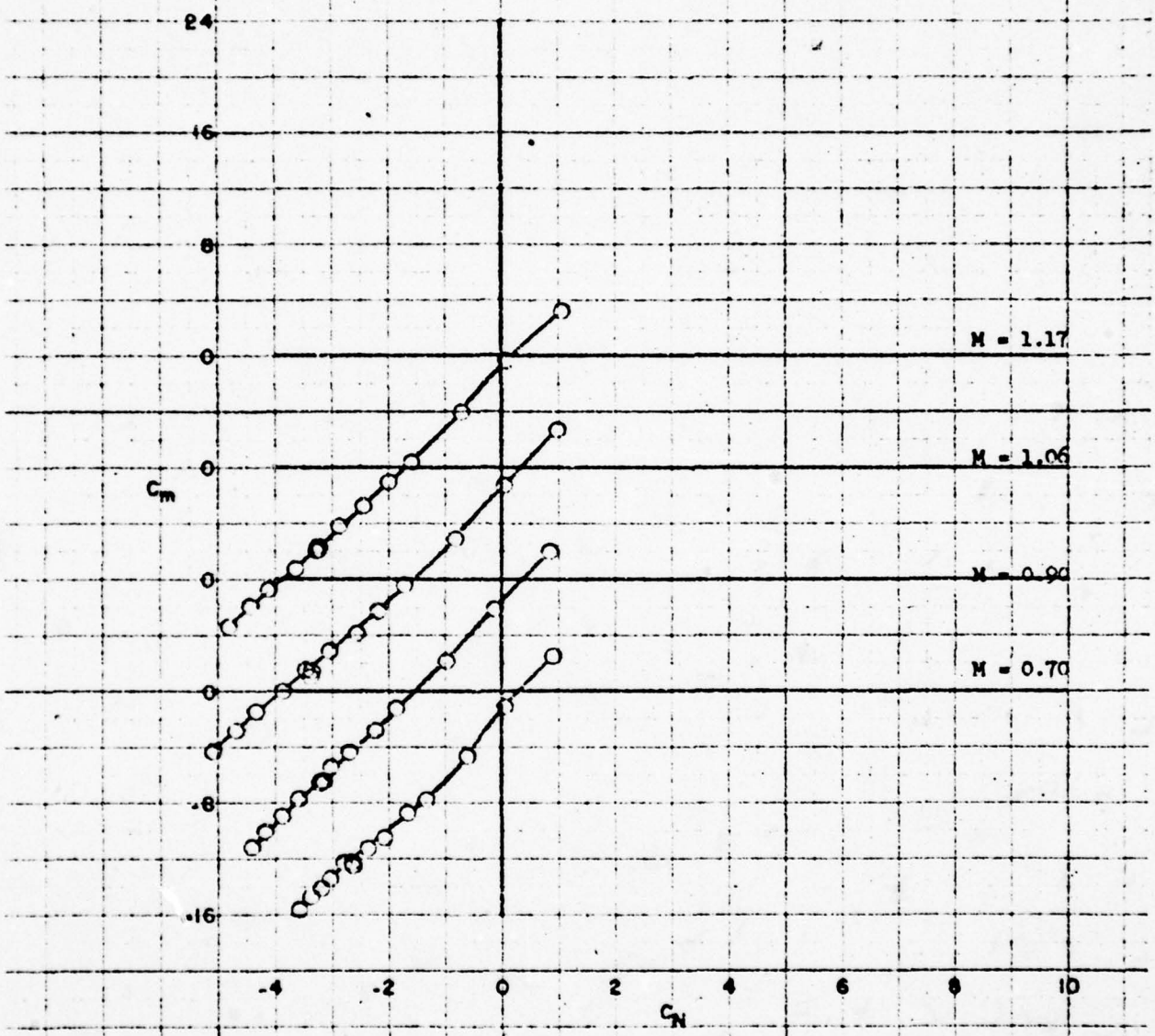

Figure 17 (Continued)
(b) ϕ=-45°; i=i'=-10°; δ=δ'=0°

FIGURE 17b

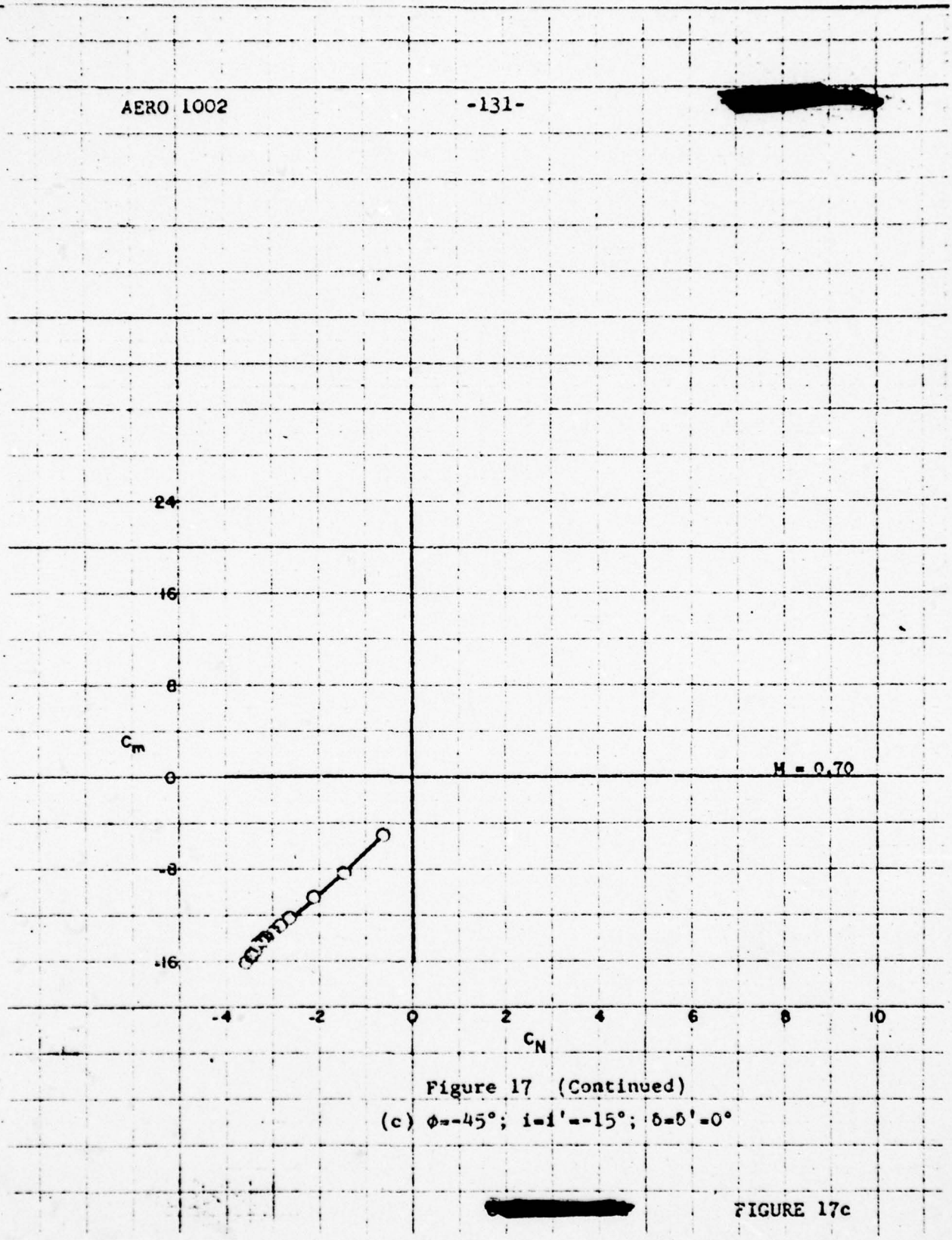

Figure 17 (Continued)

(c) ϕ=-45°; i=i'=-15°; δ=δ'=0°

FIGURE 17c

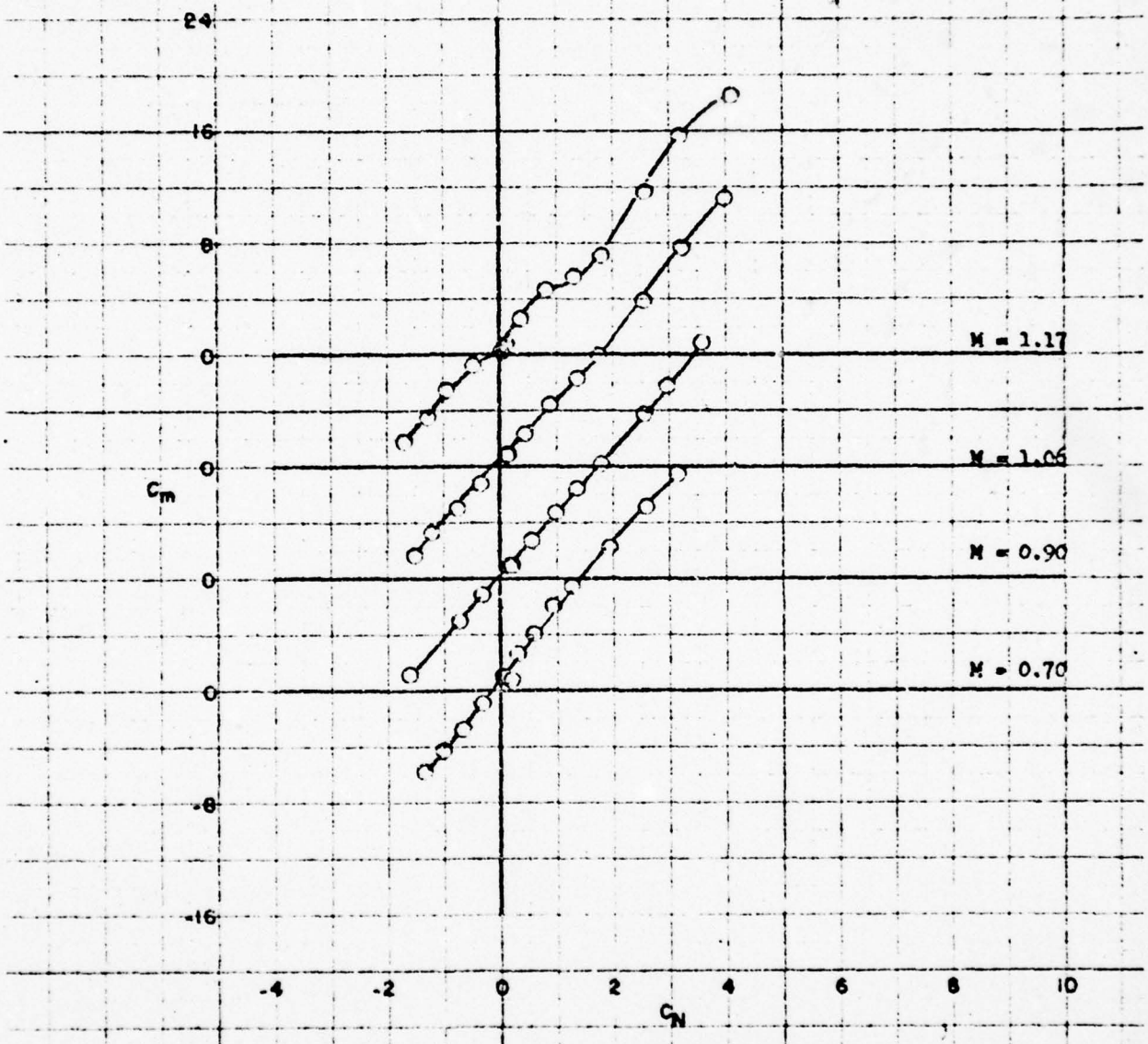

Figure 17 (Continued)

(d) ϕ=-45°; i=i'=0°; δ=δ'=5°

FIGURE 17d

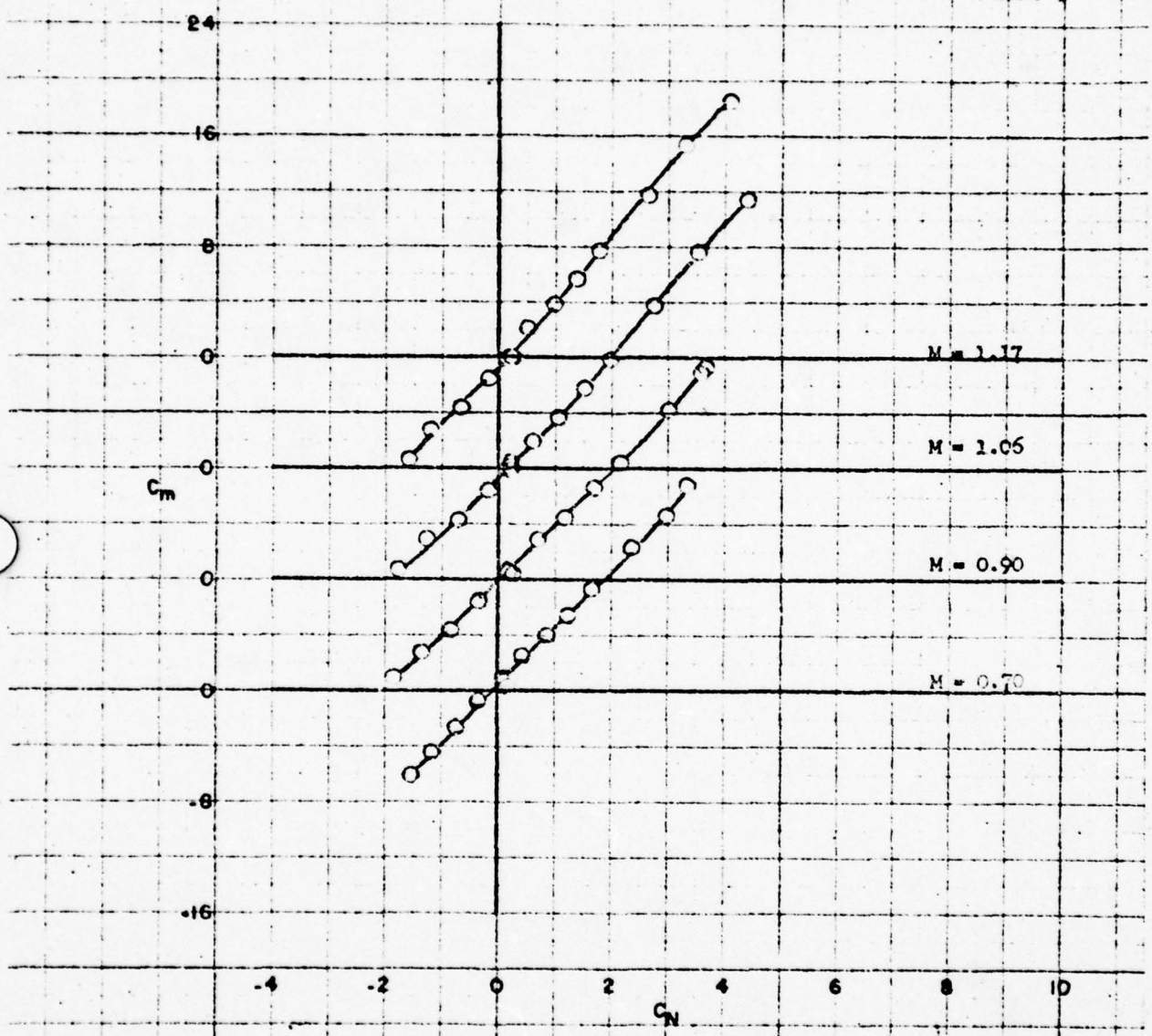

Figure 17 (Continued)

(e) ϕ=0°; i=i'=0°; δ=δ'=0°

FIGURE 17e

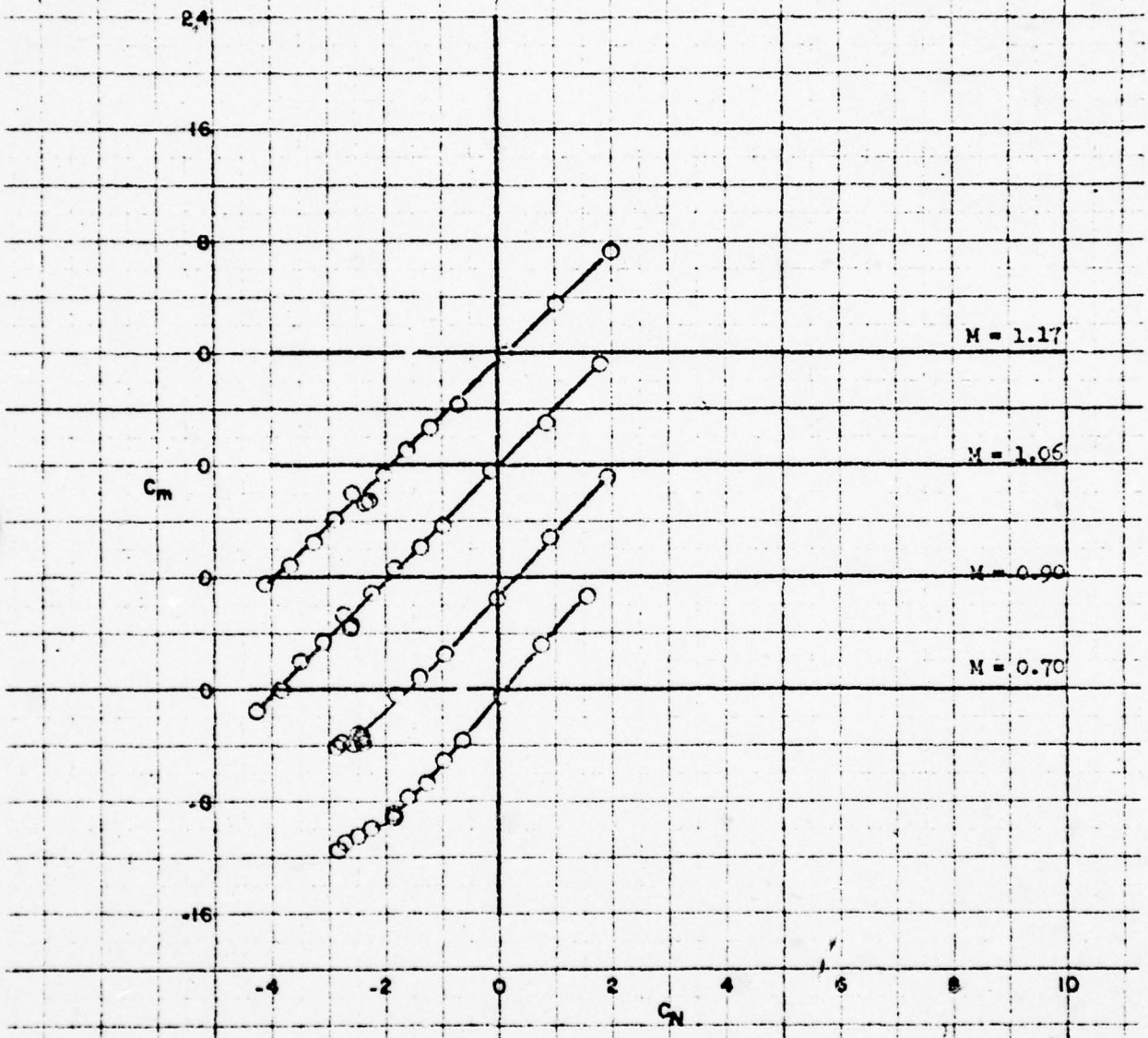

Figure 17 (Concluded)

(f) ϕ=0°; i=-10°, i'=0°; δ=δ'=0°

FIGURE 17f

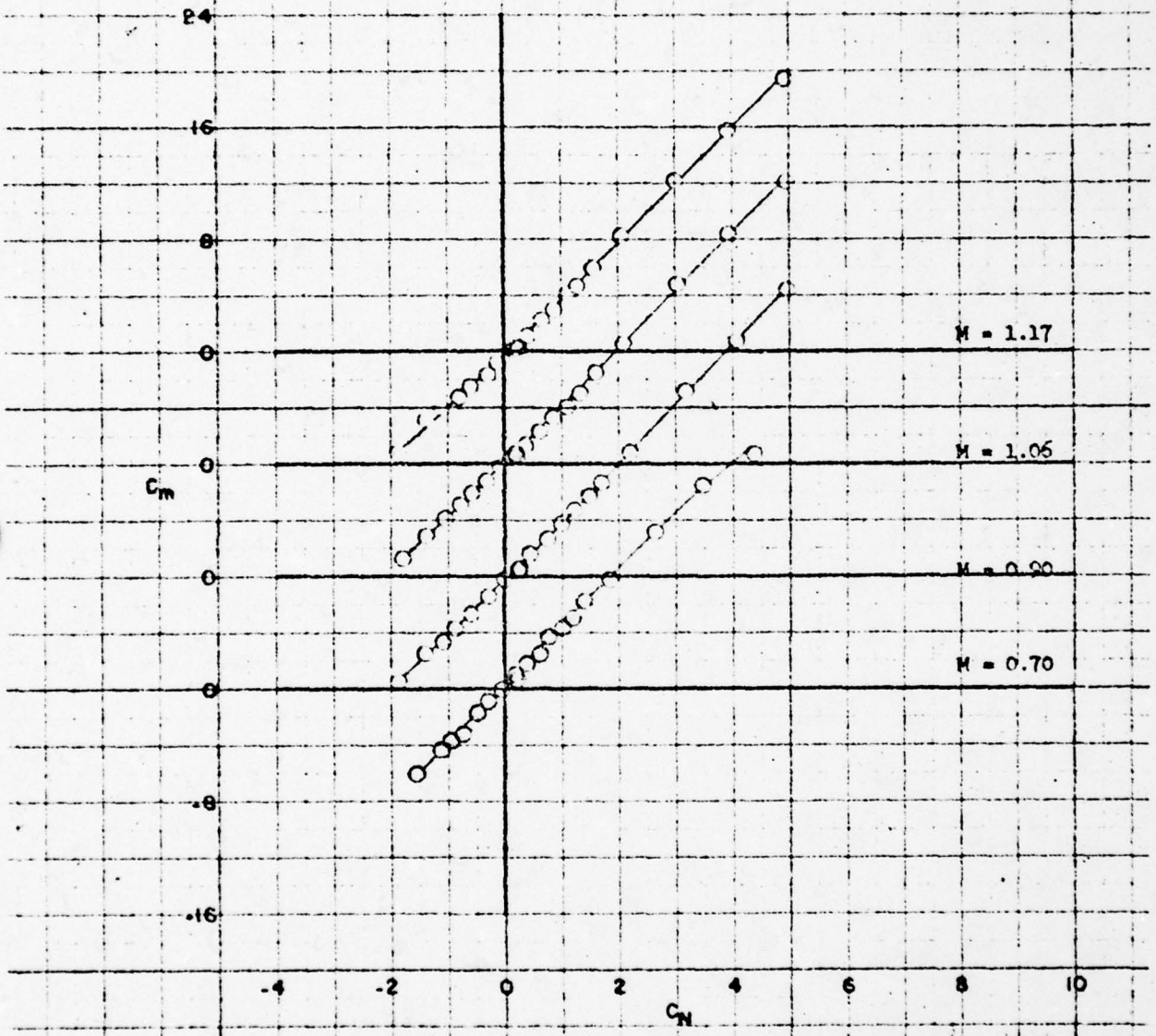

Figure 18 - Variation of Pitching-Moment Coefficient With Normal-Force Coefficient for Configuration $B_{22}R_5H_{10}WT_{10}$

(a) ϕ=-45°; i=i'=0°; δ=δ'=0°

FIGURE 18a

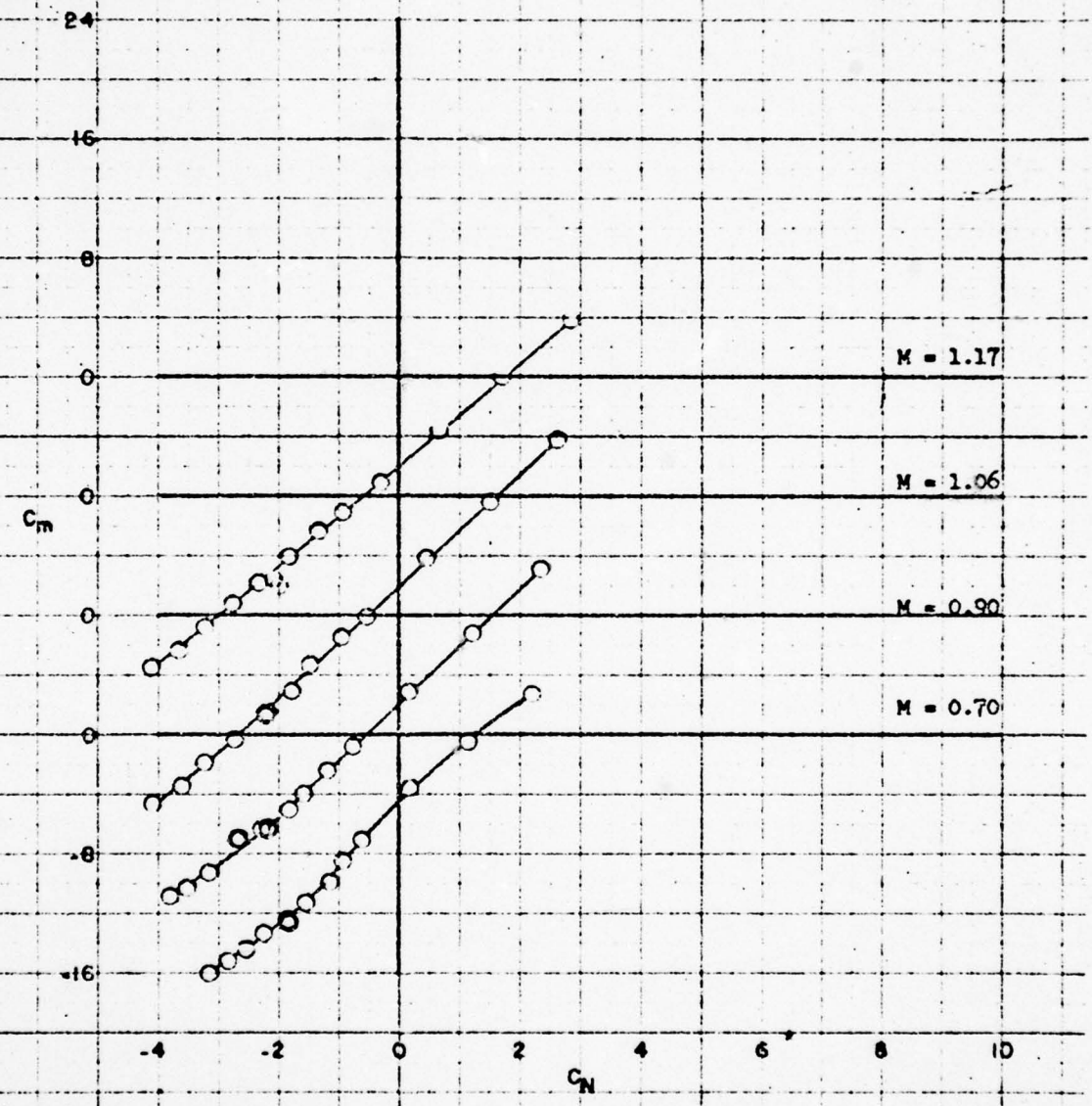

Figure 18 (Continued)

(b) ϕ=-45°; i=i'=-10°; δ=δ'=0°

[redacted]

FIGURE 18b

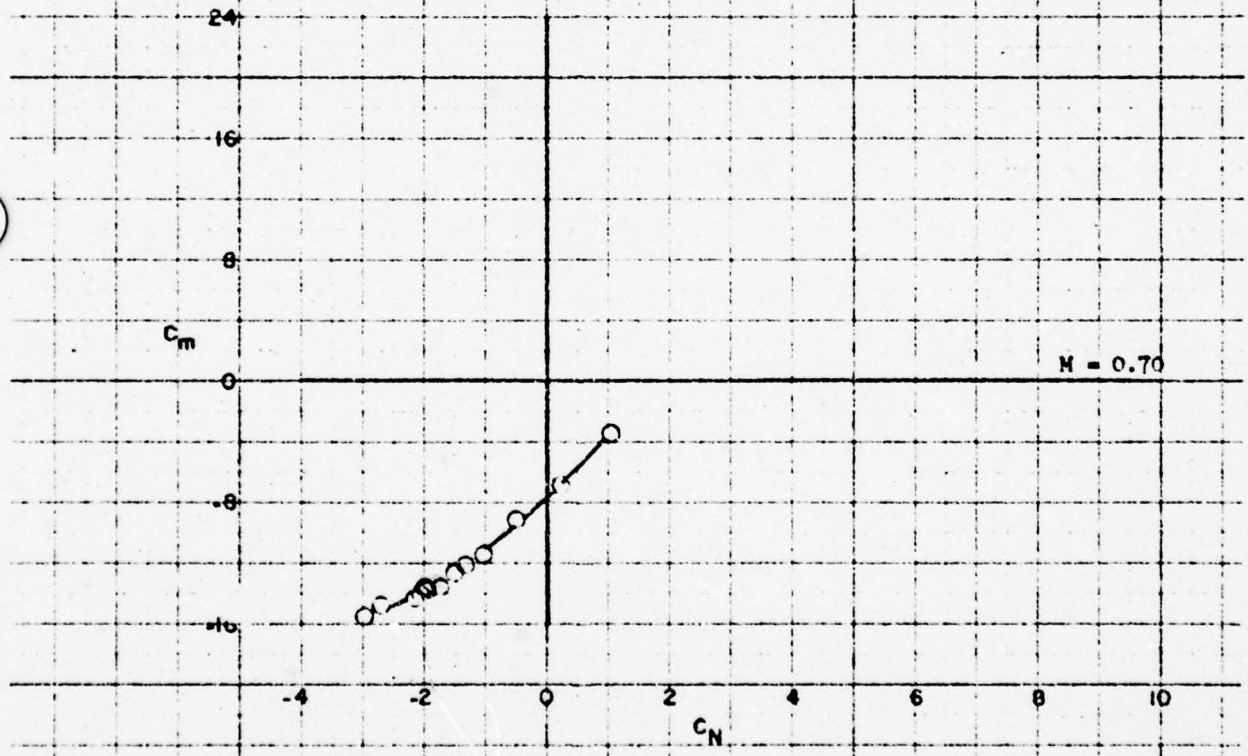

Figure 18 (Continued)

(c) ϕ=-45°; i=i'=-15°; δ=δ'=0°

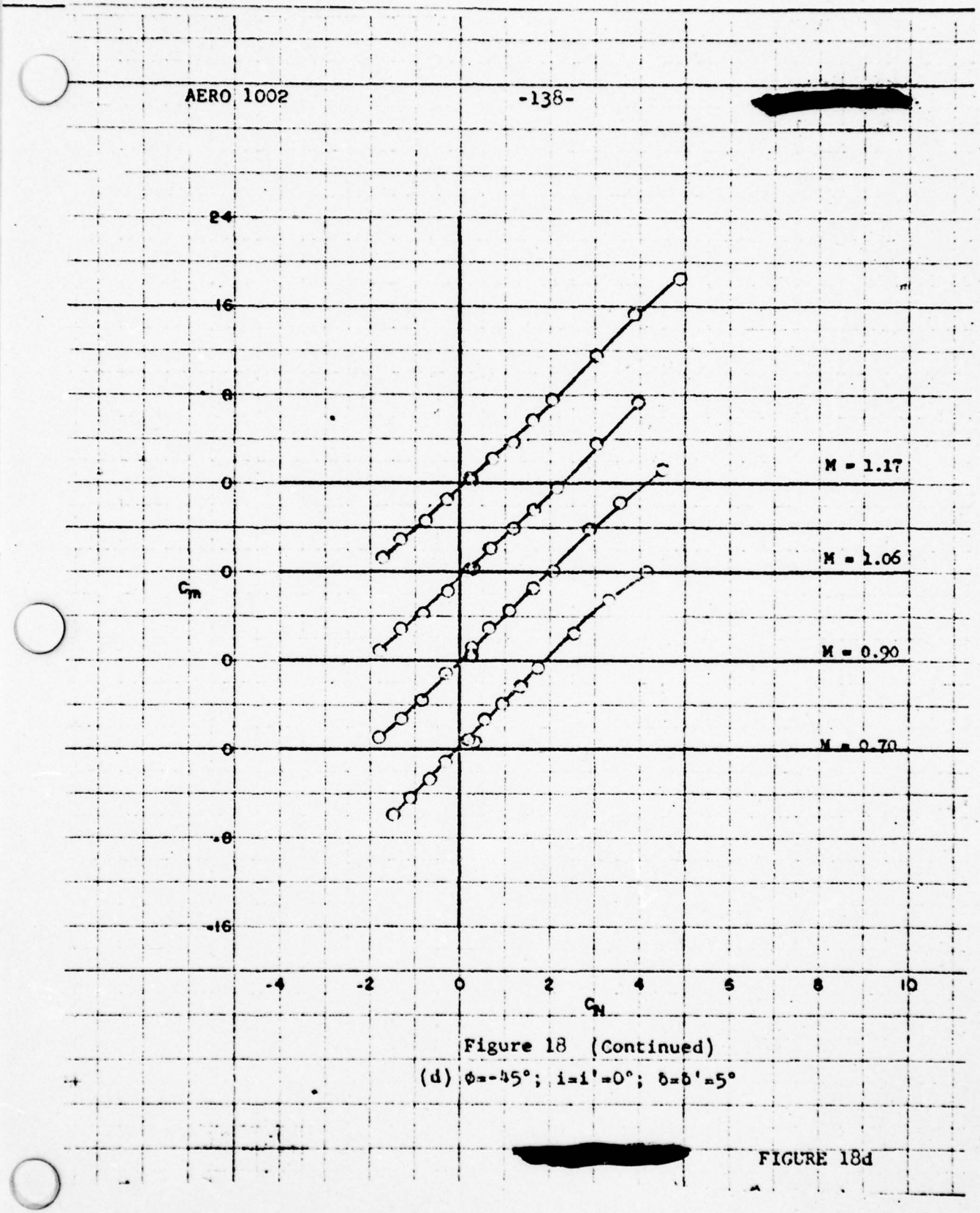

Figure 18 (Continued)

(d) ϕ=-45°; i=i'=0°; δ=δ'=5°

FIGURE 18d

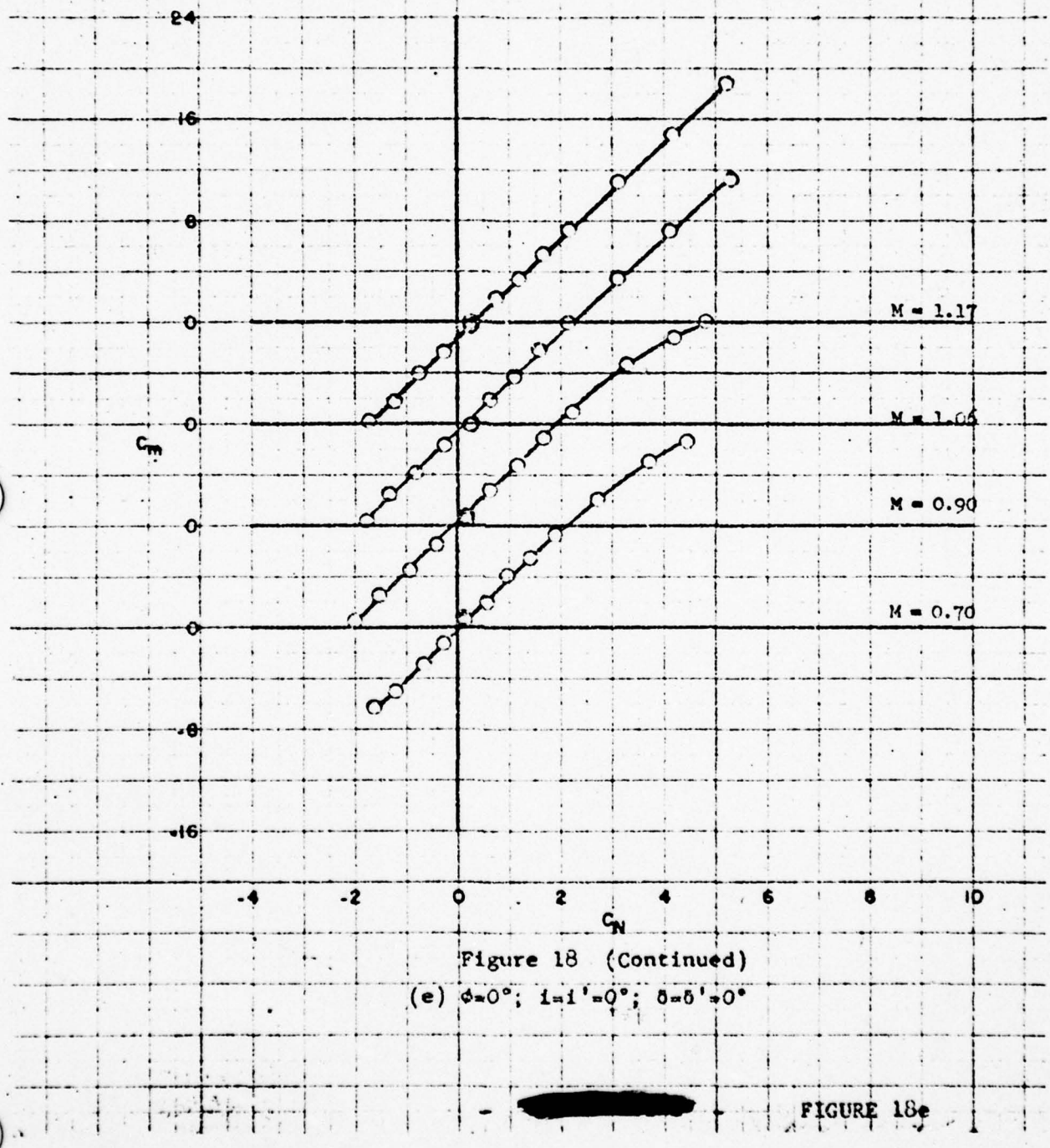

Figure 18 (Continued)

(e) $\phi=0°$; $i=i'=0°$; $\delta=\delta'=0°$

[redacted]

FIGURE 18e

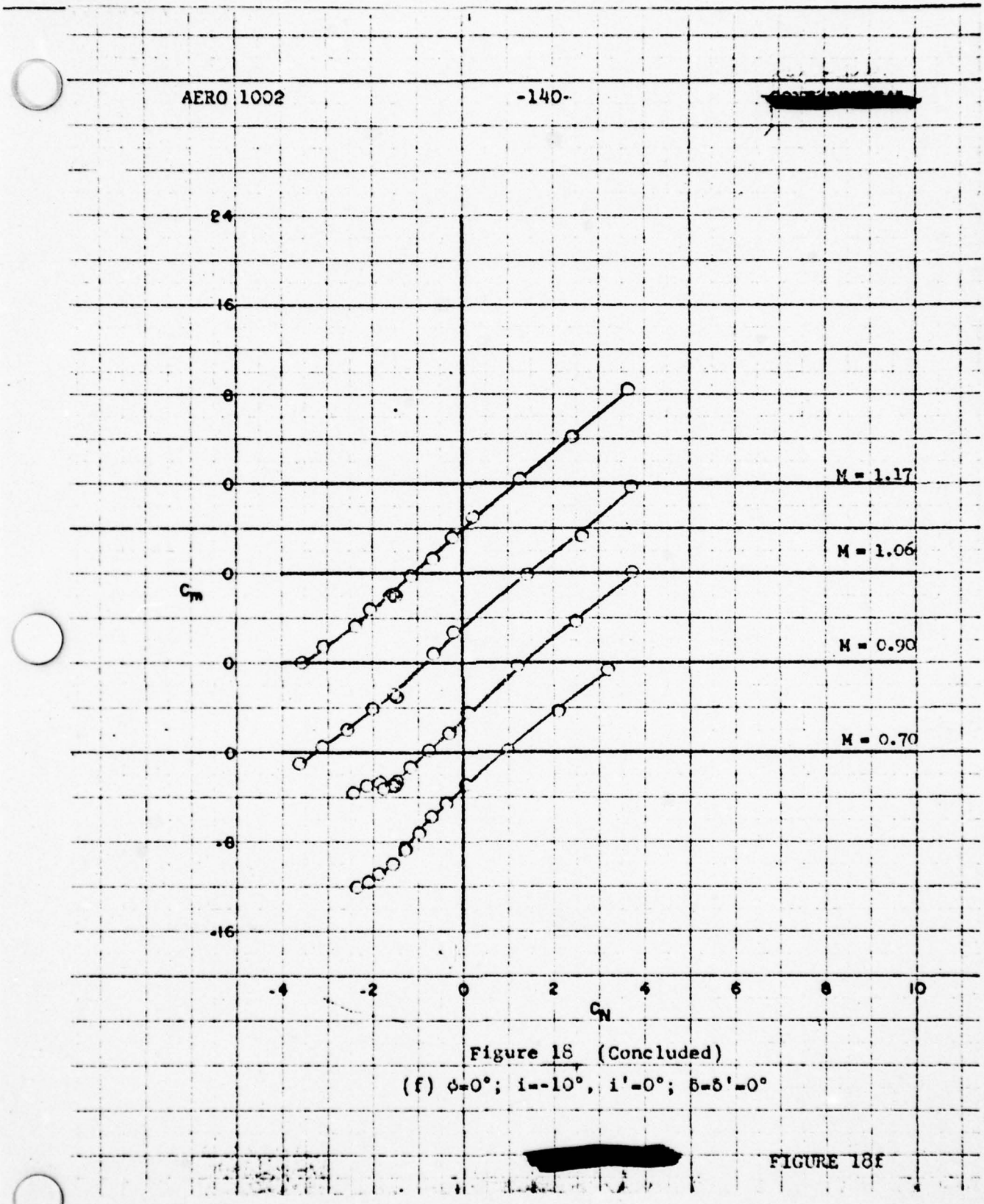

Figure 18 (Concluded)

(f) ϕ=0°; i=-10°, i'=0°; δ-δ'=0°

FIGURE 18f

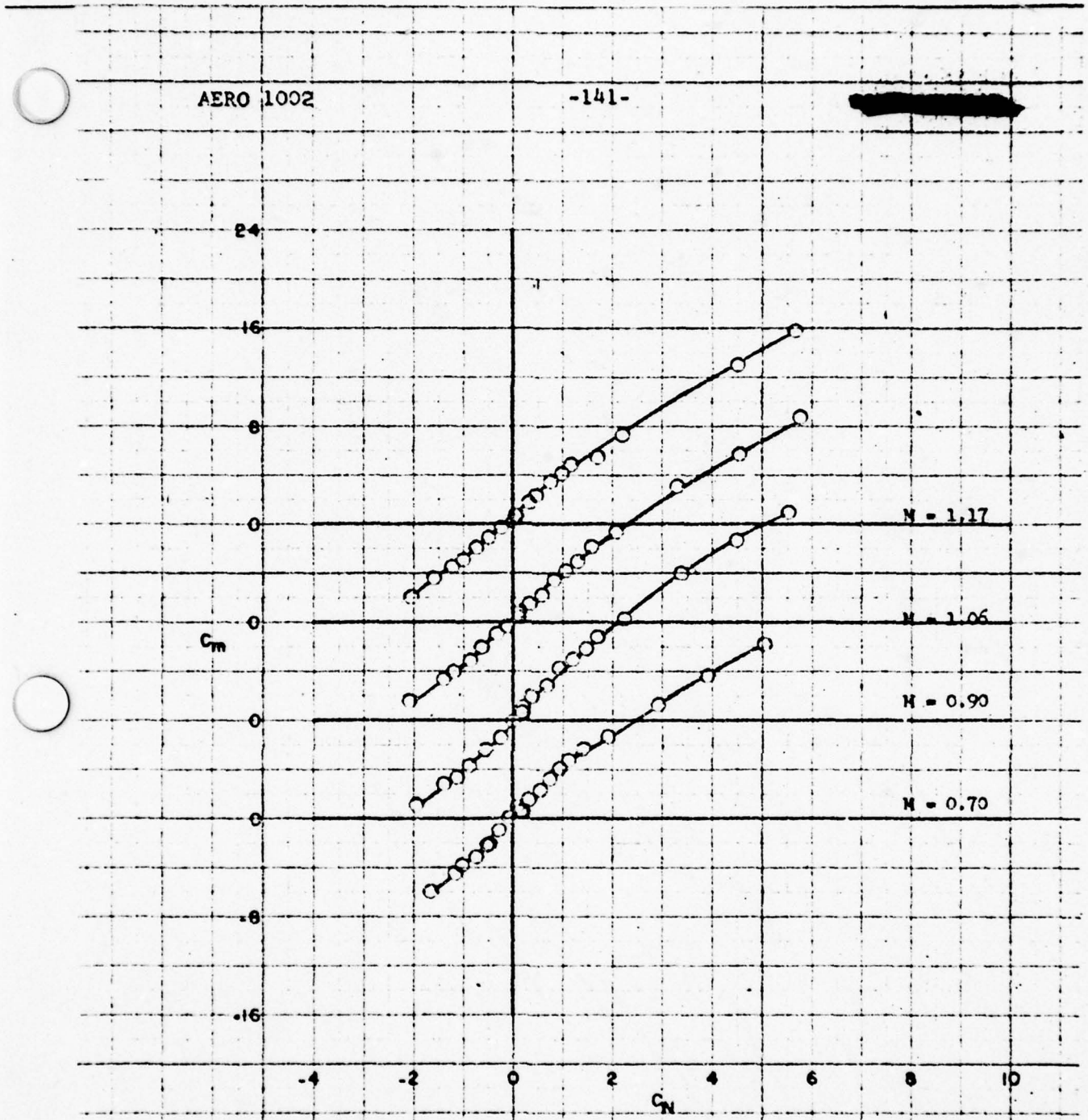

Figure 19 - Variation of Pitching-Moment Coefficient With Normal-Force Coefficient for Configuration $B_{22}R_5H_{10}WT_{10}F_{18}$

(a) ϕ=-45°; i=i'=0°; δ=δ'=0°

[redacted] FIGURE 19a

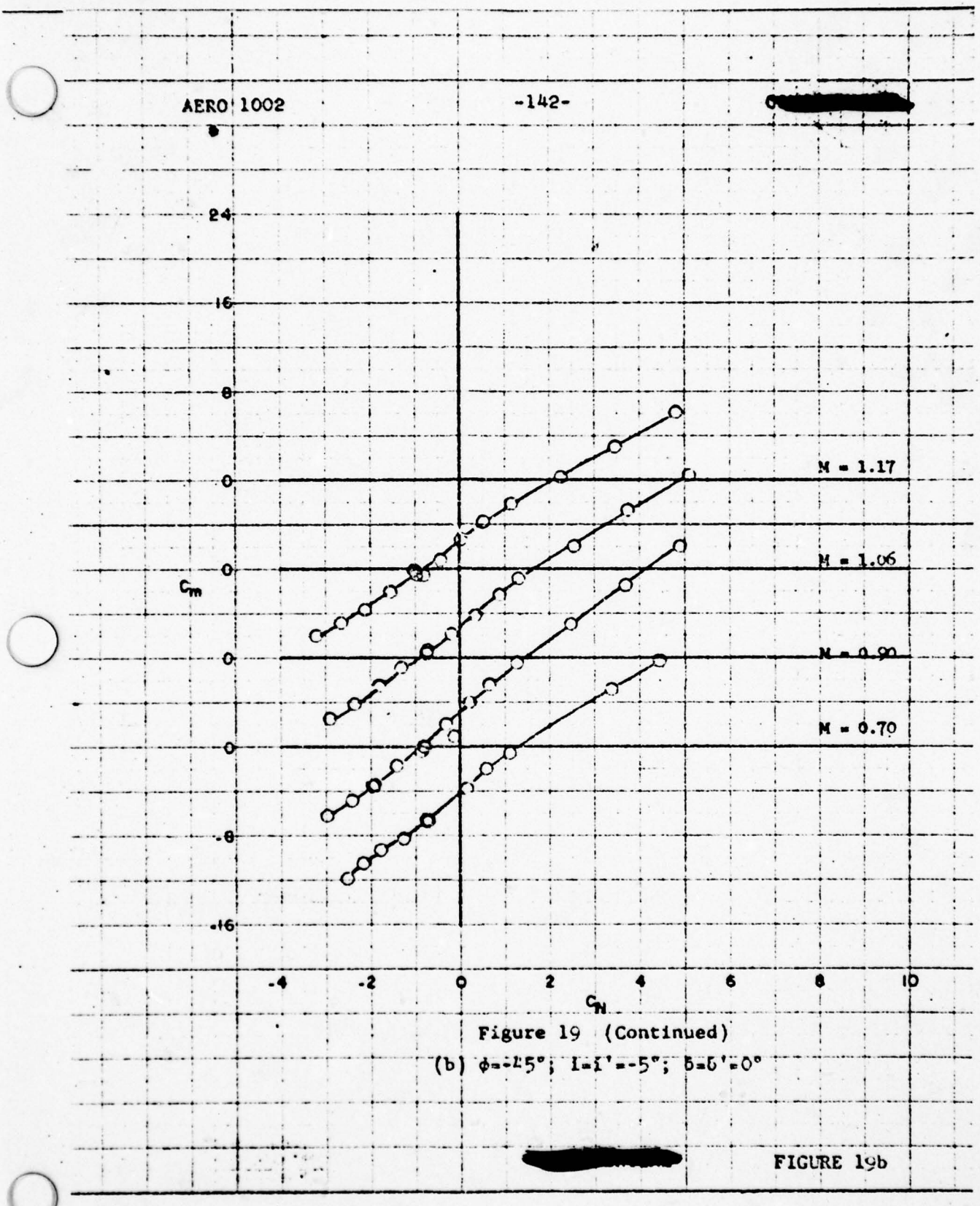

Figure 19 (Continued)

(b) ϕ=-45°; i=i'=-5°; β=β'=0°

FIGURE 19b

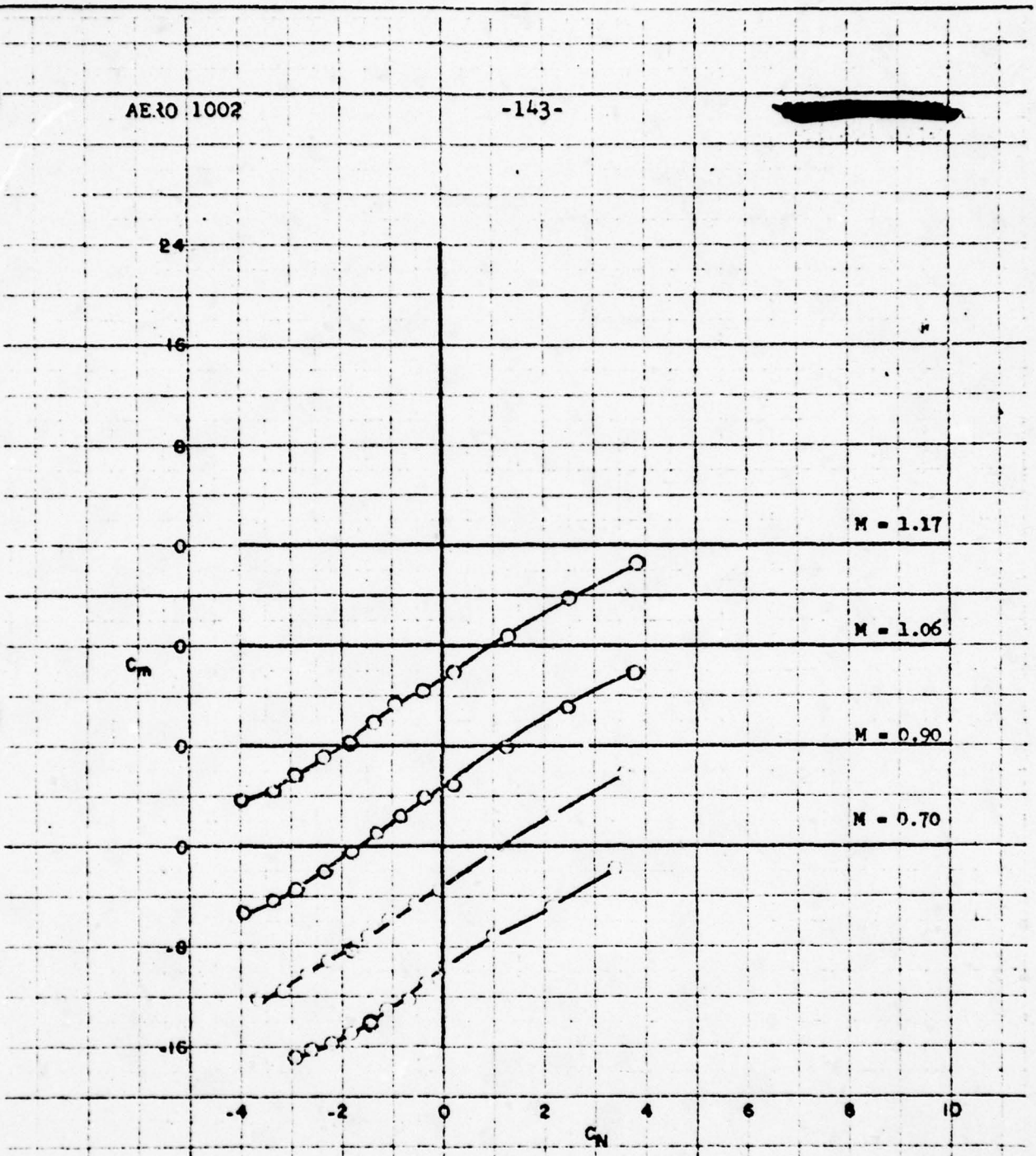

Figure 19 (Continued)

(c) ϕ=-45°; i=i'=-10°; δ=δ'=0°

[redacted] FIGURE 19c

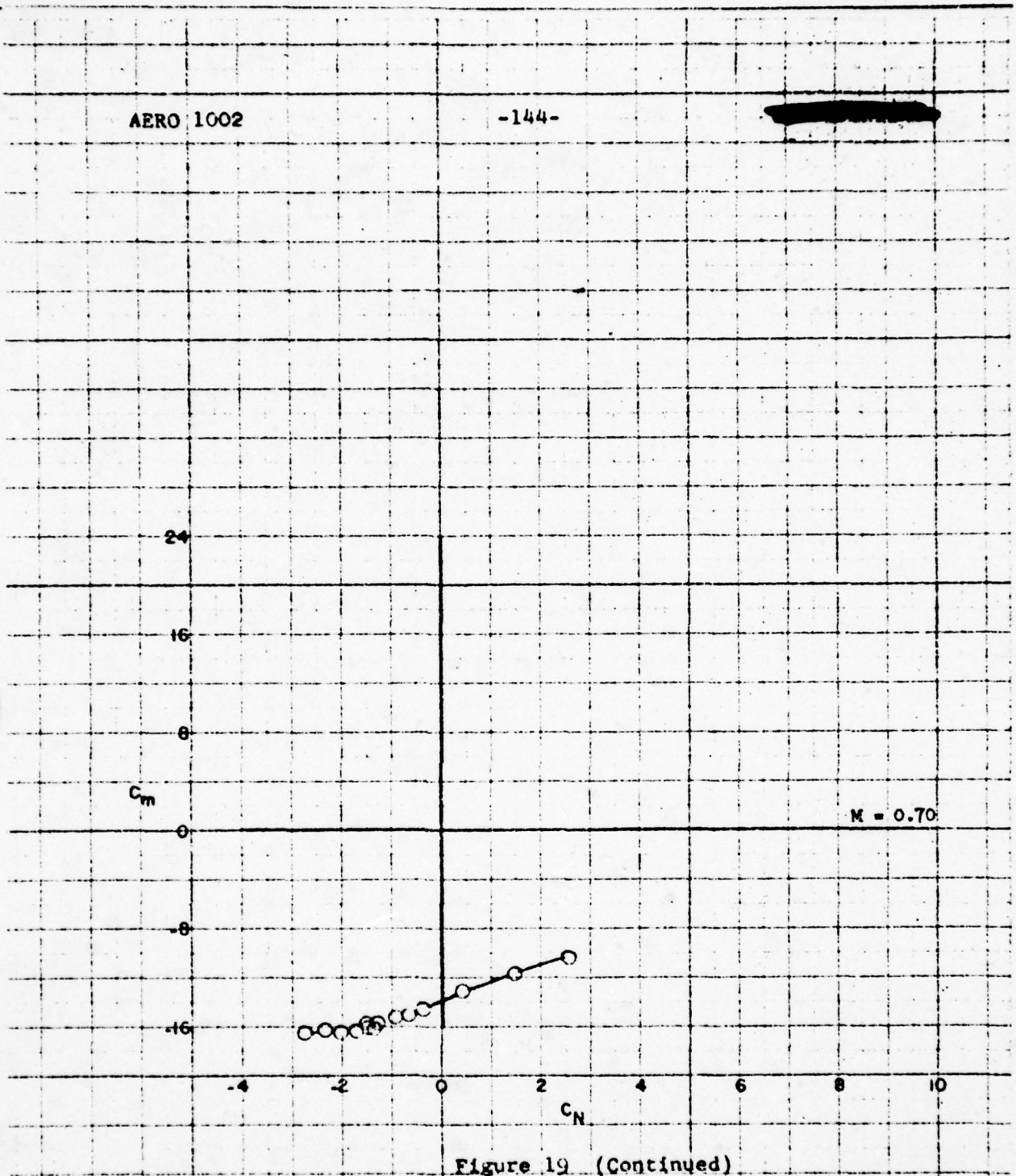

Figure 19 (Continued)

(d) ϕ=-45°; i=i'=-15°; δ=δ'=0°

FIGURE 19d

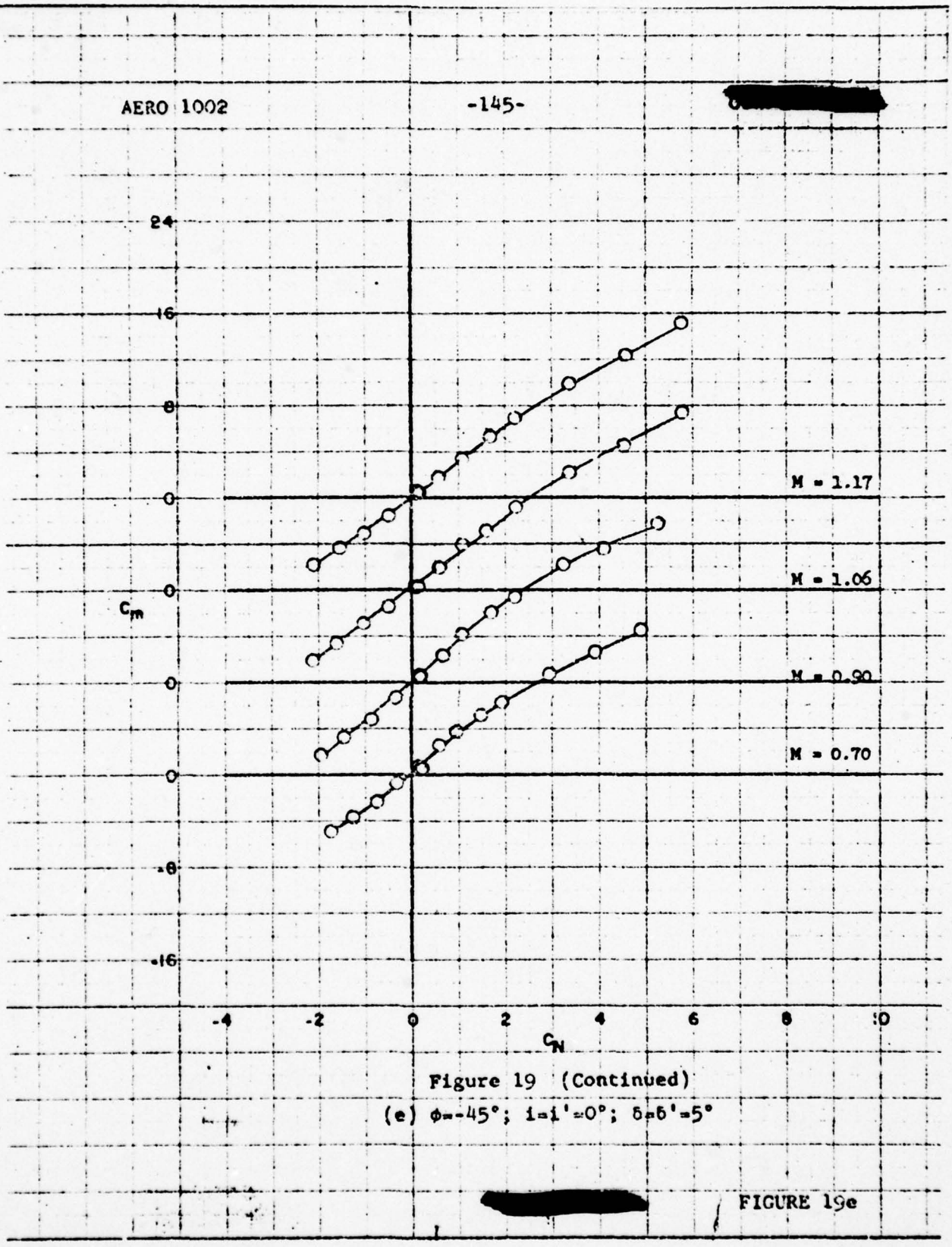

Figure 19 (Continued)

(e) ϕ=-45°; i=i'=0°; δ=δ'=5°

FIGURE 19e

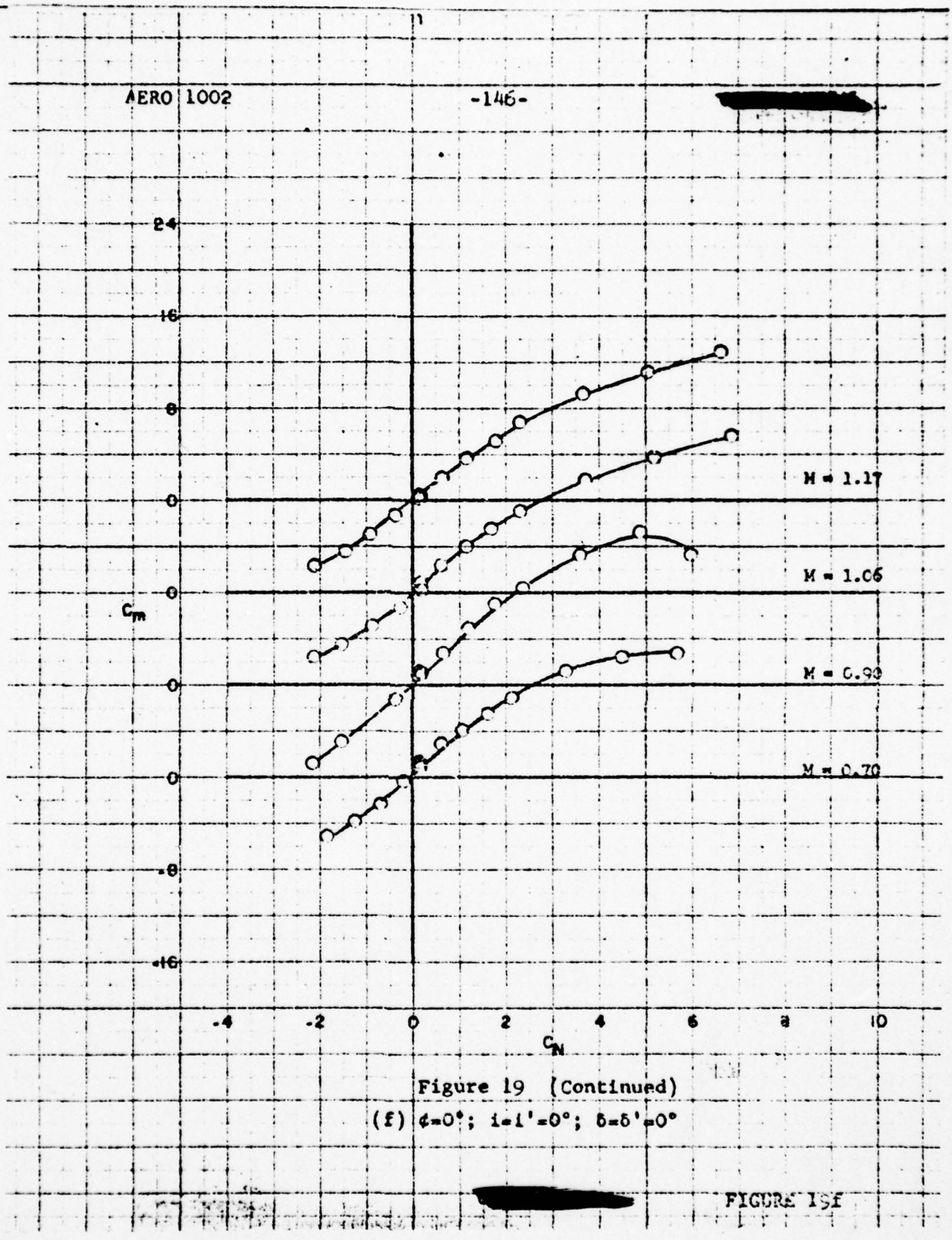

Figure 19 (Continued)

(f) ϕ=0°; i=i'=0°; δ=δ'=0°

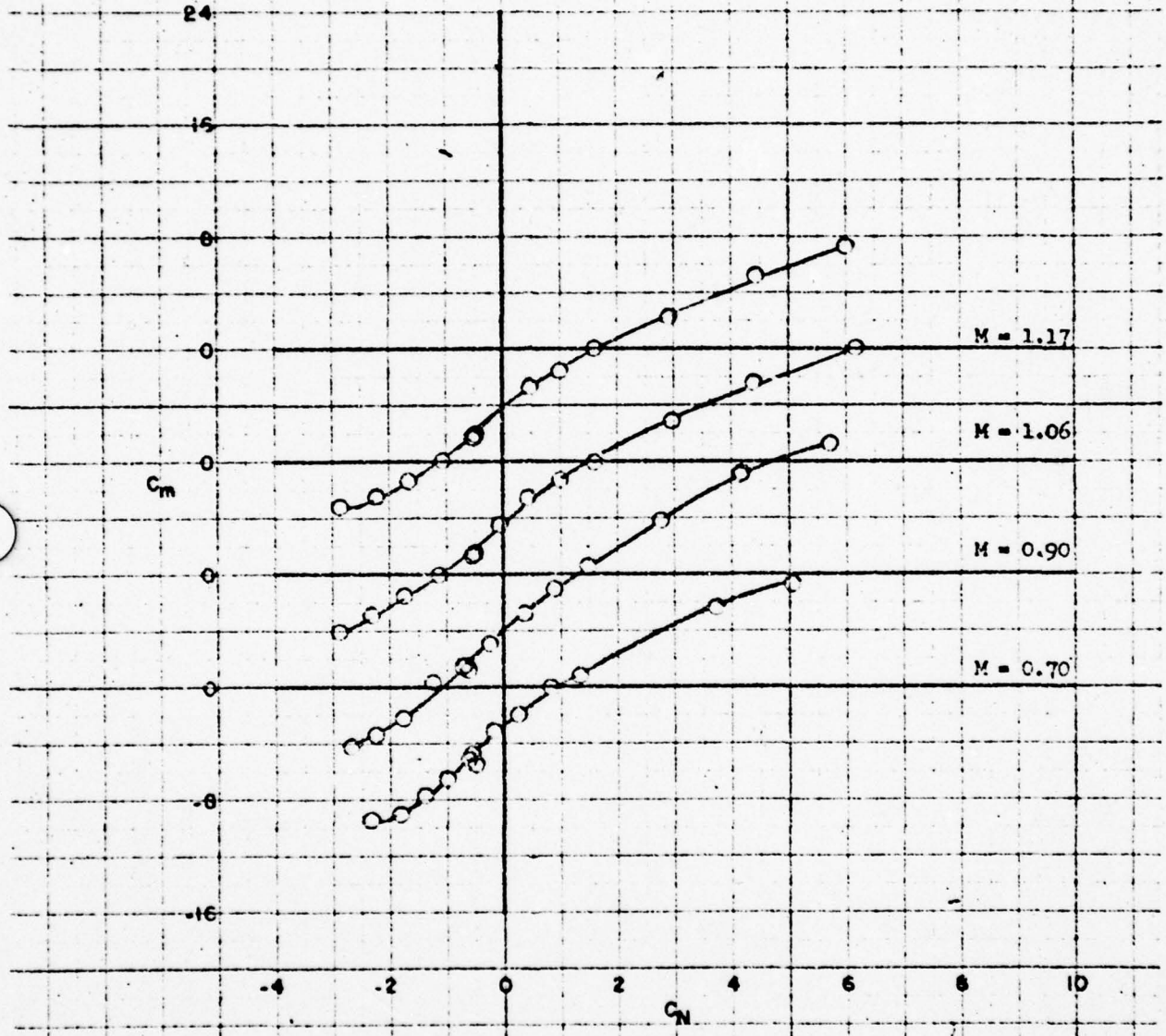

Figure 19 (Continued)

(g) ϕ=0°; i=-5°, i'=0°; δ=δ'=0°

FIGURE 19g

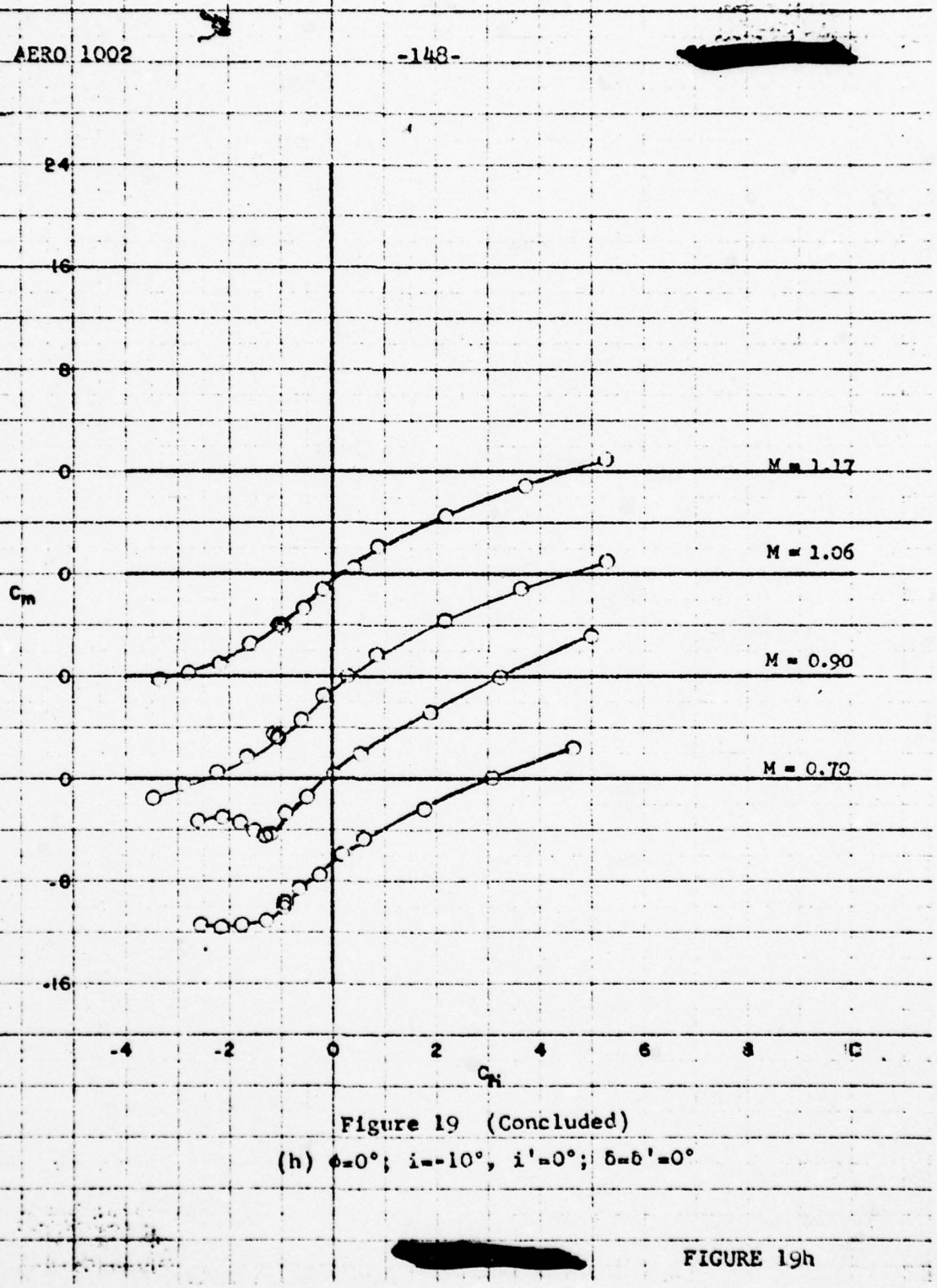

Figure 19 (Concluded)

(h) ϕ=0°; i=-10°, i'=0°; δ=δ'=0°

FIGURE 19h

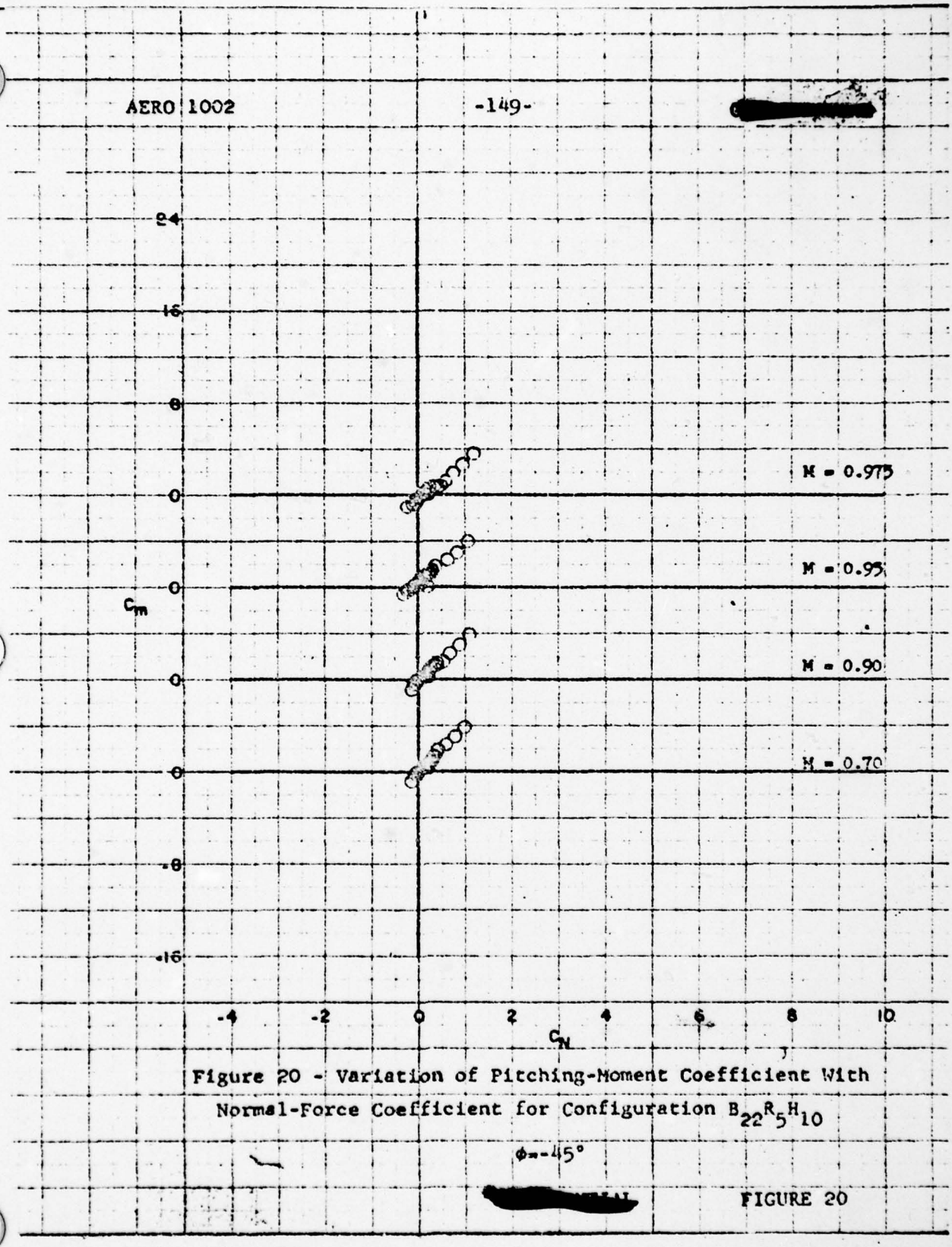

Figure 20 - Variation of Pitching-Moment Coefficient With Normal-Force Coefficient for Configuration $B_{22}R_5H_{10}$

ϕ=-45°

[redacted]

FIGURE 20

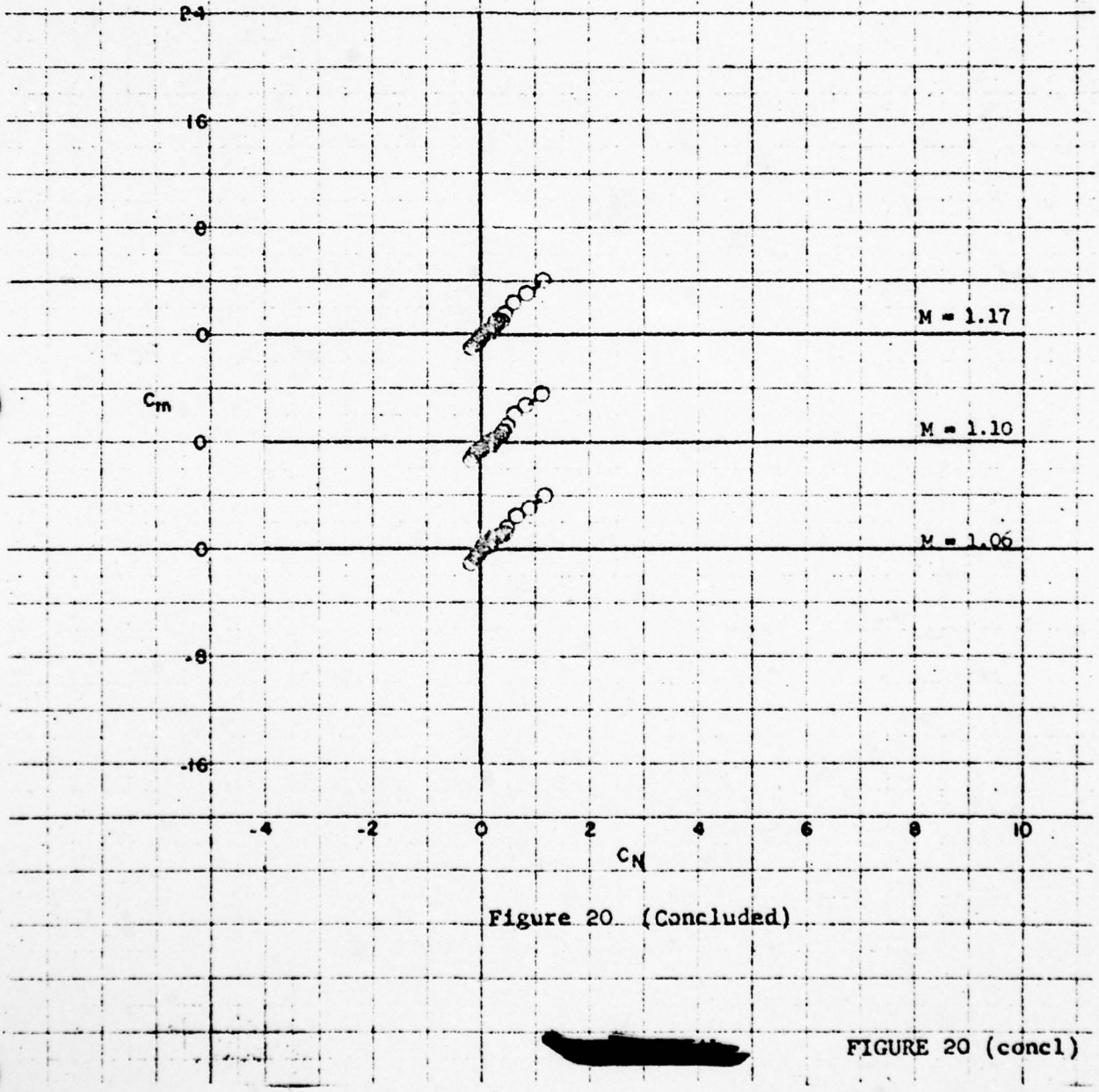

Figure 20. (Concluded)

FIGURE 20 (concl)

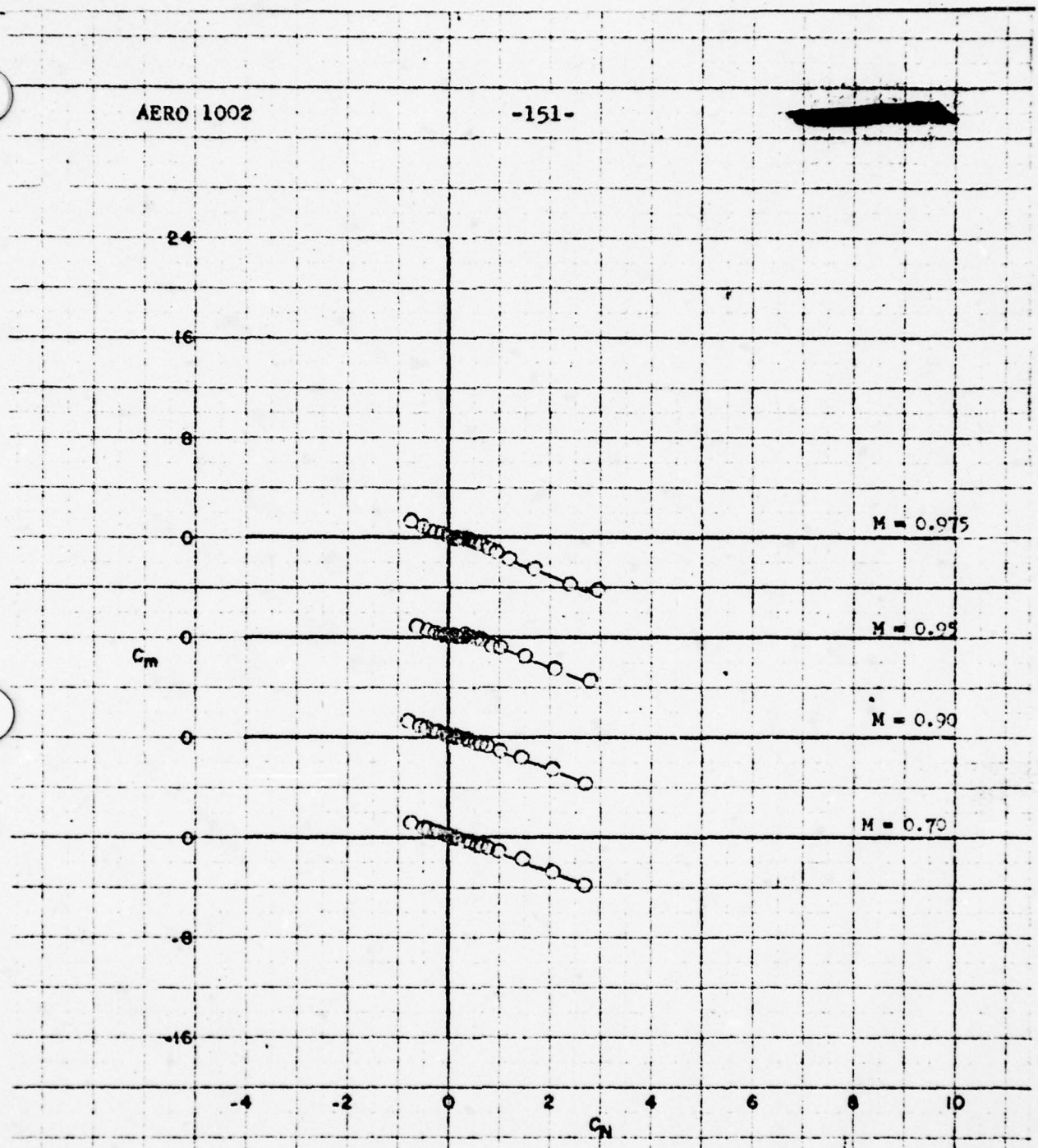

Figure 21 - Variation of Pitching-Moment Coefficient With Normal-Force Coefficient for Configuration $B_{22}R_5H_{10}F_{18}$

ϕ=-45°

[redacted]

FIGURE 21

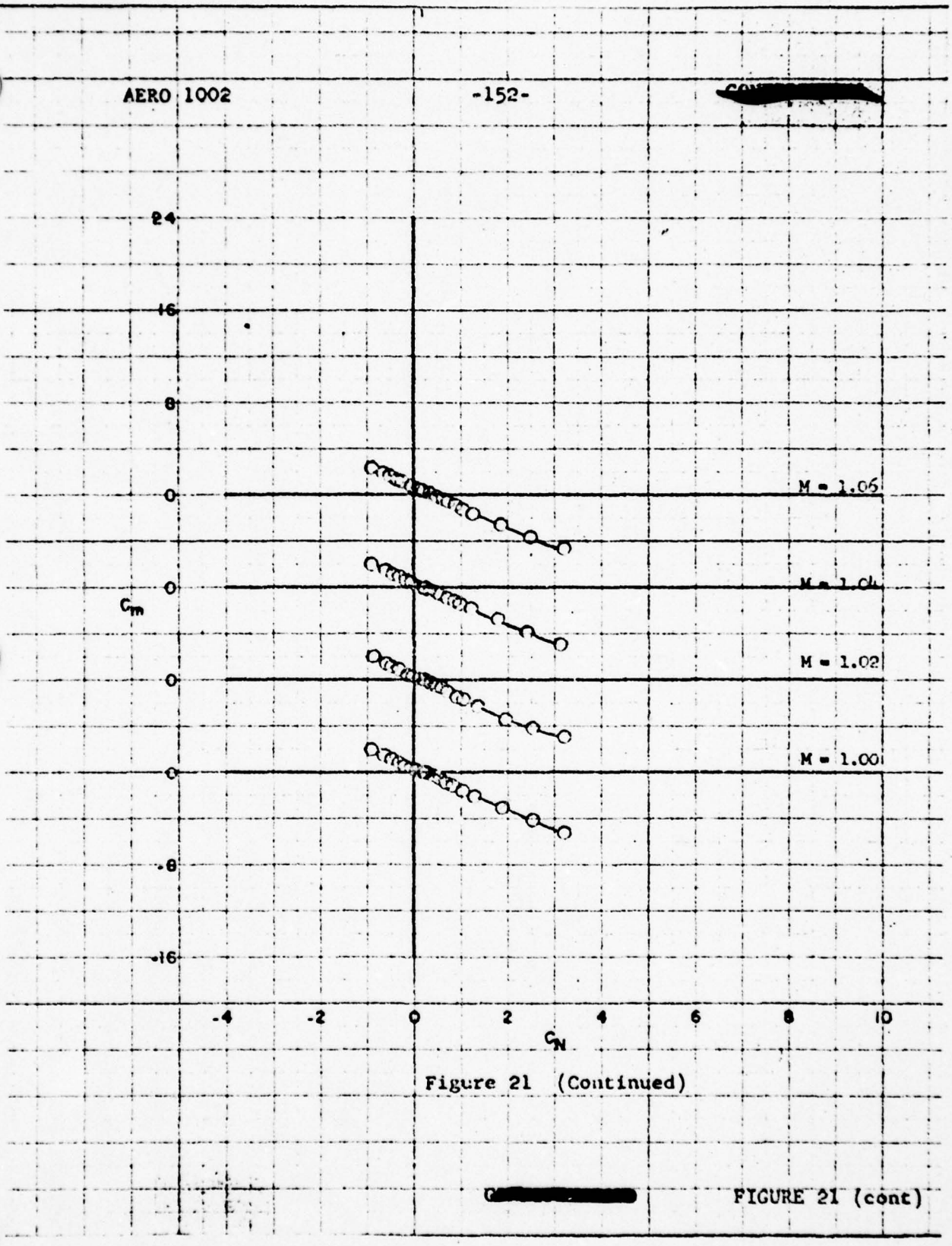

Figure 21 (Continued)

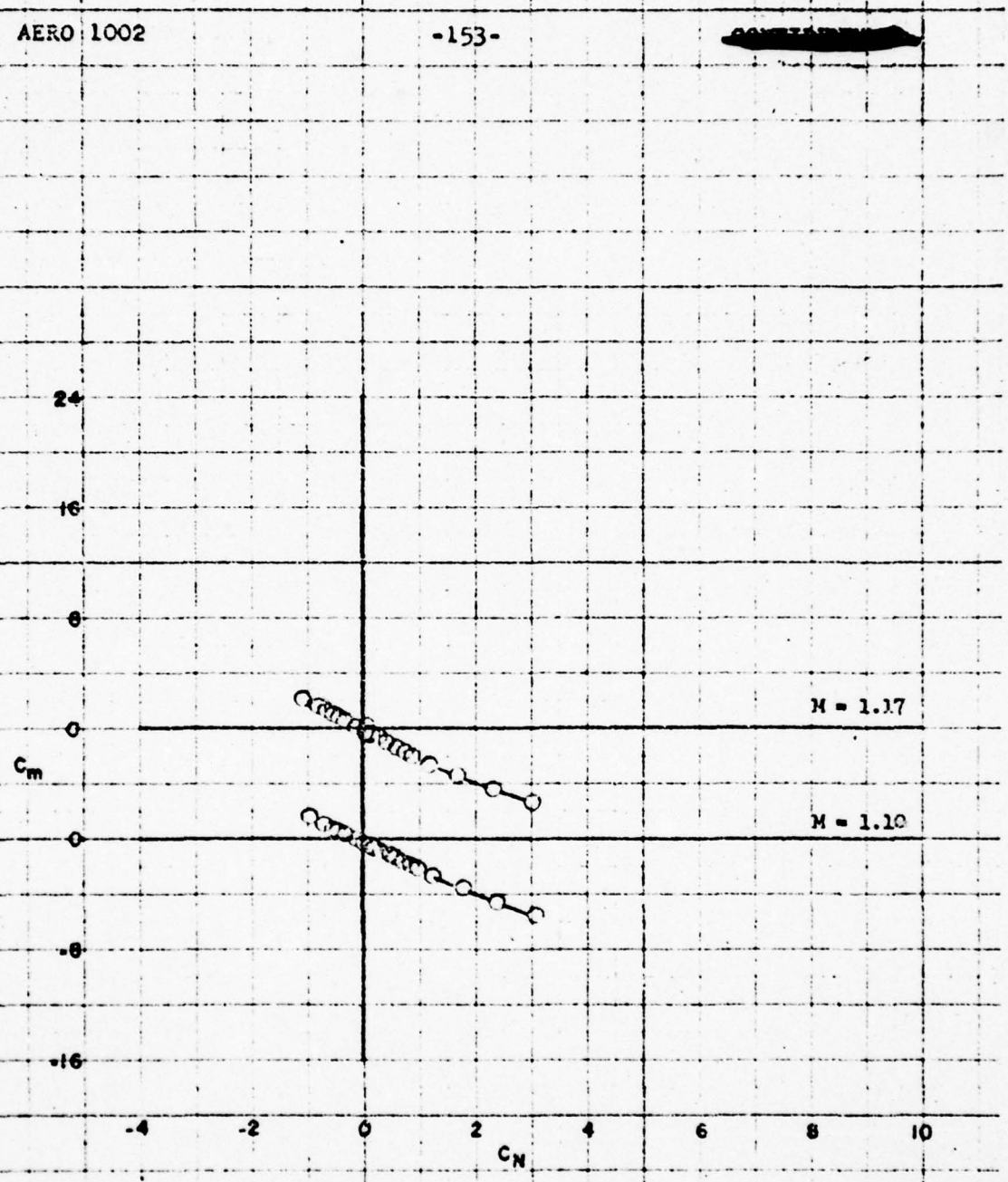

Figure 21 (Concluded)

[redacted] FIGURE 21 (concl)

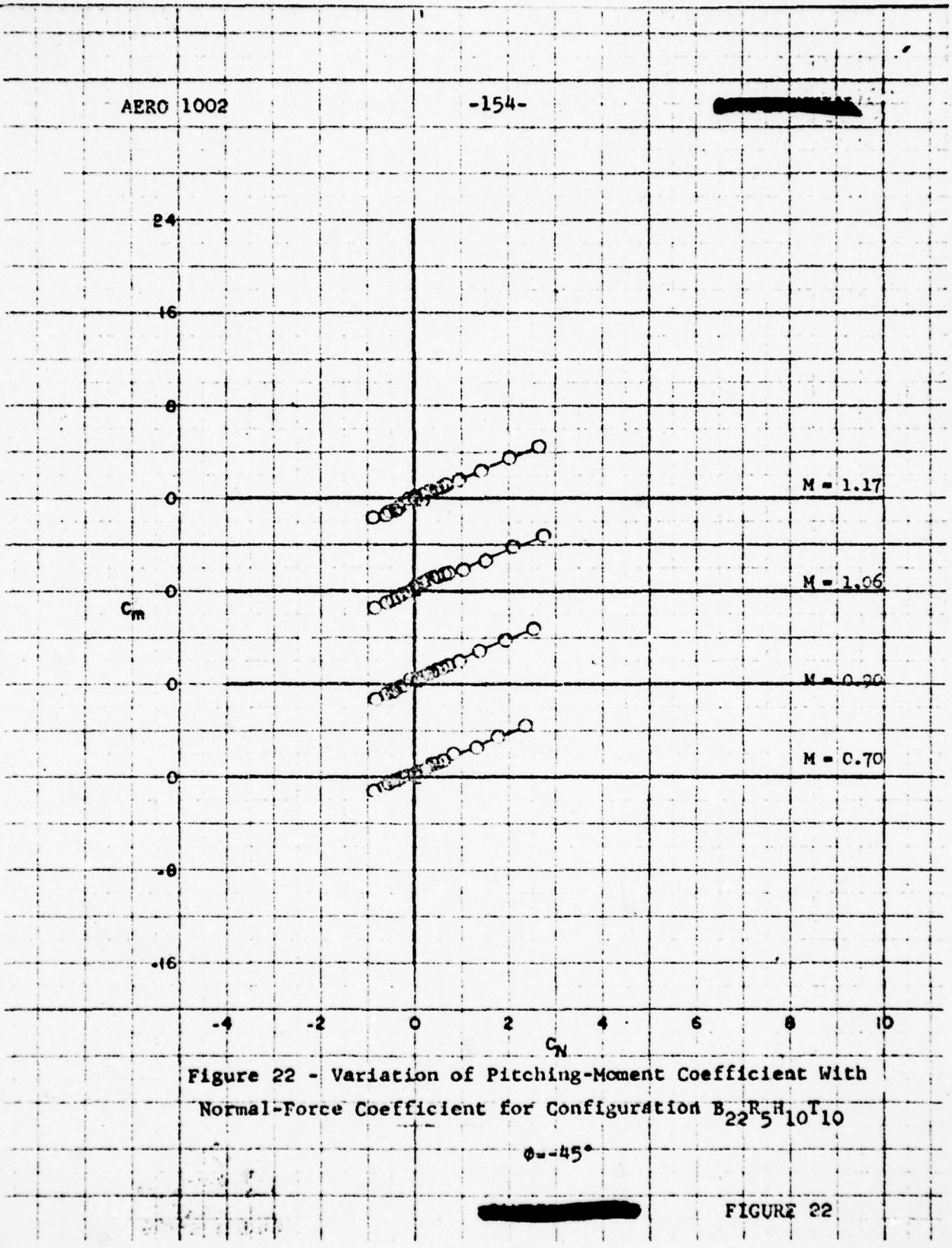

Figure 22 - Variation of Pitching-Moment Coefficient With Normal-Force Coefficient for Configuration $B_{22}R_5H_{10}T_{10}$

$\phi = -45°$

[redacted] FIGURE 22

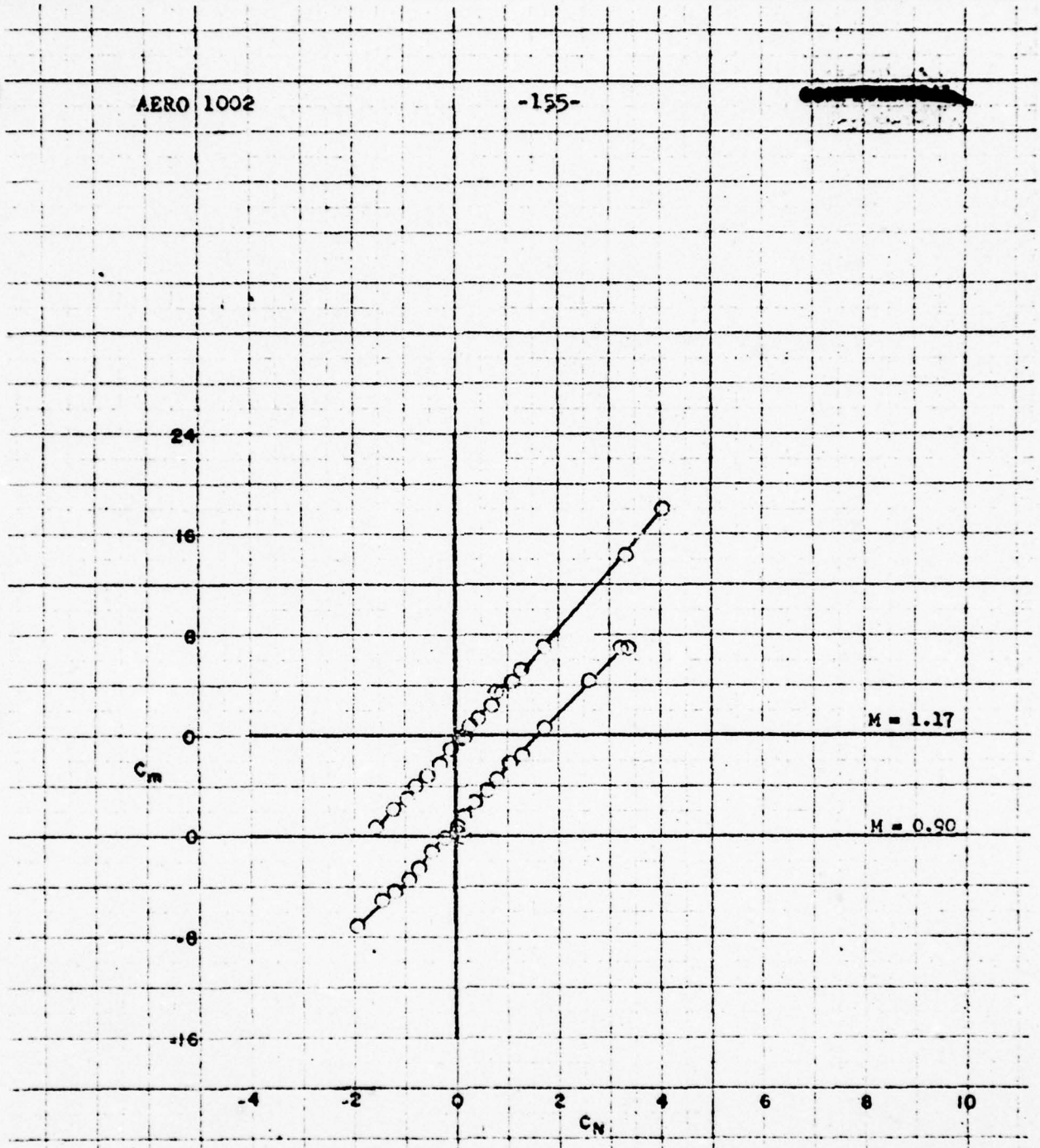

Figure 23 - Variation of Pitching-Moment Coefficient With Normal-Force Coefficient for Configuration $B_{22}R_5H_{10}WC$

(a) ϕ=0°; i=i'=0°; δ=δ'=0°

FIGURE 23a

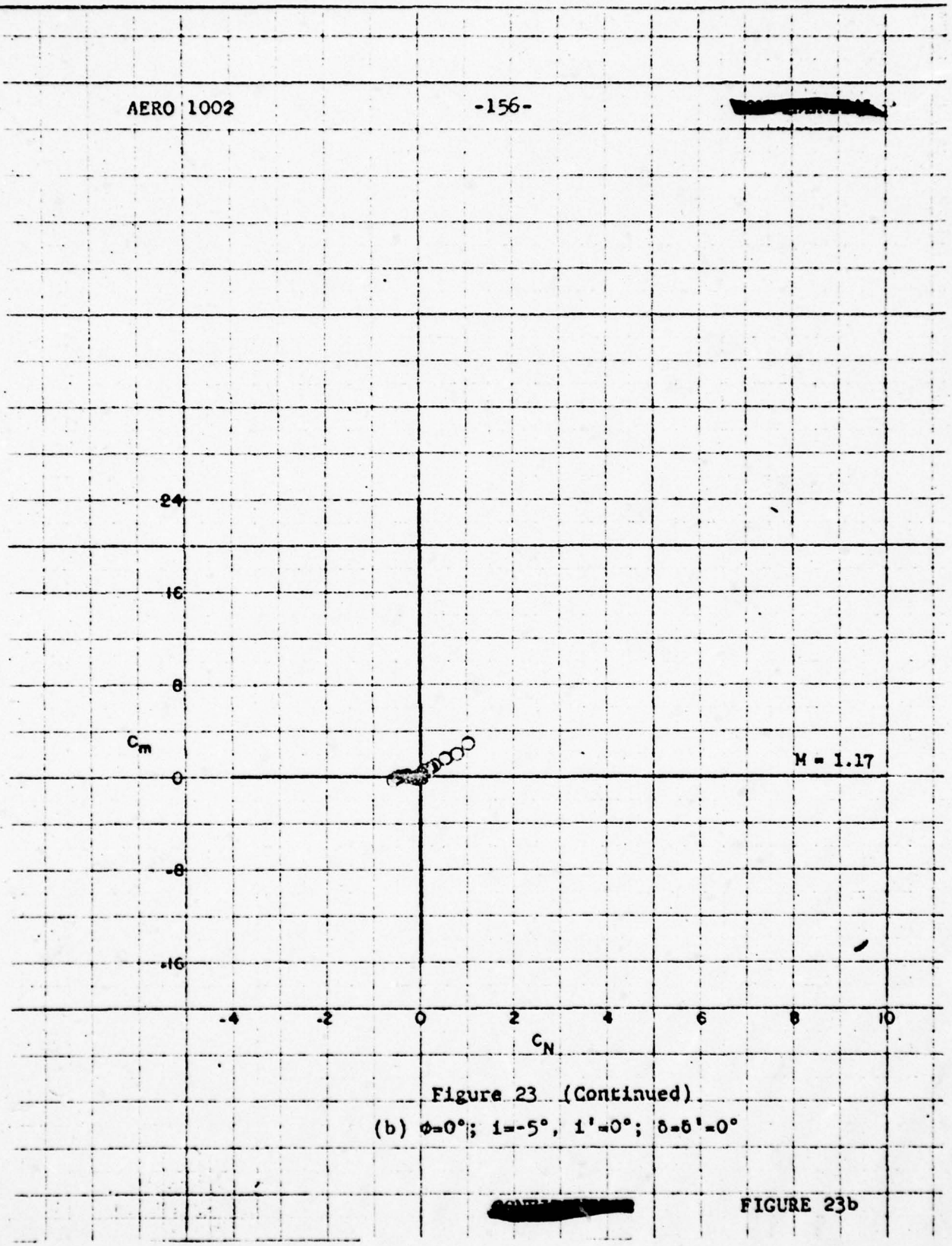

Figure 23 (Continued)

(b) ϕ=0°; i=-5°, i'=0°; δ=δ'=0°

FIGURE 23b

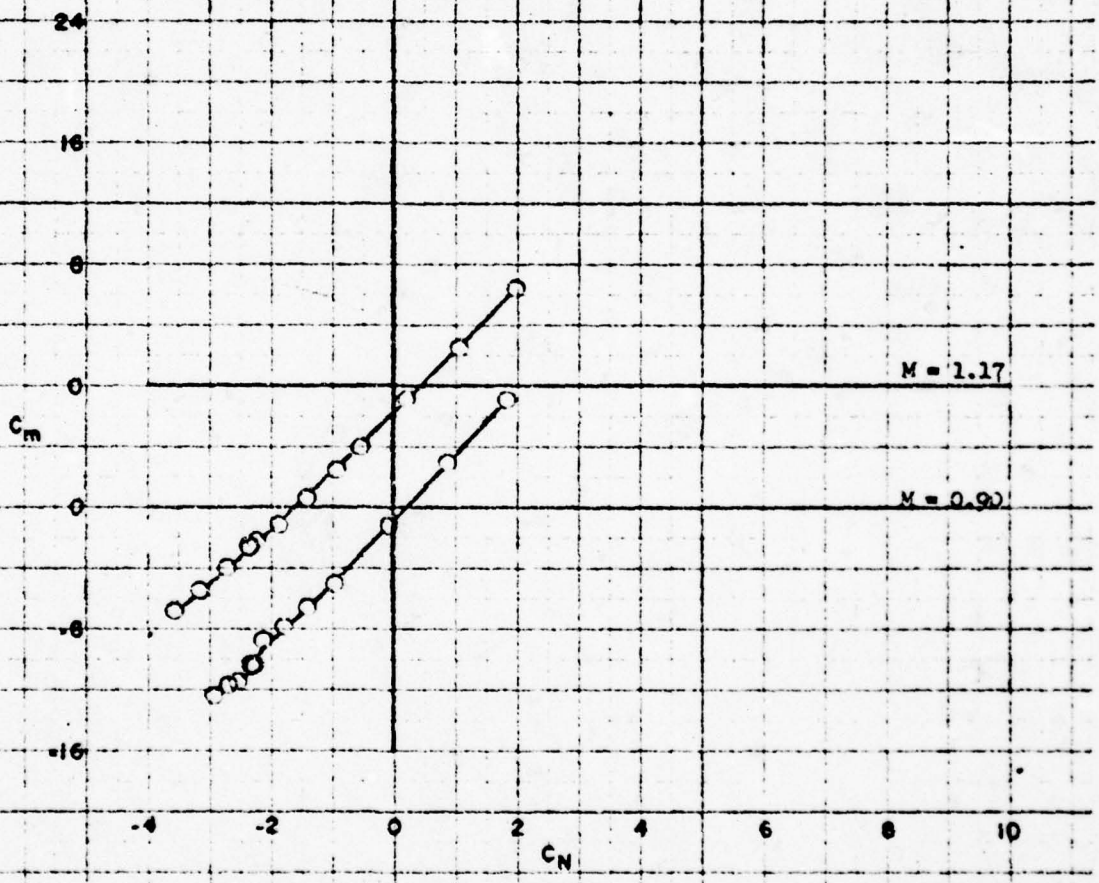

Figure 23 (Concluded)

(c) ϕ=0°; i=-10°, i'=0°; δ=δ'=0°

FIGURE 23c

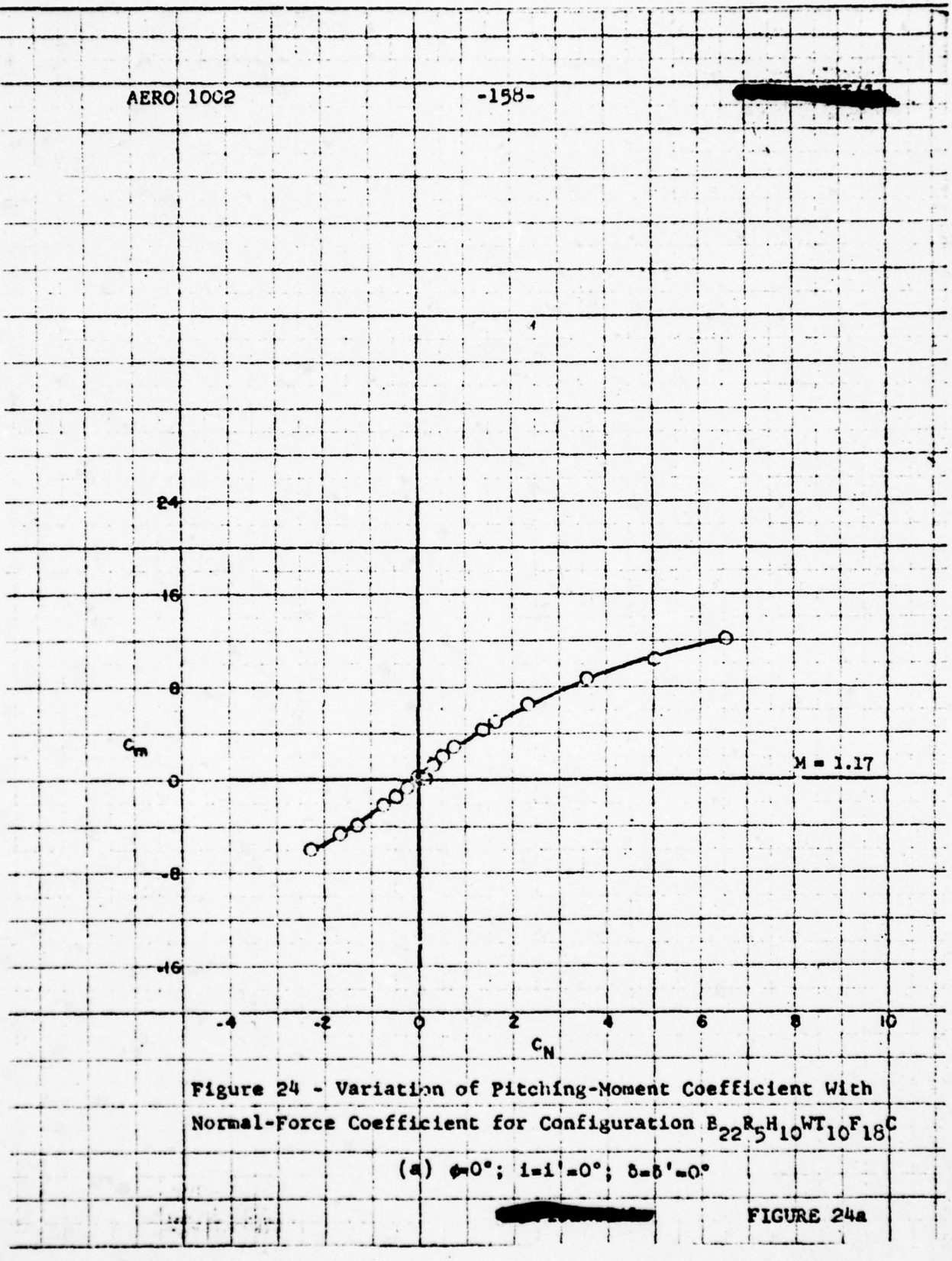

Figure 24 - Variation of Pitching-Moment Coefficient With Normal-Force Coefficient for Configuration $B_{22}R_5H_{10}WT_{10}F_{18}C$

(a) ϕ=0°; i=i'=0°; δ=δ'=0°

[redacted] FIGURE 24a

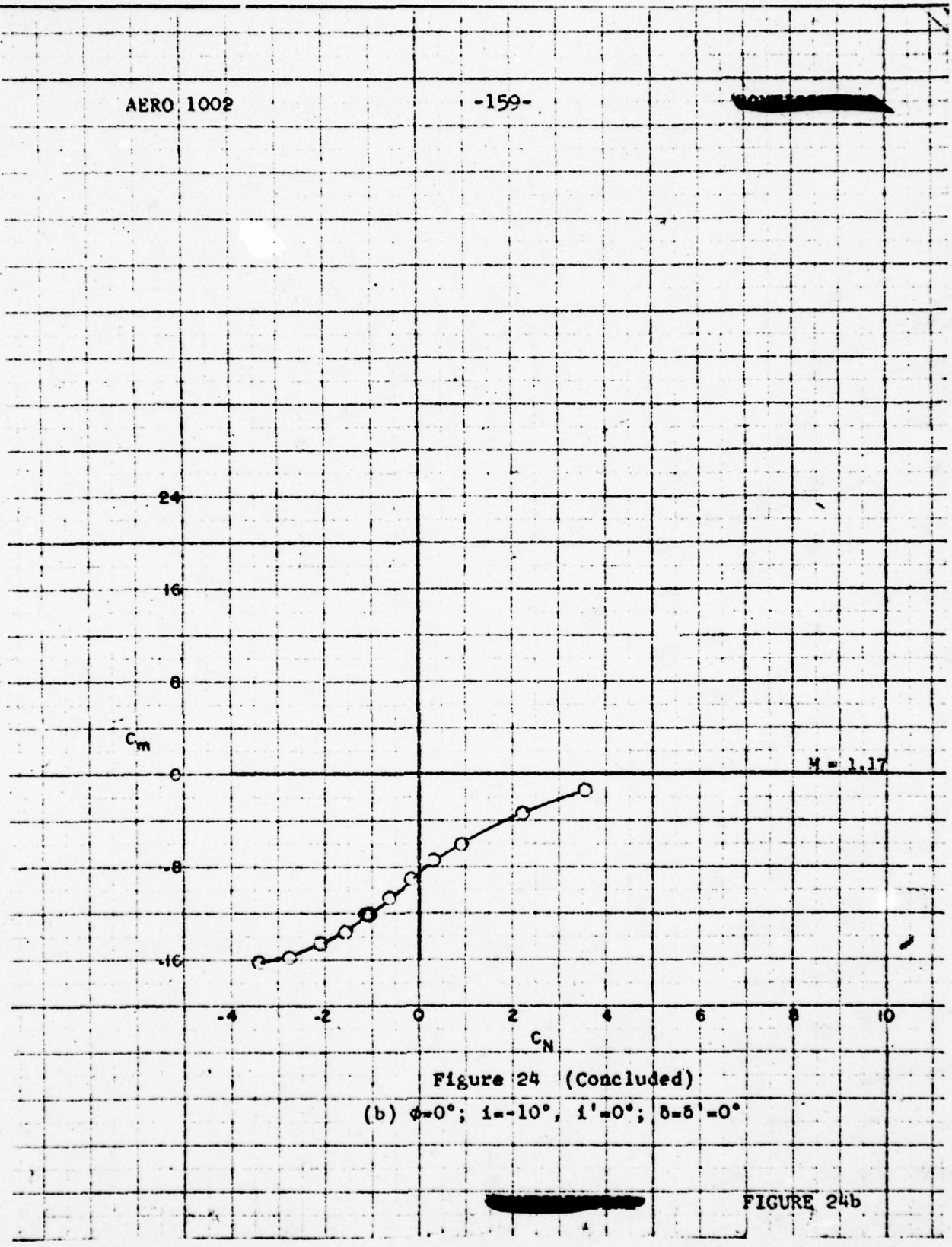

Figure 24 (Concluded)

(b) ϕ=0°; i=-10°, i'=0°; δ=δ'=0°

FIGURE 24b

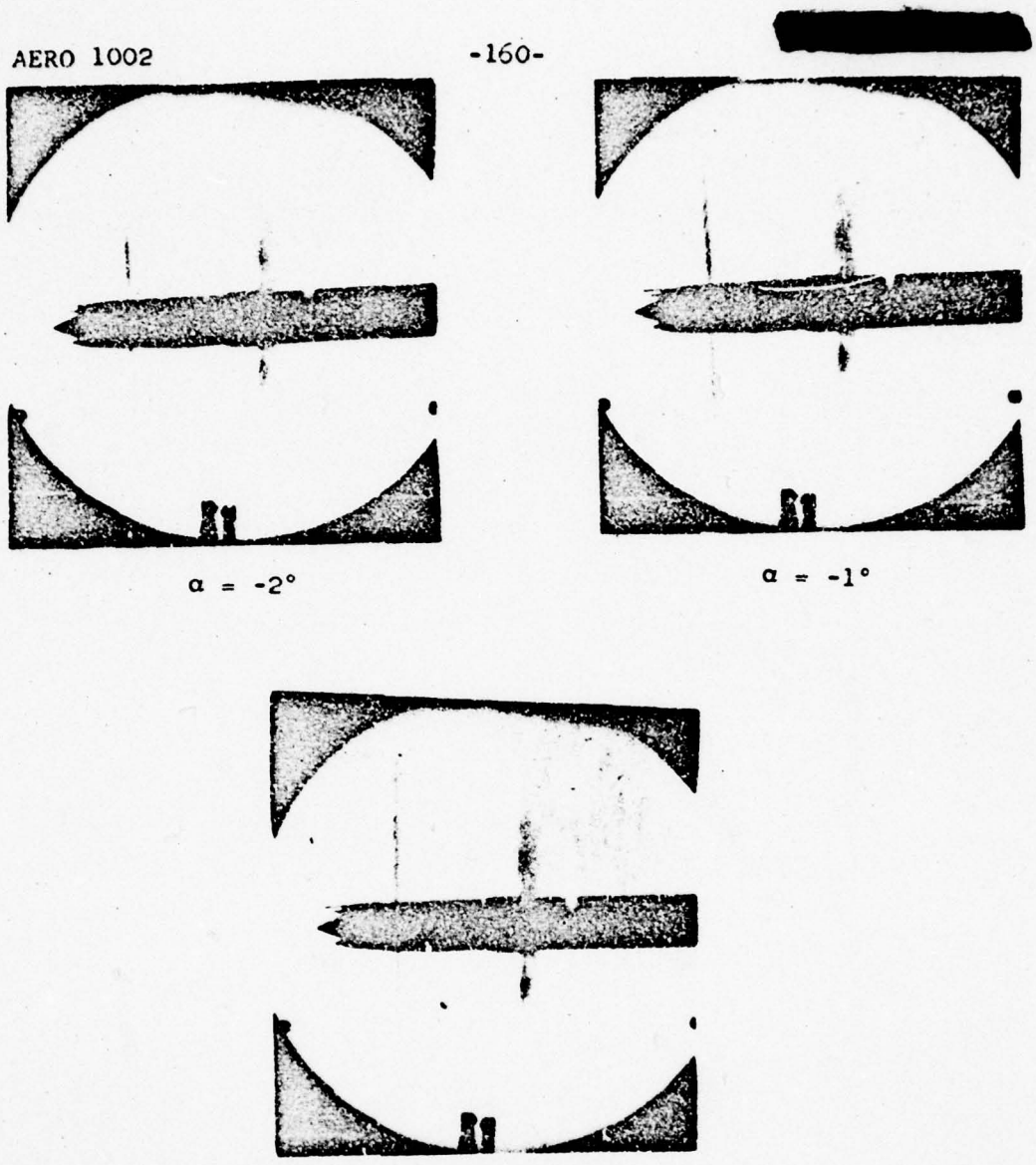

α = -2°

α = -1°

α = -0.5°

Figure 25 - Schlieren Photographs of the Missile.
Configuration $B_{22}R_5H_{10}$
(a) M = 0.95

PSD - 302, 763

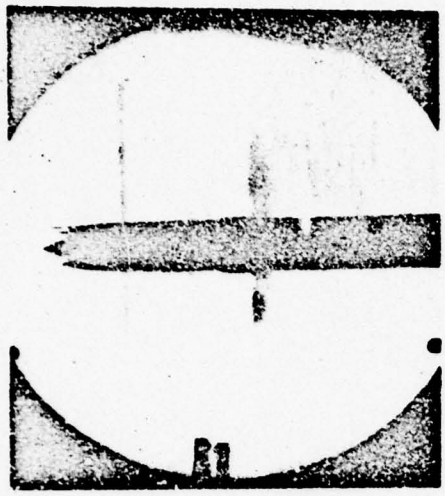

α = 0°

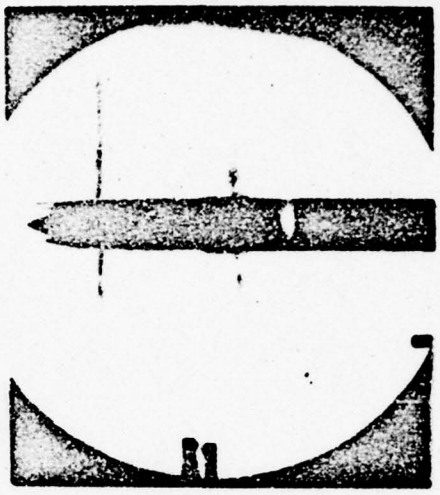

α = 0.5°

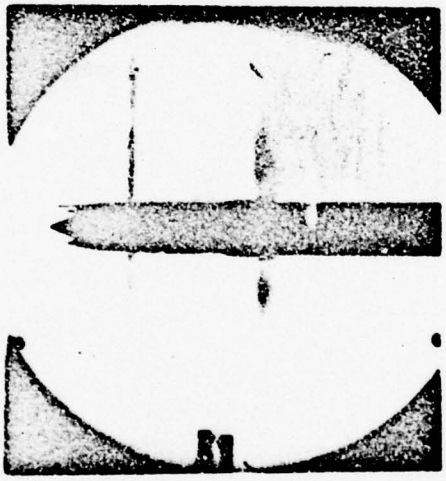

α = 1°

Figure 25 (Continued)
(a) Continued

PSD - 302, 764

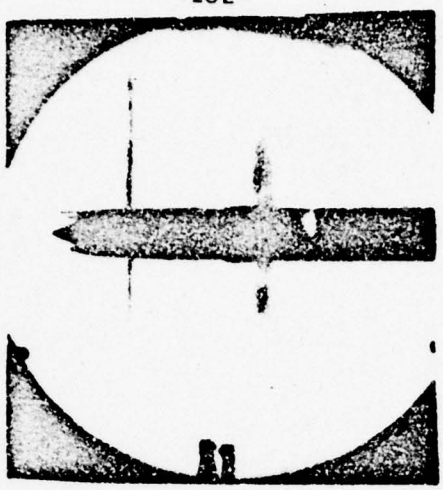

$\alpha = 1.5°$

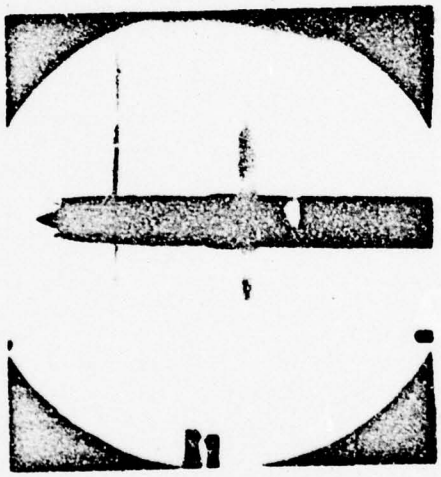

$\alpha = 2°$

Figure 25 (Continued)
(a) Concluded

PSD - 302, 765

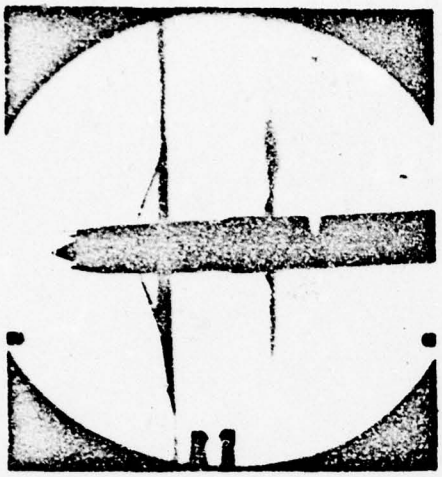

α = -2°

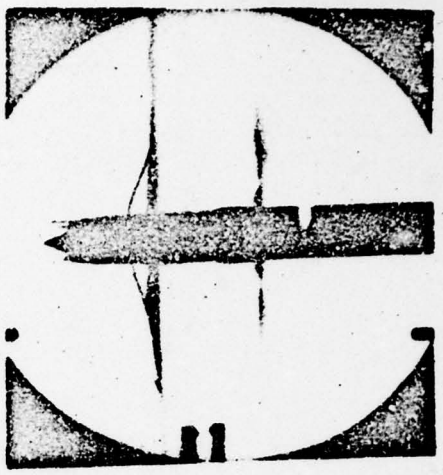

α = -1.5°

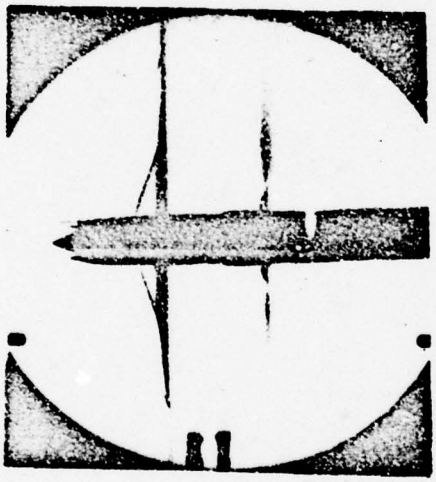

α = -1°

Figure 25 (Continued)
(b) M = 0.975

PSD - 302, 766

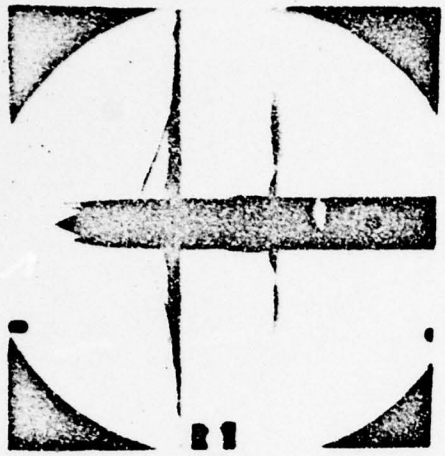

α = -0.5°

α = 0.5°

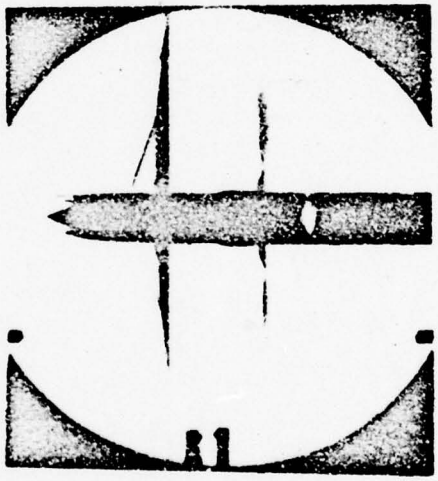

α = 1°

Figure 25 (Continued)
(b) Continued

PSD - 302, 767

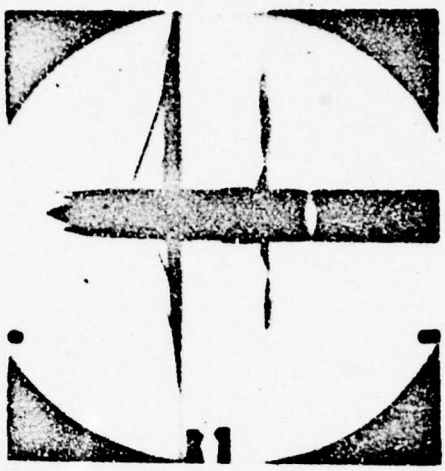

$\alpha = 1.5°$

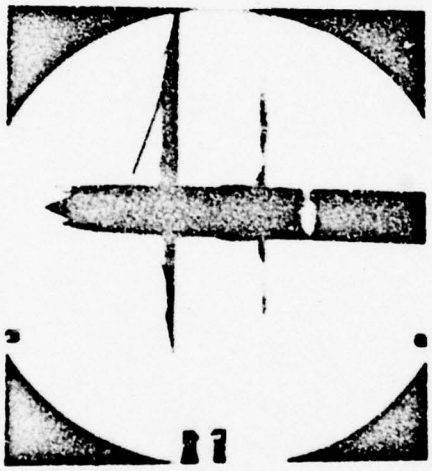

$\alpha = 2°$

Figure 25 (Continued)
(b) Concluded

PSD - 302, 768

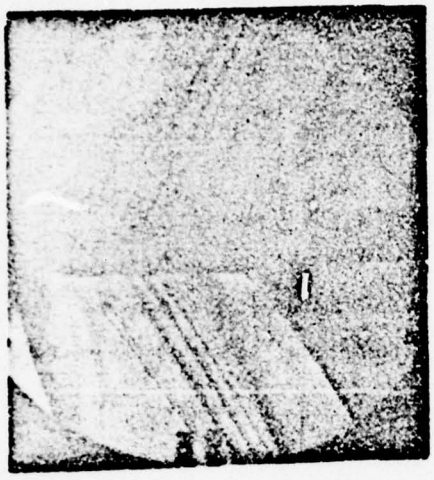

$\alpha = -2°$

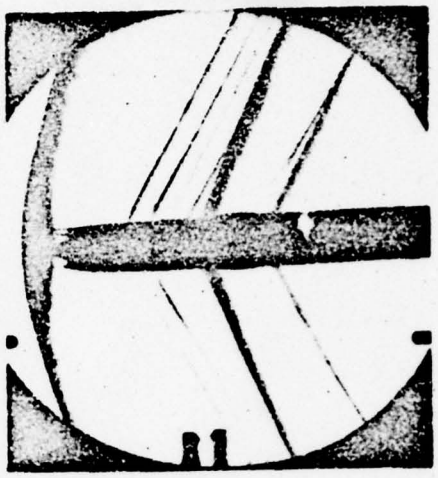

$\alpha = -1.5°$

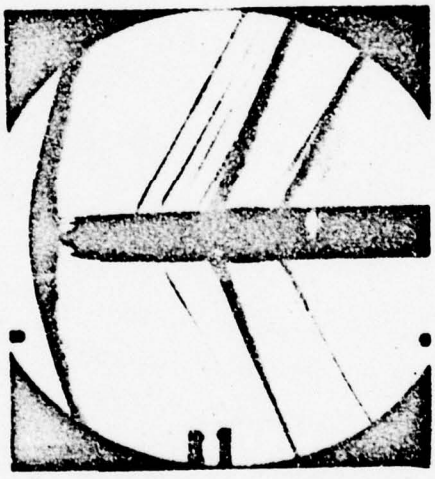

$\alpha = -1°$

Figure 25 (Continued)
(c) M = 1.10

PSD - 302, 769

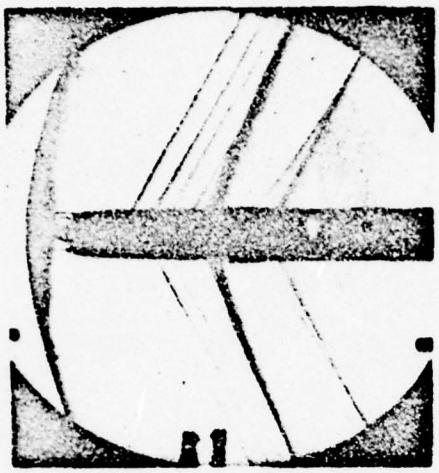

α = -0.5°

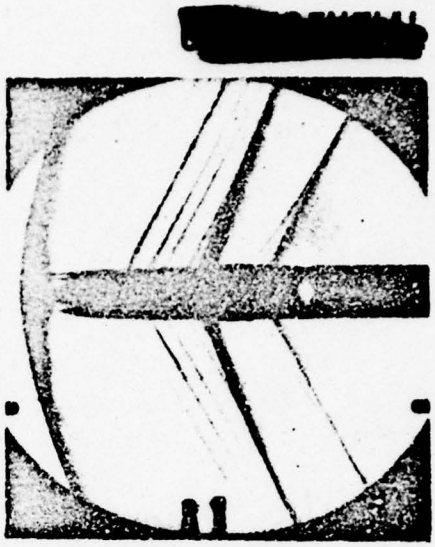

α = 0.5°

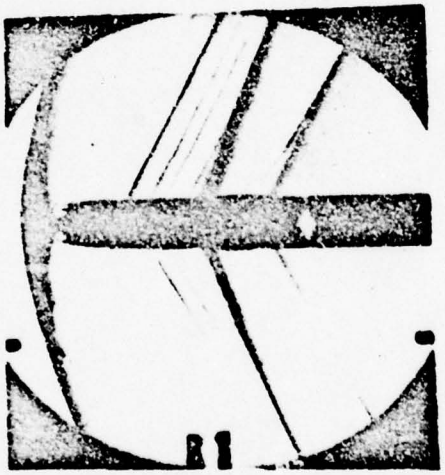

α = 1°

Figure 25 (Continued)
(c) Continued

PSD - 302, 770

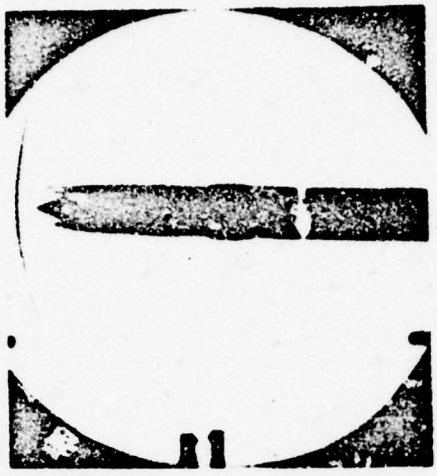

$\alpha = 1.5°$

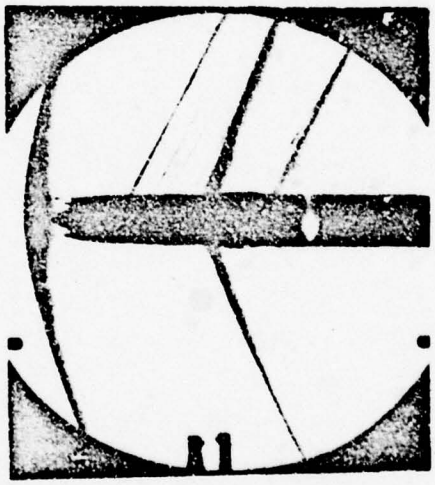

$\alpha = 2°$

Figure 25 (Concluded)
(c) Concluded

PSD - 302, 771

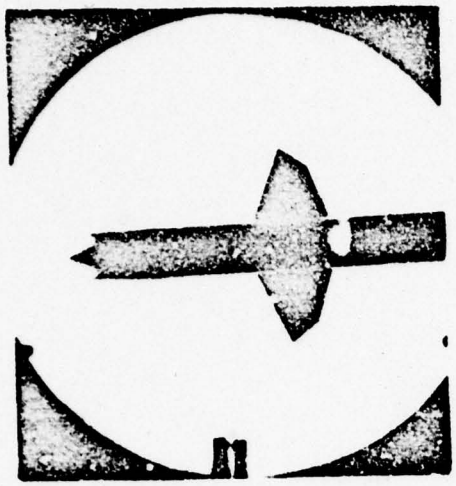

α = -2°

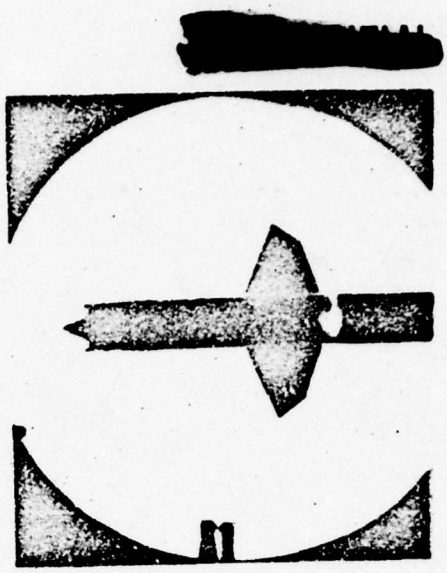

α = -1°

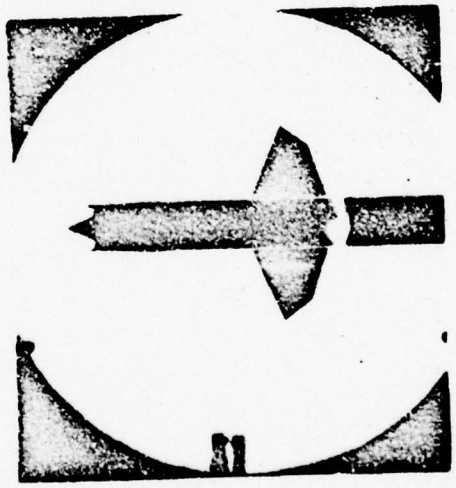

α = 0°

Figure 26 - Schlieren Photographs of the Missile.
Configuration $B_{22}R_5H_{10}W$
(a) M = 0.90

PSD - 302, 772

[redacted]

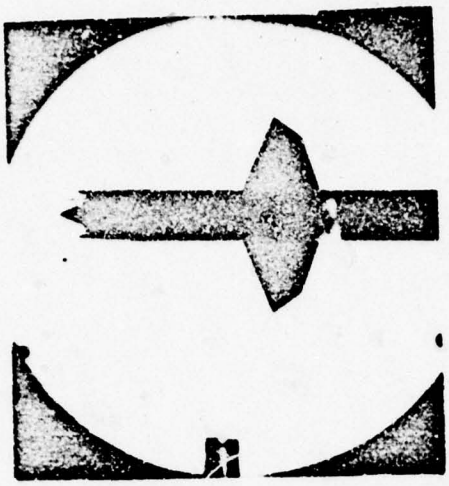

$\alpha = 1°$

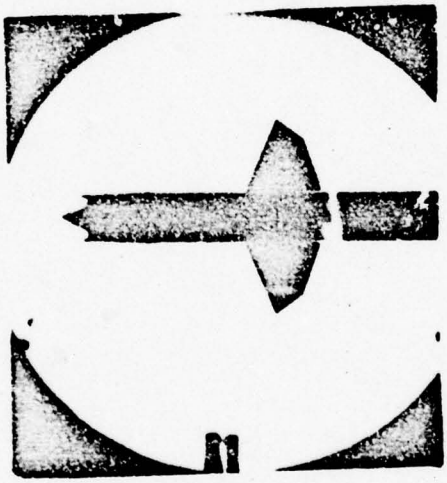

$\alpha = 2°$

Figure 26 (Continued)
(a) Concluded

PSD - 302, 773

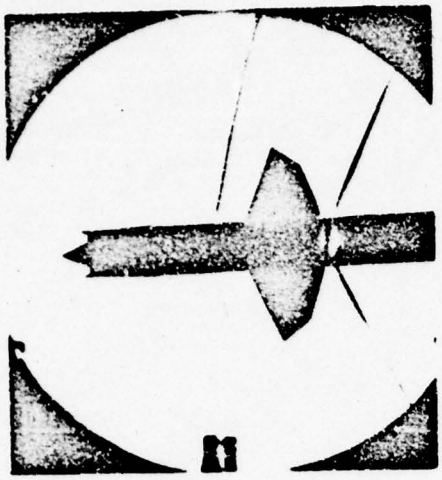

α = -2°

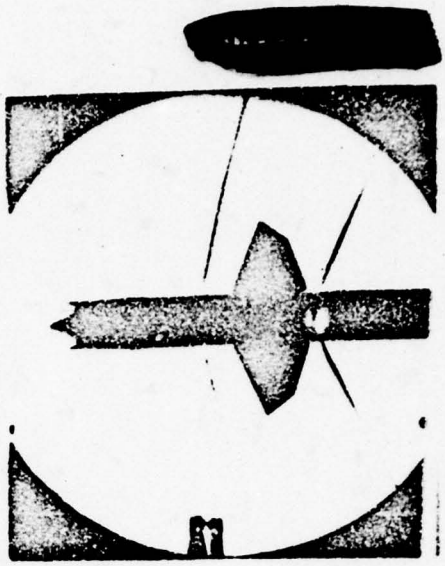

α = -1°

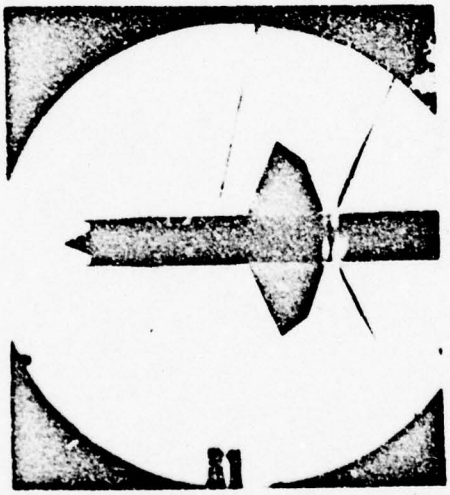

α = 0°

Figure 26 (Continued)
(b) M = 1.06

PSD - 302, 774

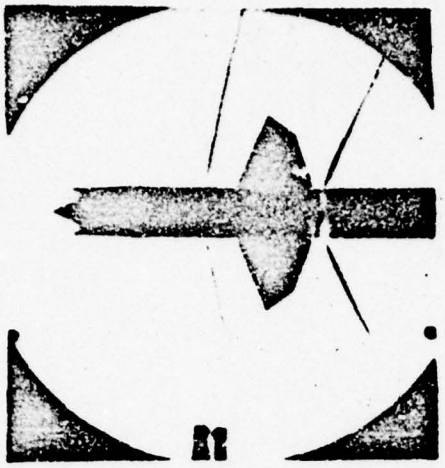

α = 1°

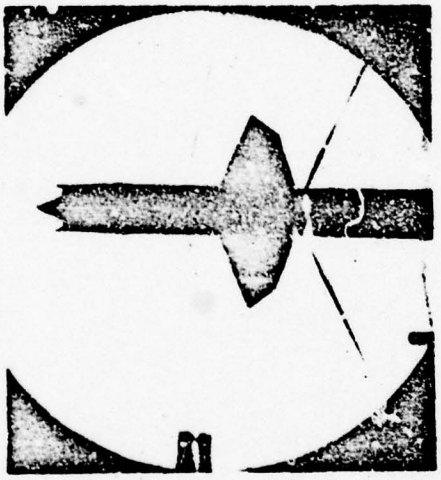

α = 2°

Figure 26 (Continued)
(b) Concluded

PSD - 302, 775

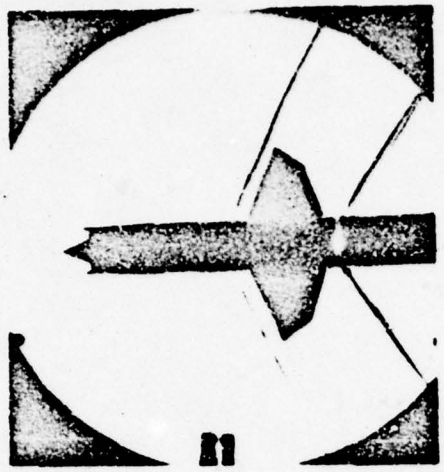

$\alpha = -2°$

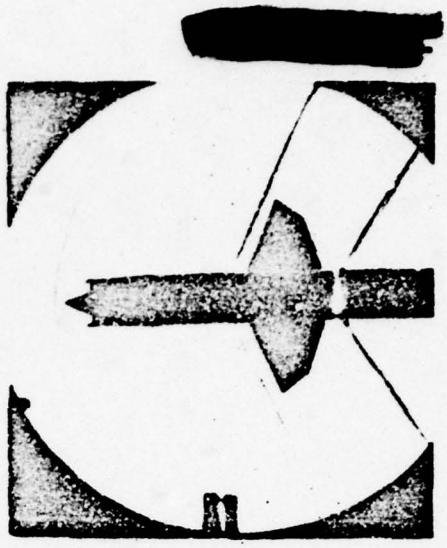

$\alpha = -1°$

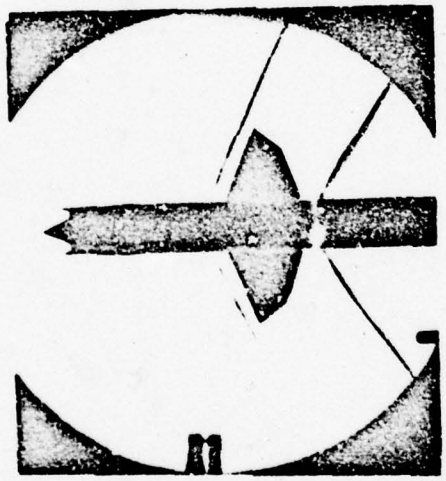

$\alpha = 0°$

Figure 26 (Continued)
(c) M = 1.17

PSD - 302, 776

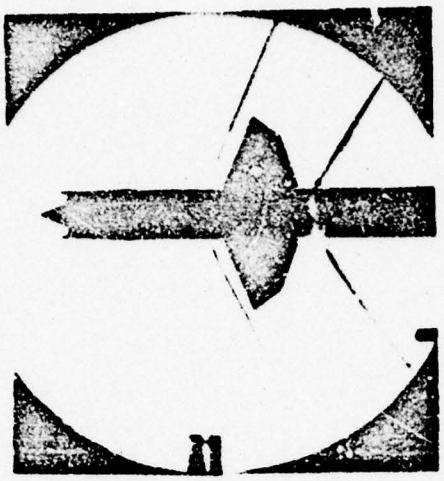

α = 1°

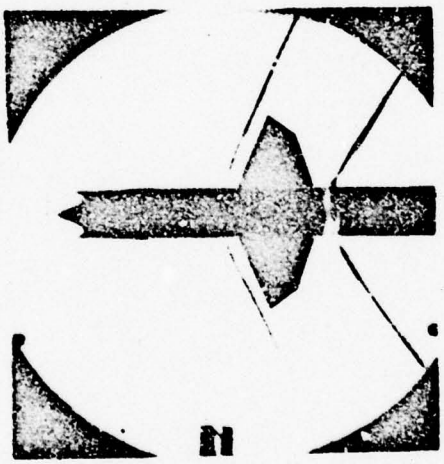

α = 2°

Figure 26 (Concluded)

(c) Concluded

PSD - 302, 777

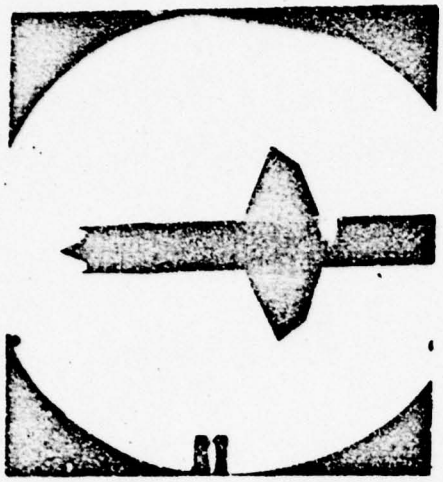

α = -2°

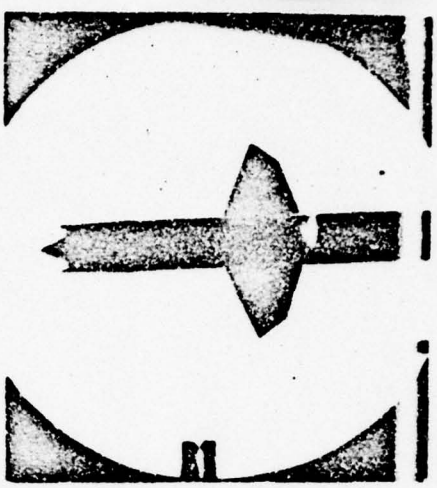

α = -1°

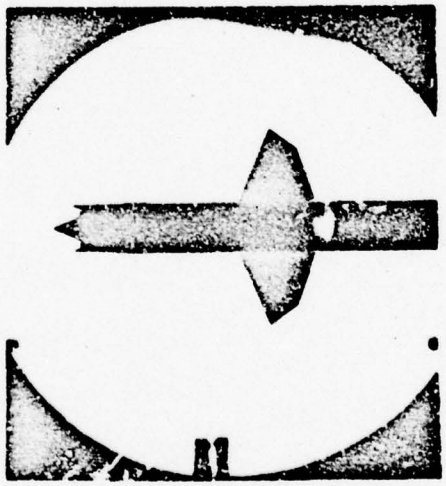

α = 0°

Figure 27 - Schlieren Photographs of the Missile.
Configuration $W_{22}R_5H_{10}T_{10}W$

PSD - 302, 778 (a) M = 0.90

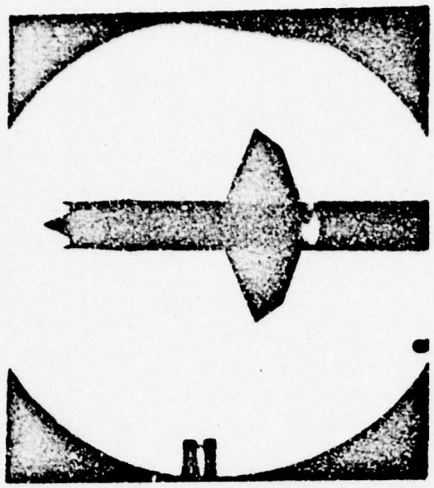

$\alpha = 1^c$

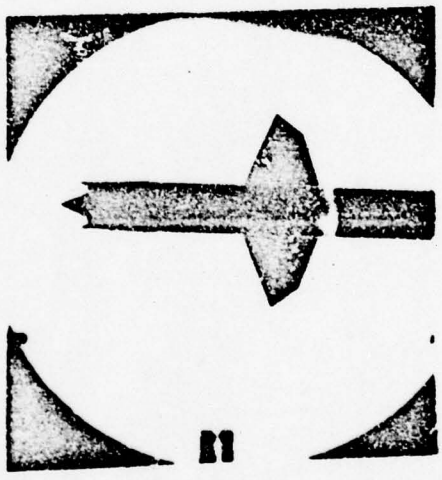

$\alpha = 2°$

Figure 27 (Continued)
(a) Concluded

PSD - 302, 779

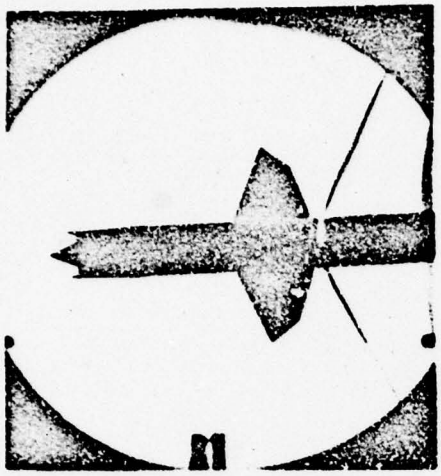

$\alpha = -2°$

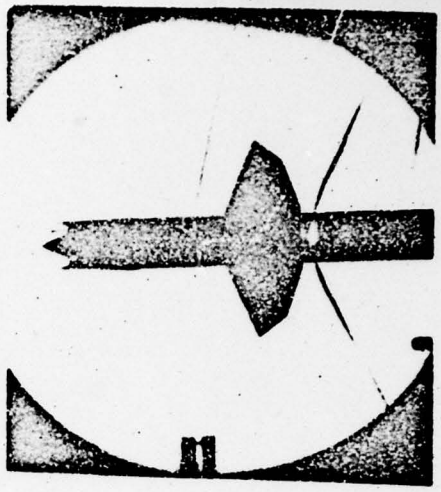

$\alpha = -1°$

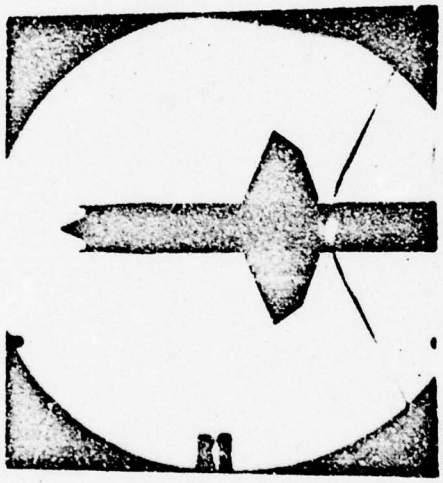

$\alpha = 0°$

Figure 27 (Continued)
(b) M = 1.06

PSD - 302, 780

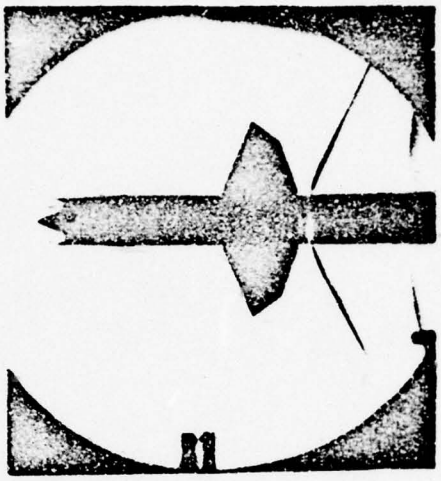

$\alpha = 1°$

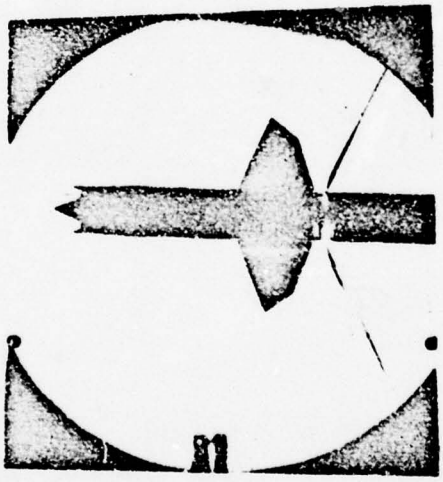

$\alpha = 2°$

Figure 27 (Concluded)
(b) Concluded

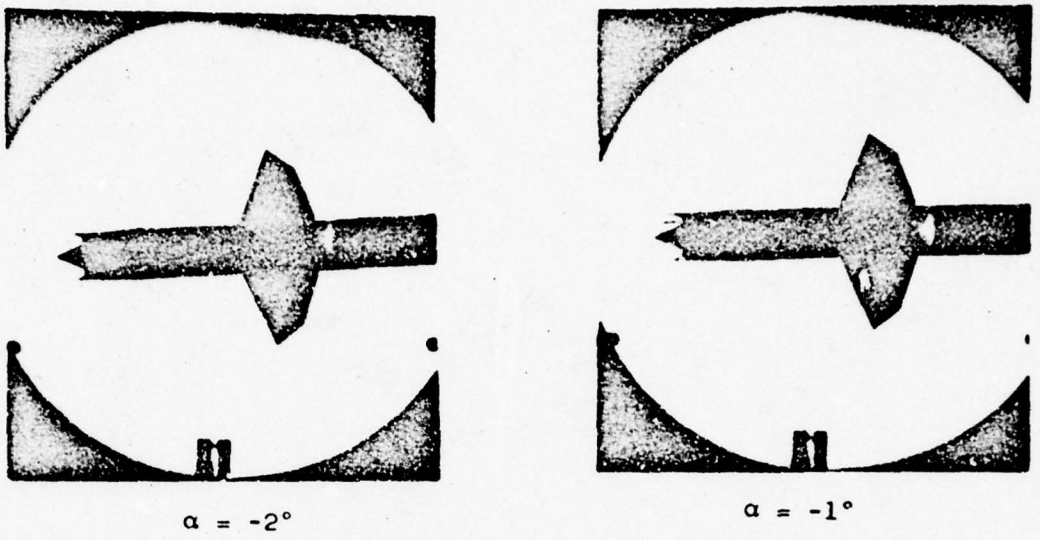

α = -2°

α = -1°

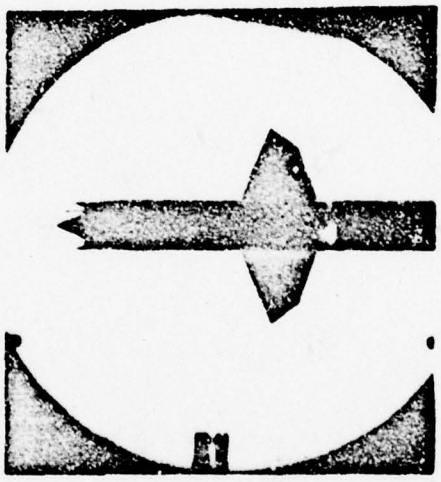

α = 0°

Figure 28 - Schlieren Photographs of the Missile.
Configuration $B_{22}R_5H_{10}WT_{10}F_{18}$

(a) M = 0.90

PSD - 302, 782

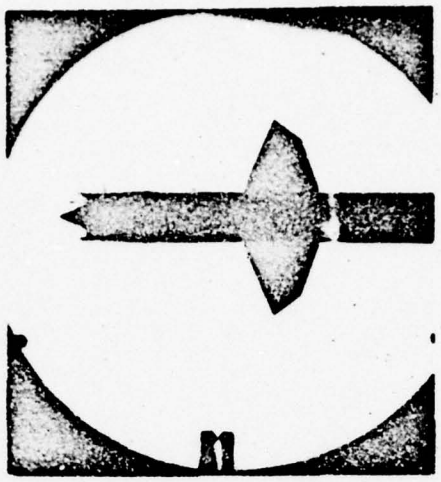

$\alpha = 1°$

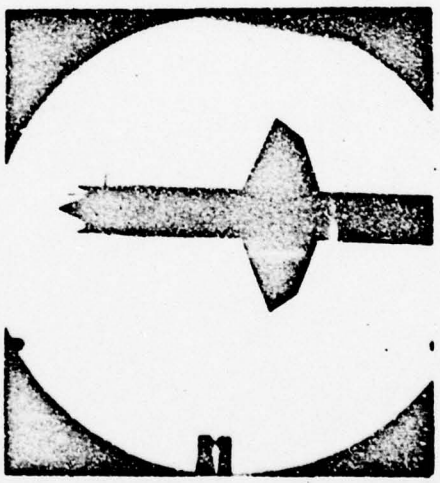

$\alpha = 2°$

Figure 28 (Continued)
(a) Concluded)

PSD - 302, 783

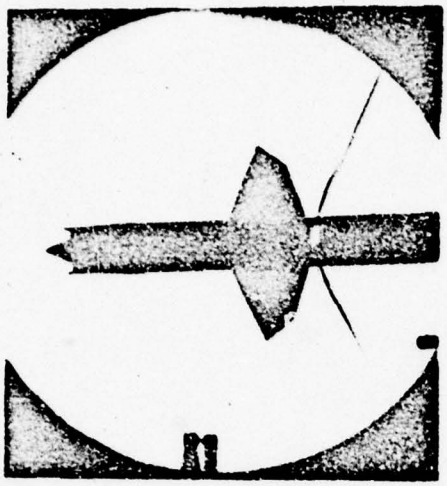

α = -2°

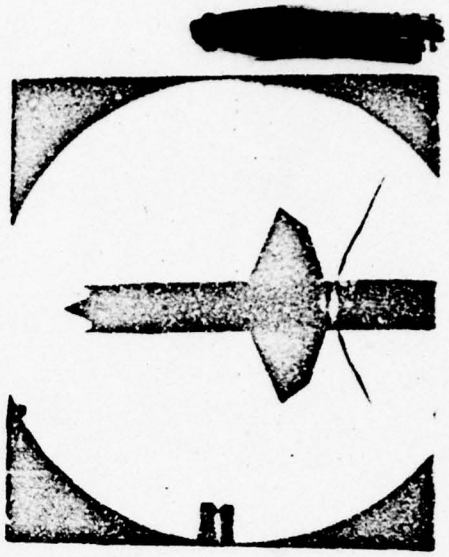

α = -1°

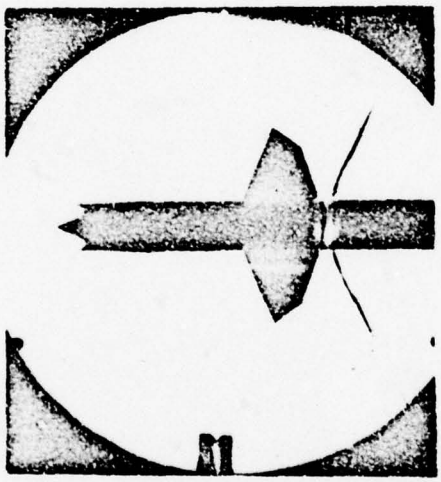

α = 0°

Figure 28 (Continued)
(b) M = 1.06

PSD - 302, 784

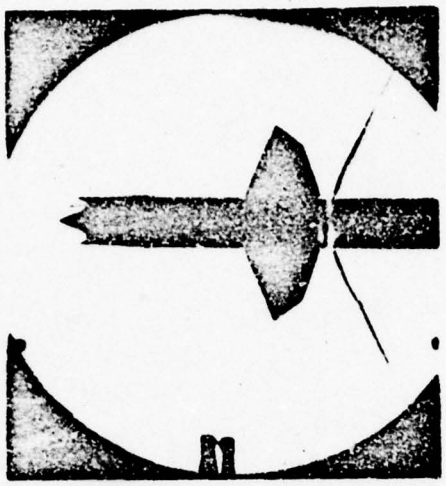

$\alpha = 1°$

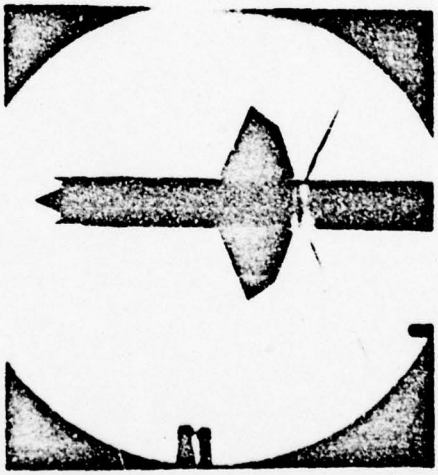

$\alpha = 2°$

Figure 28 (Continued)
(b) Concluded

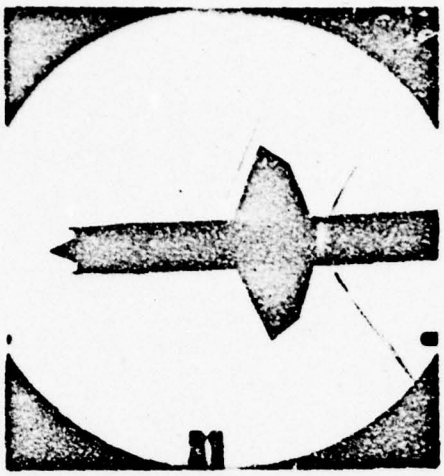

$\alpha = -2°$

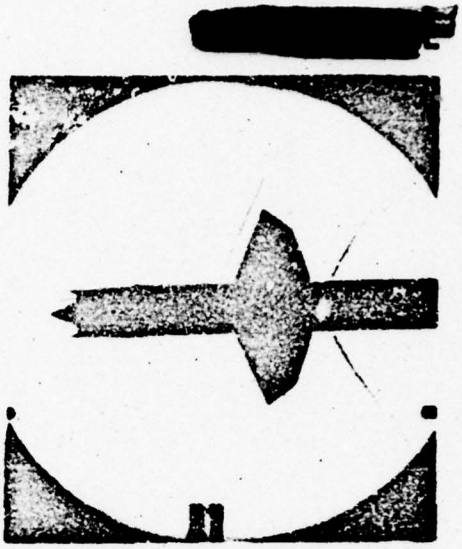

$\alpha = -1°$

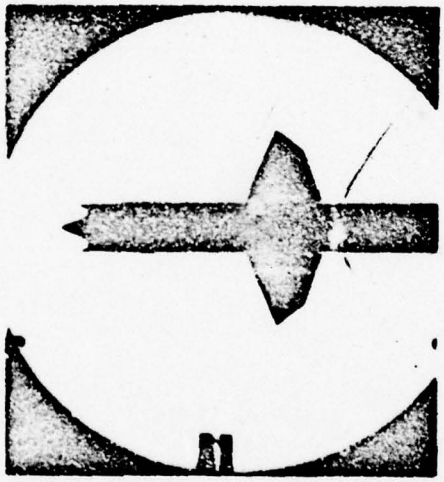

$\alpha = 0°$

Figure 28 (Continued)
(c) M = 1.17

PSD - 302, 786

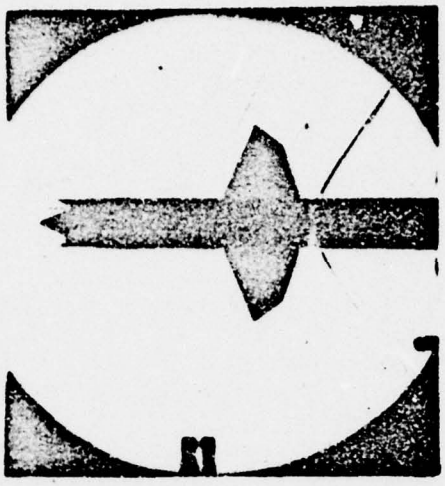

$\alpha = 1°$

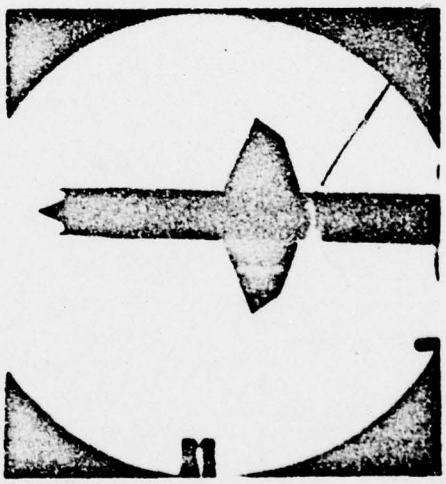

$\alpha = 2°$

Figure 28 (Concluded)
(c) Concluded

PSD - 302, 787

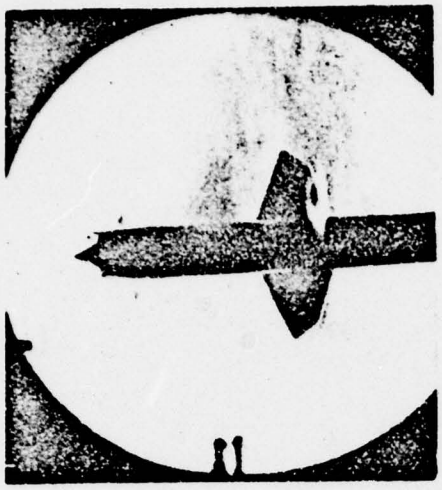

$\alpha = -2°$

$\alpha = -1.5°$

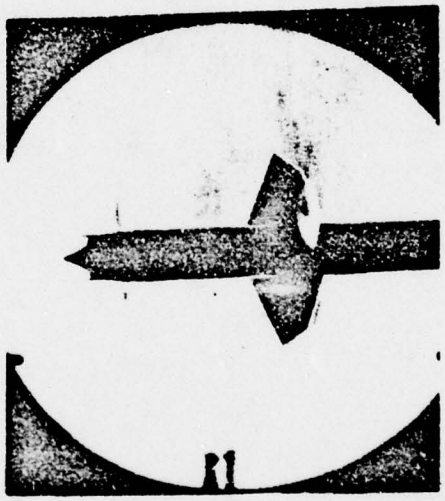

$\alpha = -1°$

Figure 29 - Schlieren Photographs of the Missile.
Configuration $B_{22}R_5H_{10}WC$

PSD - 302, 788

(a) M = 0.90

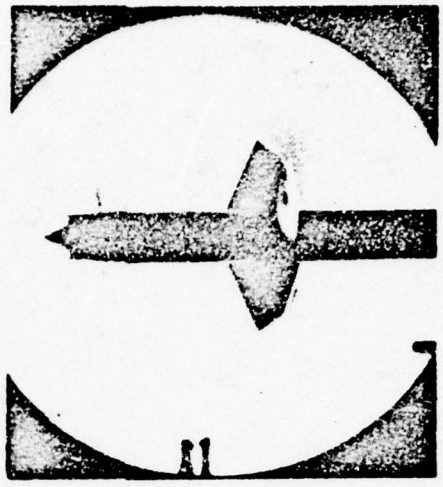

$\alpha = -0.5°$

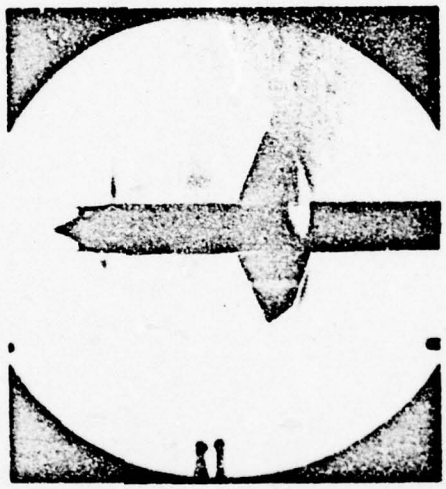

$\alpha = 0.5°$

Figure 29 (Continued)
(a) Continued

PSD - 302, 789

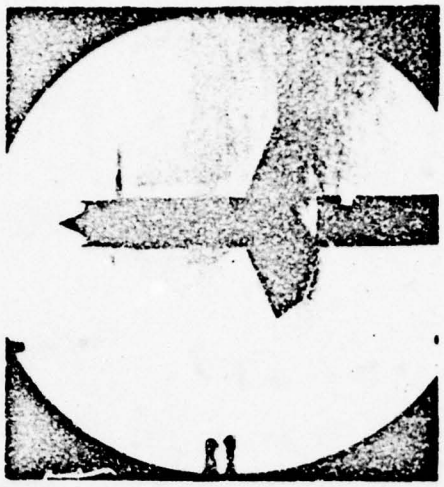

α = 1°

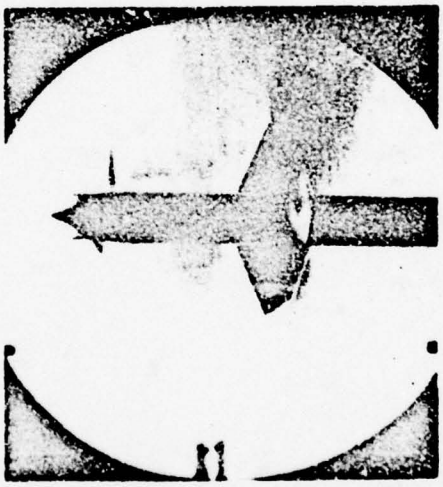

α = 1.5°

Figure 29 (Continued)
(a) Concluded

PSD - 302, 790

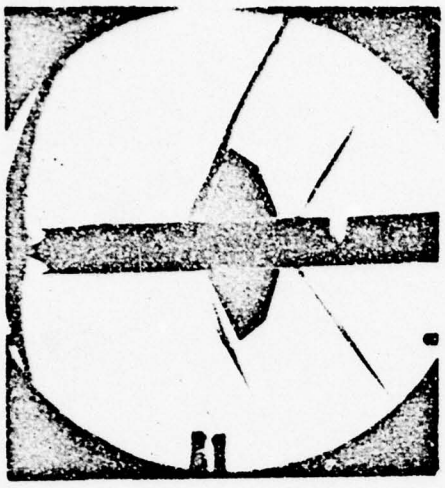

$\alpha = -2°$

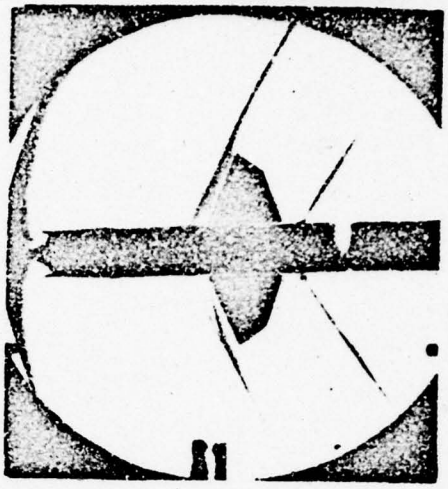

$\alpha = -1.5°$

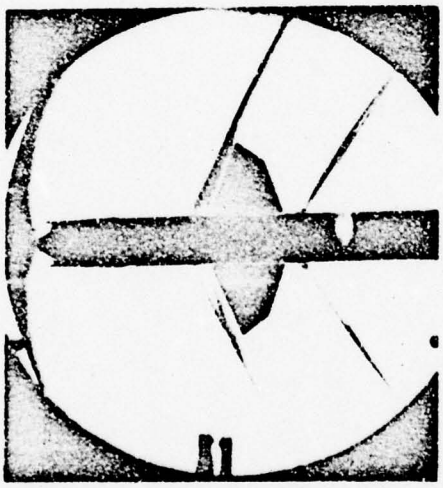

$\alpha = -1°$

Figure 29 (Continued)
(b) M = 1.17

PSD - 302, 791

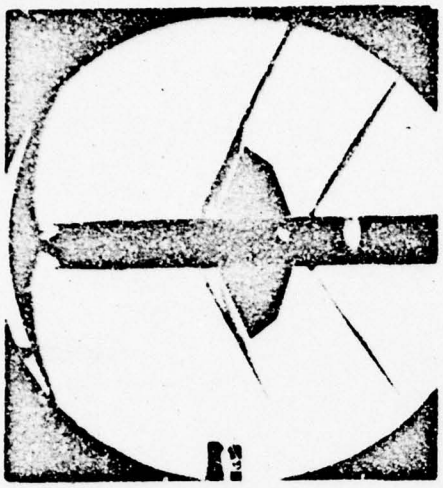

$\alpha = -0.5°$

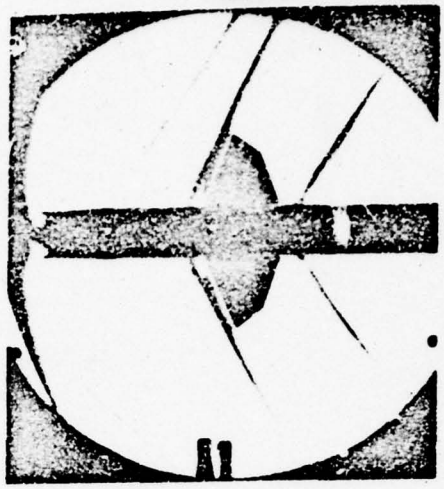

$\alpha = 0.5°$

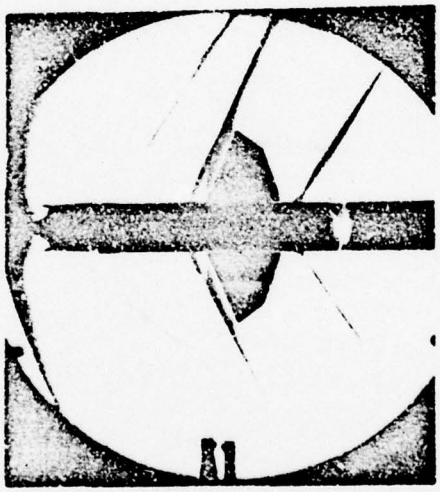

$\alpha = 1°$

Figure 29 (Continued)
(b) Continued

PSD - 302, 792

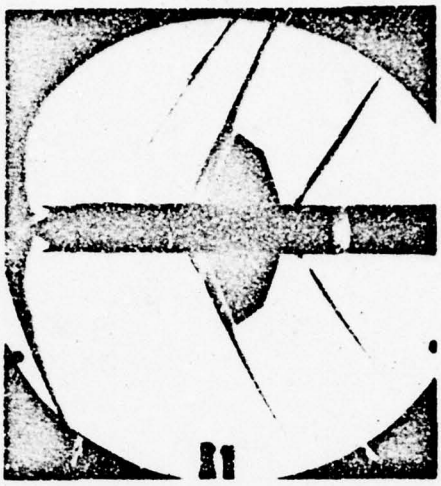

α = 1.5°

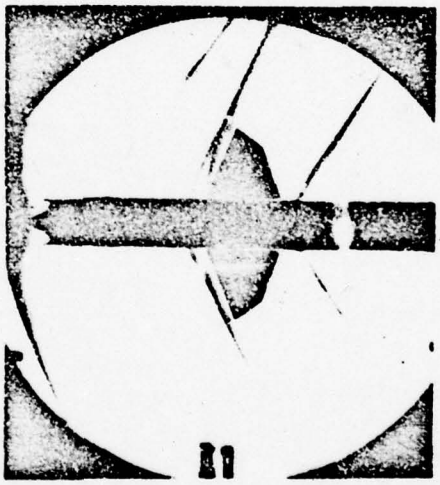

α = 2°

Figure 29 (Concluded)
(b) Concluded

PSD - 302, 793

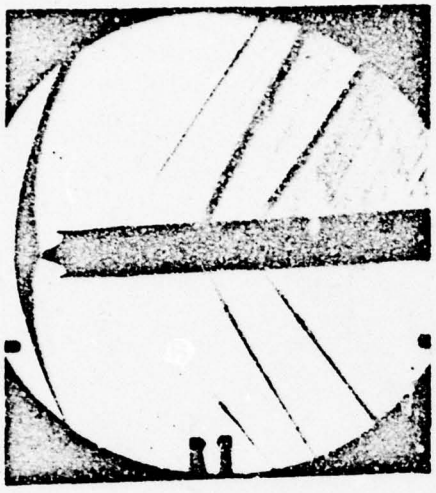

α = -2°

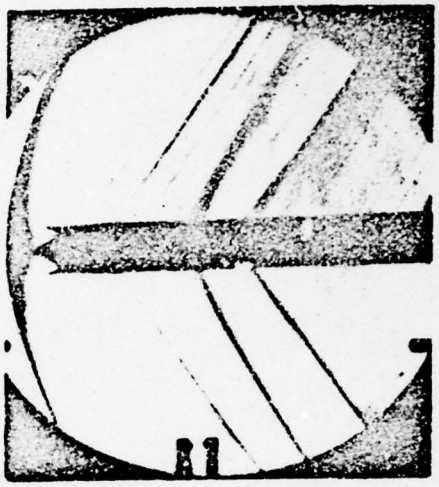

α = -1.5°

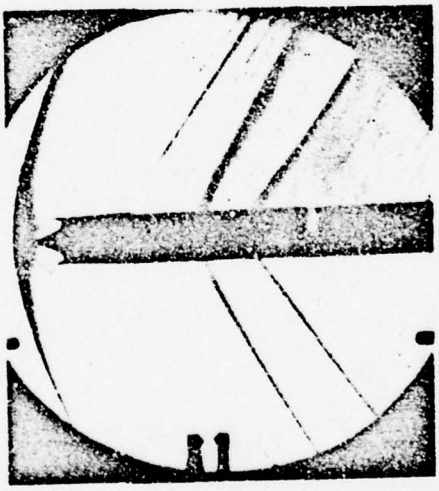

α = -1°

Figure 30 - Schlieren Photographs of the Missile.
Configuration $B_{22}R_5H_{10}C$

M = 1.17

PSD - 302, 794

AD-A062 289 DAVID TAYLOR MODEL BASIN WASHINGTON D C AERODYNAMICS LAB F/G 16/4.2
TRANSONIC WIND-TUNNEL TESTS OF A 1/15-SCALE MODEL OF THE TALOS --ETC(U)
MAR 61 M E MCDONALD

UNCLASSIFIED AERO-1002 NL

3 OF 3
ADA
062289

END
DATE
FILMED
3 -79
DDC

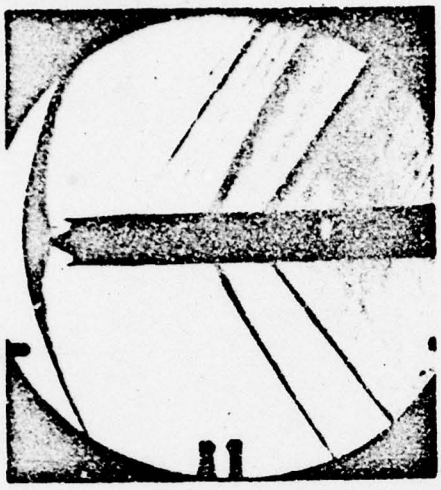

$\alpha = -0.5°$

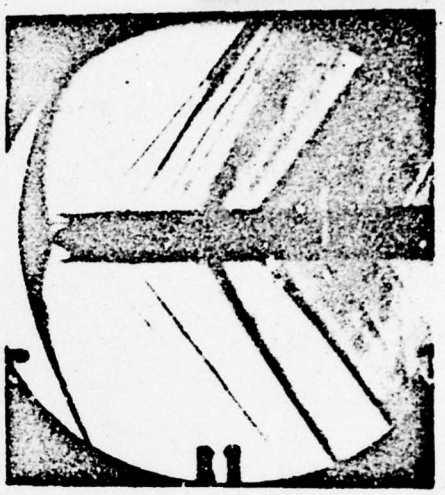

$\alpha = 0.5°$

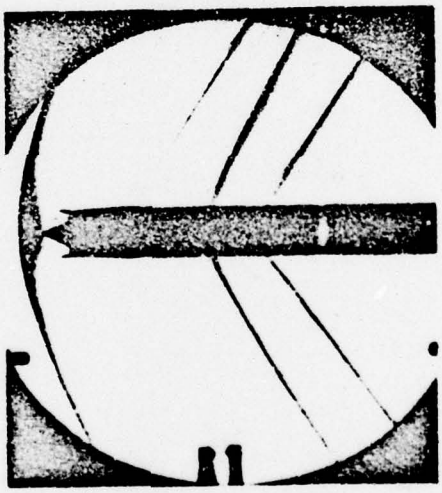

$\alpha = 1°$

Figure 30 (Continued)

PSD - 302, 795

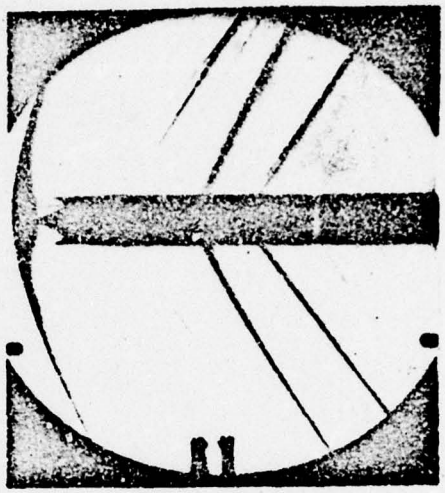

α = 1.5°

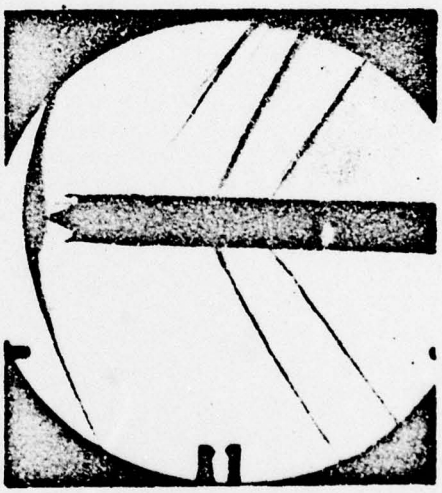

α = 2°

Figure 30 (Concluded)

PSD - 302, 796

DISTRIBUTION LIST

Copies	
5	Chief, BUWEPS (DIS-3) Navy Dept., Wash., D. C.
1	CO, NADC Johnsville, Pa.
1	CO, NAMC (Asst., NAF) Phila., Pa.
1	CO, SPCVD, Phila., Pa.
1	CDR, NOTS Point Mugu, Calif.
1	Chief of Naval Research Navy Dept., Wash., D. C.
1	Chief of Ordnance Dept. of Army, Wash., D. C.
1	CDR, NATC (Dir., TPTD) Patuxent River, Md.
2	[illegible] Wright-Patterson AFB, O.
5	DIR, NASA Wash., D. C.
2	APL, JHU Silver Spring, Md.
2	Bendix Products Div. Mishawaka, Ind.

DTMB Aero Rpt 1002
David Taylor Model Basin
TRANSONIC WIND-TUNNEL TESTS OF A 1/15-SCALE MODEL OF THE TALOS 6c1 MISSILE (Title Unclassified), by Michael E. McDonald. Wash., Mar 1961. 195 l. incl. illus. 2 refs. (Aerodynamics Lab. Aero Problem 6a0-116) CONFIDENTIAL

On cover: [Buweps] Problem Assignment 3-34-11.

Surface-to-air, supersonic guided missile tested at Mach 0.7 to 1.17, angles of attack of -4° to 10°, and roll angles of 0° and -45°. Effects of ram-air bleed at base of 2nd stage and longitudinal stability and control effectiveness of missile and components evaluated. Small scale of model affected positioning of six-component balances.

Bendix Products Div. is prime contractor for Talos.

Data-type report.

CONFIDENTIAL
1. GUIDED MISSILES (SAM-N-6c1)--STABILITY
2. JET ENGINES, RAM--BLEED-OFF
3. EXHAUST LOUVERS
4. STRAIN GAGE BALANCES, SIX-COMPONENT
5. MODELS--SIZE
6. PHOTOGRAPHY, SCHLIEREN
I. McDonald, Michael E.
II. Aero Test C-116
III. Buweps Prob Assigt 3-34-11